COMPUTATIONAL MODELING OF MULTIPHASE TURBULENT FLUID FLOW AND HEAT TRANSFER IN THE CONTINUOUS SLAB CASTING MOLD

BY

DAVID THOMAS CREECH

B.S., University of Illinois, 1997

THESIS

Submitted in partial fulfillment of the requirements
for the degree of Master of Science in Mechanical Engineering
in the Graduate College of the
University of Illinois at Urbana-Champaign, 1999

Urbana, Illinois

Abstract

The quality of continuously cast steel is known to be related to the fluid flow and heat transfer in the strand. Computational models of turbulent flow, multiphase flow and heat transfer have been developed to analyze phenomena related to steel quality and to compare modeling techniques for flow in the continuous casting nozzle and strand. The effects of grid size, turbulence model and boundary conditions on the heat transfer solution in the mold are compared using a combined turbulent fluid flow and heat transfer model, and solved with the computational fluid dynamics package CFX. It is found that the choice of these three modeling aspects has a large effect on the heat transfer results, and that the standard K-ε model with a user supplied wall law for enthalpy produces results that most closely match experiments. Models implementing three different strategies for treating the solidification of the steel shell are compared. Including the shape of the shell in the domain without modeling the mass flow across the shell interface creates an unphysical acceleration of flow into the mold. More accurate flow results are achieved by neglecting the shape of the shell completely. A parametric study is performed on a multiphase model of fluid and gas flow in the strand. The effects of gas flow rate, gas bubble diameter, casting speed, nozzle submergence depth and mold width on steel quality issues are quantified. It is found that the maximum surface velocity can be lowered by adding gas until the flow pattern becomes single roll, at which point the surface velocity increases. The maximum gas penetration depth is deepest for cases with small gas bubbles, high casting speed and shallow submergence. Single roll flow patterns decrease the gas penetration depth. The maximum steel level at the mold edges decreases when gas is added, but increases for high casting speeds and single roll flow. Surface level fluctuations are reduced by adding a moderate amount of gas (6% volume fraction), but are increased if the gas injection rate becomes too high. Single roll flow increases the surface fluctuations because the liquid jet moves close to the surface. Increasing the mold width increases the maximum surface velocity and surface fluctuations because the steel flow rate must be increased to maintain a constant casting speed.

Table of Contents

Page

List of Tables

Page

List of Figures

Page

Nomenclature

$\mathbf{B}$	Body force
$c_{liq\ gas}^{(drag)}$	Inter-phase drag terms
C_1	Constant in turbulence models, 1.44
C_2	Constant in turbulence models, 1.92
C_D	Drag Coefficient
C_p	Specific Heat
C_μ	Constant in turbulence models, 0.09
E	Log-Layer Constant for Velocity, 9.7930
E_H	Log-Layer Constant for Enthalpy, 0.2689
f_{liq}	Volume fraction of liquid phase
f_{gas}	Volume fraction of gas phase
F_2	Function in Low K-ε model
F_3	Function in Low K-ε model
F_4	Function in Low K-ε model
F_μ	Function in Low K-ε model
h	Static Enthalpy
H	Total Enthalpy
K	Turbulent kinetic energy
k_{eff}	Effective conductivity
k_o	Molecular conductivity
k_t	Turbulent conductivity
p	Pressure
Pr_t	Turbulent Prandtl number for Velocity, 1.0
Pr_K	Turbulent Prandtl number for Turbulence Kinetic Energy, 1.0
Pr_ε	Turbulent Prandtl number for Turbulence dissipation, 1.217
Pr_H	Turbulent Prandtl number for Enthalpy, 0.9
Re_b	Bubble Reynolds number
Re_T	Local turbulent Reynolds number in Low K-ε model
S_{massss}, $\mathbf{S}_{mom}$	Source term in continuity and momentum equations
T	Temperature

T_{liq}	Liquidus Temperature of Steel
$\mathbf{V}$	fluid velocity
$\mathbf{V}_{liq}$	Velocity of liquid phase
$\mathbf{V}_{gas}$	Velocity of gas phase
x	Distance in model domain from centerplane to Narrow Face
y	Distance in model domain from centerplane to Wide Face
y^+	Non-Dimensional Distance
y^+_{cell}	Non-Dimensional Size of the Cell at the Wall
y^+_o	Crossover Point for Velocity, 11.23
y^+_H	Crossover Point for Enthalpy, 31.77
z	Distance in model domain from Top Surface to Mold Exit
β	Under-Relaxation Factor
Φ	Shear Production in turbulence models
α	Inlet Jet angle
ε	Turbulent dissipation rate
κ	Von-Karmen Constant, 0.419
μ_{eff}	Effective viscosity
μ_o	Molecular viscosity
μ_t	Turbulent viscosity
ρ	fluid density
σ_K	Constant in turbulence models, 1.00
σ_ε	Constant in turbulence models, 1.30

1 Introduction

Continuous casting is the predominant way by which steel is produced in the world. A schematic of part of the continuous casting process is depicted in Figure 1.1. Molten steel flows through the “tundish,” and then it exits down through a ceramic Submerged Entry Nozzle (SEN) and into the mold. Here, the steel freezes against the water-cooled copper walls to form a solid shell, which is continuously withdrawn from the bottom of the mold at a “casting speed” that matches the flowrate of the incoming metal.

Heat transfer in the mold is important for shell growth and steel quality. There are several forms of heat transfer-related problems that occur in continuous casting. One problem is the formation of a solid hook of steel at the top surface meniscus. Steel solidifies around the hook as the shell is pulled down, creating a hook defect. Another problem is breakouts. Breakouts occur when the jet of liquid steel from the nozzle melts through the solid shell. When the melted hole reaches the end of the mold the shell can no longer contain the liquid steel. The liquid steel empties out of the mold, creating a hollow breakout shell. By modeling heat transfer in a fluid flow simulation, the heat flux delivered to the shell can be calculated. This heat flux is then correlated to a shell thickness. The shell thickness of actual breakout shells from a thin-slab caster has been measured [1]. These measurements can be used to validate the model predictions of heat flux delivered to the solidifying shell. Accurate heat transfer models can help determine what conditions lead to breakouts and hook defects.

Plant observations have found that many serious quality problems are directly associated with the flow pattern in the mold [2]. Specifically:

- If the horizontal surface velocity of the liquid steel is large, the resulting shear forces can entrain liquid flux into the steel flow [3]. The resulting flux globules then circulate with the steel flow and can be entrapped in the solidifying shell, forming internal solid inclusions.
- The vertical momentum of the liquid steel jet can lift the level of the top surface, creating a variation in the interface level or “standing wave.” A high standing wave at the mold wall can prevent liquid flux from filling the gap between the steel shell and

the mold where the surface level is high. Without lubrication from the liquid flux in the gap, the shell can “stick” in the mold instead of pulling out at the casting speed. The flux is also important for heat transfer between the steel shell and the mold. A lack of flux in the gap can create non-uniform heat flow on the shell. Finally, lack of flux in the gap can cause cracks in the steel shell due to thermal stresses and mold friction [4].

- Fluctuations in surface level of the liquid steel are caused by random turbulent motion of the flow. Large surface fluctuations cause time-variations in the interface level that could lead to surface defects such as entrapped mold powder [5].
- Bubbles of the injected argon gas can become trapped in the steel shell. The bubbles collect alumina inclusions while in the liquid steel. When the steel shell solidifies around the trapped bubbles, “pencil-pipe” defects are formed.

Clearly, the flow pattern must be understood in order to address these problems. There are many parameters that affect the flow in the mold. These include the gas flow rate, gas bubble diameter, casting speed, nozzle submergence depth and mold width. Previous studies on multiphase flow in continuous casting focus on the numerical methods of modeling multiphase flow [6, 7]. However, further work is needed to fully quantify the relationships between fluid flow and steel quality, because there are so many important flow parameters that interact.

Entrainment of the liquid flux layer was studied by Emling, Waugaman, Feldbauer and Cramb [3] with water modeling, using silicon oil as the flux modeling fluid. Their work showed that for a particular casting speed there is a critical argon flow rate that causes flux entrainment. Therefore, both the maximum surface velocity and the critical argon flow rate must be taken into account when determining the chance of entrainment for a given set of flow conditions.

The level of the steel-flux interface has been experimentally determined in several previous studies. McDavid measured the interface between the liquid flux and liquid steel using “nail boards” containing a grid of steel rods [4]. The rods melt at the flux-steel interface, showing the depth of the steel at a particular point on the surface. Bergeles used numerical models of the free surface in a simulated water model to predict the free

surface shape and compared this shape to water model measurements [8, 9]. Bergeles presents a correlation between pressure and interface level, allowing the calculation of level from pressure in a numerical model that does not include the free surface.

When argon gas bubbles are trapped in the solidifying shell, a “pencil-pipe” defect can occur. Experimental measurements by Huang of the depth below the meniscus of argon bubble entrapment for different casting speeds show that defects caused by entrapped bubbles which located between 0.5 m and 3.0 m below the meniscus [10]. The average percent argon trapped as defects was found by Shang to range from 1E-4% to 1E-3% [11].

The assumptions made in the computational models are also important. The choice of turbulence model, numerical grid size and boundary condition are essential in properly modeling heat transfer between the fluid and the mold. Guthrie used the Low Reynolds Number turbulence model in a study on heat transfer in the strand [12]. However, the Low Reynolds Number model requires a fine numerical mesh to resolve boundary layers at the walls, and therefore significantly increases the computer resources required for a given problem, when compared to the standard K-ε model.

Another choice in both water and mathematical flow models is of how to treat the solidifying shell. Simplification of the model can be made if the solidification of the shell is not included in the flow model. The domain boundaries must then be chosen. Sometimes, the curvature of the liquid domain due to the shell is included in the water model [3] and sometimes the shell is neglected entirely. In previous mathematical models [5, 13] the assumption that the shell can be neglected was made. The effect on the fluid flow solution that this simplification causes has not been studied.

Mathematical models can increase understanding of flow in continuous casting, and help to determine how to avoid and minimize problems and defects in the casting process. The objective of this work is to achieve the following:

- Develop a computational model of turbulent multiphase flow and heat transfer to analyze phenomena related to steel quality and to compare modeling techniques for

flow in the continuous casting nozzle and strand. Modeling techniques to be compared include grid size, turbulence model and boundary conditions, and their effect on the heat transfer solution in the mold.

- Determine the effect on the fluid flow solution of computational modeling strategies for treating the solidification of the steel shell. A model which does not include the shape of the shell in the domain is to be compared to two models: one that includes the shape of the shell but does not include the transfer of mass across the solidification boundary, and one that includes the shape of the shell and the transfer of mass across the solidification boundary.

- Determine the effects of inlet casting parameters on steel quality. These parameters include gas flow rate, bubble diameter, casting speed, submergence depth, and mold width. Criteria that quantify the tendency towards defects are to be extracted from the results. These include surface level, level fluctuation, top surface tangential velocity and bubble penetration depth.

This work is a step in determining what can be done to minimize defects in continuous casting. By understanding how fluid flow relates to steel quality, an optimum flow pattern that minimizes defects can be found. The modeling techniques studied in this work will help to improve numerical models of fluid flow and heat transfer in continuous casting. The parametric study will help to confirm and quantify plant observations of quality related parameters.

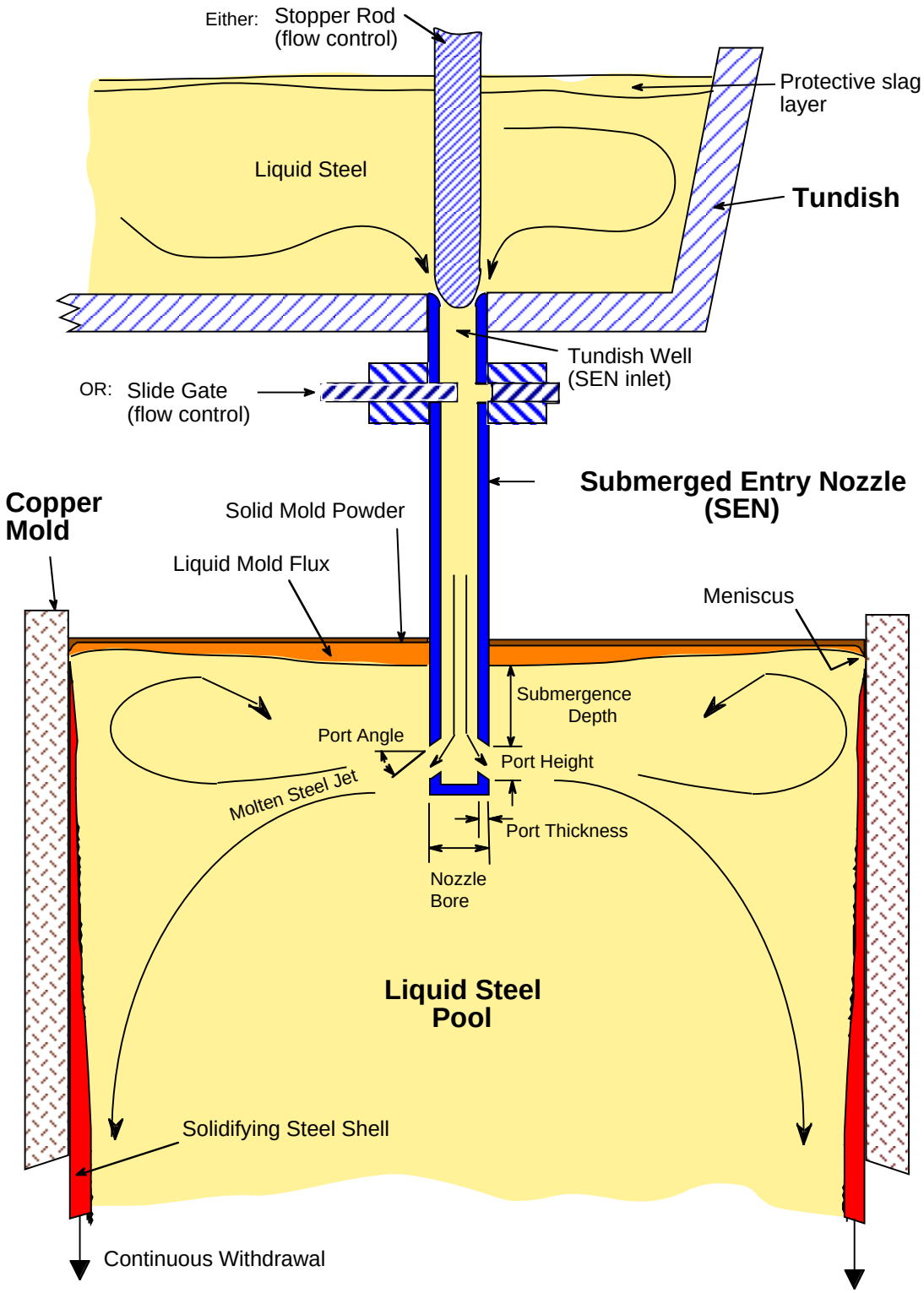

Figure 1.1. Schematic of tundish and mold region of continuous casting process [14]

2 Model Formulation

Numerical models of fluid flow and heat transfer solve governing equations that should describe the important physics of the problem. The domain of interest in this work includes the top portion of the strand and in some cases the submerged entry nozzle of the caster. To model heat transfer and fluid flow the nozzle and in the strand, governing equations for turbulent flow are needed. Including the effects of argon gas injection in the flow solution requires the equations to be extended to account for momentum transfer between the phases. Additionally, boundary conditions must be set for all variables at each boundary in the domain. Special boundary conditions for the model accounting for the shell are also derived.

2.1 Governing Equations for Turbulent Flow

Turbulent flows are governed by the unsteady Navier-Stokes equations, but the extreme complexity of the flow makes a direct numerical simulation possible only for simple geometries at low Reynolds numbers with current computer technology. To solve complex high-velocity flows, approximate modeling methods are used. The Reynolds averaged Navier-Stokes (RANS) equations use the time-averaged Navier-Stokes equations. The averaging of the Navier-Stokes equations produces new terms, called the Reynolds stress and the Reynolds flux. These are in turn defined using the variables K and ε, which are solved for using additional transport equations.

The continuity equation for mass conservation is

$$\nabla \cdot \mathbf{V} = S_{mass} \tag{2.1}$$

where $\mathbf{V}$ is the fluid velocity vector $\{V_x\ V_y\ V_z\}$. The term S_{mass} is a source term for creation or destruction of mass. This is used at some domain boundaries as an alternative to a standard boundary condition.

The time-averaged Navier Stokes equations for momentum transport are

$$\nabla \cdot (\rho \mathbf{V} \otimes \mathbf{V}) = \nabla\left(\mu_{eff}\left(\nabla \mathbf{V} + (\nabla \mathbf{V})^T\right)\right) - \nabla \mathbf{p} + \mathbf{B} + \mathbf{S}_{mom} \tag{2.2}$$

where ρ is the fluid density, p is the pressure, $\mathbf{B}$ is the body force vector representing buoyancy and $\mathbf{S}_{mom} = \{S_{mom_x}, S_{mom_y}, S_{mom_z}\}$ is a source term for creation and destruction of momentum. The effective viscosity, μ_{eff} is defined as

$$\mu_{eff} = \mu_o + \mu_t \tag{2.3}$$

where μ_o is the molecular viscosity and μ_t is the turbulent viscosity, which is defined in the turbulence model.

The temperature distribution is found by solving the energy equation

$$\nabla \cdot (\rho H \mathbf{V}) = \nabla \cdot (k_{eff} \nabla T) \tag{2.4}$$

where T is the temperature and where H is the total enthalpy, defined in terms of static enthalpy as

$$H = h + \frac{1}{2}|\mathbf{V} \cdot \mathbf{V}| \tag{2.5}$$

A constitutive equation is used to relate static enthalpy, h, to temperature and pressure. The static enthalpy is assumed to be

$$h = \int_0^T C_p(T')dT' - \int_0^{T_{ref}} C_p(T')dT' \tag{2.6}$$

where C_p is the specific heat, T' is a temporary variable for the integration, and T_{ref} is a reference temperature where static enthalpy is defined to be zero. The effective conductivity, k_{eff}, is defined as

$$k_{eff} = k_o + k_t \tag{2.7}$$

where k_o is the conductivity and k_t is the turbulent conductivity, which is defined as

$$k_t = \frac{C_p \mu_t}{\mathrm{Pr}_t} \tag{2.8}$$

where Pr_t is the turbulent Prandtl number constant.

The hydrostatic pressure is ignored in all equations. Therefore, pressure in the model is equal to the actual pressure less the hydrostatic pressure:

$$p = p_{tot} - \rho g z \tag{2.9}$$

In Cartesian coordinates, the tensor product is a rank two tensor defined as

$$(\mathbf{V}\otimes\mathbf{V}) = \begin{bmatrix} V_x V_x & V_x V_y & V_x V_z \\ V_y V_x & V_y V_y & V_y V_z \\ V_z V_x & V_z V_y & V_z V_z \end{bmatrix} \tag{2.10}$$

The vector gradient is defined as

$$\nabla\mathbf{V} = \left\{ \frac{\partial V_x}{\partial x} \quad \frac{\partial V_y}{\partial y} \quad \frac{\partial V_z}{\partial z} \right\} \tag{2.11}$$

$$\nabla^2\mathbf{V} = \left\{ \frac{\partial^2 V_x}{\partial x^2} \quad \frac{\partial^2 V_y}{\partial y^2} \quad \frac{\partial^2 V_z}{\partial z^2} \right\} \tag{2.12}$$

The vector divergence is defined as

$$\nabla\cdot\mathbf{V} = \frac{\partial V_x}{\partial x} + \frac{\partial V_y}{\partial y} + \frac{\partial V_z}{\partial z} \tag{2.13}$$

The divergence of a rank two tensor is defined as

$$\begin{aligned} \nabla\cdot(\mathbf{V}\otimes\mathbf{V}) = {} & \frac{\partial V_x}{\partial x}V_x + \frac{\partial V_x}{\partial x}V_y + \frac{\partial V_x}{\partial x}V_z \\ & + \frac{\partial V_y}{\partial y}V_x + \frac{\partial V_y}{\partial y}V_y + \frac{\partial V_y}{\partial y}V_z \\ & + \frac{\partial V_z}{\partial z}V_x + \frac{\partial V_z}{\partial z}V_y + \frac{\partial V_z}{\partial z}V_z \end{aligned} \tag{2.14}$$

The magnitude of a vector is defined as

$$|\mathbf{V}| = \sqrt{V_x^2 + V_y^2 + V_z^2} \tag{2.15}$$

The multiplication of two vectors in the source term equation is defined as

$$\mathbf{SV} = \{S_x V_x,\ S_y V_y,\ S_z V_z\} \tag{2.16}$$

2.2 Turbulence Models

To solve turbulent flows, viscosity is increased (by introducing the turbulent viscosity, μ_t) in the Navier-Stokes equations, so that relatively course grids can be used, and consequently only large scale turbulent eddies are simulated. The most commonly used model is the standard *K*-ε model. The Low *K*-ε model is a modification of the standard *K*-ε model. The Low *K*-ε model is supposed to extend the range of applicable Reynolds numbers to allow calculation of turbulent flows at Reynolds numbers in the additional range of 5,000 to 30,000.

2.2.1 The Standard K-ε model

The turbulent viscosity, μ_t, is calculated from the K and ε turbulence parameters:

$$\mu_t = C_\mu \rho \frac{K^2}{\varepsilon} \tag{2.17}$$

The turbulent viscosity depends on the turbulent kinetic energy, K, and its rate of dissipation, ε. The parameters are found by solving two transport equations:

$$\nabla \cdot (\rho K \mathbf{V}) = \nabla \cdot \left(\left(\mu + \frac{\mu_t}{\mathrm{Pr}_K} \right) \nabla K \right) + \Phi - \rho\varepsilon \tag{2.18}$$

$$\nabla \cdot (\rho \varepsilon \mathbf{V}) = \nabla \cdot \left(\left(\mu + \frac{\mu_t}{\mathrm{Pr}_\varepsilon} \right) \nabla \varepsilon \right) + C_1 \frac{\varepsilon}{K} \Phi + C_2 \rho \frac{\varepsilon^2}{K} \tag{2.19}$$

where the shear production, Φ, is defined by

$$\Phi = \mu_{eff} \nabla \mathbf{V} \cdot \left(\nabla \mathbf{V} + (\nabla \mathbf{V})^T \right) - \frac{2}{3} \nabla \cdot \mathbf{V} \left(\mu_{eff} \nabla \cdot \mathbf{V} + \rho K \right) \tag{2.20}$$

The transport equations also include the empirical constants C_1 and C_2.

2.2.2 The Low K-ε model

The turbulent viscosity, μ_t, is calculated from the K and ε turbulence parameters:

$$\mu_t = C_\mu F_\mu \rho \frac{K^2}{\varepsilon} \tag{2.21}$$

where the function F_μ is defined as

$$F_\mu = \exp\left(\frac{-3.4}{\left(1 + \mathrm{Re}_T / 50\right)^2} \right) \tag{2.22}$$

where the local turbulent Reynolds number is defined as

$$\mathrm{Re}_T = \frac{\rho K^2}{\mu \varepsilon} \tag{2.23}$$

The equations for the turbulent kinetic energy K and turbulence dissipation rate ε are:

$$\nabla \cdot (\rho K \mathbf{V}) = \nabla \cdot \left(\left(\mu + \frac{\mu_t}{\mathrm{Pr}_K} \right) \nabla K \right) + \Phi - F_3 - \rho\varepsilon \tag{2.24}$$

$$\nabla \cdot (\rho \varepsilon \mathbf{V}) = \nabla \cdot \left(\left(\mu + \frac{\mu_t}{\mathrm{Pr}_\varepsilon} \right) \nabla \varepsilon \right) + C_1 \frac{\varepsilon}{K} \Phi + C_2 F_2 \rho \frac{\varepsilon^2}{K} + F_4 \tag{2.25}$$

where the shear production, Φ is defined as

$$\Phi = \mu_t \nabla \mathbf{V} \cdot \left(\nabla \mathbf{V} + (\nabla \mathbf{V})^T \right) - \frac{2}{3} \nabla \cdot \mathbf{V} \left(\mu_t \nabla \cdot \mathbf{V} + \rho K \right) \tag{2.26}$$

and the functions F_2, F_3 and F_4 are defined as

$$F_2 = 1 - 0.3 \exp\left(-\mathrm{Re}_T^2 \right) \tag{2.27}$$

$$F_3 = 2\mu \left(\nabla K^{1/2} \right)^2 \tag{2.28}$$

$$F_4 = 2 \frac{\mu \mu_t}{\rho} \left(\nabla^2 \mathbf{V} \right)^2 \tag{2.29}$$

2.3 Multiphase Model

An Eulerian multiphase multi-fluid model is used to simulate the flow of gas bubbles in the liquid steel. Each phase has it's own velocity, K and ε fields. The pressure field is shared for the two phases. The velocity fields are coupled by an empirical inter-phase drag model, which handles the transfer of momentum between the phases.

2.3.1 Governing Equations

The governing equations for multiphase flow are based on the single phase governing equations. The two continuity equations become:

$$\nabla \cdot \mathbf{V}_{liq} = S_{mass_{liq}} \tag{2.30}$$

$$\nabla \cdot \mathbf{V}_{gas} = S_{mass_{gas}} \tag{2.31}$$

Each of the two sets of momentum equations is similar to those for single phase flow, with the exception that an extra tem for momentum transfer is present:

$$\begin{aligned} \nabla \cdot \left(f_{liq} \left(\rho_{liq} \mathbf{V}_{liq} \otimes \mathbf{V}_{liq} \right) \right) = \nabla \left(f_{liq} \mu_{eff} \left(\nabla \mathbf{V}_{liq} + \left(\nabla \mathbf{V}_{liq} \right)^T \right) \right) - \\ f_{liq} \nabla \mathbf{p} + c_{liq\ gas}^{(drag)} \left(\mathbf{V}_{gas} - \mathbf{V}_{liq} \right) + \mathbf{S}_{mom_{liq}} \end{aligned} \tag{2.32}$$

$$\begin{aligned} \nabla \cdot \left(f_{gas} \left(\rho_{gas} \mathbf{V}_{gas} \otimes \mathbf{V}_{gas} \right) \right) = \nabla \left(f_{gas} \mu_{eff} \left(\nabla \mathbf{V}_{gas} + \left(\nabla \mathbf{V}_{gas} \right)^T \right) \right) + \\ f_{gas} \left(\mathbf{B}_{gas} - \nabla \mathbf{p} \right) + c_{gas\ liq}^{(drag)} \left(\mathbf{V}_{liq} - \mathbf{V}_{gas} \right) + \mathbf{S}_{mom_{gas}} \end{aligned} \tag{2.33}$$

where f_{liq} and f_{gas} are the liquid volume fraction and the gas volume fraction, respectively. The inter-phase drag terms, $c_{liq\ gas}^{(drag)}$ and $c_{gas\ liq}^{(drag)}$ are defined in Equations 2.40 and 2.41.

The standard K-ε model is used to solve for the K and ε turbulence parameters in the liquid phase. The gas phase is assumed to be laminar. The transport equations for the liquid phase are

$$\nabla \cdot \left(f_{liq} \left(\rho_{liq} K_{liq} \mathbf{V}_{liq} \right) \right) = \nabla \cdot \left(f_{liq} \left(\mu_{liq} + \frac{\mu_{liq_t}}{\mathrm{Pr}_K} \right) \nabla K_{liq} \right) + f_{liq} \Phi_{liq} - f_{liq} \rho_{liq} \varepsilon_{liq} \tag{2.34}$$

$$\begin{aligned} \nabla \cdot \left(f_{liq} \left(\rho_{liq} \varepsilon_{liq} \mathbf{V}_{liq} \right) \right) = \nabla \cdot \left(f_{liq} \left(\mu_{liq} + \frac{\mu_{liq_t}}{\mathrm{Pr}_\varepsilon} \right) \nabla \varepsilon_{liq} \right) + C_1 f_{liq} \frac{\varepsilon_{liq}}{K_{liq}} \Phi_{liq} \\ + C_2 f_{liq} \rho_{liq} \frac{\varepsilon_{liq}^2}{K_{liq}} \end{aligned} \tag{2.35}$$

where the shear production, Φ_{liq} is defined as

$$\Phi_{liq} = \mu_{liq_{eff}} \nabla \mathbf{V}_{liq} \cdot \left(\nabla \mathbf{V}_{liq} + \left(\nabla \mathbf{V}_{liq} \right)^T \right) - \frac{2}{3} \nabla \cdot \mathbf{V}_{liq} \left(\mu_{liq_{eff}} \nabla \cdot \mathbf{V}_{liq} + \rho_{liq} K_{liq} \right) \tag{2.36}$$

The transport equations for the gas phase are

$$\nabla \cdot \left(f_{gas} \left(\rho_{gas} K_{gas} \mathbf{V}_{gas} \right) \right) = \nabla \cdot \left(f_{gas} \left(\mu_{gas} + \frac{\mu_{gas_t}}{\mathrm{Pr}_K} \right) \nabla K_{gas} \right) + f_{gas} \Phi_{gas} - f_{gas} \rho_{gas} \varepsilon_{gas} \tag{2.37}$$

$$\begin{aligned} \nabla \cdot \left(f_{gas} \left(\rho_{gas} \varepsilon_{gas} \mathbf{V}_{gas} \right) \right) = \nabla \cdot \left(f_{gas} \left(\mu_{gas} + \frac{\mu_{gas_t}}{\mathrm{Pr}_\varepsilon} \right) \nabla \varepsilon_{gas} \right) + C_1 f_{gas} \frac{\varepsilon_{gas}}{K_{gas}} \Phi_{gas} \\ + C_2 f_{gas} \rho_{gas} \frac{\varepsilon_{gas}^2}{K_{gas}} \end{aligned} \tag{2.38}$$

where the shear production, Φ_{gas} is defined as

$$\Phi_{gas} = \mu_{gas_{eff}} \nabla \mathbf{V}_{gas} \cdot \left(\nabla \mathbf{V}_{gas} + \left(\nabla \mathbf{V}_{gas} \right)^T \right) - \frac{2}{3} \nabla \cdot \mathbf{V}_{gas} \left(\mu_{gas_{eff}} \nabla \cdot \mathbf{V}_{gas} + \rho_{gas} K_{gas} \right) \tag{2.39}$$

2.3.2 Inter-Phase Drag Model

The inter-phase drag terms $c_{liq\ gas}^{(drag)}$ and $c_{gas\ liq}^{(drag)}$ are defined as

$$c_{liq\ gas}^{(drag)} = \frac{3}{4} \frac{C_D}{d} f_{gas} \rho_{liq} \left| \mathbf{V}_{gas} - \mathbf{V}_{liq} \right| \tag{2.40}$$

$$c_{gas\ liq}^{(drag)} = \frac{3}{4} \frac{C_D}{d} f_{liq} \rho_{gas} \left| \mathbf{V}_{liq} - \mathbf{V}_{gas} \right| \tag{2.41}$$

The drag coefficient, C_D is a function of the bubble Reynolds number Re_b:

$$\mathrm{Re}_b = \frac{\rho_{liq}\left|\mathbf{V}_{liq} - \mathbf{V}_{gas}\right| d}{\mu_{o_{liq}}} \tag{2.42}$$

The function $C_D(\mathrm{Re}_b)$ is determined experimentally, and is known as the drag curve. In our case, the bubbles move closely with the liquid, and the bubble Reynolds number is about 125 for a 1 mm bubble. For $0 \le \mathrm{Re}_b \le 1000$, the drag curve is in the Allen regime:

$$C_D = \frac{24}{\mathrm{Re}_b}\left(1 + 0.15\,\mathrm{Re}_b^{0.687}\right) \tag{2.43}$$

2.3.3 Buoyancy

Because there is a large difference in density between liquid steel and argon gas, buoyancy is important in the flow calculation of the gas phase. The buoyancy force is what causes most of the gas to leave the domain through the top surface instead of getting trapped in the solidifying steel.

The buoyancy force is introduced into the momentum equation as the body force, **B**:

$$\mathbf{B}_{gas} = \left(\rho_{liq} - \rho_{gas}\right)\mathbf{g} \tag{2.44}$$

where **g** is the gravity vector {0, 0, 9.8}. The Boussinesq approximation is employed, whereby gas compressibility and thermal effects on ρ are ignored.

2.4 Boundary Conditions

Boundary conditions must be set for each variable at every boundary on the domain. The following boundary conditions are used except when noted in the individual model descriptions.

2.4.1 Wall Boundary Conditions for Turbulent Flow

The walls in the domain correspond to the solidification interface between the liquid and the solid shell in the caster. The velocity at this wall is given a no-slip condition (i.e. $V_x=V_y=V_z=0$). The velocity profile in the boundary layer is either solved for numerically or calculated with a wall law, depending on the turbulence model used. In heat transfer

calculations, the temperature of the wall is set to the liquidus temperature of steel [13]. This avoids having to specify a variable heat flux boundary condition along the walls. Pressure is given a zero-normal gradient boundary condition. The turbulence parameters at the wall are calculated by a turbulence model, described next.

Standard K-ε model

The boundary condition for velocity is specified using wall laws in the standard K-ε model. Wall laws calculate the high gradients of velocity in the boundary layer region using an empirical correlation based on the shear stress at the wall. This allows a coarse mesh to be used and still include the behavior in the boundary layer. The non-dimensional distance normal to the wall, y^+, is defined as

$$y^+ = \frac{\left(\rho^2 C_\mu^{1/2} K\right)^{1/2}}{\mu} n \tag{2.45}$$

where *n* is distance normal to the wall. The tangential velocity profile as a function of y^+ is

$$V_t = \begin{cases} -\left(C_\mu K\right)^{1/2} y^+, & for \;\; y^+ < y_o^+ \\ \dfrac{-\left(C_\mu K\right)^{1/2}}{\kappa} \log\left(E y^+\right), & for \;\; y^+ \geq y_o^+ \end{cases} \tag{2.46}$$

where V_t is the velocity tangential to the wall, *E* is the constant log-layer thickness, κ is the Von-Karmen constant and y_o^+ is the cross over point between the viscous sub-layer and the logarithmic region.

The turbulence kinetic energy *K* is solved in the control volume adjacent to the wall using Equations 2.18. The production terms in the K equation are treated differently so that only quantities interior to the flow and the specified boundary conditions on velocity. The turbulence dissipation is calculated from K using the relation [15]:

$$\varepsilon_{\left(y^+=0\right)} = \frac{C_\mu^{3/4} K^{3/2}}{\kappa \; n} \tag{2.47}$$

The boundary conditions for heat transfer calculations are similar to the velocity boundary conditions.

The enthalpy in the wall layer is assumed to be

$$H = \begin{cases} \dfrac{\mathrm{Pr}_H E_H y^+ \left(\dfrac{\partial H}{\partial n}\right)_{y^+=0}}{\rho C_\mu^{1/4} K^{1/2}}, & for\ y^+ \le y_H^+ \\ \dfrac{\dfrac{\mathrm{Pr}_t}{\kappa}\log\left(E_H y^+\right)\left(\dfrac{\partial H}{\partial n}\right)_{y^+=0}}{\rho C_\mu^{1/4} K^{1/2}}, & for\ y^+ > y_H^+ \end{cases} \tag{2.48}$$

where y_H^+ is the cross over point between the viscous sub-layer and the logarithmic region for enthalpy, and E_H is the formula of Jayatilleke

$$E_H = E\exp\left[9.0\kappa\left(\left(\frac{\mathrm{Pr}}{\mathrm{Pr}_H}\right)^{0.75} - 1\right)\left(1 + 0.28\exp\left(-0.007\frac{\mathrm{Pr}}{\mathrm{Pr}_H}\right)\right)\right] \tag{2.49}$$

where Pr is the fluid Prandtl number ($C_p\mu_o/k_o$) and Pr_H is the Prandtl number for enthalpy [15].

Low K-ε model

The low Reynolds number version of the K-ε model solves the governing equations to the wall, and does not use wall laws. A no-slip boundary condition is set on velocity (i.e. $V_x = V_y = V_z = 0$), and zero values are set for K and ε. The heat transfer boundary conditions are the same as those for the standard K-ε model.

2.4.2 Top Surface Boundary Condition

The top surface is modeled as a wall with no-slip velocity boundary conditions. This was chosen over a zero shear stress condition because previous work [16] revealed that the shear stress imposed from the viscous molten flux layer that floats on the top surface is very large. A convective boundary condition is set for temperature.

2.4.3 Inlet Boundary Condition

At the inlet boundary, constant values for all variables except pressure are specified. Pressure is extrapolated from the outlet boundary. The inlet velocity is derived from the imposed casting speed V_c using a mass balance:

$$V_i = V_c A_m / A_n \tag{2.50}$$

where V_i is the inlet velocity normal to the inlet, A_m is the cross-sectional area of the mold exit and A_n is the cross-sectional area of the inlet boundary.

Inlet values for K and ε must also be specified. In models that include the nozzle geometry in the domain, the inlet values of K and ε at the top of the nozzle are assigned average values calculated from a mixing-length model for turbulent pipe flow [14, 17, 18]. When the nozzle geometry is not included in the domain (such as in the multiphase parametric study) the values of K and ε at the inlet are set to the average calculated values at the nozzle port outlet obtained from simulations of flow in the nozzle [19].

2.4.4 Outlet Boundary Condition

A pressure boundary condition is used for the mold outlet boundary. This choice was made over other possible boundary conditions, such as a specified mass flow boundary, because previous work showed that the pressure boundary condition can handle outlets where flow is not fully developed better than the mass flow boundary can [20]. A constant pressure of zero (an arbitrary reference value) is specified for the mold outlet boundary at the bottom of the domain. Zero normal gradients are applied to all other variables.

2.4.5 Symmetry Boundary Condition

At planes of symmetry, the velocity component normal to the boundary is set to zero. For all other variables, including pressure, zero normal gradient boundary conditions are specified.

2.5 Solution Method

A multi-block, body-fitted coordinate numerical grid was used to allow for complex domain geometry. The governing equations are discretized and solved using the commercial finite difference program CFX 4.2 by AEA Technologies. Iteration is used at

two levels: an inner iteration that solves for the spatial coupling for each variable, and an outer variable that solves for the spatial coupling between variables [15]. The inner iteration was run with an under-relaxation factor between $\beta = 0.3$ and $\beta = 0.7$ for each equation, where $\beta = 1.0$ would be no under-relaxation (successive substitution). The inner iterations are run for each equation in the following order: U momentum, V momentum, W momentum, pressure, volume fraction, K, ε and enthalpy. The Full Field Stone's Method linear solver is used to solve for the momentum, volume fraction and enthalpy equations. The Preconditioned Conjugate Gradients solver is used to solve the pressure equation. The K and ε equations are solved using the Line Relaxation solver [15].

The source term *S* is used in the multiphase model and the model accounting for shell growth to specify non-standard boundary conditions for the multiphase models. The source term is expressed mathematically for one control volume as

$$S_{mass} = \sum_{m} A_m \left(\phi_p - \phi_m \right) = S_{mass_u} + S_{mass_p} \phi_p \tag{2.51}$$

$$\mathbf{S}_{mom} = \sum_{m} A_m \left(\phi_p - \phi_m \right) = \mathbf{S}_{mom_u} + \mathbf{S}_{mom_p} \phi_p \tag{2.52}$$

where the summation m is over the six neighboring cells of the control volume *p* [15]. In this equation A_m contains the off-diagonal terms of the coefficient matrix ϕ is the variable in the equation that the source term is applied to, S_p is the contribution of the source terms to the diagonal terms in the coefficient matrix and S_u contains the off-diagonal source terms.

In the multiphase model, the Inter-Phase Slip Algorithm of Spalding [15] is used to solve the coupled equations. Because the gas phase is specified at the boundaries using source terms, CFX does not automatically know that there is a second phase present. Therefore, a gas volume fraction of 1E-6 % is specified at the inlet so that CFX recognizes that the problem is multiphase and applies the correct equations and gas parameters to the problem.

CFX allows a solution run to use the results of a previous run as an initial condition. For instance, a fluid flow solution can be run and used as the initial condition for a heat transfer calculation. This allows for rapid changes in the solution parameters without

having to solve the flow solution from a zero initial condition. For most cases, the solver is run for 2000 to 4000 iterations to achieve a converged flow solution. Residuals of less than 1E-4 where found to be sufficient for this work. Additional models are then added, such as heat transfer or multiphase flow, and the solver is restarted using the flow calculation as the initial condition. A typical convergence history, measured by the absolute residuals of each equation being solved, is shown in Figure 2.1. This run is for a 20% gas multiphase calculation (Case 17), and shows only the residuals for the liquid phase. The gas phase residuals are similar to the liquid phase residuals in last 1000 iterations. The first 2000 iterations are for the single phase flow solution (Case 16). When the solver is restarted for the multiphase calculation, the residuals rise during the first few iterations. The solution quickly converges to a maximum residual level of 1E-4 within 1000 iterations, opposed to the 2000 or more iterations that would be necessary for convergence if the solution was started without the single phase initial condition.

For turbulent flow, a common problem is rapid divergence, where the residuals suddenly increase to extremely large numbers and the solver crashes. This problem is usually due to the cross-diffusion terms in the *K* and ε equations [15]. The cross diffusion terms are the terms in the K transport equation (Equation 2.18) that contain ε, and the terms in the ε equation (Equation 2.19) that contain K. This behavior can be prevented by under-relaxing these terms, which is referred to as deferred correction in CFX. It was found that turning off these terms until the last 200 iterations ($\beta = 0$) and then linearly increasing them to the full value ($\beta = 1$) by the last iteration resulted in faster convergence and with no decrease in the accuracy of the solution. On a Cray Origin 2000, running on a single processor, the single phase calculation took 3 hours per 1000 iterations. The multiphase calculation took 7 hours per 1000 iterations.

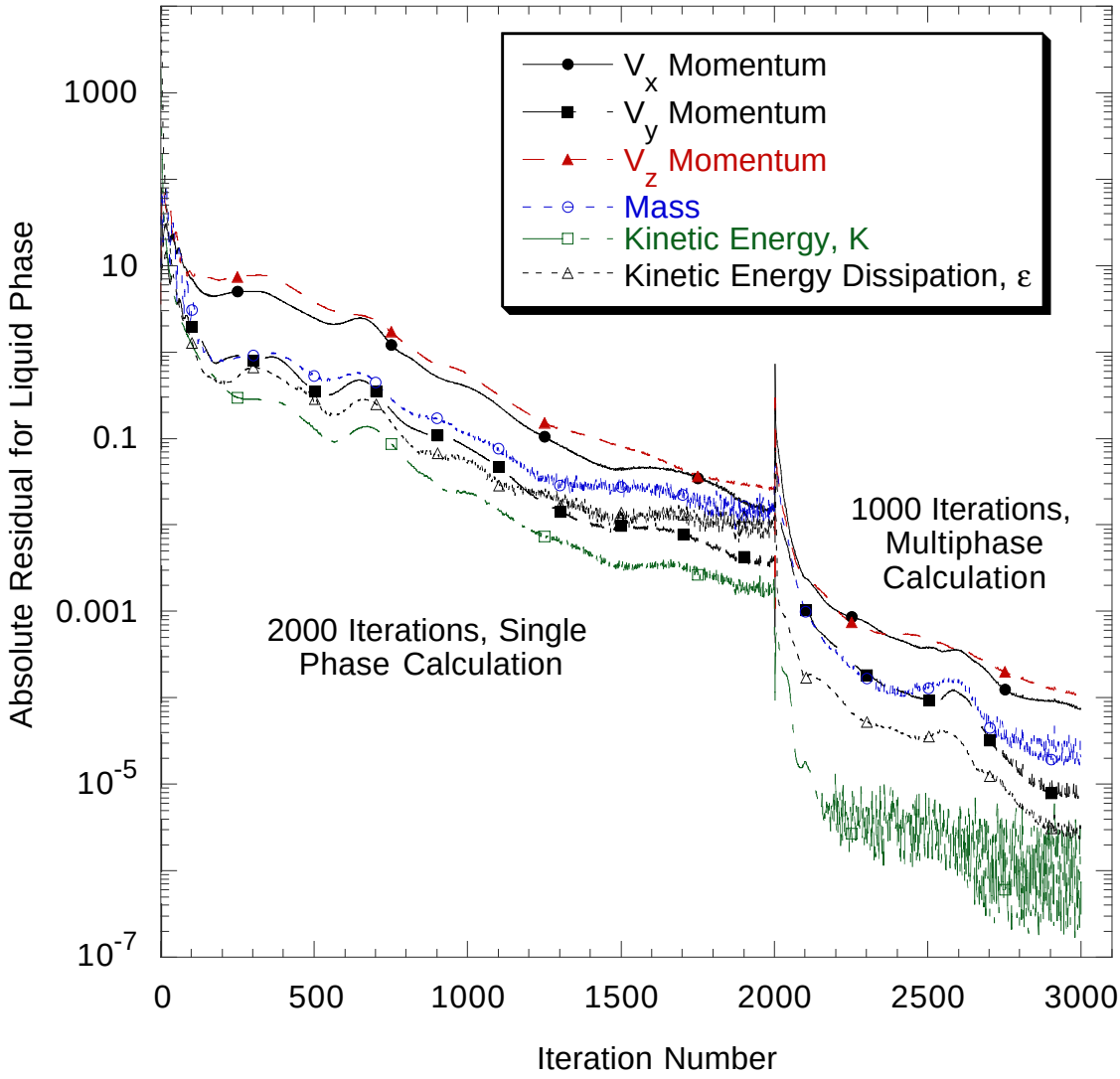

Figure 2.1. Convergence History for Typical Multiphase Solution (Cases 16 and 17)

3 Evaluation of Turbulence Models

Flow in a continuous casting mold has several features that make heat transfer calculations difficult. The flow has a high speed jet impinging against the domain wall. Most wall laws in the standard K-ε model have difficulty in accurately modeling flow that is not parallel to the flow boundary. Liquid steel is also a fluid with a low Prandtl number. There is little work in the literature on jet impingement for low Prandtl number fluids.

The shell thickness of actual breakout shells from a thin-slab caster has been measured [1]. The model predictions of wall heat flux are used as input to CON1D, a program that predicts the growth of the shell [21]. The predicted shell profiles are compared to the experimental measurements. This validation is used to compare different turbulence models and grid resolutions.

The model domain is shown in Figure 3.1. The model is based on the thin-slab caster used at Armco Steel from which the breakout shells were obtained. The nozzle is a 3-Port design, with two ports angled 15° downward from the horizontal and one port directly downwards into the mold. The nozzle geometry is included in the model because the nozzle is highly three-dimensional. The simulation exploits symmetry by modeling a quarter of the mold and nozzle.

3.1 Model Cases

In this study, flow and heat transfer predictions are compared for several different grid resolutions and wall laws using both the Standard K-ε and Low K-ε turbulence models. Heat transfer predictions from several different simulations using the Low K-ε model are compared for various grid resolutions. The grid resolutions are expressed in terms of the non-dimensional size of the cell near the wall, y^+_{cell}, which is defined as

$$y^+_{cell} = \frac{\left(\rho^2 C_\mu^{1/2} K\right)^{1/2}}{\mu} \Delta y \tag{3.1}$$

where Δy is the thickness of the first element along the wall. Five cases using different turbulence models, wall laws and grid resolutions were compared.

3.1.1 Standard K-ε Model Cases

Simulations were run for the standard K-ε model with a coarse grid (y^+=30) containing 294,317 nodes and 236,669 elements. The standard enthalpy wall law is used (see section 2.4.1).

The same coarse grid is run with the standard K-ε model, except that the wall law for enthalpy is replaced with a user wall law. This wall law is derived in Appendix A, and is implemented as a user Fortran subroutine, which is provided in Appendix B.

3.1.2 Low K-ε Model Cases

Simulations were run for coarse (y^+<30), fine (y^+<6) and very fine (y^+<1) grids using the Low K-ε model. The fine (y^+<6) grid contains 549,728 nodes and 509,153 elements, and the very fine (y^+<1) contains 843,607 nodes and 791,634 elements.

3.2 Solution Methodology

The simulation was first run without heat transfer for 4000 iterations to generate a converged flow solution such that the largest of the momentum residuals, R, is smaller than 1E-4 for the momentum equations. Then, another 500 iterations were run with the heat transfer model to generate a temperature solution. To eliminate sudden divergence in the solution the cross-diffusion term for the K and ε equations were deferred, and increased from 0% to 100% in the last 100 iterations of the solution.

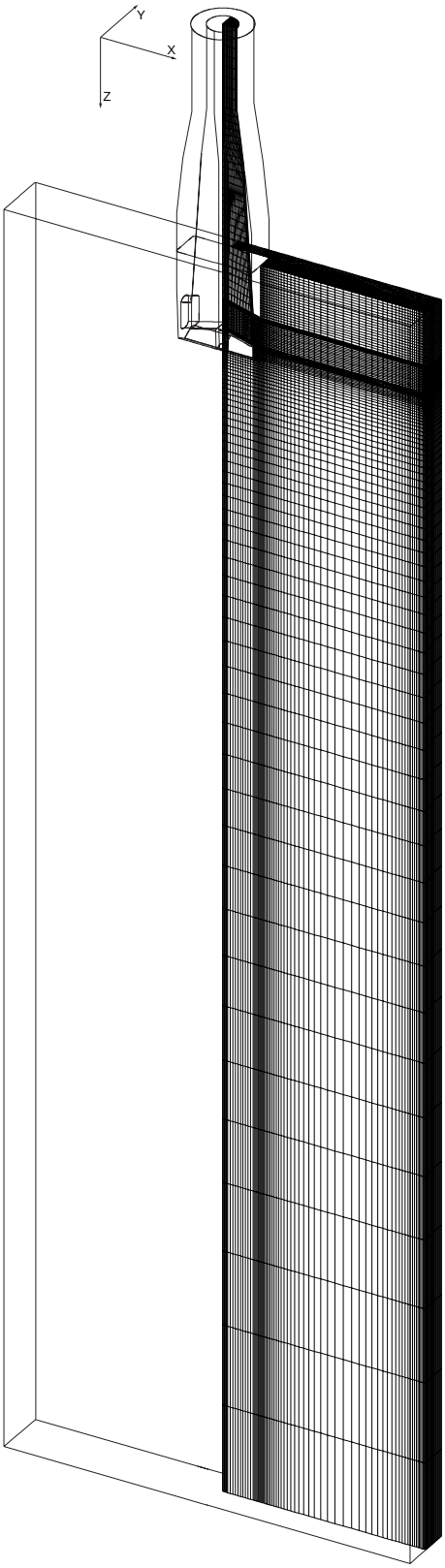

Figure 3.1. Turbulence Model Evaluation Domain

3.3 Turbulence Model Results

The flow and heat transfer solutions produced by the models are used to compare the different turbulence models. The heat transfer solutions is correlated to a shell thickness and compared by Stone [1] to experimental measurements. The simulation parameters for the cases compared are listed in Table 3.1.

3.3.1 Velocity Solution

Figure 3.2 shows profiles of downward velocity at the solidifying shell normal to the narrow face wall, 0.741 mm below the steel-flux interface at the top surface of the domain. The results for four different flow solutions are compared. Each point on the graph represents a grid point, so this figure also illustrates the great differences in mesh refinement between the grids. The dashed line for the Standard K-ε model illustrates the wall function solution for velocity assumed in this model.

This high-speed flow system is known (through experiments and computational models) to develop a high velocity gradient near the wall. The standard and Low K-ε model with the fine and very fine grids predict this high velocity gradient. The Low K-ε model with the coarse grid predicts a much lower velocity gradient. The unrealistic result illustrates the inaccuracy in the flow prediction that can result from using a coarse mesh with the Low K-ε model. Because the Low K-ε model does not use wall laws, a fine mesh should be used to resolve the boundary layer. The standard wall law is able to capture the steep gradient even with the coarse mesh.

Figure 3.6 shows the turbulent viscosity for the standard K-ε using the user specified wall law. The viscosity is scaled as μ_t/μ_o, so this plot shows how the turbulence model increases viscosity to account for turbulence.

3.3.2 Heat Transfer Solution

The heat transfer prediction is much more sensitive to the turbulence model and grid size than is the flow prediction. The CFX implementation of the standard K-ε model wall laws, including the wall law for enthalpy, is compared to user-subroutine form of the same equations. The models are compared in Table 3.2 using the total heat flux and the peak heat flux along the narrow face centerline. The total heat removed along the narrow face was integrated along the centerline of the narrow face. Figure 3.4 shows the centerplane temperature predictions for each turbulence model. The corresponding wall heat flux profiles are shown in Figure 3.5. The size of the hot area (light shades) shows how much heat is removed from the jet by the walls. The standard K-ε model (a) has the largest hot area, consistent with the prediction that only 680 kW/m is removed along the narrow face centerline for this model. The User subroutine and Low K-ε models have much smaller hot areas, corresponding with a larger amount of heat removed by the wall. The coarse grid Low K-ε model (e) has the coldest fluid (largest dark area) and corresponding highest heat flux of 1490 kW/m.

The K-ε model with user wall law delivers 17% more heat to the wall than the standard K-ε model. The Low K-ε models with $y^+<30$ and $y^+<6$ grids delivers considerably more heat to the wall than the user-modified K-ε model. The total heat delivered to the wall by the Low K-ε model with $y^+<1$ grid is comparable to the user-modified K-ε model.

The peak of the heat flux profile occurs at the jet impingement point in all cases, as expected. The standard K-ε model has a heat flux peak of 720 kW/m^2 at this point, while the user modified K-ε model has a peak of 1400 kW/m^2. The Low K-ε models all have extremely high and narrow peaks, which do not appear to be realistic. The Low K-ε model is very sensitive to grid refinement, and produces unreliable results at coarse grid sizes of $y^+=30$. The Low K-ε model for the $y^+=30$ grid predicts the total heat flux at the narrow face mold wall to be 85% greater than the user–modified K-ε model, and the peak heat flux at the jet impingement point to be 240% greater. For the $y^+=6$ grid the total and peak heat flux are 25% greater and 240% greater, respectively.

The heat flux predicted by Low K-ε model with the $y^+<1$ grid and the user–modified K-ε model differ mainly by the shape of the heat flux peak in the impingement region. The total heat flux is 10% greater than for the user–modified K-ε model. The peak for the Low K-ε model is approximately 80 mm wide, while the peak for the standard K-ε model is approximately 250 mm wide. It is not known which shape is correct, but it is suspected that the user–modified K-ε model prediction is better. In real life, the jet moves between several steady flow patterns, spreading out the region where heat is delivered. Thus, the sharp heat flux peak predicted by the Low K-ε model appears to be unrealistic.

The heat transfer predictions of the different models were input by Stone to a solidification model [1, 22] and the predicted shell growth was compared with experimental measurements obtained from a shell obtained from an operating caster [22]. The user-subroutine K-ε model prediction matched the experimental data well. The standard K-ε model would over-predict shell growth and miss the important shell thinning effect that was observed at the impingement point. The Low K-ε model with $y^+<30$ would significantly under-predict shell growth.

Table 3.1. Simulation Parameters for Armco Heat Transfer Model

Mold Width	984 *mm*
Mold Thickness	132 *mm*
Mold Cross-sectional Area, A_m	129888 mm^2
Nozzle Cross-sectional Area, A_n	3848 mm^2
Nozzle Submergence Depth	265 *mm*
Nozzle Port Angle, α	15° down
Caster Domain Modeled	1/4 Mold
Numerical Grid, Maximum y^+ at Wall	30, 6, 1
Casting Speed, V_c	25.4 *mm/s*
Inlet Velocity, V_x,V_y	0
Inlet Velocity, V_z	0.857 *m/s*
Inlet Turbulent Kinetic Energy, K_o	0.00425 m^2/s^2
Inlet Dissipation Rate, ε_o	0.020 m^2/s^3
Steel Density, ρ	7020 kg/m^3
Laminar Conductivity, k_o	26 $kg\text{-}m/s^3\text{-}K$
Specific Heat, C_p	680 $m^2/s^2\text{-}K$
Laminar (Molecular) Viscosity, μ_o	0.0056 *kg/m s*
Turbulence Model	Standard K-ε, Low K-ε
Inlet Casting Temperature, T_o	1836 *K*
Liquidus Temperature, T_{liq}	1775 *K*
Top Surface Heat Transfer Coefficient, h	40 W/m^2K
Top Surface Ambient Temperature, T_∞	300 *K*

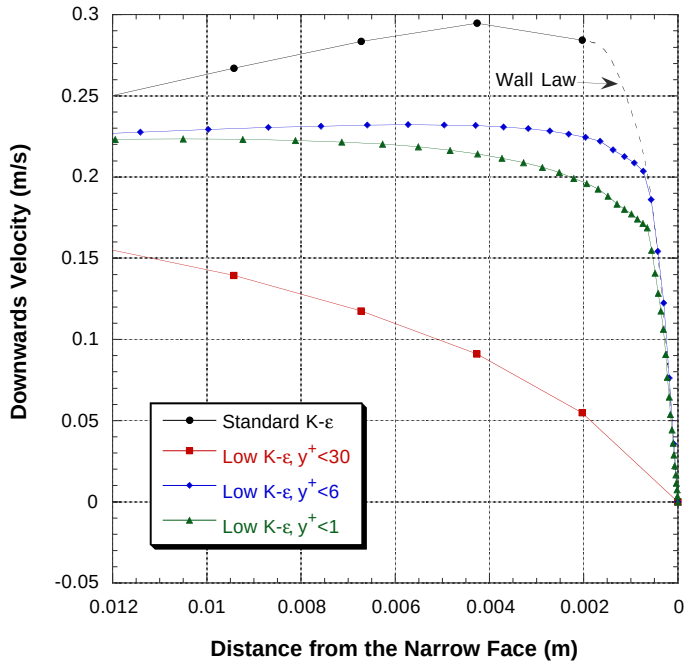

Figure 3.2. Wall velocity profiles at 0.741 m below the meniscus on the Centerplane Parallel to the Wide Face.

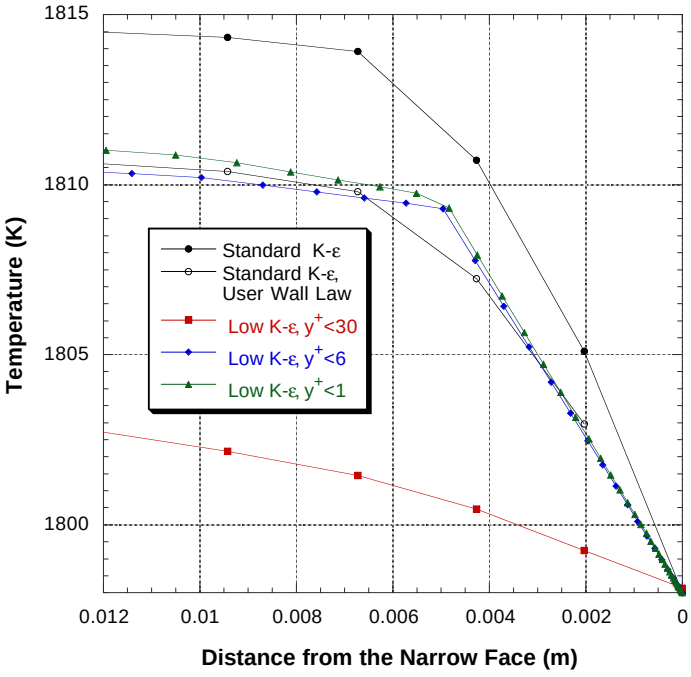

Figure 3.3. Wall temperature profiles at 0.741 m below the meniscus on the Centerplane Parallel to the Wide Face.

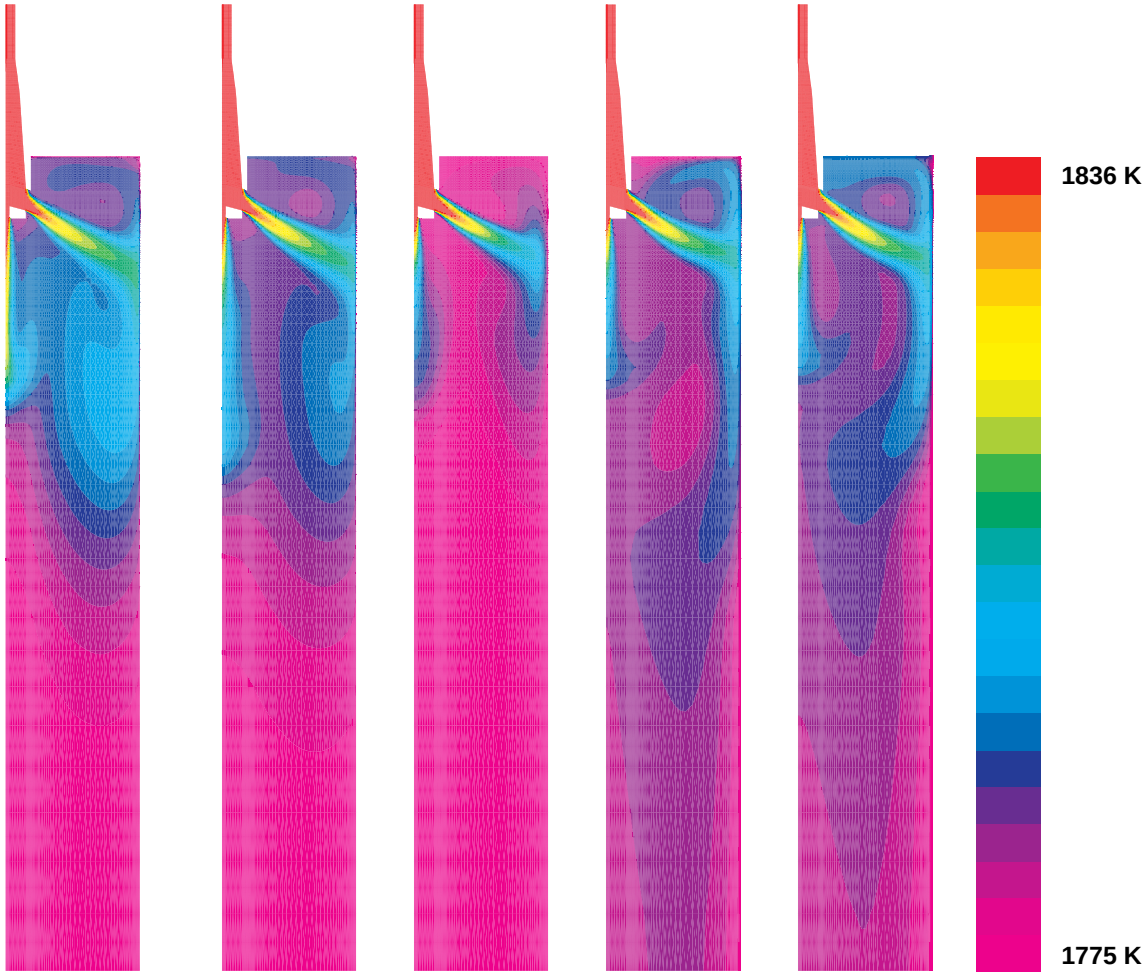

Figure 3.4. Temperature predictions for a) Standard K-ε model, b) User K-ε model, c) Low K-ε model with $y^+<30$, d) Low K-ε model with $y^+<6$ and e) Low K-ε model with $y^+<1$ grid.

Table 3.2. Integrated and Peak Wall Heat Flux at the Solidifying Shell

Turbulence Model, Grid Size, and Wall Law	Total Heat Flux (kW/m)	Peak Heat Flux (kW/m^2)
High K-ε Turbulence Model, $y^+<30$	680.3	720
High K-ε Turbulence Model, $y^+<30$, Fortran Wall Law	798.9	1400
Low K-ε Turbulence Model, $y^+<30$	1490.1	4808
Low K-ε Turbulence Model, $y^+<6$	996.5	4832
Low K-ε Turbulence Model, $y^+<1$	901.2	3837

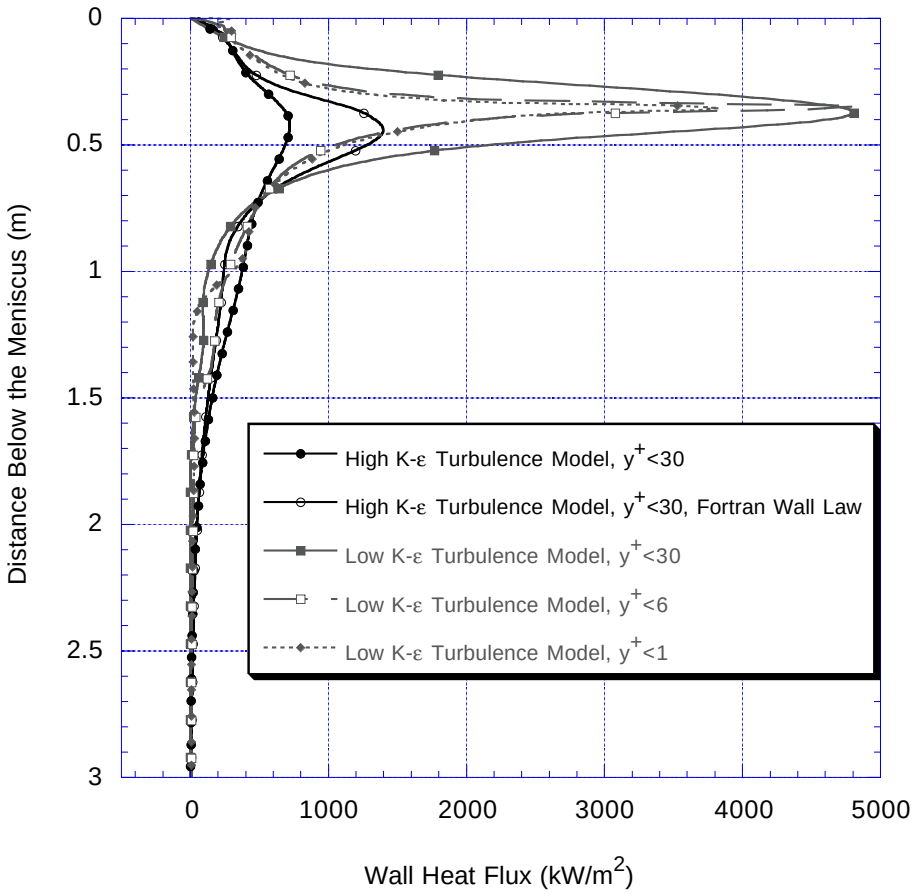

Figure 3.5. Profiles of wall heat flux at the solidifying shell

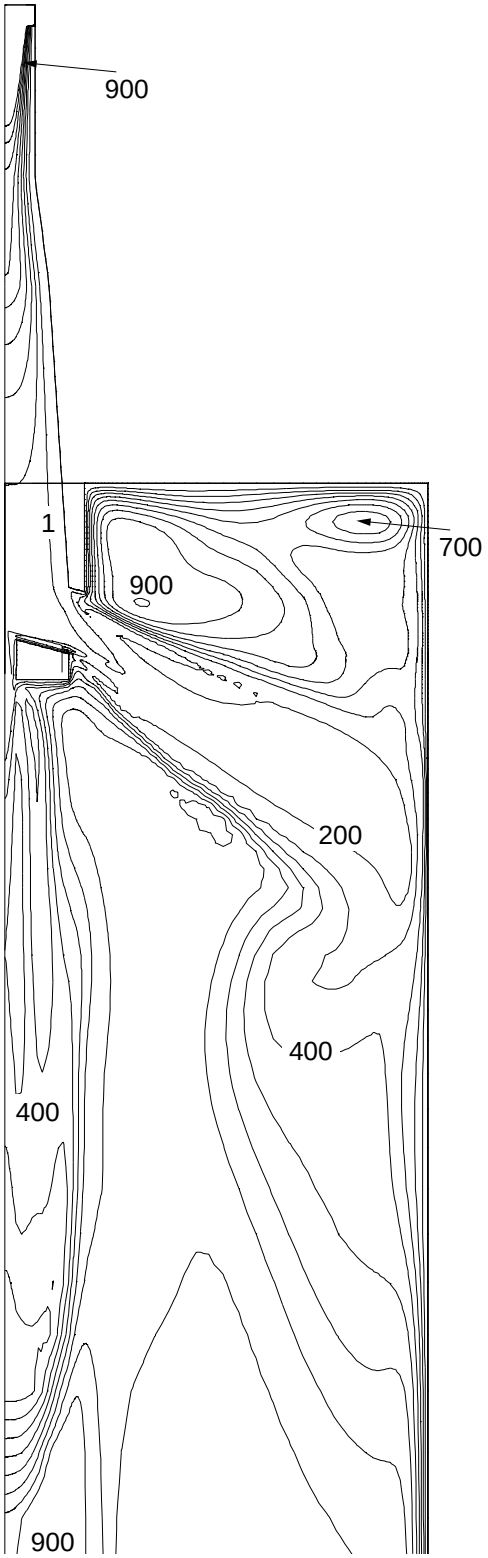

Figure 3.6. Non-dimensional Turbulent Viscosity, μ_{eff}/μ_o.
Standard K-ε model with User Wall Law

4 Effect of the Shell on Fluid Flow

In the continuous casting process, the liquid steel solidifies against the cooled mold. This steel shell is then pulled from the mold at a constant rate. At steady state, the location of the solidification front is constant with respect to a laboratory frame of reference. As the shell is pulled from the mold, new fluid has to cross the solidification front in order to fulfill the mass balance. In both the present work and in some physical water models of the process, the solidification front is the domain boundary. Thus, there should be a small flow across the model walls that represent the shell boundary. The importance of this effect is investigated in this chapter.

In water models of fluid flow in the mold, the presence of the solidifying shell is assumed to have negligible effect on the flow result. The assumption that the shell can be neglected allows for simplification of the model. To determine the importance of this assumption on the resulting flow field, the results from three different models were compared. In all of these models, only flow in the liquid pool is considered.

The geometry for this model is based on the geometry used in the Turbulence Model Evaluations Chapter. This geometry was used because it is an extreme case; the effects of the shell are large relative to standard molds. Two domains are compared: the Standard domain with straight walls, and the Shell domain with walls that include the curvature of the shell.

4.1 Model Cases

Three cases are compared. The Standard Conditions case models the strand as if there was no solid shell. This is what is commonly done in most water models and several previous computational models. The Solid Shell case models the mold with a tapering curved wall, so that only the liquid pool is in the domain and the shell is accounted for using a geometrically accurate domain. This case corresponds to a water model that includes the shell in the geometry but does not remove liquid through the walls. The Porous Shell case models the mold with the shell in the geometry and includes negative mass source and negative momentum source terms to remove fluid and momentum at the

boundary without interfering with the wall laws. This case is the closest approximation to the actual flow in the mold.

4.1.1 Standard Conditions.

The Standard Conditions case is identical to the High K-ε case of turbulence models comparison, with the exception that heat transfer is not modeled. The solid shell is treated as liquid. The domain is unmodified (same as actual caster), and no mass or momentum is removed at the domain walls.

4.1.2 Solid Shell

In the Solid Shell case, the domain walls are modified to include the curvature of the liquid domain due to the solid shell. The shape of the shell is built into the geometry (except for Oscillation marks and variations in shell thickness related to heat transfer, which are ignored). The shell thickness is calculated using Equation 4.3. No mass is removed at the domain walls.

4.1.3 Porous Shell

The Porous Shell model treats the solidifying shell as a fixed interface with the appropriate amount of fluid crossing it. Negative mass and momentum sources on the domain walls simulate the steel that moves across the shell interface as the shell is pulled from the mold. The shape of the shell is built into the geometry (except for Oscillation marks and variations in shell thickness related to heat transfer, which are ignored). The shell thickness is calculated using Equation 4.3. The mass and momentum sources are derived in the next section.

In the caster, liquid steel solidifies in the solid shell and is pulled from the mold. When the shell geometry is included in the domain, the mass that is pulled out with the shell must be accounted for. To do this, the boundary condition on the walls is modified with the source term in the governing equations so that fluid is removed through the wall. The source term for the continuity equation is

$$S_{mass_p} = -\dot{m}(z) \tag{4.1}$$

The variable $\dot{m}(z)$ is the mass flux across the shell interface as a function of distance below the top surface. For the momentum equations, the source term is

$$\mathbf{S}_{mom_p} = -\dot{m}(z)\mathbf{V} \tag{4.2}$$

Calculation of Wall Mass-Flux for Porous Shell Case

Because the curvature of the shell varies as a function of distance below the top surface the mass flux $\dot{m}$ will also vary with distance below the surface. A schematic of an increment of the solid shell is shown in Figure 4.1.

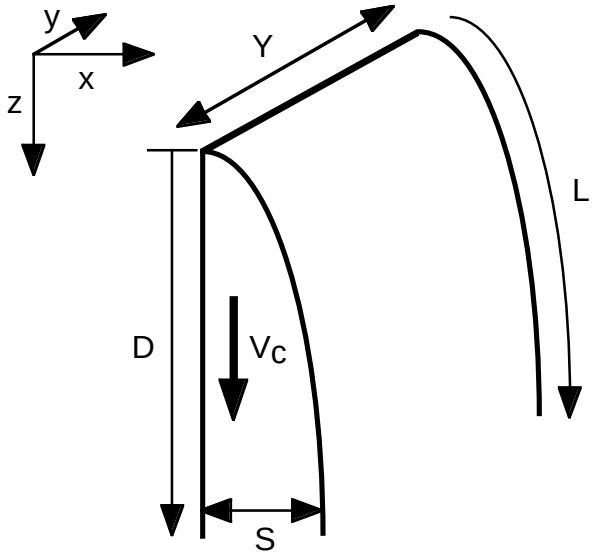

Figure 4.1. Schematic of Shell

The thickness of the solidifying shell, *S*, can be expressed as a function of distance down the strand (below the meniscus), *D*, by:

$$S(D) = C\sqrt{D/V_c} \tag{4.3}$$

Where C is an empirical constant for the shell growth rate and V_c is the casting speed [23].

The mass flux across the solidification interface can be written as a function of *D*. The mass flux across an arbitrary cell face on the solidification interface of the shell is

$$\dot{m}_i = \rho A_i V_N \tag{4.4}$$

where ρ is the density of steel, A_i is the area of the cell face and V_N is the normal velocity across the interface.

To express the normal velocity V_N in terms of the casting speed V_c, an increment of the shell is examined, as shown in Figure 4.2.

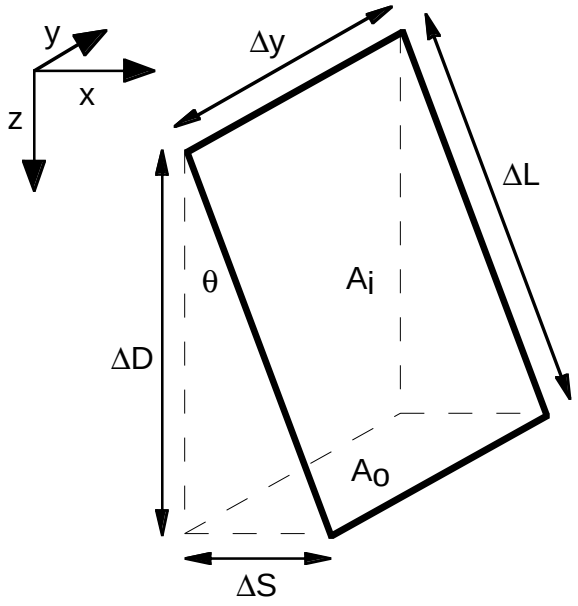

Figure 4.2. Incremental Shell Section

$$\Delta S = \Delta D \tan\theta \tag{4.5}$$

$$A_o = \Delta D \tan\theta \Delta y \tag{4.6}$$

$$A_i = \frac{\Delta D \Delta y}{\cos\theta} \tag{4.7}$$

$$A_o = \Delta D \tan\theta \Delta y \tag{4.8}$$

Performing a mass balance on this section reveals that the mass flux into area A_i must equal the mass flux out of area A_o:

$$\dot{m}_i = \dot{m}_o \tag{4.9}$$

$$\rho V_N A_i = \rho V_C A_o \tag{4.10}$$

$$\rho V_N \frac{\Delta D \Delta y}{\cos\theta} = \rho V_C \Delta D \tan\theta \Delta y \tag{4.11}$$

By rearranging Equation 4.11, the normal velocity can be rewritten in terms of the casting speed

$$\begin{aligned} V_N &= V_C \tan\theta \cos\theta \\ &= V_C \sin\theta \end{aligned} \tag{4.12}$$

V_N can be written as a function of distance D only. Sin θ can be written as:

$$\sin\theta = \frac{\Delta D}{\sqrt{\Delta D^2 + \Delta S^2}} \approx \frac{dD}{\sqrt{dD^2 + dS^2}} = \frac{1}{\sqrt{1 + \left(\frac{dS}{dD}\right)^2}} \tag{4.13}$$

Taking the derivative of *S(D)* in Equation 4.3 gives

$$\frac{dS}{dD} = \frac{C}{2\sqrt{V_C D}} \tag{4.14}$$

Substituting Equation 4.14 into Equation 4.13 yields sin θ as a function of D:

$$\sin\theta = \frac{1}{\sqrt{1 + \left(\frac{C}{2\sqrt{V_C D}}\right)^2}} \tag{4.15}$$

Substituting Equation 4.15 into Equation 4.12, the equation for normal velocity, gives:

$$V_N = \frac{V_C}{\sqrt{1 + \left(\frac{C}{2\sqrt{V_C D}}\right)^2}} \tag{4.16}$$

From Equation 4.4, the mass flux can now be rewritten as a function of D only:

$$\dot{m}(D) = \frac{\rho A_i V_C}{\sqrt{1 + \left(\frac{C}{2\sqrt{V_C D}}\right)^2}} \tag{4.17}$$

For a curved strand, the distance down the shell, D, is a not a simple function of vertical distance, but also depends on the radius of curvature, R:

$$D = \frac{\theta z}{\sin\theta} = \theta R \tag{4.18}$$

$$D = R \arcsin\left(\frac{z}{R}\right) \tag{4.19}$$

For a radius R of 11 meters, at z=3 meters D is 3.0385 meters. Therefore, the curved strand does not have a significant effect on the distance D, and the coordinate z can be used in the finite difference equations for the mass flux term for both curved and straight-mold casters.

$$\dot{m}(z) = \frac{\rho A_i V_C}{\sqrt{1+\left(\frac{C}{2\sqrt{V_C z}}\right)^2}} \tag{4.20}$$

The casting speed is positive, so the mass flux term is a positive number. Because the source term is defined as the negative mass flux, the source is a negative source, or "sink" that removes mass from the liquid domain

4.2 Solution Methodology

Typically, 4000 iterations were performed for the each simulation in order to produce a converged solution. The results of the No Shell model can not be used as an initial condition for the Solid and Porous Shell models because the domains are different, and the results do not directly apply on a node by node basis. It was also found that using the Solid Shell solution as an initial condition for the Porous Shell model produced slower convergence than starting the Porous Shell model from zero initial conditions. This is because the velocity solutions of the two models vary significantly because of the acceleration of flow in the Solid Shell model. To eliminate sudden divergence in the solution the cross-diffusion term for the K and ε equations were deferred, and increased from 0% to 100% in the last 100 iterations of the solution.

4.3 Results

Flow results were obtained for each of the three cases to study the effect of each method of treating the shell on mold flow. The simulation parameters for each case are listed in Table 4.1.

Velocity profiles at different regions in the domain are shown in Figure 4.4 through Figure 4.9. In Figure 4.4, at 1 m below the meniscus, the velocity profiles for the three cases are fairly similar. There is a very sharp boundary layer (10 mm) along the shell, which is characteristic of high-speed flow. At 2 m below the meniscus, Figure 4.5, the velocity profile for the Solid Shell case is significantly higher than the profiles for the No Shell and Porous Shell cases. The maximum velocities near the shell are very similar for the No Shell and Porous Shell cases. At 3 m below the meniscus, Figure 4.6, the velocity

profile for the Solid Shell case is more than double the magnitude of the profiles for the other cases. This shows that a model with the shell included in the domain that does not have a sink will accelerate the flow through the outlet. A water model that includes the shape of the shell will have this problem. This is especially important deeper in the caster, and for thin slab casters, where the shell is a large section of the cross section. For the Solid Shell case, this acceleration increases the average outlet velocity by 134%. The boundary layer at this depth is much wider (70 mm) because the flow near the wall is much slower than in the top of the domain.

The velocity solution at the centerplane, 1 mm inside the wide face, 1 mm inside the narrow face and 1 mm below the top surface is shown in Figure 4.10 for the No Shell case. Because the wide face and narrow face in the Solid and Porous Shell cases are curved, velocity solutions for these locations are plotted on a plane tangential to the wall at 0.3 m below the top surface. The velocity solution is shown in Figure 4.11 for the Solid Shell case and Figure 4.12 for the Porous Shell case. In the upper region of the domain, the flow pattern of the Solid Shell case is closest to the Porous Shell Case. The influence of the porous shell is to reduce the magnitude of small vortexes and eddies near the shell, particularly near the meniscus.

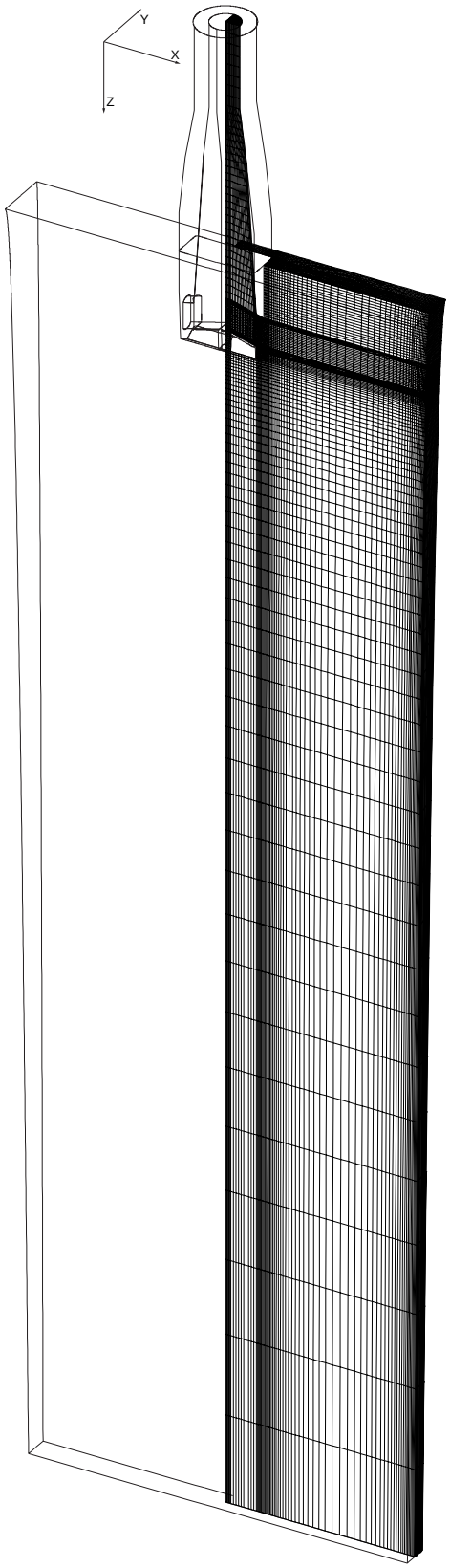

Figure 4.3. Geometry of Porous and Solid Shell Cases

Table 4.1. Standard Model Parameters

Mold Width	984 *mm*
Mold Thickness	132 *mm*
Nozzle Submergence Depth	265 *mm*
Nozzle Angle, α	15° down
Jet Height	56 *mm*
Jet Width	16 *mm*
Jet Angle	40° down
Shell Growth Constant, C	3.27912 $mm/\sqrt{s}$
Caster Domain Modeled	1/4 Mold
Numerical Grid, Maximum y^+ at Wall	30
Casting Speed, V_c	25.4 *mm/s*
Inlet Velocity, V_z	0.857 *m/s*
Inlet Turbulent Kinetic Energy, K_o	0.0035 m^2/s^2
Inlet Dissipation Rate, ε_o	0.020 m^2/s^3
Steel Density, ρ	7020 kg/m^3
Laminar (Molecular) Viscosity, μ_o	0.0056 *kg/m s*
Turbulence Models	Standard K-ε, Low K-ε

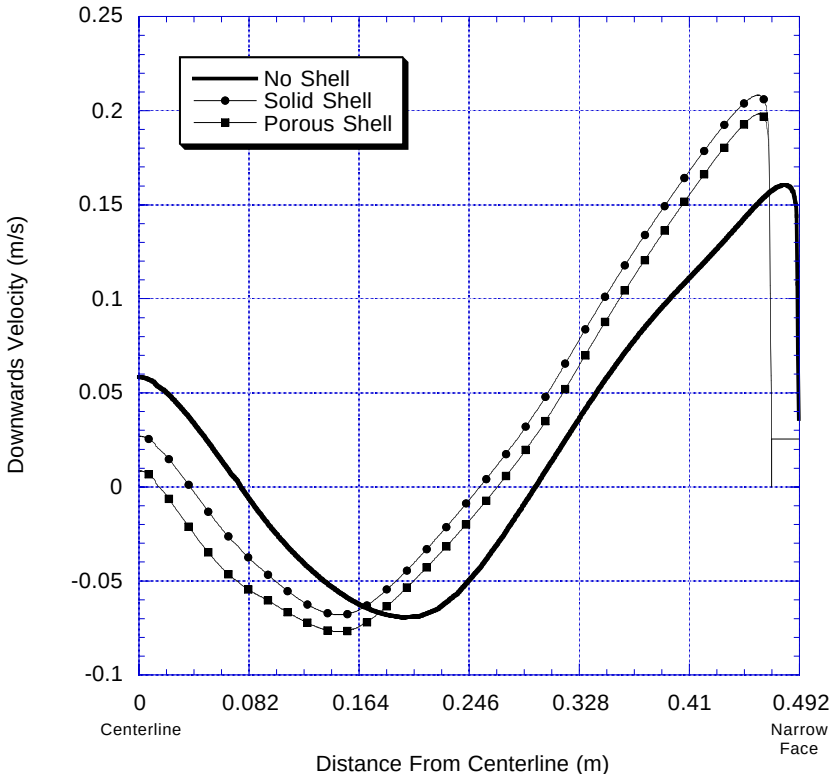

Figure 4.4. Velocity Comparison at 1 m Below Meniscus, 66 mm from Wide Face.

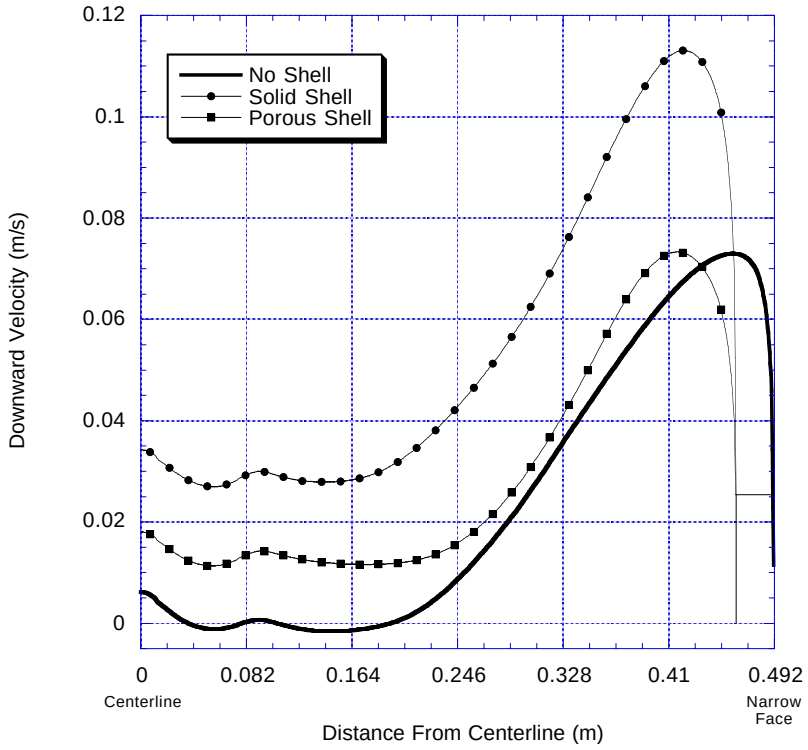

Figure 4.5. Velocity Comparison at 2 m Below Meniscus, 66 mm from Wide Face.

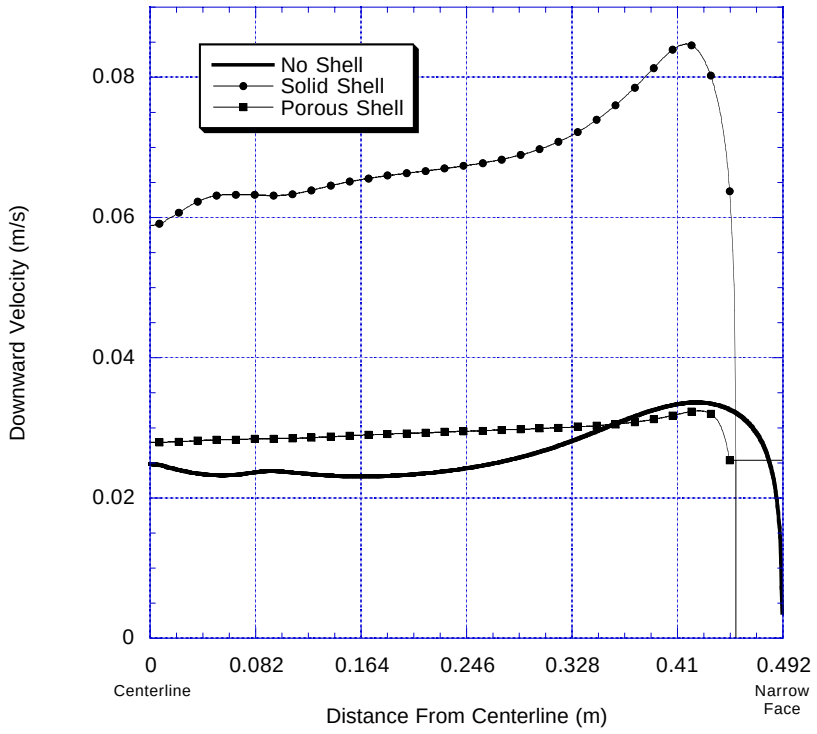

Figure 4.6. Velocity Comparison at 3 m Below Meniscus, 66 mm from Wide Face.

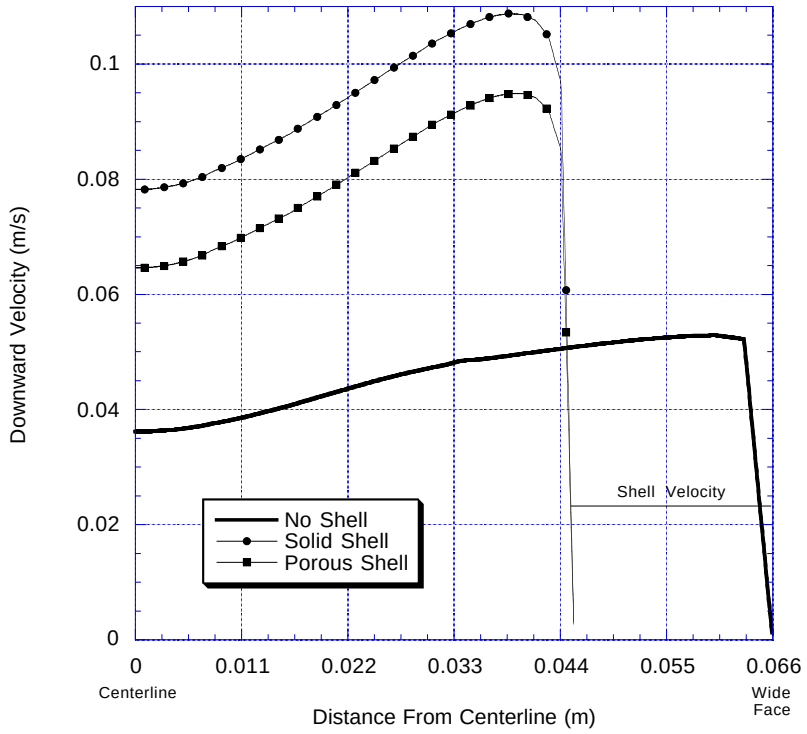

Figure 4.7. Velocity Comparison at 1 m Below Meniscus, 164 mm from Narrow Face.

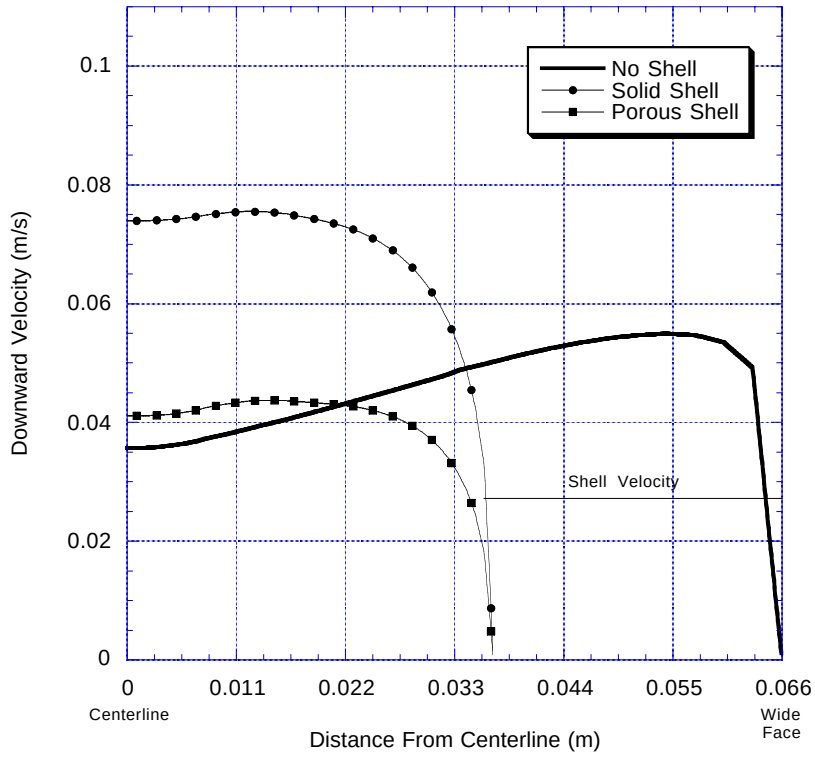

Figure 4.8. Velocity Comparison at 2 m Below Meniscus, 164 mm from Narrow Face.

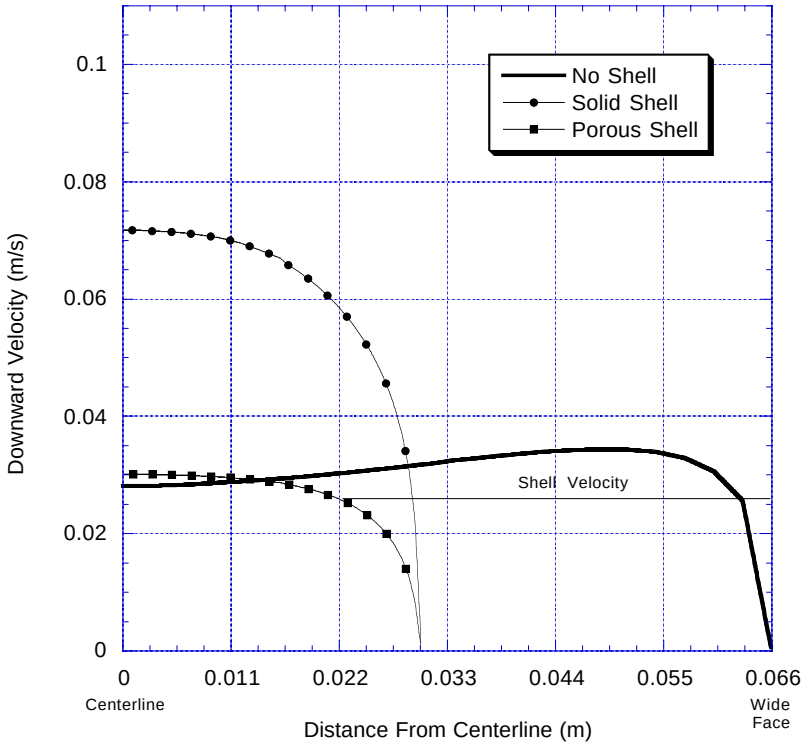

Figure 4.9. Velocity Comparison at 3 m Below Meniscus, 164 mm from Narrow Face.

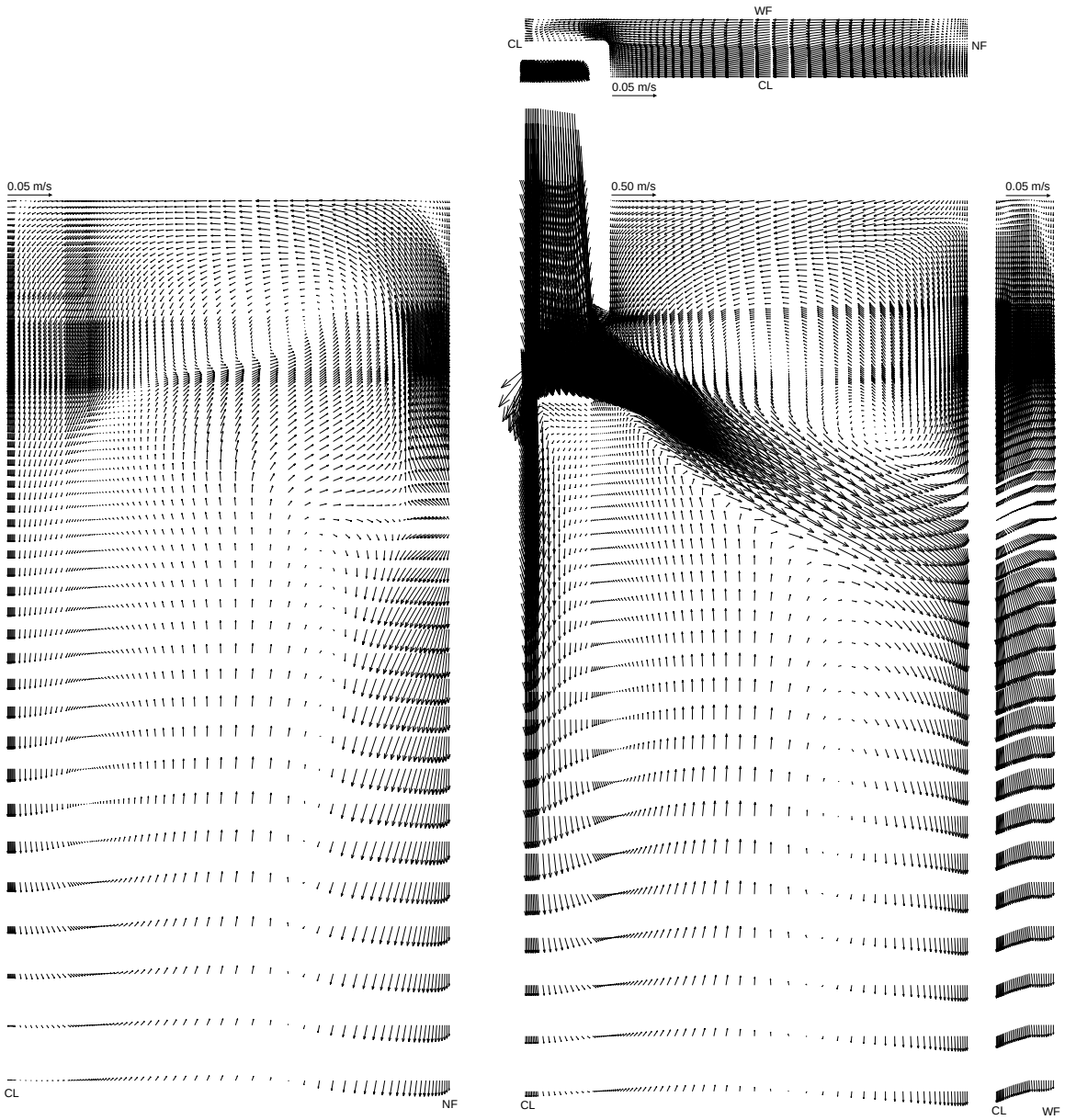

Figure 4.10. No Shell. Centerplane (center), Wide Face (left), Narrow Face (right) and Top Surface (top) Velocity.

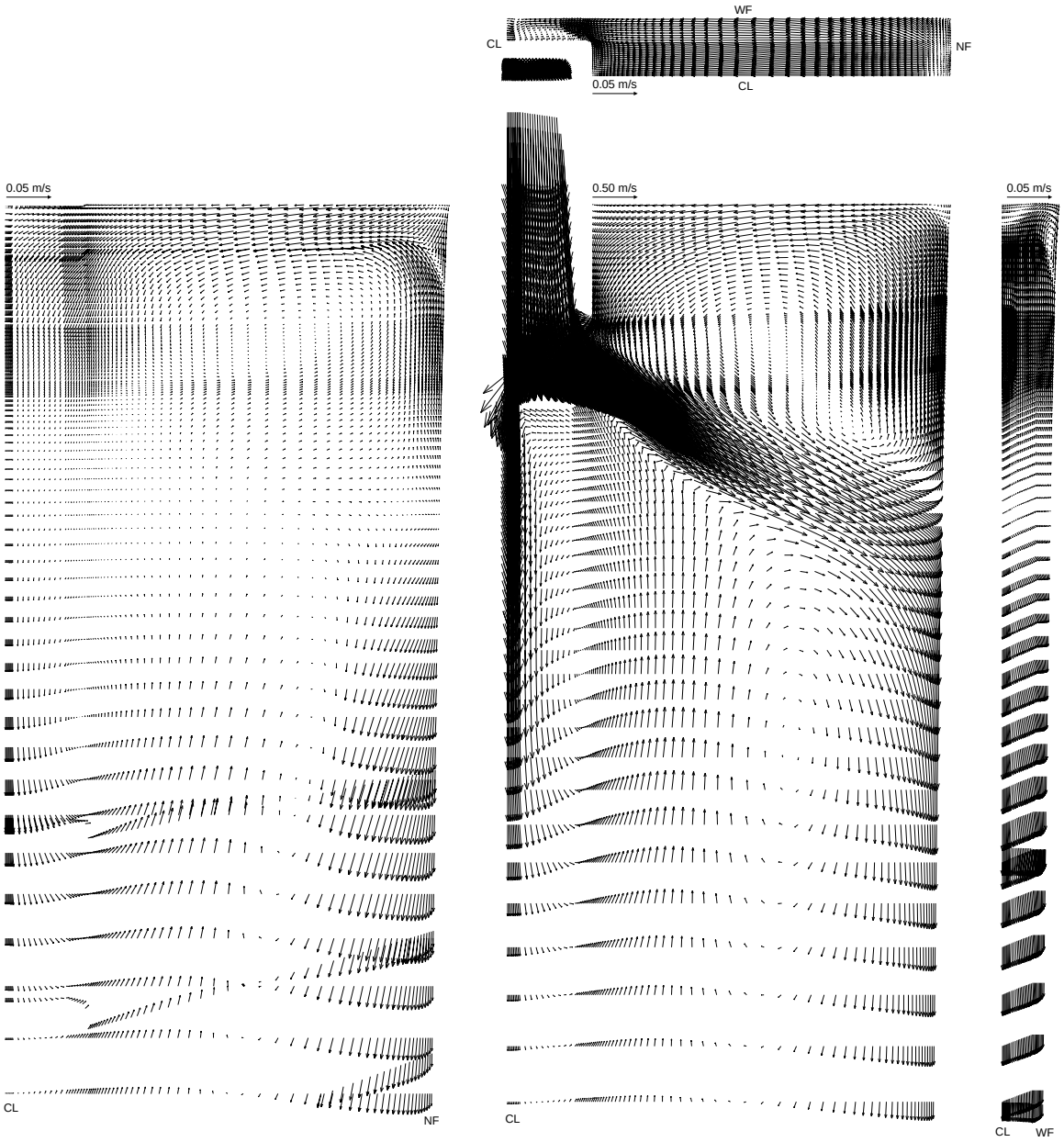

Figure 4.11. Solid Shell. Centerplane (center), Wide Face (left), Narrow Face (right) and Top Surface (top) Velocity.

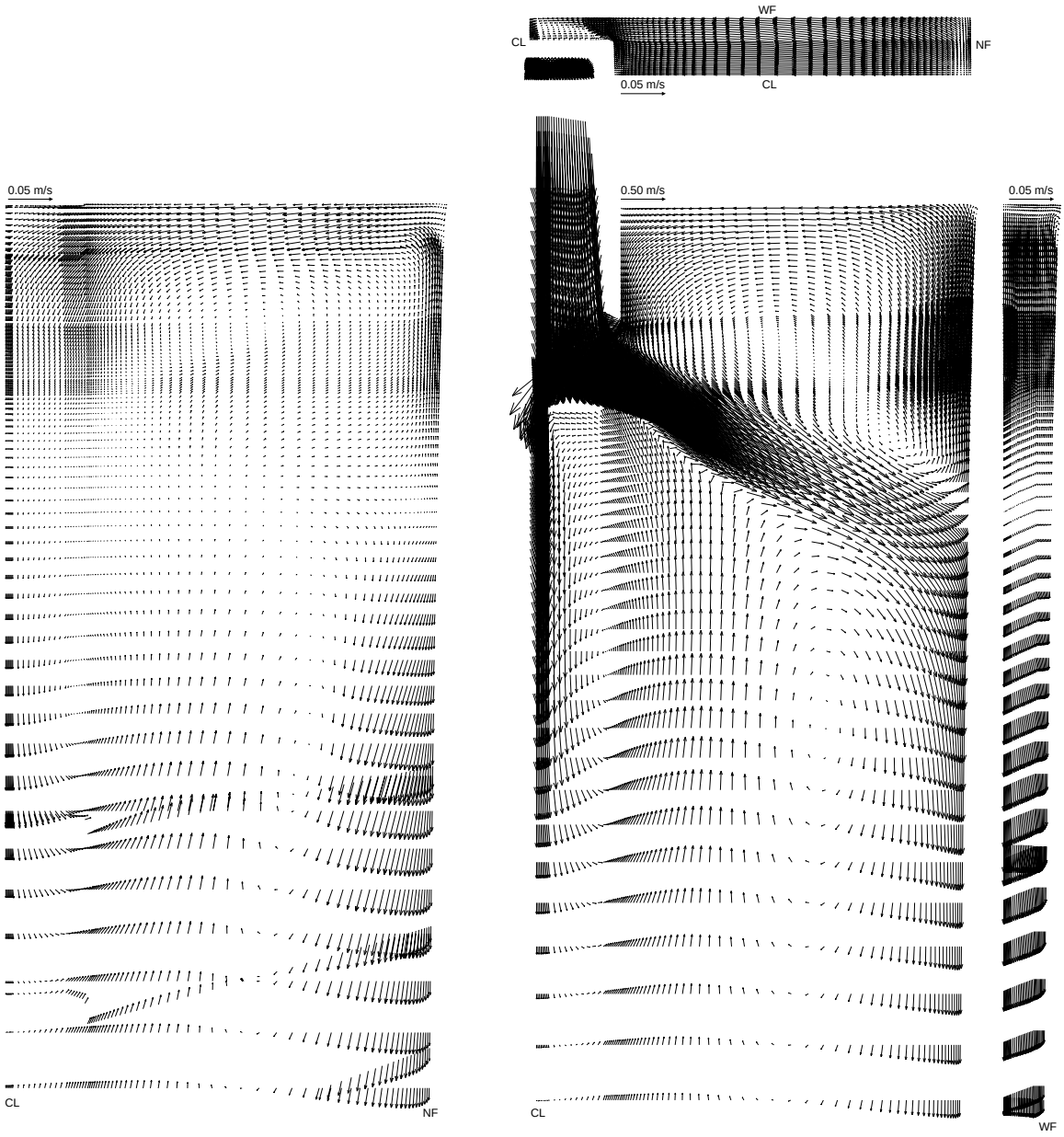

Figure 4.12. Porous Shell. Centerplane (center), Wide Face (left), Narrow Face (right) and Top Surface (top) Velocity.

5 Multiphase Mold Flow Model

Argon gas is injected into the nozzle during casting to prevent clogging. Because of their buoyancy, the bubbles can significantly change the flow pattern in the mold. Bubbles can also be trapped in the solidifying shell. The effect that the gas has on the casting process is dependent on several other parameters, such as bubble diameter, casting speed, submergence depth, and mold width. A study comparing the numerical results and experimental results is performed to validate the multiphase model used. In Chapter 6 a parametric study is performed to determine how these casting parameters affect the casting process.

5.1 Simulation Conditions

The domain for the Standard Conditions case is shown in Figure 5.1. A quarter domain is used, so no asymmetric flow effects are studied. There is no strand or mold curvature included in the domain. The nozzle is modeled as an inlet with appropriate average flow and turbulence quantities.

Input conditions for the validation case are listed in Table 5.1. Input conditions for the parametric study are listed in Table 6.1. The jet of steel leaving the nozzle port is modeled as an inlet boundary with appropriate smaller size and constant flow parameters (V_x, V_y, V_z, K, ε and f). The inlet velocity is defined as the average velocity leaving the nozzle ports, and the width and height of the inlet jet are chosen to represent the actual size of the jet leaving the nozzle ports. The actual port dimensions are larger than the inlet dimensions because in most nozzles the area of the port is not completely filled by the jet. The actual nozzle dimensions represented by these inlet dimensions are estimated from previous calculations [14] and included in Table 6.1. The normal component of the inlet velocity is calculated from a mass balance on the casting speed:

$$V_{normal} = V_c \frac{Area\ \ of\ \ Inlet}{Area\ \ of\ \ Domain\ \ Outlet} \tag{5.1}$$

The tangential velocity is calculated from the normal velocity and the jet angle:

$$V_{tangential} = V_{normal}(\tan\alpha) \tag{5.2}$$

In the parametric study, the 1.60 m width case has the same casting speed as standard conditions. To maintain this casting speed in a larger mold, the inlet velocity must be increased by the ratio of the cross sectional mold areas. The inlet values for K and ε are calculated in a previous model of flow in a nozzle [19]. The gas volume fraction is calculated from the gas mass flow rate using Equation 5.5. The bubble diameter is the size of the gas bubbles injected into the domain. In a real caster, there will be a range of bubble sizes, but in this model only a constant bubble size is modeled per case. The standard K-e model is used to solve for the turbulence parameters. The numerical grid size is measured by the non-dimensional cell size at the wall.

5.2 Boundary Conditions

Due to buoyant forces, the argon gas bubbles tend to float towards the top surface and out of the domain through the flux layers instead of leaving the domain through the outlet with the liquid steel. Source terms are used to set the boundary conditions on the gas phase at the inlet and the top surface because of limitations in CFX on the types of boundary conditions that can be set.

5.2.1 Inlet Boundary Condition

Both liquid steel and argon gas enter the domain at the inlet. A constant velocity boundary condition is specified for the steel phase. The argon phase cannot be specified in this manner due to limitations in CFX. Specifically, the gas phase cannot be injected into the domain using an inlet boundary, because CFX would force this flow to go out the domain bottom (pressure boundary outlet) with the liquid phase. The gas phase is instead injected into the domain using a mass source at the inlet boundary. For the gas continuity equation, Equation 2.1, the source term is

$$S_{p_{gas}} = \dot{m}_{gas} \tag{5.3}$$

where $\dot{m}_{gas}$ is the mass flux of the injected gas.

The source term for the gas momentum equation, Equation 2.2, is

$$\mathbf{S}_{p_{gas}} = \dot{m}_{gas}\mathbf{V}_{gas} \tag{5.4}$$

where $\mathbf{V}_{gas}$ is the velocity of the injected gas, which is assumed to be equal to the inlet velocity of the liquid phase.

The gas is specified in terms of the volume fraction of gas compared to liquid at the inlet. This volume fraction is calculated at the casting temperature. Because the gas density is much lower at the casting temperature than at standard temperature and pressure (STP), a gas volume fraction measured at the casting temperature and pressure will be much larger than for the same mass flow rate when measured at STP. The gas fraction is calculated in terms of the gas mass flow rate (which is the value used in the source term) as

$$f_{gas} = \frac{\frac{\dot{m}_{gas}}{\rho_{gas_{inlet}}}}{V_{x_{liq}} A_{inlet} + \frac{\dot{m}_{gas}}{\rho_{gas_{inlet}}}} \tag{5.5}$$

where $V_{x_{liq}}$ is the normal liquid velocity through the inlet, A_{inlet} is the area of the inlet, and $\rho_{gas_{inlet}}$ is the density of the gas at the hot inlet temperature. At standard temperature and pressure (STP), the density of argon gas is 1.61 kg/m^3. As the inlet, the gas density $\rho_{gas_{inlet}}$ is calculated to be 0.322 kg/m^3, or one fifth of the density at STP [24].

Hershey performed a three dimensional model of a nozzle and validated this model with experiments [25]. Najjar used this validation as a basis for a parametric study on nozzle design [14]. He presents outlet turbulence values for a variety of nozzle designs. These turbulence values K_o and ε_o used as the inlet boundary conditions in this model were taken from a nozzle calculated in Najjar's study that had similar jet characteristics to standard conditions.

5.2.2 Top Surface Boundary Condition

The appropriate amount of the gas phase is removed from the top surface of the domain using a negative source term. The top surface is treated as a wall for the liquid steel phase. For the volume fraction equation, the source is

$$S_{p_{gas}} = \rho_{gas} A V_{z_{gas}} \tag{5.6}$$

where A is the area of the control volume at which the source is being applied to and $V_{z_{gas}}$ is the downwards component of velocity in the control volumes adjacent to the top surface. Because the gas velocity at the top surface is actually upwards, $V_{z_{gas}}$ is a negative quantity. This makes $S_{p_{gas}}$ a negative source that removes any gas that physically crosses the top interface.

For the continuity and momentum equations, the source is

$$S_{p_{gas}} = f_{gas}\rho_{gas}A \times \max\left(V_{z_{gas}}, 0\right) \tag{5.7}$$

where f_{gas} is the volume fraction of the argon phase, ρ_{gas} is the density of the argon phase, A is the area of the control volume at which the source is being applied to and $V_{z_{gas}}$ is the downwards component of velocity in the control volume.

5.3 Solution Methodology

Single phase (0% gas) solutions for each case were calculated and used as an initial condition for the multiphase simulation. To eliminate sudden divergence in the solution the cross-diffusion term for the K and ε equations were deferred, and slowly increased at the last 100 iterations of the solution. Typically, 2000 iterations were performed for the single phase simulation, and another 1000 iterations were needed for the multiphase simulation to get the residual down to the same level.

5.4 Validation

To determine that the gas injection and gas removal conditions are valid, the fluid flow solution is compared to experimental measurements found in the literature [26]. The simulation parameters for the validation case are listed in Table 5.1. Two cases are modeled: Case A with a casting speed of 1.1 *m/min*, and Case B with a casting speed of 0.6 *m/min*. The mass flow rate of gas is held constant for each case. This results in a different gas volume fraction for each casting speed modeled. The domain is similar to the domain shown in Figure 5.1, with the exception that the mold is very wide.

The single phase flow pattern for Case A, shown in Figure 5.2, is a typical casting flow pattern known as double roll flow. When gas is added to the flow, the impingement of the jet moves up. Figure 5.3a shows multiphase flow results predicted by the model. The predicted flow pattern matches quite well with the experimental measurements shown in Figure 5.3b.

The single phase flow pattern for Case B, shown in Figure 5.4, is extremely similar to the flow pattern for Case A. The major difference is in the flow speed, which is different because Case B is for a lower casting speed. When the liquid flowrate is decreased and the gas flowrate is held constant, the gas volume fraction increases. The multiphase flow pattern, shown in Figure 5.5a, is very different from the multiphase flow pattern for Case A. The steel jet impinges on the top surface instead of the narrow face as usual. This flow pattern is known as single roll flow. As in Case A, the flow prediction closely matches the experimental measurements, shown in Figure 5.5b, both qualitatively and quantitatively. The jet angle in the bulk of flow is about the same, between 20° and 30° up.

The fact that model prediction can match experimental results for double roll and single roll flow patterns is an indication that the multiphase model is a good approximation of multiphase flow in an actual caster.

Table 5.1. Validation Model Parameters. Unlisted Values are the same as Case A.

	Case A	Case B
Mold Width	2765 *mm*	
Mold Thickness	220 *mm*	
Nozzle Submergence Depth (top surface to top of port)	100 *mm*	
Nozzle Bore Inner Diameter	85 *mm*	
Port Wall Thickness	27 *mm*	
Nozzle Port Height	95 *mm*	
Nozzle Port Width	75 *mm*	
Inlet Jet Height, L_h	38 *mm*	
Inlet Jet Width, L_w	75 *mm*	
Nominal Vertical Angle of Port Edges	15° down	
Inlet Jet Vertical Angle	25° down	
Inlet Jet Spread Angle	0°	
Casting Speed, V_c	18.1 *mm/s* (1.1 *m/min*)	9.9 *mm/s* (0.6 *m/min*)
Inlet Velocity, V_x	1.96 *m/s*	1.07 *m/s*
Inlet Velocity, V_z	0.87 *m/s*	0.48 *m/s*
Jet Angle at Inlet, α	24° down	
Inlet Turbulent Kinetic Energy, K_o	0.0502 m^2/s^2	
Inlet Turbulence Dissipation Rate, ε_o	0.457 m^2/s^3	
Liquid Steel Density, ρ	7020 kg/m^3	
Steel Laminar (Molecular) Viscosity, μ_o	0.00560 *kg/m s*	
Volumetric Steel Flow Rate	110 x 10^{-4} m^3/s	60 x 10^{-4} m^3/s
Inlet Gas Flow Rate	0, 0.030 m^3/min	0, 0.030 m^3/min
Inlet Gas Volume Fraction, f_{gas}	0%, 4.3%	0%, 7.7%
Average Gas Bubble Diameter, D_o	1.0 *mm*	
Gravitational Acceleration, g	9.8 m/s^2	

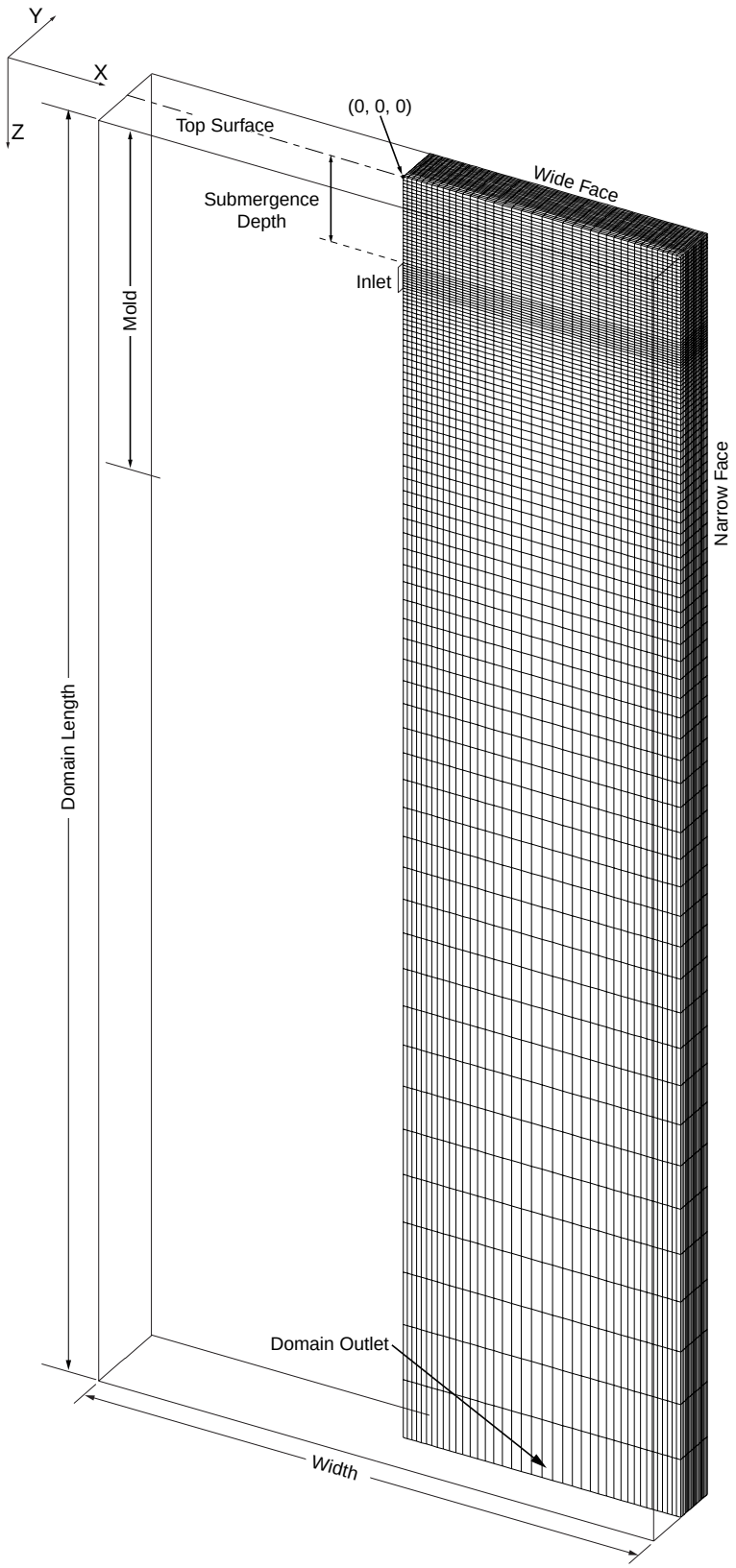

Figure 5.1. Standard Conditions Domain.

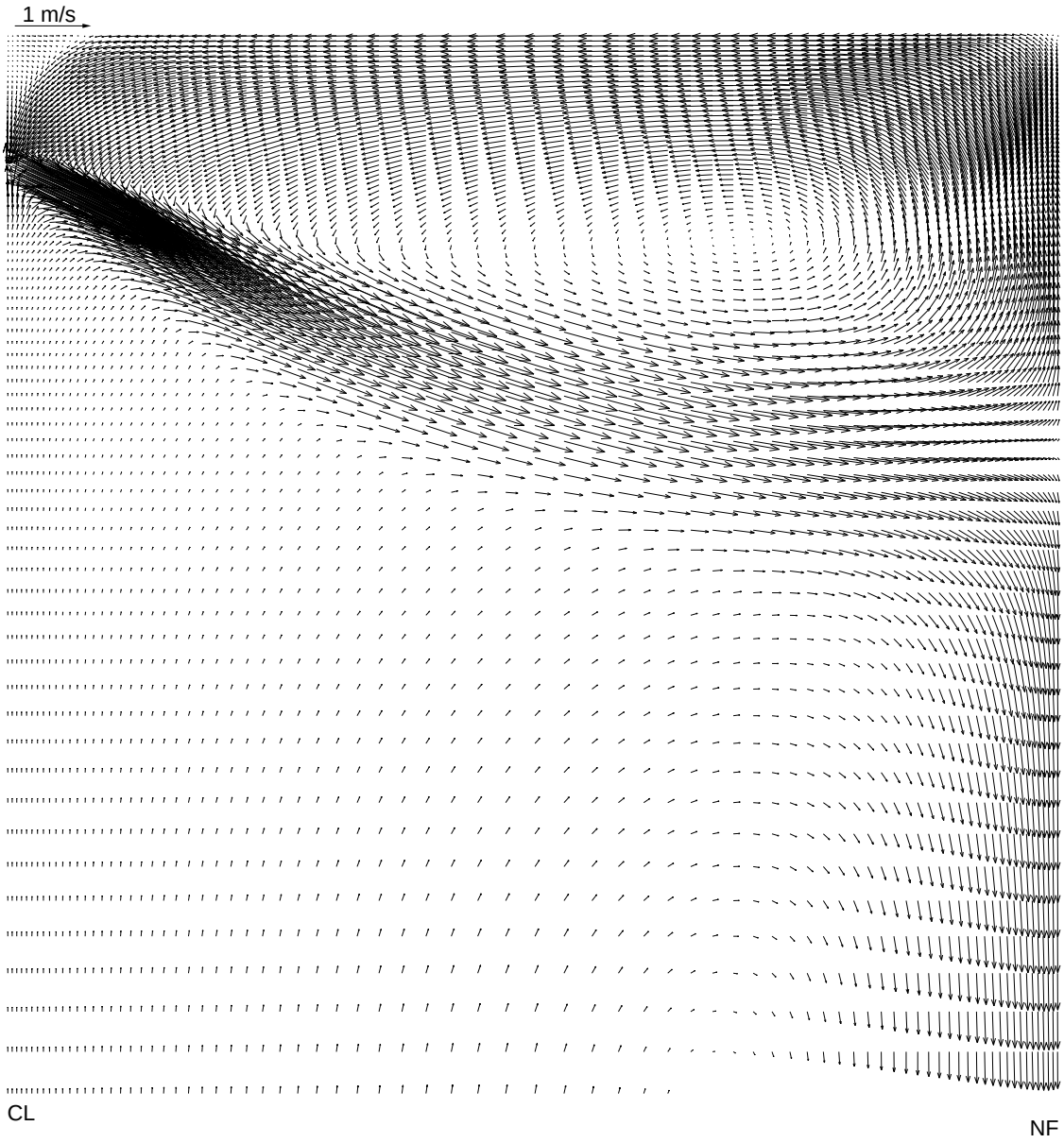

Figure 5.2. Case A, 0% Gas. Centerplane Velocity

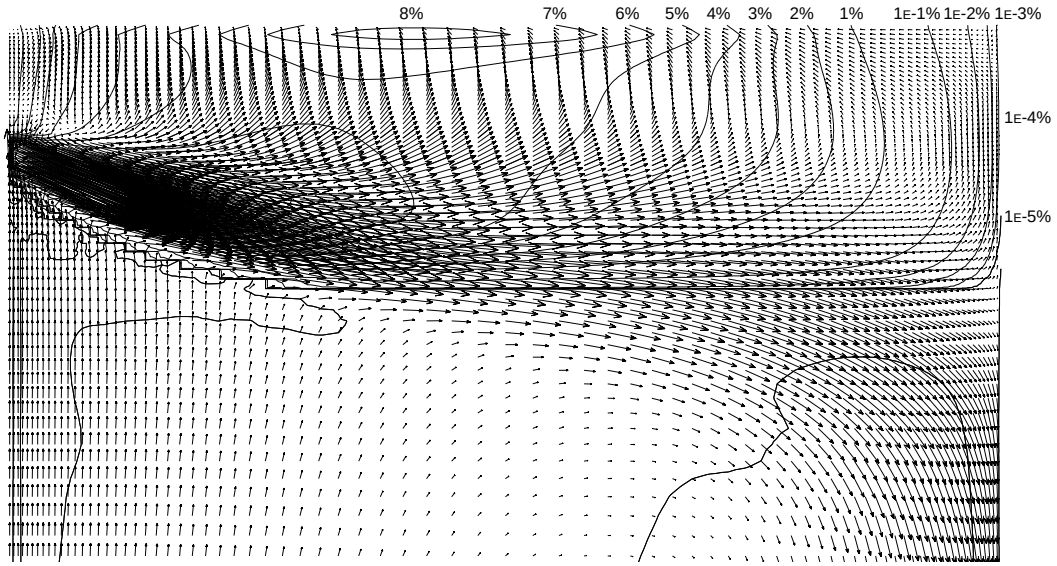

a.

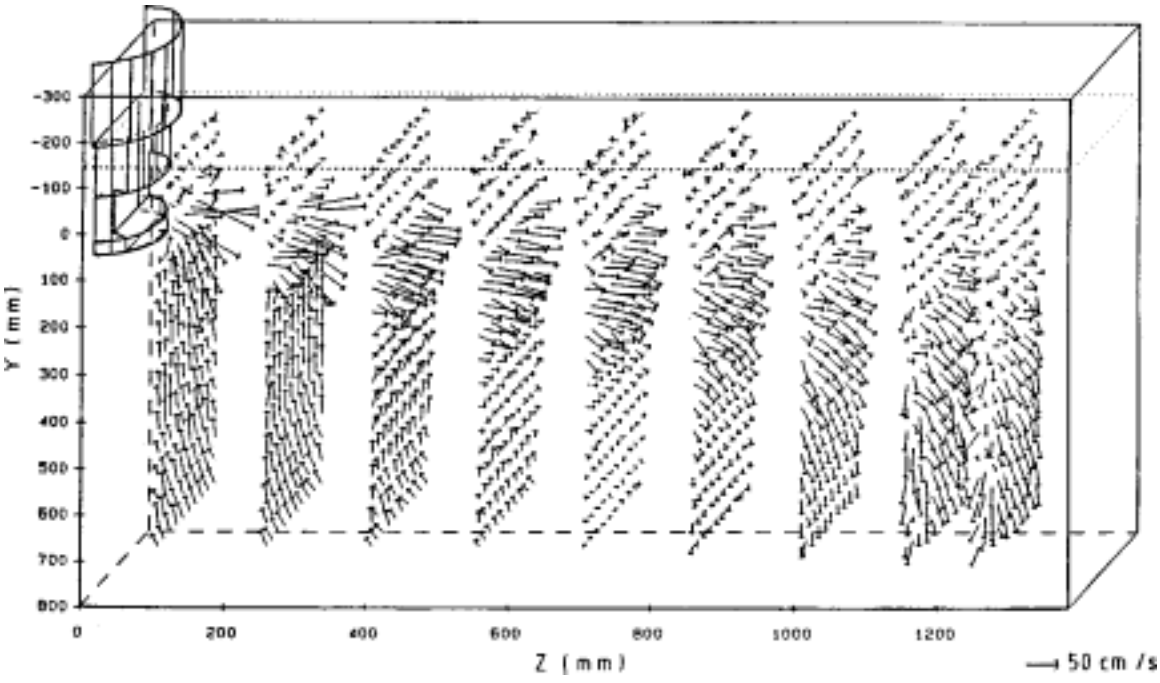

b.

Figure 5.3. Comparison of velocity profiles in continuous casting mold centerplane for Case A conditions, a) predicted by current CFX model, and b) measured in a water model [26]

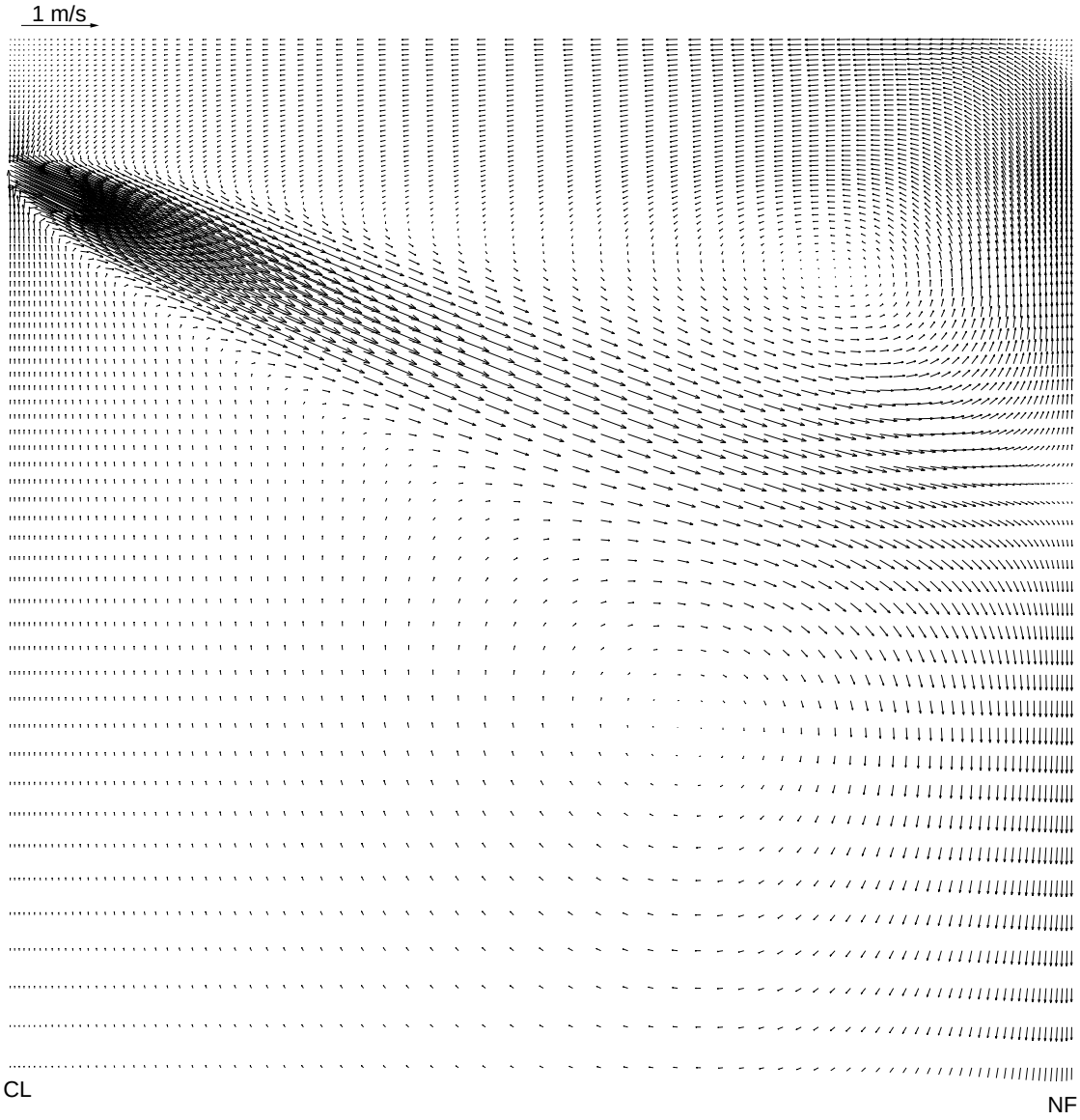

Figure 5.4. Case B, 0% Gas. Centerplane Velocity

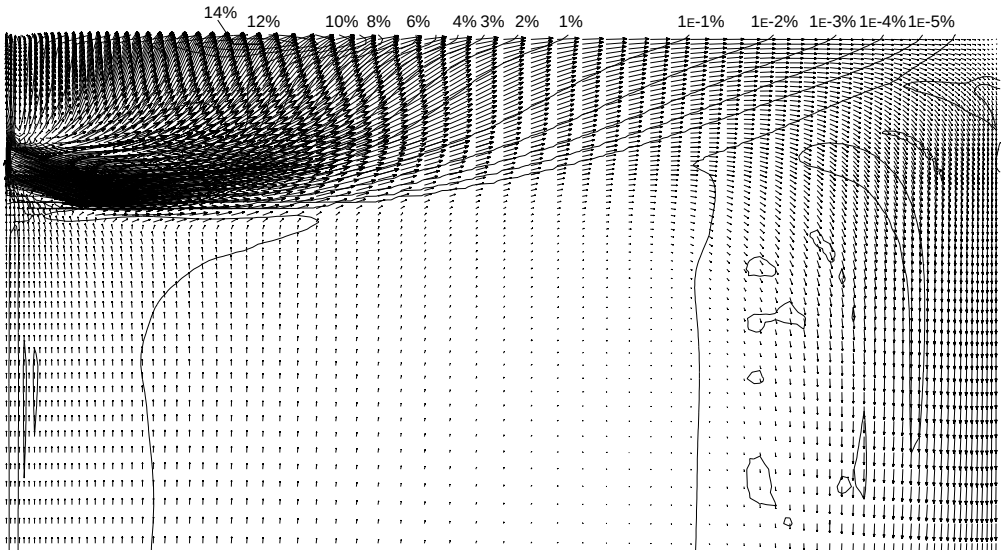

a.

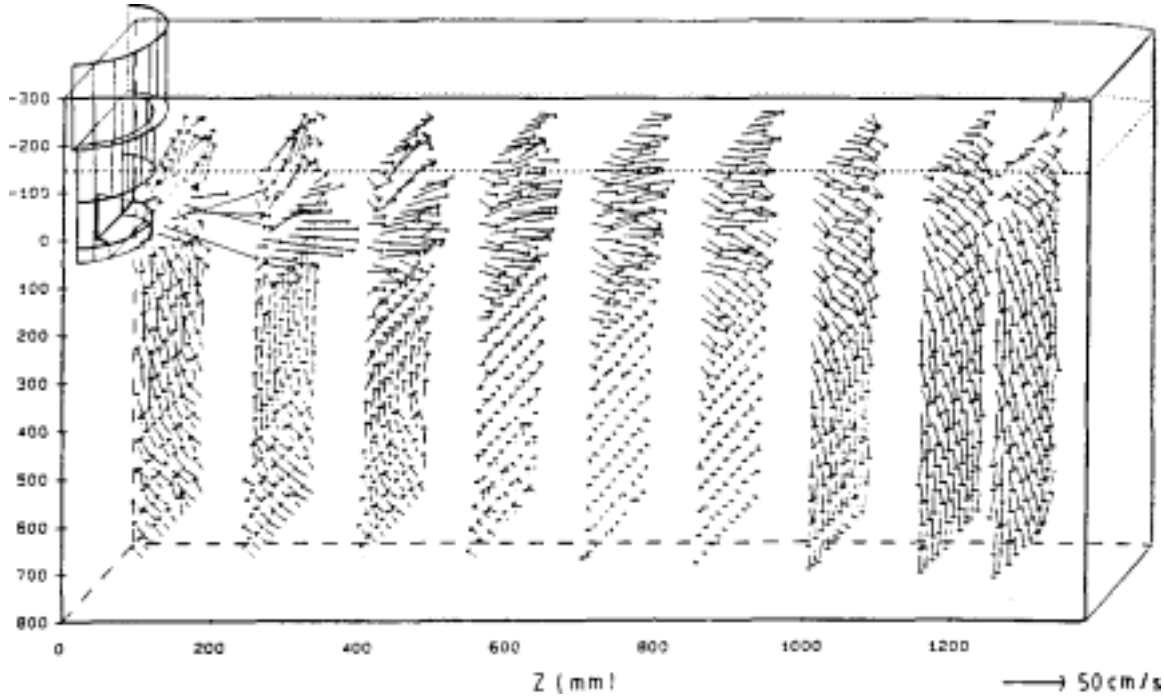

b.

Figure 5.5. Comparison of velocity profiles in continuous casting mold centerplane for Case B conditions, a) predicted by current CFX model, and b) measured in a water model [26]

6 Multiphase Flow Model Parametric Study

A parametric study was performed to study the effects of gas flow rate, bubble diameter, casting speed, submergence depth, and mold width on parameters important to casting product quality. The simulation parameters are listed in Table 6.1. The range of parameters was chosen to span the extreme range of those encountered in practice, with a low, high and typical value for each parameter. The Standard Conditions are listed in bold. The conditions for each case are identical to the Standard Conditions case except for noted values. Values for nozzle port height, width, vertical angle and nozzle bore diameter are estimated values for a new nozzle that has the jet characteristics imposed at the domain inlet. The same inlet turbulence values (K_o and ε_o) taken from Najjar's work [14] were used for all simulations .

Submergence depth is measured from the average level of the steel-flux interface to the top of the steel jet. For the particular example of Standard Conditions, the submergence of 205 mm corresponds to 190 mm when measured to the top of the port. Similarly, the submergence of 120 mm corresponds to 105 mm and the submergence of 50 mm corresponds to 35 mm measured to the top of the port. A simplified geometry is used for the study. The domain is for a straight mold and strand. It is assumed that two-fold symmetry exists in the mold. Therefore, the domain modeled is one quarter of the mold. This assumption means that any asymmetric flow effects will not be modeled. The nozzle geometry is not included in the domain.

A single bubble diameter is a simplification made in the multiphase model. In a real caster, a range of bubble sizes will be present. Steel plant observations have found 0.5 mm bubbles that are trapped as pencil-pipe defects. Other studies of gas injection through porous nozzle refractories [27] have measured bubble diameters of 2 mm in the nozzle for casting conditions similar to those used in this study.

Using Equation 5.5 and the correct values for argon density, the volume flowrate of gas can be calculated from the gas volume fraction. For standard conditions, 6% and 20% gas volume fractions correspond to volume flowrates of 4.67 LPM and 18.28 LPM respectively when measured at the liquid steel temperature. This corresponds to flow

rates of 0.93 SLPM and 3.66 SLPM (standard liters per minute) respectively when measured at standard temperature and pressure. These volumetric flowrate values change with casting speed and width.

6.1 Parametric Study Results

Table 6.2, Table 6.3 and Table 6.4 summarize important results for each of the 20 simulations in this study, including the location of the upper eye, the location of impingement below the top surface on the narrow face, the maximum surface velocity, the maximum gas penetration depth, the maximum turbulence kinetic energy and the average and maximum top surface pressure. Additional results for each case are presented in Appendix E.

The upper eye is defined as the center of the upper recirculation zone that usually forms at the top of the mold when the jet splits after impinging on the narrow face. The distance x is the distance from the centerline through the nozzle and z is the distance below the top surface in meters. This point will have a velocity close to zero.

The impingement point is defined as the distance below the no-flow steel-flux interface. Level changes due to pressure gradients are not accounted for in the impingement point's calculation.

The maximum surface velocity is measured at 8 mm below the top surface the first node. The surface velocity is defined as positive when moving from the narrow face to the centerline of the nozzle, as is the case in a double roll flow pattern. Velocities moving in this direction are denoted by + in the table. Velocities moving from the centerline to the narrow face are denoted by – in the table. Only the magnitude is given for velocities that are not moving in a consistent direction across the top surface.

The maximum gas penetration depth is defined as the deepest point that the 1E-5% gas volume fraction contour reaches in the domain. This value was picked because it is an order of magnitude less than the volume fraction of gas that was trapped as pencil-pipe

defects, according to statistical studies. This volume fraction was found to be between 1% and 1E-4 % [11].

A high level of the steel-flux interface at the mold walls can prevent the liquid flux from filling the gap between the shell and the mold. The maximum height of the standing wave on the mold perimeter is important because it is the point where liquid flux is least likely to fill the gap. In this model, the free surface is not modeled, so a direct solution of level is not performed. However, the pressure at the top surface can be used to predict the surface level. Pressure may be correlated to a standing wave level using the following equation:

$$Level = \frac{p - p_{atm}}{\left(\rho_{steel} - \rho_{flux}\right)g} \tag{6.1}$$

In single phase flow a simplified version of this equation that does not include the effect of the flux layer was found to reasonable relate pressure calculated using a flat interface with predicted surface level [8]. These results were also validated with a water model [8]. The multiphase model for the parametric study uses a pressure boundary condition for the outlet, at which the reference pressure can arbitrarily be set. Therefore, p_{atm} is defined as the average pressure over the area of the top surface. For this calculation, pressure was evaluated at 1 mm below the top surface, but generally pressure gradients normal to the top surface are negligible so this is not important.

The turbulence kinetic energy is measured 16 mm below the top surface at the second node, where the *K* gradient becomes nearly zero, as shown in Figure 6.13. A correlation between the turbulent kinetic energy, *K*, and level fluctuations of the top surface was proposed by Huang [28]:

$$\rho_{steel} K = 0.5\left(\rho_{steel} - \rho_{flux}\right)g\left(Level \;\; Fluctuation \;\; Height\right) \tag{6.2}$$

This relation was found to produce level fluctuations with a flat top surface that roughly matched measured level fluctuations [28]. For the parameters in Table 6.1, and assuming a liquid flux density equal to 3000 kg/m^3, this equation yields the correlation:

$$Level \;\; Fluctuation \;\; Height \approx \left(0.356 \;\; s^2/m\right)K \tag{6.3}$$

6.2 Typical Results

There are two basic flow patterns that occur in the continuous casting strand: double roll patterns and single roll patterns. Typical flow results that demonstrate these patterns and the flow parameters associated with them are described in the next section.

6.2.1 Single Phase Double Roll Flow

The velocity solution for the single phase Standard Conditions case (Case 1) are shown in Figure 6.1, Figure 6.2 and Figure 6.3. The flow pattern for Case 1 is a double roll pattern, where the jet of liquid steel impinges against the narrow face. The jet then splits and forms two recirculation zones, one above and one below the jet. The upper recirculation zone flows along the top surface towards the nozzle, where it turns down and joins the jet. The lower recirculation zone is much larger, and circulates in the area one to two meters below the jet. Near the domain outlet (3 m down the strand) the flow begins to move downward, as shown in Figure 6.3. Further down the strand, the velocity becomes more uniform and eventually all moves directly downwards at the casting speed.

As the jet moves from the inlet across the mold it entrains surrounding fluid. This effect can be seen in the plot of velocity on a plane through the jet, Figure 6.1. The jet widens until it reaches the wide face. The area where the jet reaches the wide face can be seen in Figure 6.2 near the narrow face.

The pressure distribution on the centerplane parallel to the wide face is shown in Figure 6.4. The maximum value of pressure along the top surface mold perimeter and the corresponding maximum level for each case are listed in Table 6.3. The pressure is highest where the jet impinges on the narrow face. A local maximum occurs at the corner of the top surface and the narrow face. There is a highly negative region of pressure directly under the jet inlet. This is caused by the jet entraining fluid as it enters the mold. The pressure distribution across the top surface is shown in Figure 6.6. The level of the standing wave can be calculated from the surface pressure. The highest surface level occurs at the narrow face where the jet reaches the top surface. The surface level is

lowest in the center, and rises again in the center of the wide face. This result is commonly observed in the plant and is well known.

The distribution of kinetic energy on the centerplane parallel to the wide face is shown in Figure 6.5. The highest value of *K* occurs on the top and bottom of the jet, where the shear layers are high. The distribution of *K* across the top surface is shown in Figure 6.12. The maximum value of *K* occurs at the center of the domain. The maximum value along the mold perimeter is at the wide face, and the minimum value is along the narrow face. The turbulence kinetic energy can be correlated to a level fluctuation using Equation 6.3. A high level fluctuation on the mold perimeter can cause defects in the shell.

6.2.2 Multiphase Double Roll Flow

The flow results for the standard conditions with 20% gas case are shown in Figure 6.8 through Figure 6.15. When gas is injected into the mold, the jet is generally lifted by the bubbles. This raises the impingement point, and tends to raise the maximum surface pressure. The upper eye is not well defined, because a large portion of the jet is deflected upward by the gas. The rest of the jet penetrates across the mold to the narrow face. This tends to lower the maximum tangential surface velocity. In addition, the velocities do not move consistantly across the top surface, so shearing entrainment of liquid flux may be more difficult. The velocity of the gas phase is shown in Figure 6.10 for the centerplane and the wide face. The velocity solution for the gas phase must be interpreted with the gas contours, because the CFX plots non-zero velocity values in areas where the volume fraction of the gas phase is close to zero. The plots of gas velocity can be thought of as potential velocity plots: if a bubble is present in a given location, it will move at the velocity shown in the plot. The gas velocity solution is very similar to the liquid velocity solution with the exception that there is an upward component of velocity due to buoyancy. For 1.0 mm bubbles, this upward velocity component is 0.12 m/s, which corresponds to the terminal velocity. The maximum penetration depth of the gas into the strand for this case is 0.338 m.

The pressure distribution on the centerplane parallel to the wide face is shown in Figure 6.11. The pressure is highest at the top surface where the bubbles leave the domain. A local maximum occurs at impingement point. The pressure distribution across the top surface is shown in Figure 6.14. The highest surface level occurs at the middle of the centerline parallel to the wide face where the bubble-laden jet reaches the surface. Across the thickness of the mold the surface level is lowest midway between the centerplane and the wide face. A local maximum occurs at the wide face, midway between the centerplane and the narrow face.

The distribution of kinetic energy on the centerplane parallel to the wide face is shown in Figure 6.12. The maximum value of K is still at the inlet, but the value of K at the top surface, where most of the gas bubbles are leaving the domain, is much higher. The distribution of K across the top surface is shown in Figure 6.15. The maximum value of K occurs at the middle of the centerline parallel to the wide face. The maximum value along the mold perimeter is at the wide face, and the minimum value is along the narrow face. The maximum value is higher than that for the single phase case.

6.2.3 Single Roll Flow

When the submergence depth is decreased to 0.120 m, the flow pattern can completely change when the gas flow rate is high. Figure 6.16 shows the single phase flow pattern for Case 16 with a submergence depth of 0.120 m and all other conditions standard. The flow with no gas injection is a double roll pattern. With 20% volume fraction gas injection the flow becomes a “single roll” flow pattern. The centerplane velocity for the 20% gas case is shown in Figure 6.22. The jet impinges on the top surface instead of at the narrow face. The jet flow across the top surface towards the narrow face, where it then turns down into the strand. The plot of the top surface (Figure 6.9) shows that the flow is moving in the direction opposite that of the double roll cases. A lower recirculation zone is still present as in double roll flow.

The pressure and K distributions for the single roll pattern are similar to the single phase standard conditions results. The top surface pressure and K distributions for the 20% gas

case (Case 17) are shown in Figure 6.26 and Figure 6.27. The magnitude of the *K* distribution is similar to the *K* distribution of Case 3, but the distribution is shifted towards the narrow face. The pressure distribution differs in that the pressure at the narrow face is higher than in the standard conditions case. The calculated maximum surface level is 5 mm, compared to 3 mm for standard conditions at 20% gas.

The maximum penetration depth of the gas for this single roll case is 1.372 m. This is deeper than the penetration depth for Case 3, so there will be a greater change of bubble entrapment.

6.3 Effect of Gas Flow Rate

Increasing the gas flow rate while maintaining a double roll flow pattern will decrease the maximum surface velocity. For standard conditions, increasing the gas injection from 0% to 20% decreases the max surface velocity from 0.252 m/s to 0.062 m/s. This trend is seen for all cases with double roll flow patterns. If a single roll flow pattern develops (Cases 15 and 17) the surface velocity will increase. This is because the high speed jet first reaches the top surface, instead of impinging at the narrow face, turning and then flowing along the top surface. For a submergence depth of 0.120, the surface velocity increased from 0.248 m/s to 0.255 m/s.

The gas flow rate also changes the depth of bubble penetration into the bottom of the domain. The single phase flow pattern has a region of high speed flow along the narrow face under the jet impingement point. If a small amount of gas were added to this flow pattern (small enough to not change the flow pattern) the bubbles might penetrate deep into the strand. Adding some gas (6%) changes the flow pattern so that there is slower flow down along the narrow face. This gives the bubbles less of a chance to be sent deep into the strand. When the gas is increased further (20%) the flow pattern changes back to again having high speed flow along the wall. This again sends the gas bubbles deep into the strand. For example Case 4 (standard conditions with 0.5 mm bubbles and 6% gas) has a maximum gas penetration of 1.047 m. When the gas is increased to 20% (Case 5) the penetration depth increases to 2.063 m. This suggests that an optimum gas flowrate may exist to minimize gas penetration.

For most cases, high gas flow rates cause increased surface fluctuation levels where the bubbles leave the top surface. For the single phase Case 1 the surface fluctuations 0.83 mm. For the 20% gas Case 3 the surface fluctuations are 3.74, an increase of 350%. In cases with high casting speeds, increasing the gas flow rate can actually decrease the surface fluctuations. For the single phase Case 9 the surface fluctuations 6.69 mm. For the 20% gas Case 10 the surface fluctuations are 4.76, a decrease of 30%.

A high gas flow rate creates a high pressure region in the middle of the top surface instead of the on the narrow face. For double roll flow, the maximum surface level decreases when gas is increased. For the standard conditions Cases 1 and 3, the surface level decreased by 40% from 5 mm to 3 mm. For single roll flow, the surface level is increases when gas is increased. For Cases 16 and 17, the surface level increased by 25% from 4 mm to 5 mm. For Cases 13 and 15, the surface level increased by 100% from 5 mm to 10 mm.

Preliminary data from caster measurements suggests that the bubbles may not follow the liquid steel flow as closely as predicted by this model, and as shown in Figure 6.3 and Figure 6.28. This suggests that the drag law used in this model may not be appropriate. Decreasing the momentum transfer between the gas bubbles and the liquid phase would allow the bubble to flow through the steel to the surface more easily. The gas would also have less effect on the flow solution; more gas would have to be added to reproduce the results of this study.

Case 2 was run with the same conditions as Cases 1 and 3, except that the gas fraction was set to 6%. The results for this run do not seem to fit the patterns seen in the results of the other cases. Upon closer inspection of the convergence history, it was found that the run had not converged due to a computer failure that was unrelated to the solver.

6.4 Effect of Bubble Diameter

Changing the mean bubble diameter of the gas bubbles injected into the domain can change the shape of the jet. Small bubbles tend to stay with the flow and raise the jet,

making the impingement point higher, as found in Case 5. Large bubbles tend to immediately rise to the surface and split the jet, as found in Case 7. This agrees with the findings of Huang [6]. This results in an area of low velocity near the narrow face meniscus, which could reduce the heat delivered to the meniscus.

Small bubbles also tend to penetrate deeper into the caster than large bubbles. Comparing the standard conditions cases for 20% gas and 0.5 mm (Case 5), 1.0 mm (Case 3) and 2.0 mm bubbles (Case 7) shows that the penetration depths are 2.063 m, 0.338 m, and 0.317 m respectively.

6.5 Effect of Submergence Depth

Submergence depth greatly affects whether single roll flow will develop at a given gas flow rate. For the standard conditions submergence depth of 0.205 m, single roll flow does not develop, even at a high gas injection rate of 20%. When the submergence depth is changed to 0.120 m (Case 17) the flow pattern changes to single roll at 20% gas. This also happens for the very shallow submergence depth of 0.050 m (Case 15). Thus, shallower submergence makes single roll flow easier.

When the flow becomes single roll, the gas penetration depth, surface level, and surface level fluctuations are all significantly changed. The effect of adding 20% gas to the single roll case (Case 16 and 17) increases the maximum surface level by 25%. For double roll flow (Cases 1 and 3) the maximum surface level decreases by 40 %. Therefore when the flow pattern becomes single roll, adding gas has the opposite effect on surface level, raising the level instead of lowering it. Thus, high gas flows are more detrimental in single roll flow.

The maximum surface fluctuations for all three submergence depths studied are similar. For standard conditions single phase (Case 1), 0.120 m submergence (Case 16) and 0.050 m submergence (Case 13) the maximum surface fluctuations are 0.83, 0.88 and 0.87 respectively. For the 20% gas cases (Cases 3, 17 and 15) the maximum surface fluctuations are 3.74, 3.72, and 4.43. Therefore the submergence depth has little effect on the maximum surface fluctuations.

The penetration of gas into the strand is less for the single roll flow than for double roll flow at the same gas flowrate. For Case 14 with a submergence depth of 0.050 m and 4% gas the penetration depth is 2.353 m. When 20 % gas is added (Case 15) and the flow becomes single roll, the penetration depth is only 0.564 m, a 75% decrease. In other cases, such as standard conditions, the same trend is seen when gas is increased, but penetration depth only decreases by 9%. Suprisingly, the intermediate submergence depth (0.120 m) had the deepest bubble penetration, for the same gas flow rate and bubble size.

6.6 Effect of Casting Speed

A high casting speed will lessen the effects of the gas phase on the overall flow pattern. Increasing the gas at a casting speed of 41.75 mm/s (2.5 m/min) from 0% (Case 9) to 20% (Case 10) changed the location of the impingement point by only 7%, compared to 29% for standard conditions (Case 1 and Case 3) at a casting speed of 17.5 mm/s (1 m/min). This makes is more difficult to develop single roll flow patterns. Increasing the casting speed will also increase the gas level lower in the caster.

The top surface velocity is increased when the casting speed is increased. For 0% gas, a 150% increase in the casting speed increases the maximum surface velocity by 175%, from 0.252 m/s for Case 1 to 0.691 m/s for Case 9. For 20% gas, the surface velocity increases by 940%, from 0.062 m/s for Case 3 to 0.646 m/s for Case 10. The surface velocity difference is greater for high gas rates because for the standard conditions case with lower casting speeds the velocity is decreased by 75% when gas is added, but for the high casting speed adding gas only decreases the surface velocity by 6%. High speed also causes much higher maximum level and higher level fluctuations.

Case 12, with a high casting speed and gas injection rate, produced results that do not seem to agree with results from the other cases. These results are most likely caused by a convergence problem which is more likely with high velocity, high gas flows.

6.7 Effect of Mold Width

The effects of changing mold width on pressure, K, and gas penetration are similar to the effects of changing casting speed. In order to maintain a constant casting speed, the inlet velocity must be increased. This results in higher levels of maximum surface *K* and pressure than for the standard conditions cases at the same gas flow rates. The higher flow rate of the liquid steel also causes gas to have less effect on the flow pattern. Changing the mold width by 21% from 1.32 m to 1.60 m increases the maximum surface velocity by 33% for the single phase cases (Cases 1 and 18), and by 63% for the 20% gas cases (Cases 3 and 20).

6.8 Implications of Parametric Study Results on Steel Quality

The results of the parametric study suggest several ways that defects can be reduced through the proper selection of casting parameters. The flow parameters first can be correlated to defect mechanisms to quantify their effect on steel quality.

6.8.1 Flux Entrainment

A high tangential surface velocity of the liquid steel creates shear forces on the liquid flux layer. When the shear forces become large globules of the liquid flux can become entrained in the steel flow. The globules circulate with the steel flow and can be entrapped in the solidifying shell, forming internal solid inclusions. Adding gas to the flow reduces the surface velocity by changing the flow pattern. Adding 20% gas at a casting speed of 16.7 mm/s (1.0 m/min) will reduce the maximum surface velocity by a factor of four. At a high casting speed, adding gas has little effect on the maximum casting speed. If enough gas is added to a mold with a typical (0.120 m) or shallow (0.050 m) submergence depth and a casting speed of 16.7 mm/s (1.0 m/min), the flow will become single roll and the maximum surface velocity will increase. Increasing the mold width while keeping the casting speed constant will increase the surface velocity, because the volumetric flow rate of the liquid steel must be increased to maintain the casting speed in a larger mold.

If gas is held constant, reducing the maximum surface velocity will lower the chance that flux will become entrained. However, the critical surface velocity at which entrainment occurs is decreased when the gas flowrate is increased [3]. It is possible that increasing the gas flow rate will outweigh the benefits of reducing the surface velocity by reducing the critical surface velocity. Cramb studied the critical surface velocity in water models using silicon oil to represent the liquid flux layer [29]. Cramb found a relationship between gas flow rate and the critical surface velocity. If this work can be extended to steel/flux flow, an optimum gas flow rate may be found that minimizes entrainment. This work makes it clear that for the same maximum surface velocity, a single phase case will have less chance of entrainment than a case with gas injection.

This work suggests that if gas foaming can be avoided, then an optimal amount of gas can slow down the surface velocities and make liquid flux entrainment less likely.

6.8.2 Surface Level Height

The vertical momentum of the liquid steel jet can lift the level of the top surface, creating a variation in the interface level or “standing wave.” A high standing wave at the mold wall can prevent liquid flux from filling the gap between the steel shell and the mold where the surface level is high. Without lubrication from the liquid flux in the gap, the shell can “stick” in the mold instead of pulling out at the casting speed. The flux is also important for heat transfer between the steel shell and the mold. A lack of flux in the gap can create non-uniform heat flow on the shell. Finally, lack of flux in the gap can cause cracks in the steel shell due to thermal stresses and mold friction.

The pressure can be correlated to a surface level profile using Equation 6.1. This corresponding surface level profile can be compared to measurements of the location of the steel-flux interface in actual casters. The pressure distribution for the standard conditions case matches the standing wave shape found by McDavid for single phase flow, but the calculated height of the standing wave is 40% less than the measurements by both McDavid and Bergeles [8, 16].

Bergeles found that the wave height increases with the square of the inlet jet speed according to the relation

$$\frac{Wave\ \ Height(2g)}{V_{inlet}^2} = Constant \tag{6.4}$$

where the wave height is the difference between the maximum and minimum surface level. When calculated for the single phase cases, this constant is found to be 0.080 for Case 1, 0.082 for Case 9, and 0.0871 for Case 18, showing a slight upward trend with increased casting speed. Bergeles found a slight downward trend with increased casting speed, but this shows general agreement with the relation of Bergeles. According to the Rottman relation [8] none of the waves predicted in this study should be unstable, even at the highest casting speed considered. Thus, there is no clear reason why Equation 6.1 should not be valid.

For single phase flow, the maximum pressure occurs at the narrow face, which is observed in actual casters. For multiphase flow, the rising bubbles create a region of high pressure, and the corresponding high standing wave level, somewhere between the narrow face and the centerline through the nozzle. Therefore, defects related to flux filling of the gap will occur at this point instead of at the narrow face.

6.8.3 Surface Level Fluctuations

Fluctuations in surface level of the liquid steel are caused by random turbulent motion of the flow. Large surface fluctuations cause time-variations in the interface level which lead to surface defects such as entrapped mold powder. The surface fluctuation height can be calculated from the turbulence kinetic energy at the top surface using Equation 6.3.

For most cases, high gas flow rates cause increased surface fluctuation levels where the bubbles leave the top surface. For the single phase Case 1 the surface fluctuations 0.83 mm. For the 20% gas Case 3 the surface fluctuations are 3.74, an increase of 350%. In cases with high casting speeds, increasing the gas flow rate can actually decrease the surface fluctuations. For the single phase Case 9 the surface fluctuations are 6.69 mm. For the 20% gas Case 10 the surface fluctuations are 4.76, a decrease of 30%.

The maximum surface fluctuations for all three submergence depths studied are similar. For standard conditions single phase (Case 1), 0.120 m submergence (Case 16) and 0.050 m submergence (Case 13) the maximum surface fluctuations are 0.83, 0.88 and 0.87 respectively. For the 20% gas cases (Cases 3, 17 and 15) the maximum surface fluctuations are 3.74, 3.72, and 4.43. Therefore the submergence depth appears to have little direct effect on the maximum surface level fluctuations, if other conditions remain constant.

6.8.4 Bubble Penetration into the Strand

Small bubbles (0.5 mm) are found to penetrate the deepest into the strand. For standard conditions 1.0 mm bubbles at 20% gas (Case 3) penetrate 0.338 m, while 0.5 mm bubbles at 20% gas (Case 5) penetrate 2.063 m. Increasing the steel flow rate, either by increasing the casting speed (Cases 10 and 11) or using a wider mold (Cases 19 and 20) also increases the gas penetration depth. A shallow submergence depth is also found to increase the gas penetration depth (Case 14), but increasing the gas flow rate to create a single roll flow pattern was found to reduce the penetration depth from 2.353 m to 0.564 m (Case 15).

Bubbles of the injected argon gas can become trapped in the steel shell. The bubbles collect alumina inclusions while in the liquid steel. When the steel shell solidifies around the trapped bubbles, “pencil-pipe” defects are formed. Defects caused by bubble entrapment occur between 0.5 m and 3.0 m [10] and the gas percentage trapped is between 1E-4% to 1E-3% [11]. It is assumed that pencil-pipe defects occur when the speed of bubbles flowing down the wall (solidification front) approaches the casting speed. This region occurs between the narrow face and the centerline through the nozzle for most cases, and moves closer to the narrow face deeper into the strand. The intersection of this area with gas percentages of 1E-5% or greater shows that there is a small percentage of gas that hits the critical zone. This percentage agrees with measured values [11].

Table 6.1. Parametric Study Model Parameters (Standard Conditions in bold)

Mold Width	**1320 *mm***, 1600 *mm*
Mold Thickness	220 *mm*
Nozzle Submergence Depth	50 *mm*, 120 *mm*, **205 *mm***
Nozzle Port Height†	75 *mm*
Nozzle Port Width†	38 *mm*
Nozzle Bore Inner Diameter†	75 mm
Nominal Vertical Angle of Port Edges†	15° *down*
Inlet Jet Height, L_h	60 *mm*
Inlet Jet Width, L_w	38 *mm*
Inlet Jet Angle, α	*22° down*
Casting Speed, V_c	8.35 *mm/s*, **16.7 *mm/s***, 41.75 *mm/s*
Inlet Normal Velocity, V_x	0.531 *m/s*, **1.062 *m/s***, 2.655 *m/s*
Inlet Downwards Velocity, V_z	0.214 *m/s*, **0.427 *m/s***, 1.068 *m/s*
Inlet Turbulent Kinetic Energy, K_o	0.0502 m^2/s^2
Inlet Dissipation Rate, ε_o	0.457 m^2/s^3
Steel Density, ρ	7020 kg/m^3
Laminar (Molecular) Viscosity, μ	0.00560 *kg/m s*
Gas Volume Fraction, f_{gas}	0%, 4%, 6%, 20%
Average Bubble Diameter, D_o	0.5 *mm*, 1.0 *mm*, 2 *mm*
Gravitational Acceleration, $\boldsymbol{g}$	{0, 0, 9.8 m/s^2}
Caster Domain Modeled	1/4 Mold
Turbulence Model	Standard K-ε
Numerical Grid, Maximum y^+ at Wall	30

† Estimates

Table 6.2. Parametric Study Results.

Case No.	Conditions (Standard except as noted)	% Gas	Bubble Diameter (mm)	Upper Eye Location {x, z}	Narrow Face Impingement Point (m)	Max. Surface Velocity (m/s)
1	Standard	0 %	—	{.386, .234}	0.427	+ 0.252
2‡	Conditions	6 %	1.0	{.361, .222}	0.400	+ 0.284
3		20 %	1.0	—	0.304	0.062
4		6 %	0.5	{.255, .227}	0.371	+ 0.237
5		20 %	0.5	—	0.262	0.085
6		6 %	2.0	{.427, .165}	0.370	+ 0.060
7		20 %	2.0	{.540, .158}	0.372	0.055
8	Casting Speed 8.35 mm/s	6 %	2.0	{.429, .164}	0.354	+ 0.060
9	Casting Speed	0 %	—	{.470, .318}	0.421	+ 0.691
10	41.75 mm/s	20 %	1.0	{.451, .299}	0.449	+ 0.646
11		6 %	0.5	{.490, .328}	0.471	+ 0.580
12‡		20 %	0.5	{.501, .318}	0.455	+ 0.600
13	Submergence	0 %	—	{.461, .156}	0.290	+ 0.245
14	Depth 0.05 m	4 %	0.5	—	0.242	+ 0.128
15		20 %	0.5	—	Single Roll	- 0.302
16	Submergence	0 %	—	{.432, .236}	0.375	+ 0.248
17	Depth 0.120 m	20 %	1.0	—	Single Roll	- 0.255
18	Mold Width	0 %	—	{.458, .247}	0.435	+ 0.336
19	1.60 m	6 %	1.0	{.225, .221}	0.386	+ 0.225
20		20 %	1.0	—	0.335	+ 0.101

‡ These simulations were not properly converged

Table 6.3. Parametric Study Results.

Case No.	Conditions (Standard except as noted)	% Gas	Bubble Diameter (mm)	Average Surface Pressure (kg/ms^2)	Maximum Surface Pressure (kg/ms^2)	Maximum Surface Level (mm)
1	Standard	0 %	—	-47	133	5
2‡	Conditions	6 %	1.0	4	219	6
3		20 %	1.0	200	300	3
4		6 %	0.5	140	453	8
5		20 %	0.5	380	514	3
6		6 %	2.0	60	124	2
7		20 %	2.0	170	220	1
8	Casting Speed 8.35 mm/s	6 %	2.0	75	124	1
9	Casting Speed	0 %	—	-138	1109	32
10	41.75 mm/s	20 %	1.0	350	1438	28
11		6 %	0.5	530	1366	21
12‡		20 %	0.5	2320	3210	23
13	Submergence	0 %	—	-47	149	5
14	Depth 0.05 m	4 %	0.5	75	315	6
15		20 %	0.5	400	785	10
16	Submergence	0 %	—	-10	152	4
17	Depth 0.120 m	20 %	1.0	250	438	5
18	Mold Width	0 %	—	-63	237	8
19	1.60 m	6 %	1.0	80	226	4
20		20 %	1.0	305	359	1

‡ These simulations were not properly converged

Table 6.4. Parametric Study Results

Case No.	Conditions (Standard except as noted)	% Gas	Bubble Diameter (mm)	Max. Gas Penetration (m)	Maximum Surface K (m^2/s^2)	Maximum Surface Fluctuation (mm)
1	Standard	0 %	—	—	0.00235	0.83
2‡	Conditions	6 %	1.0	0.371	0.00303	1.08
3		20 %	1.0	0.338	0.01049	3.74
4		6 %	0.5	1.047	0.00569	2.03
5		20 %	0.5	2.063	0.01155	4.11
6		6 %	2.0	0.400	0.00143	0.51
7		20 %	2.0	0.317	0.00861	3.07
8	Casting Speed 8.35 mm/s	6 %	2.0	0.283	0.00351	1.25
9	Casting Speed	0 %	—	—	0.01878	6.69
10	41.75 mm/s	20 %	1.0	1.353	0.01337	4.76
11		6 %	0.5	2.247	0.01410	5.02
12‡		20 %	0.5	1.976	0.01326	4.72
13	Submergence	0 %	—	—	0.00243	0.87
14	Depth 0.05 m	4 %	0.5	2.353	0.00537	1.91
15		20 %	0.5	0.564	0.01244	4.43
16	Submergence	0 %	—	—	0.00247	0.88
17	Depth 0.120 m	20 %	1.0	1.372	0.01044	3.72
18	Mold Width	0 %	—	—	0.00407	1.45
19	1.60 m	6 %	1.0	0.483	0.00175	0.62
20		20 %	1.0	0.377	0.01337	4.76

‡ These simulations were not properly converged

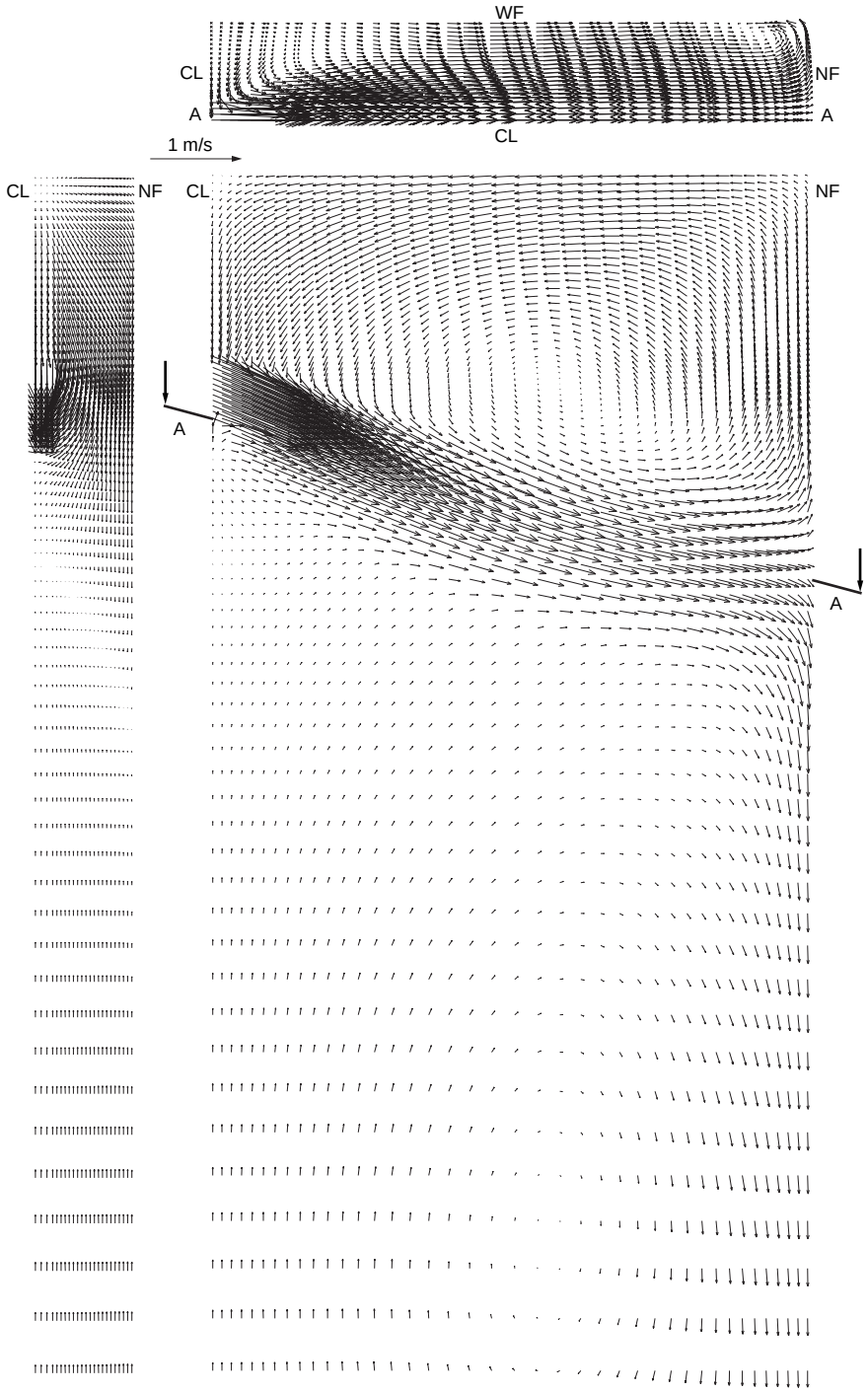

Figure 6.1. Velocity at Centerplane Parallel to Narrow Face (left), Centerplane Parallel to Wide Face (right), and at 15° Through Bottom of Inlet (Section A-A, top) [Case 1: Standard Conditions, 1.0 mm Bubble Diameter, 0% Gas]

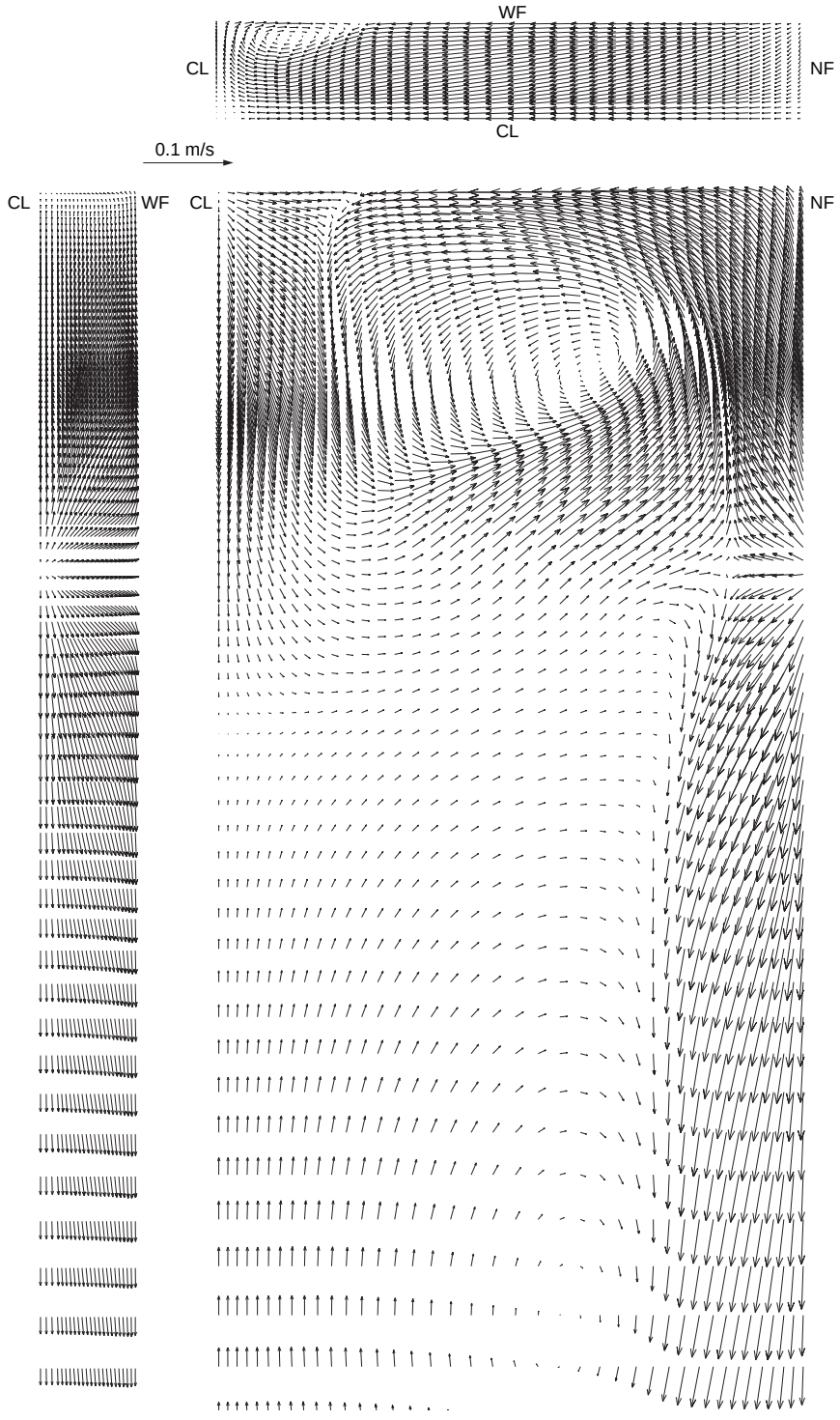

Figure 6.2. Velocity at 1 mm from Narrow Face (left), 1 mm from Wide Face (right), and 1 mm Below the Top Surface [Case 1: Standard Conditions, 0% Gas]

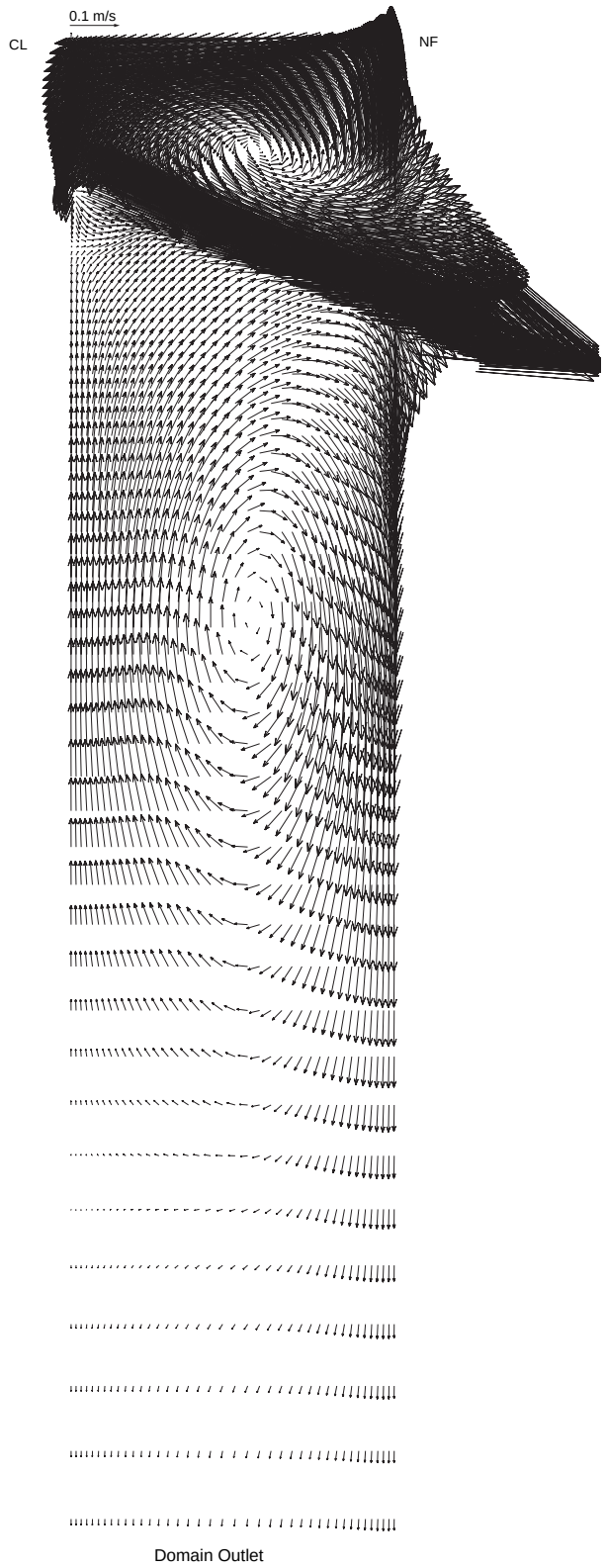

Figure 6.3. Velocity at Centerplane Parallel to Wide Face for Entire Domain. [Case 1: Standard Conditions, 0% Gas]

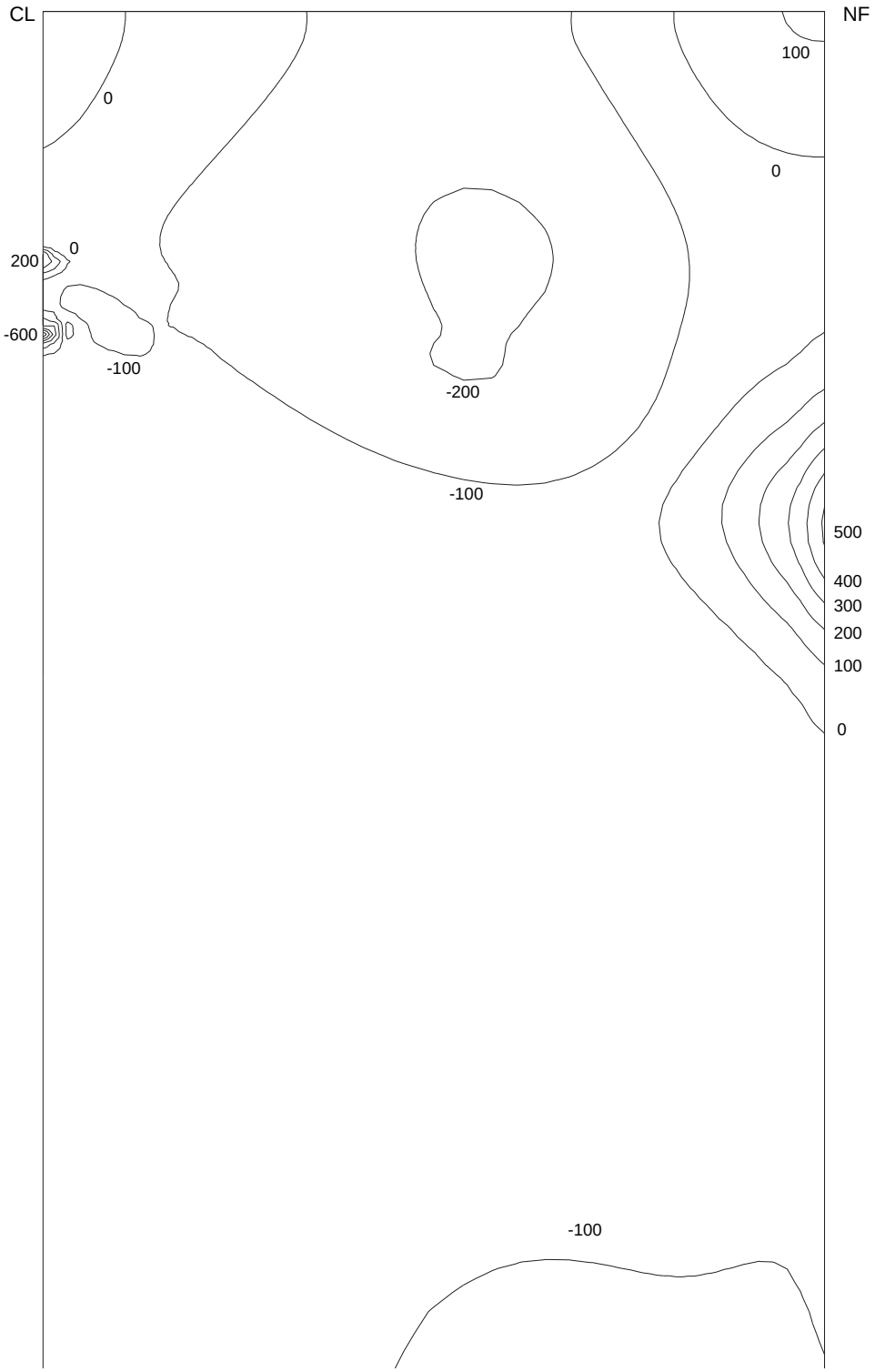

Figure 6.4. Pressure (kg/ms^2) at Centerplane Parallel to Wide Face [Case 1: Standard Conditions, 0% Gas]

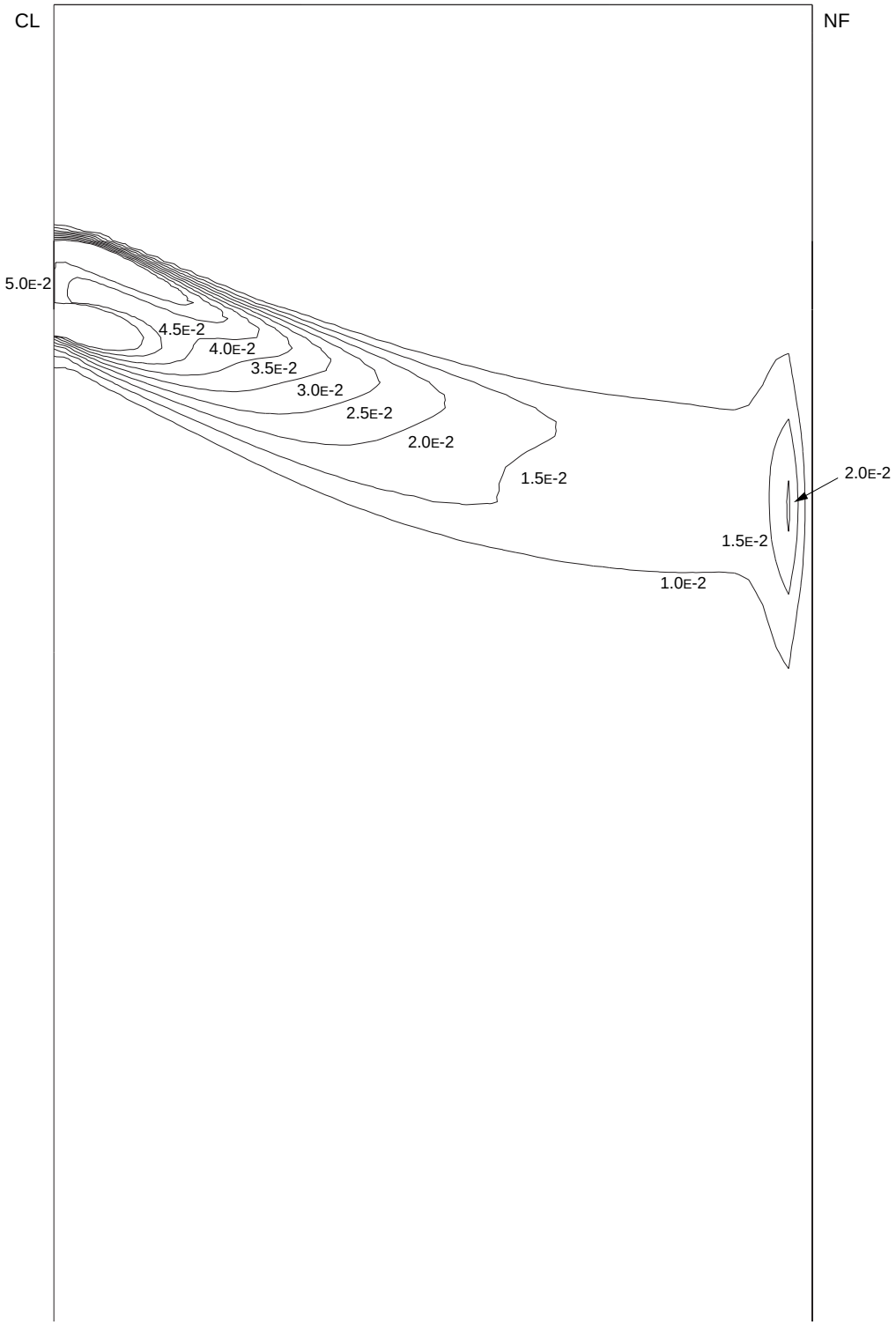

Figure 6.5. Kinetic Energy (m^2/s^2) at Centerplane Parallel to Wide Face
[Case 1: Standard Conditions, 0% Gas]

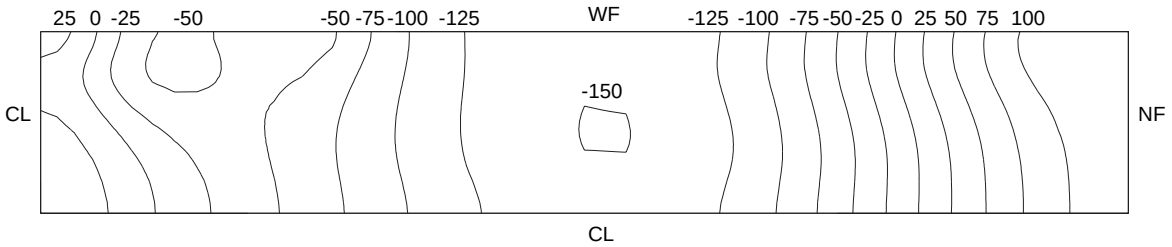

Figure 6.6. Pressure (kg/ms^2) at 1 mm Below Top Surface
[Case 1: Standard Conditions, 0% Gas]

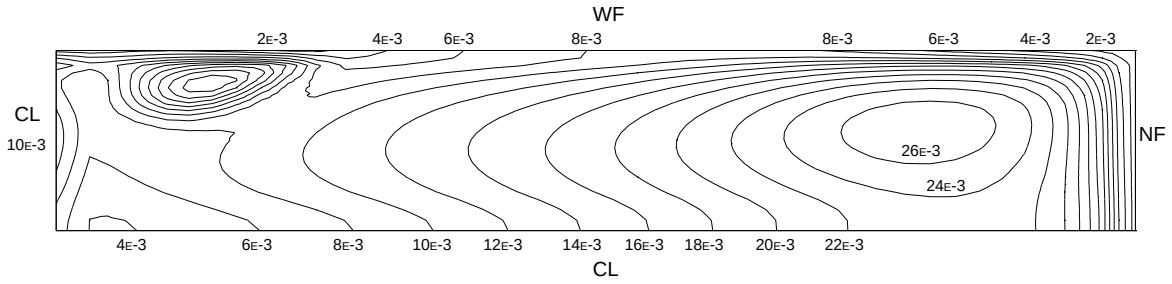

Figure 6.7. Kinetic Energy (m^2/s^2) at 1mm Below Top
Surface. [Case 1: Standard Conditions, 0% Gas]

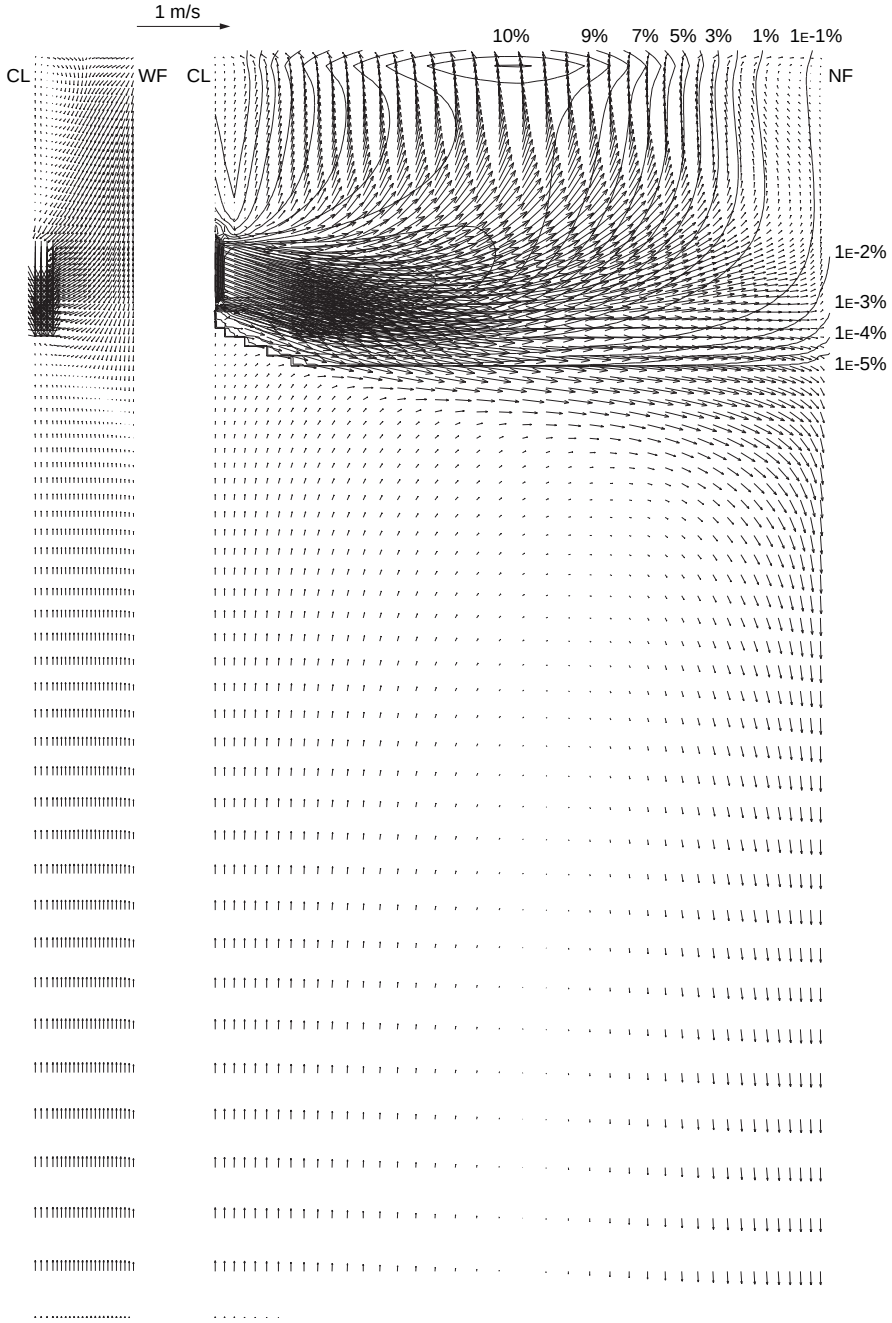

Figure 6.8. Velocity at Centerplane Parallel to Narrow Face (left) and Centerplane Parallel to Wide Face (right). [Case 3: Standard Conditions, 1.0 mm Bubble Diameter, 20% Gas]

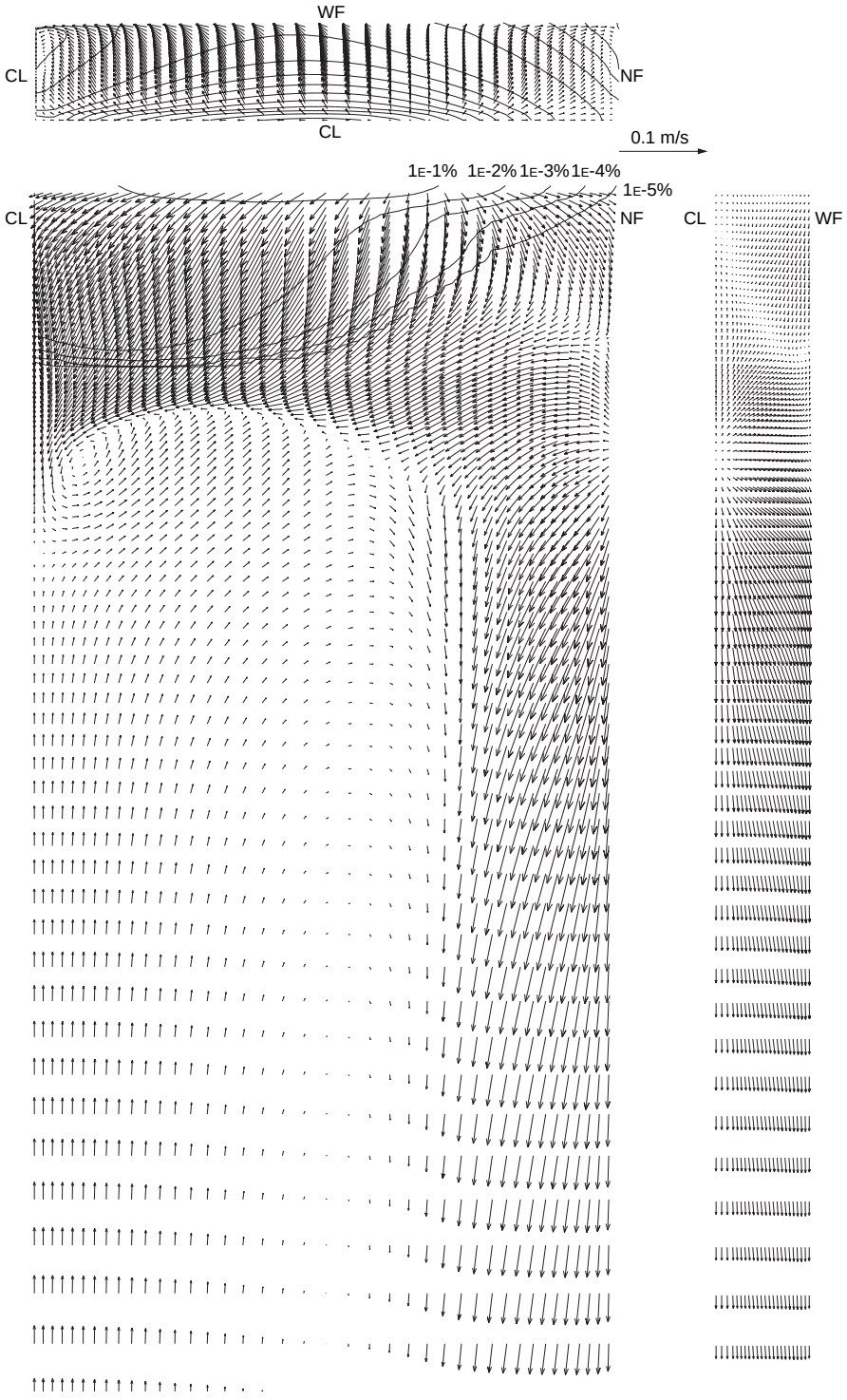

Figure 6.9. Velocity at 1 mm from Narrow Face (left), 1 mm from Wide Face (right), and 1 mm Below the Top Surface [Case3: Standard Conditions, 1.0 mm Bubble Diameter, 20% Gas]

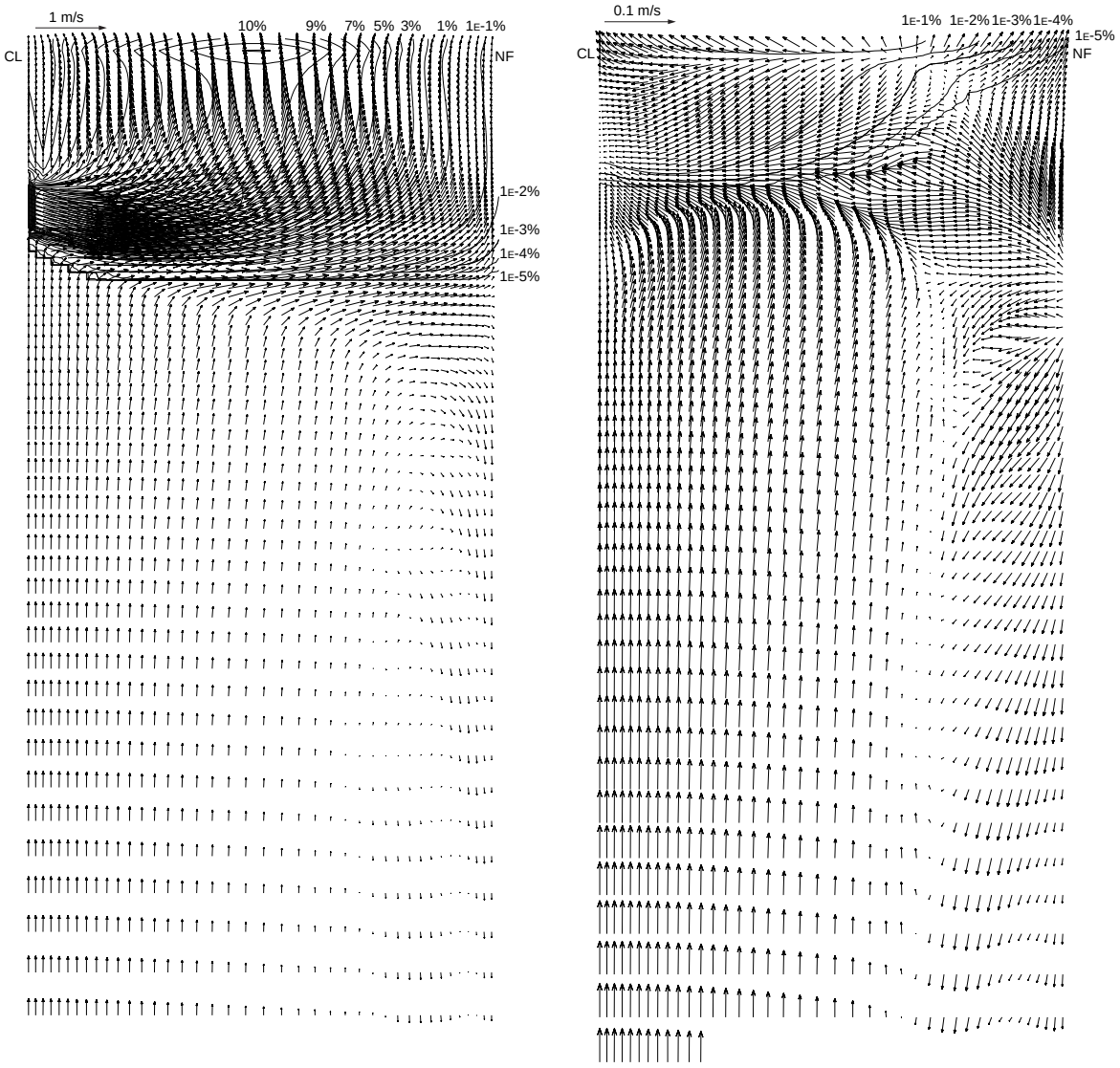

Figure 6.10. Velocity of Gas Phase for Centerplane (left) and 1 mm from Wide Face (right). [Case3: Standard Conditions, 1.0 mm Bubble Diameter, 20% Gas]

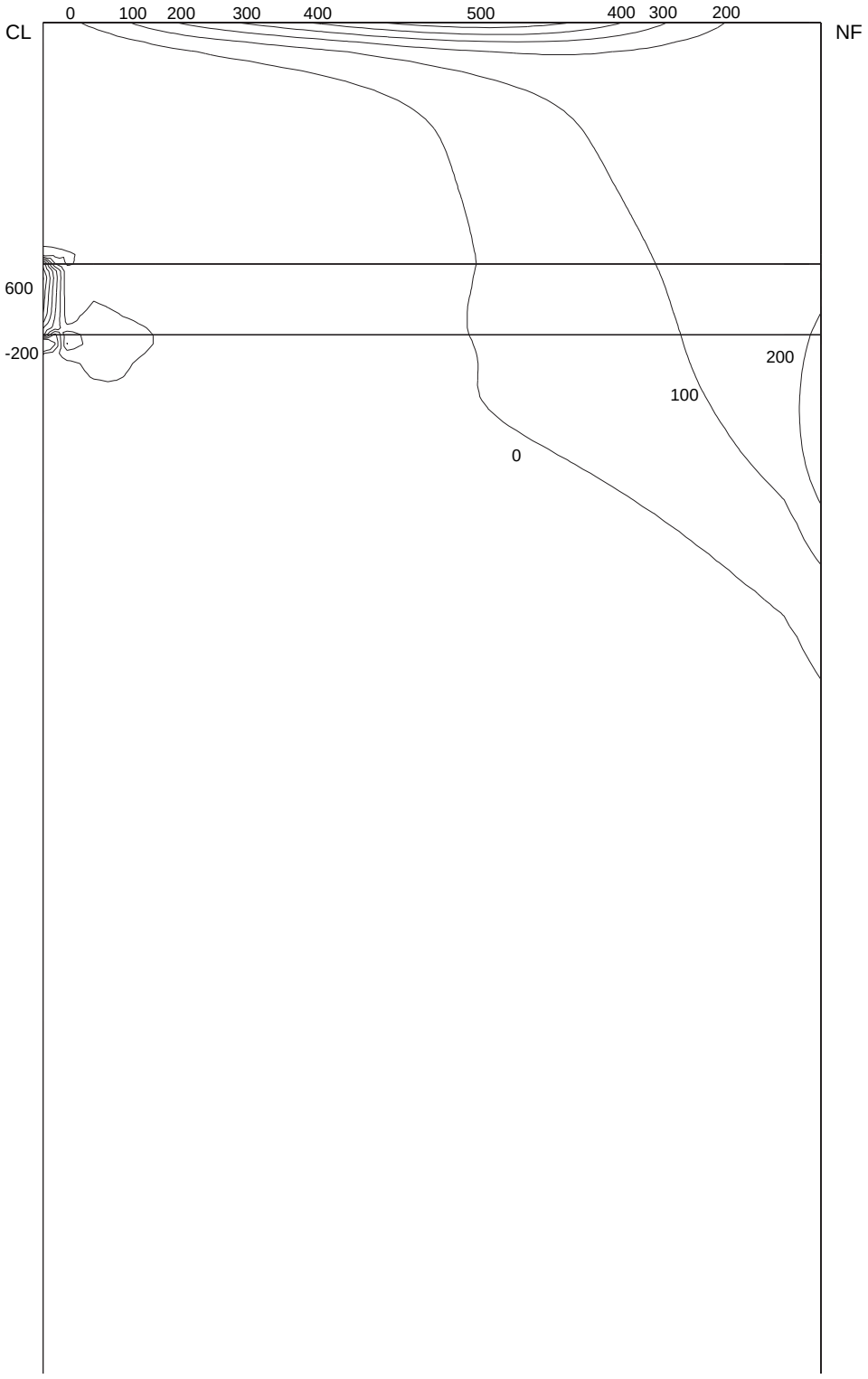

Figure 6.11. Pressure (kg/ms^2) at Centerplane Parallel to Wide Face [Case 3: Standard Conditions, 1.0 mm Bubble Diameter, 20% Gas]

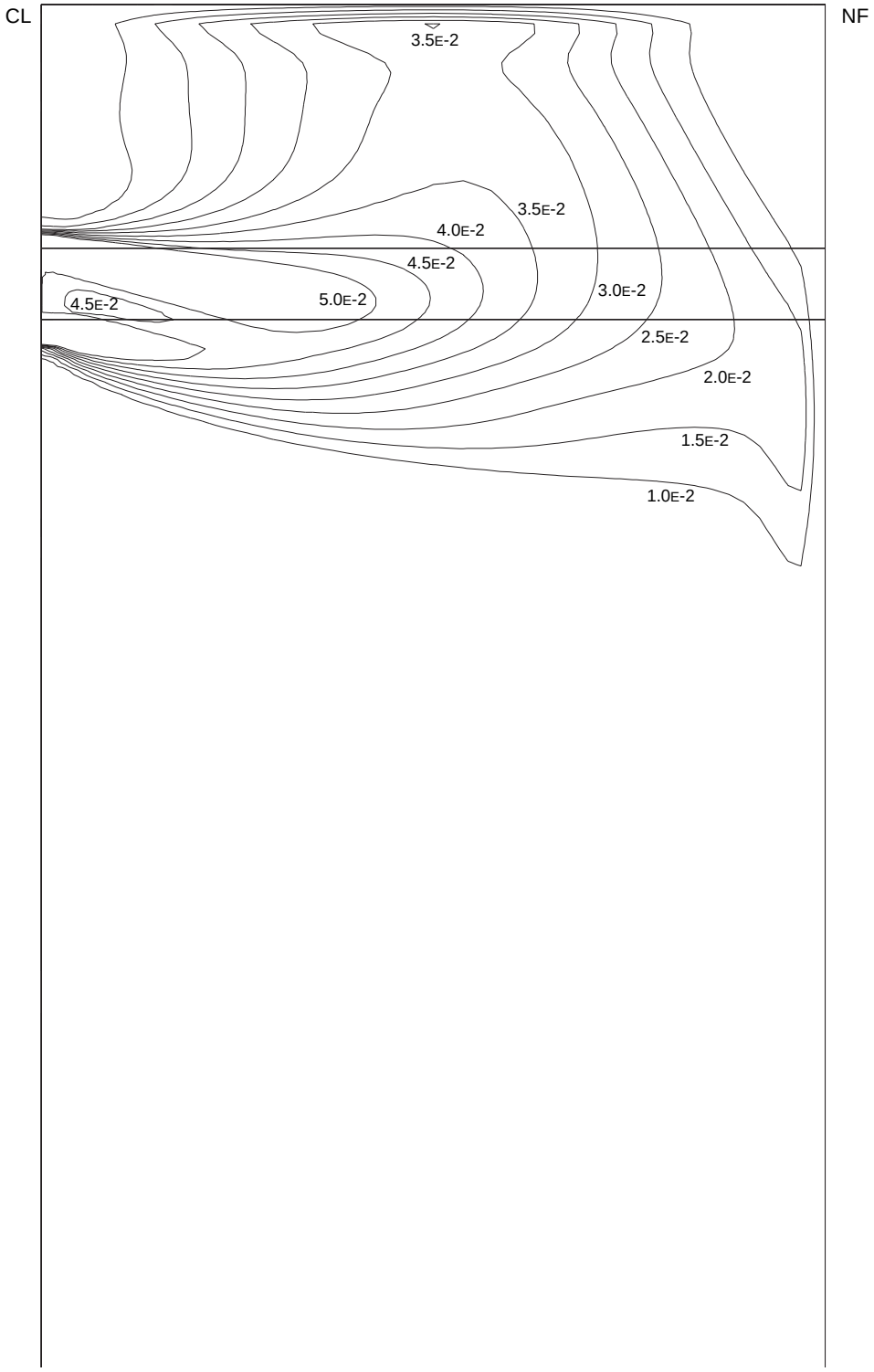

Figure 6.12. Kinetic Energy (m^2/s^2) at Centerplane Parallel to Wide Face [Case 3: Standard Conditions, 1.0 mm Bubble Diameter, 20% Gas]

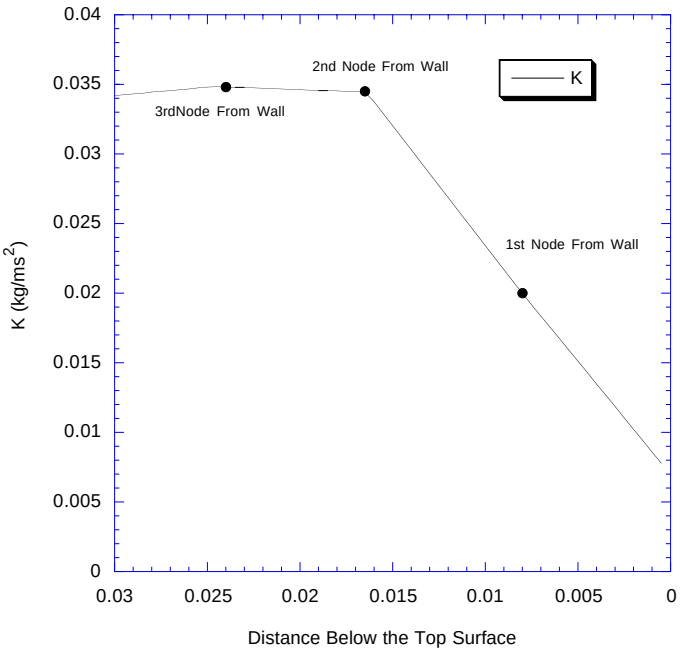

Figure 6.13. K Profile at Top Surface, Halfway between Narrow Face and Centerline Through Nozzle. [Case 3: Standard Conditions, 1.0 mm Bubble Diameter, 20% Gas]

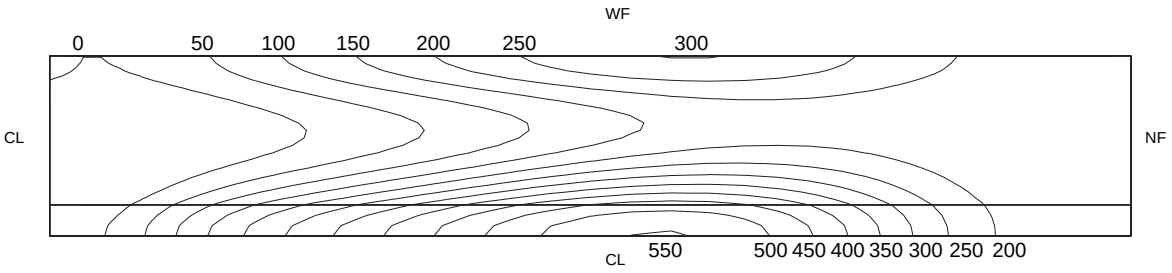

Figure 6.14. Pressure (kg/ms^2) at 1 mm Below Top Surface [Case 3: Standard Conditions, 1.0 mm Bubble Diameter, 20% Gas]

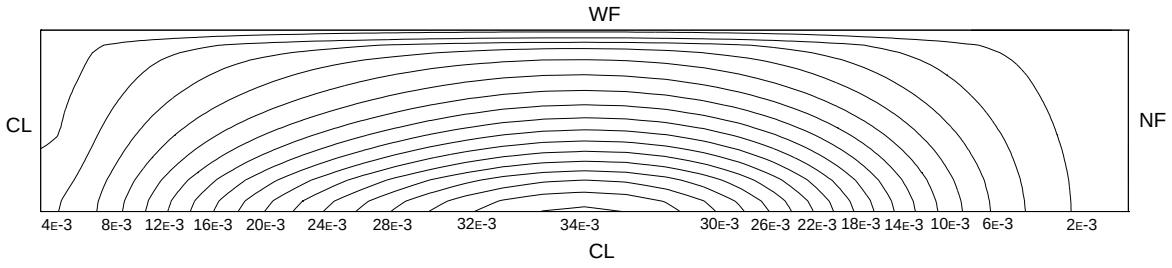

Figure 6.15. Kinetic Energy (m^2/s^2) at 1mm Below Top Surface. [Case 3: Standard Conditions, 1.0 mm Bubble Diameter, 20% Gas]

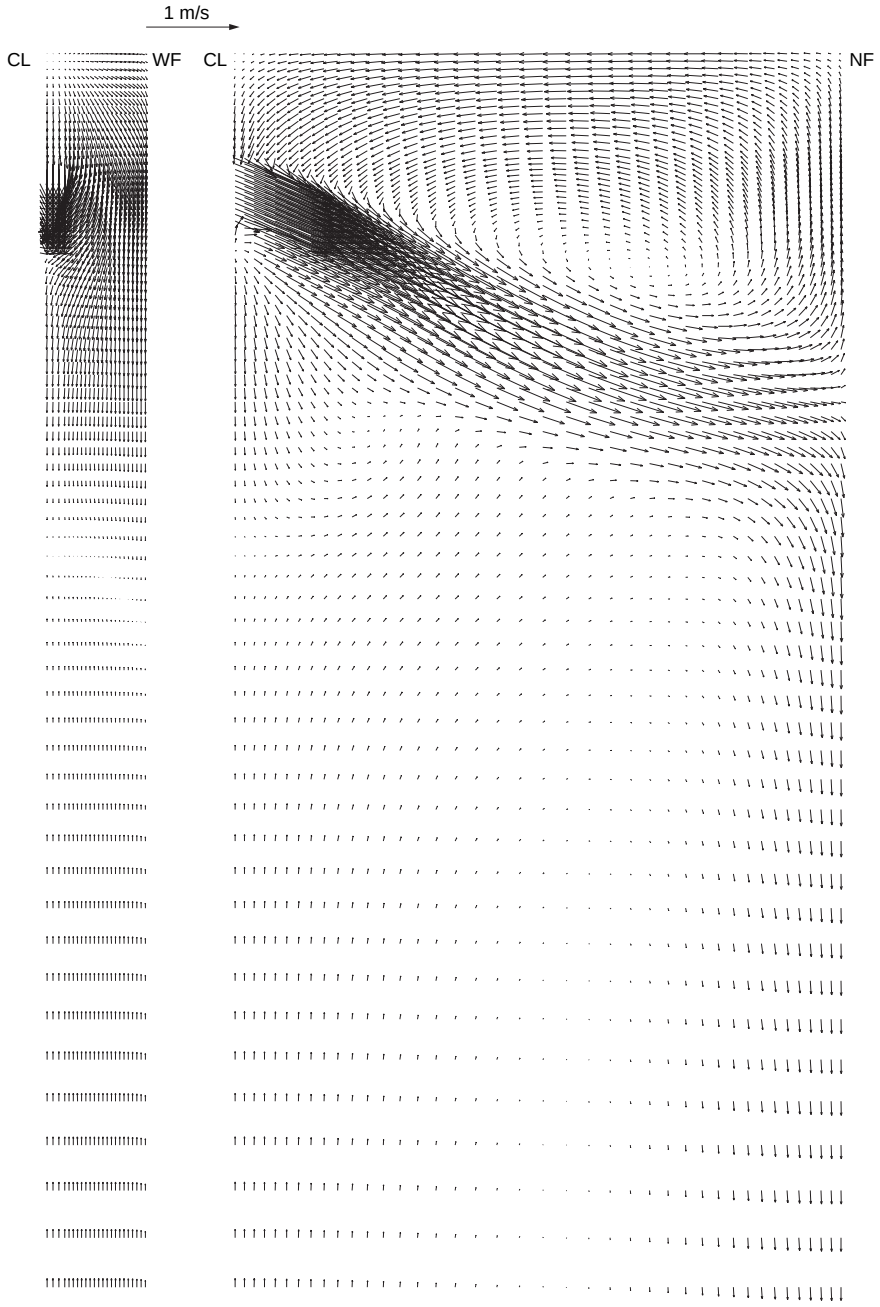

Figure 6.16. Velocity at Centerplane Parallel to Narrow Face (left) and Centerplane Parallel to Wide Face (right). [Case16: Submergence Depth 0.120m, 0% Gas]

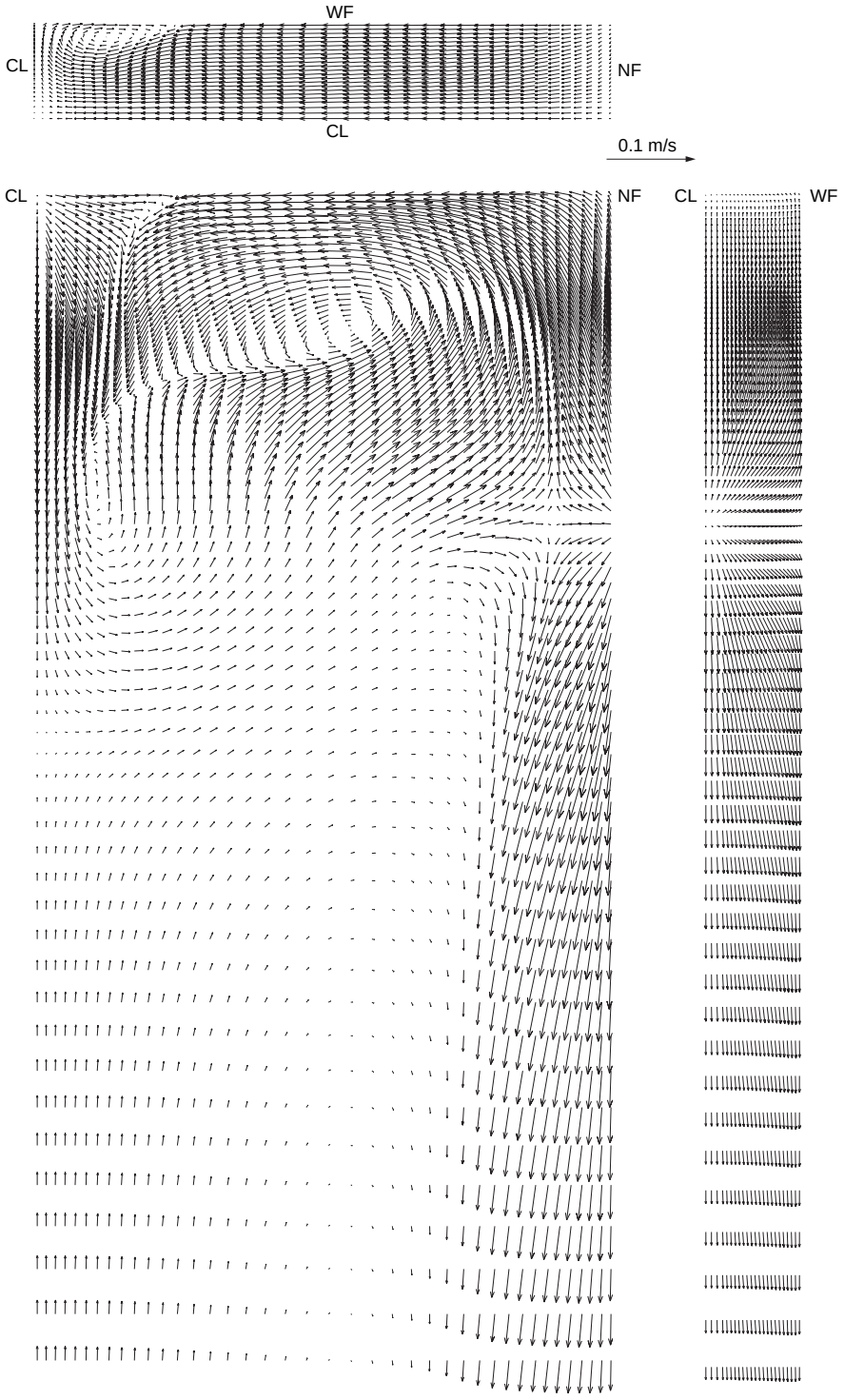

Figure 6.17. Velocity at 1 mm from Narrow Face (left), 1 mm from Wide Face (right), and 1 mm Below the Top Surface [Case16: Submergence Depth 0.120m, 0% Gas]

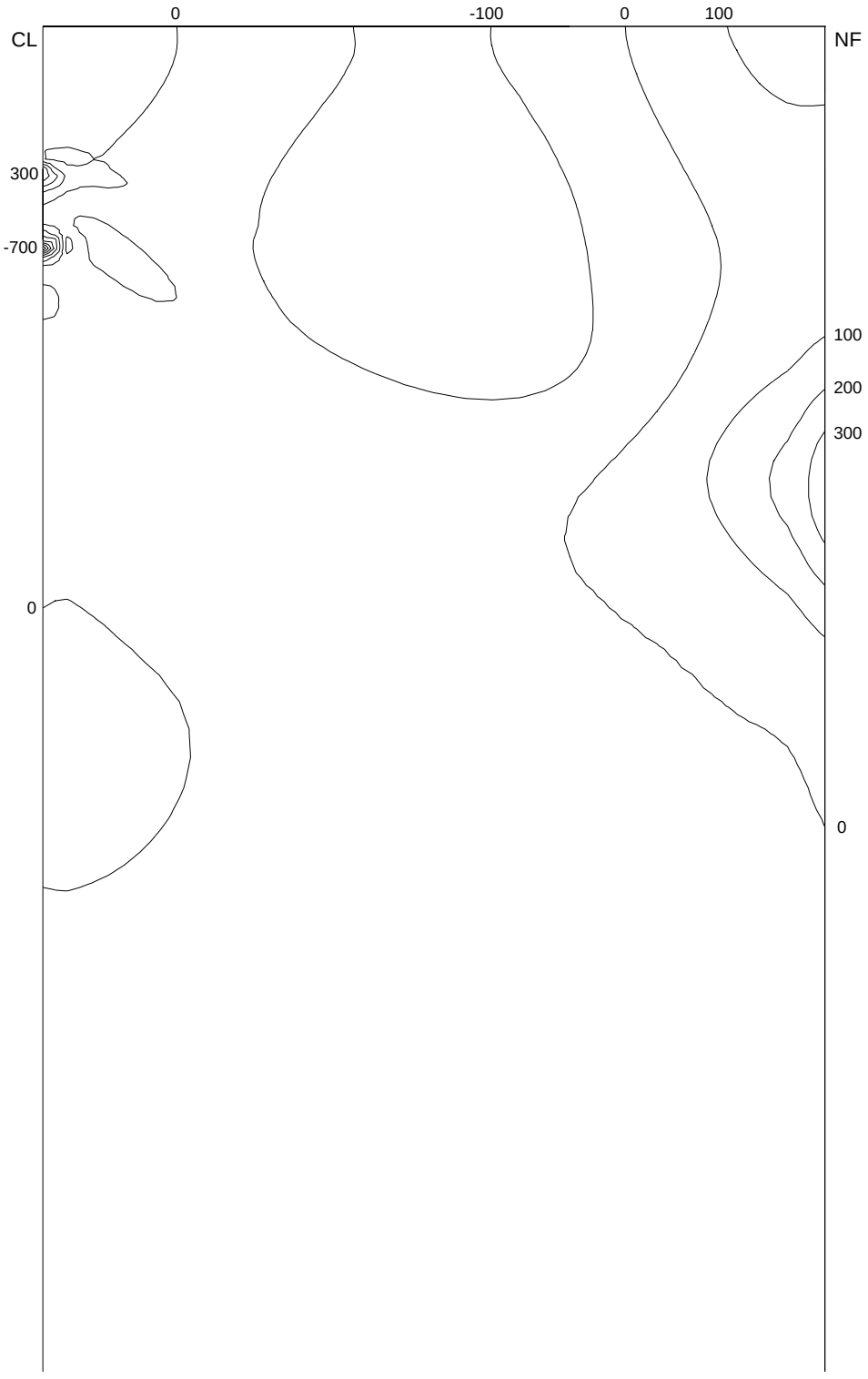

Figure 6.18. Pressure (kg/ms^2) at Centerplane Parallel to Wide Face [Case16: Submergence Depth 0.120m, 0% Gas]

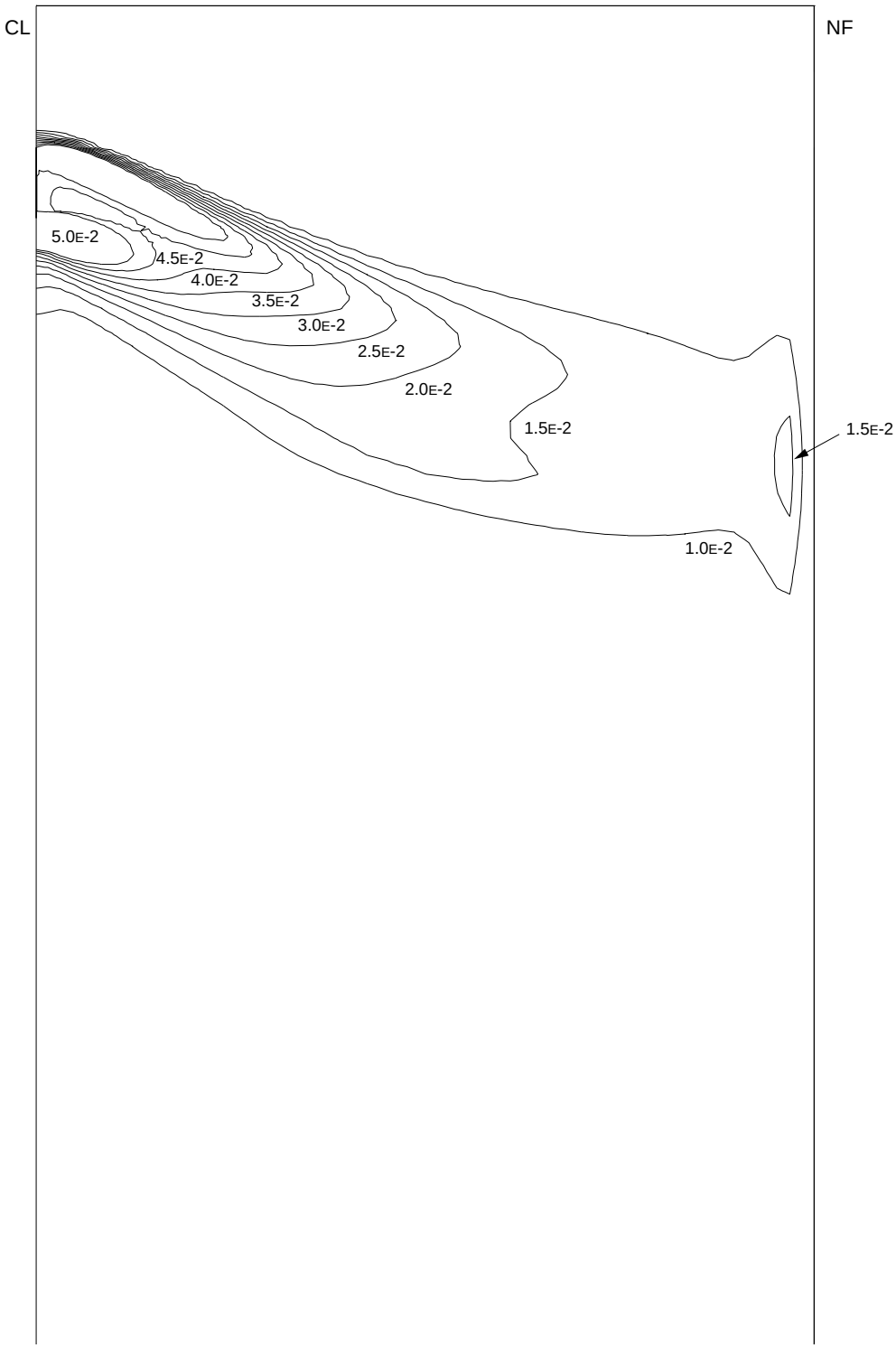

Figure 6.19. Kinetic Energy (m^2/s^2) at Centerplane Parallel to Wide Face [Case16: Submergence Depth 0.120m, 0% Gas]

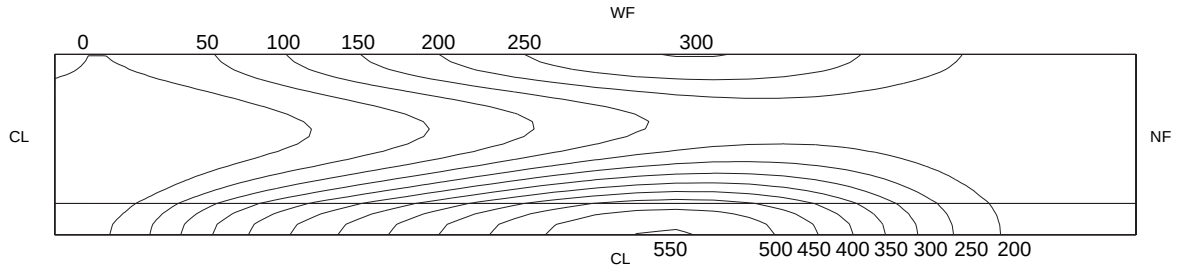

Figure 6.20. Pressure (kg/ms^2) at 1 mm Below Top Surface
[Case16: Submergence Depth 0.120m, 0% Gas]

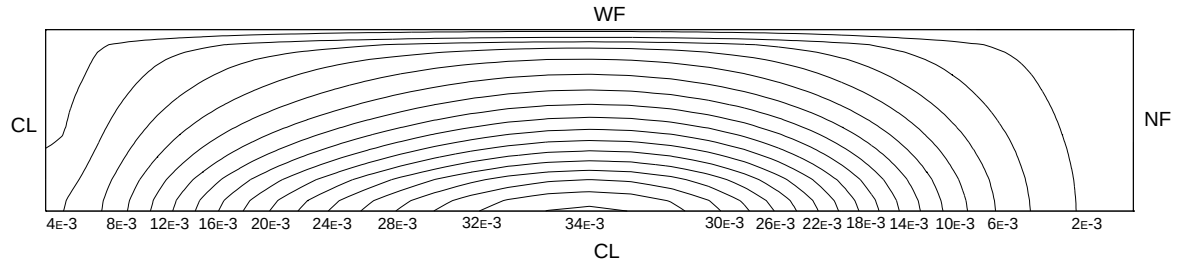

Figure 6.21. Kinetic Energy (m^2/s^2) at 1mm Below Top Surface.
[Case16: Submergence Depth 0.120m, 0% Gas]

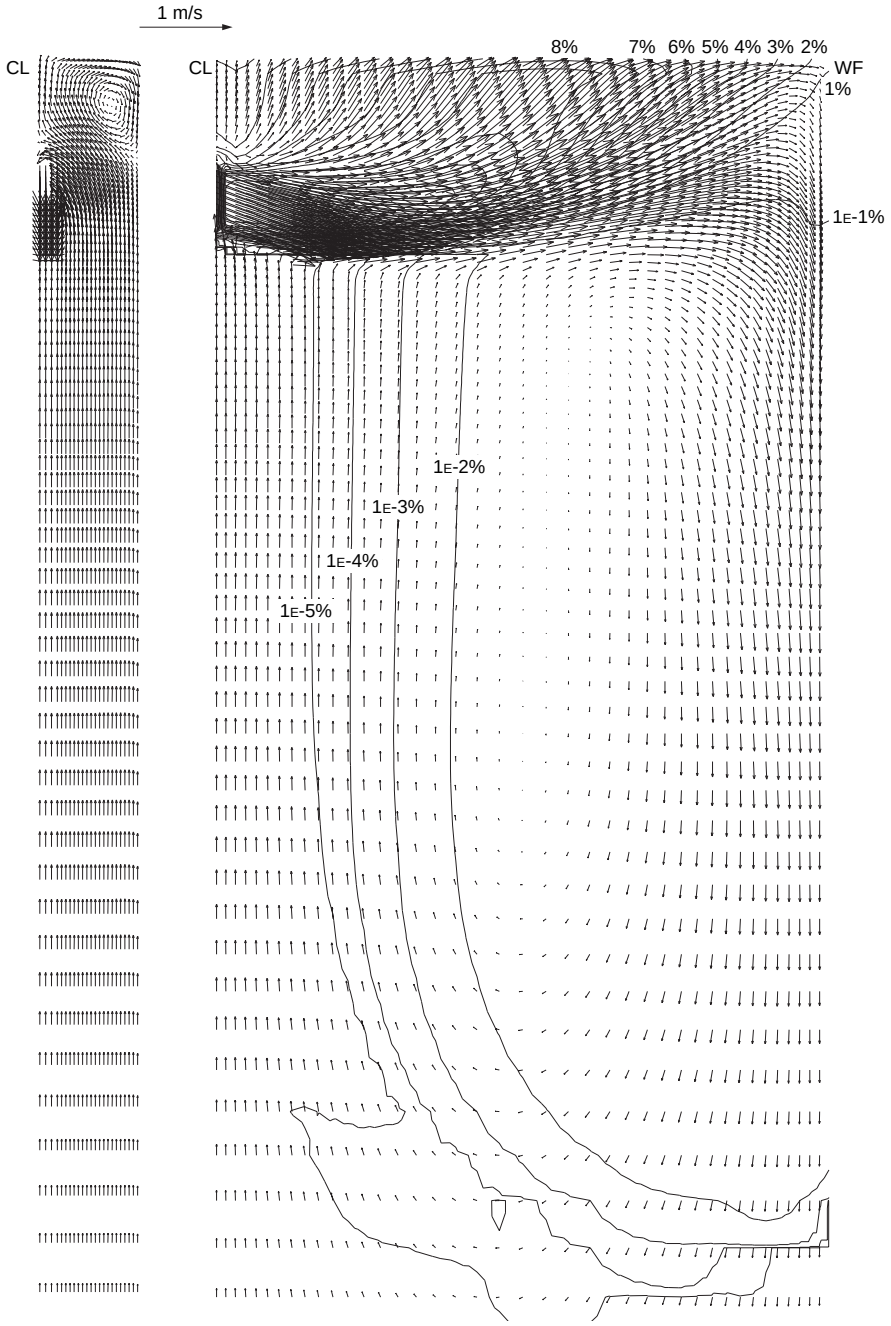

Figure 6.22. Velocity at Centerplane Parallel to Narrow Face (left) and Centerplane Parallel to Wide Face (right). [Case17: Submergence Depth 0.120m, 1.0 mm Bubble Diameter, 20% Gas]

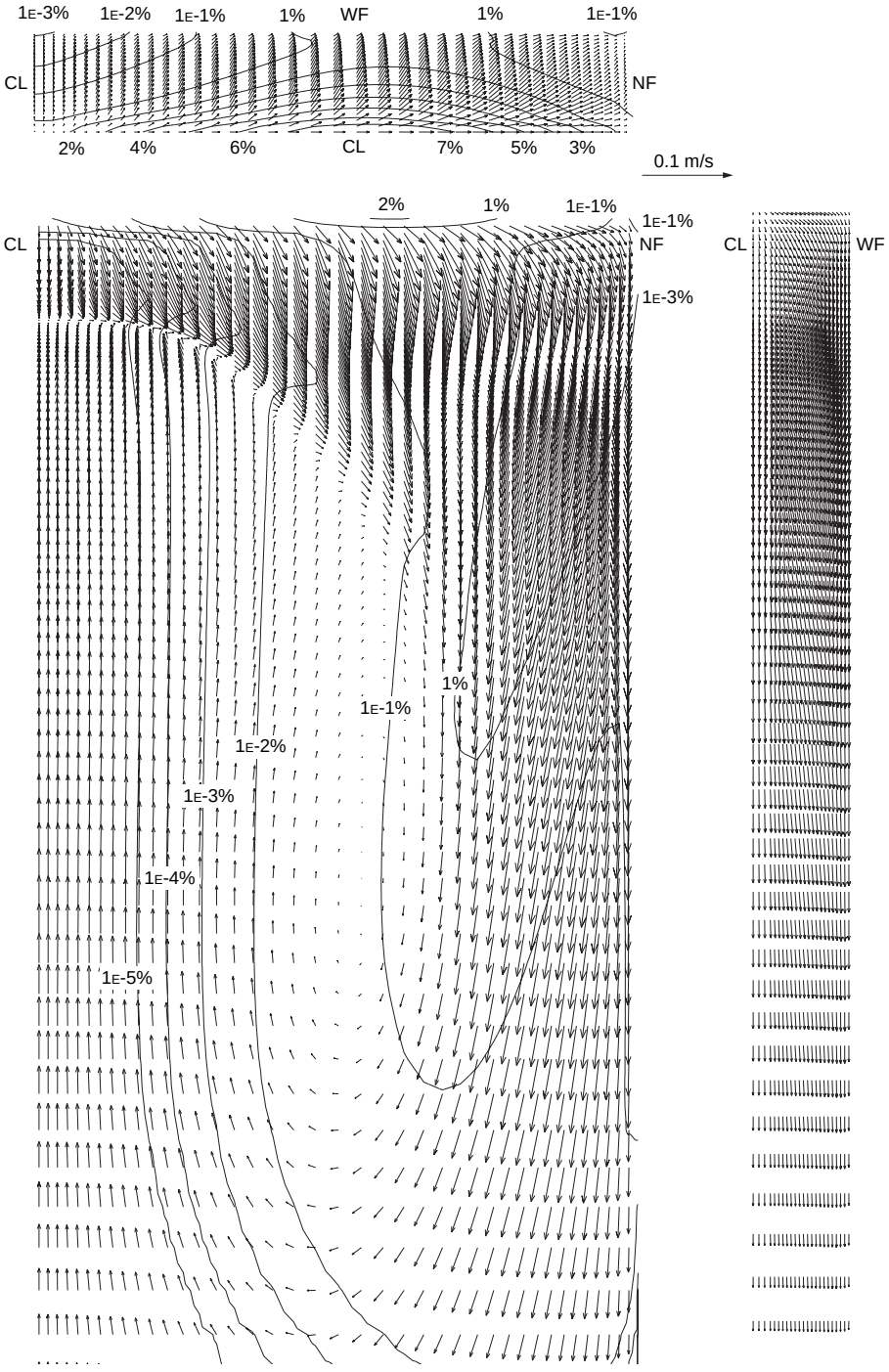

Figure 6.23. Velocity at 1 mm from Narrow Face (left), 1 mm from Wide Face (right), and 1 mm Below the Top Surface [Case17: Submergence Depth 0.120m, 1.0 mm Bubble Diameter, 20% Gas]

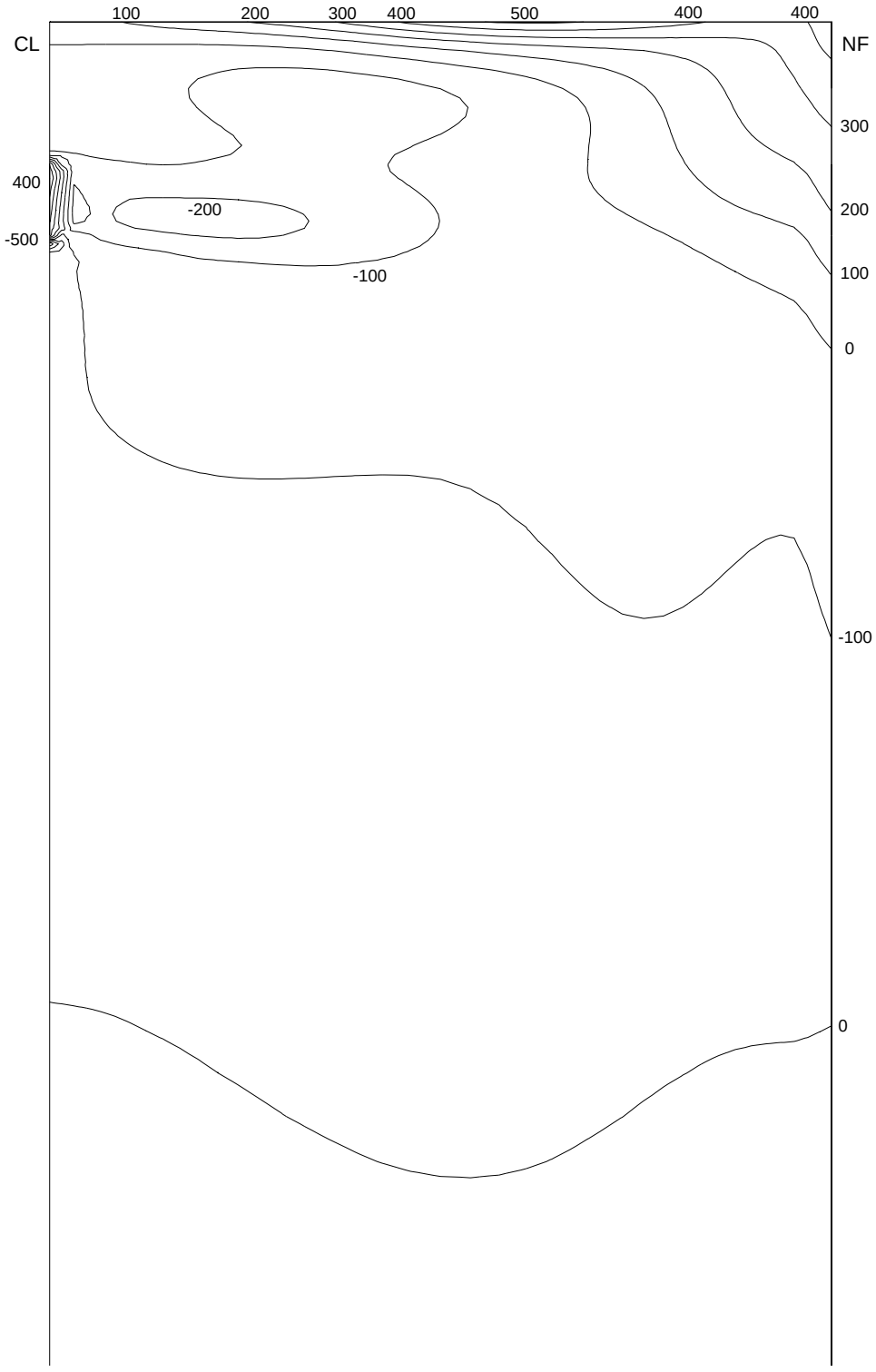

Figure 6.24. Pressure (kg/ms^2) at Centerplane Parallel to Wide Face [Case17: Submergence Depth 0.120m, 1.0 mm Bubble Diameter, 20% Gas]

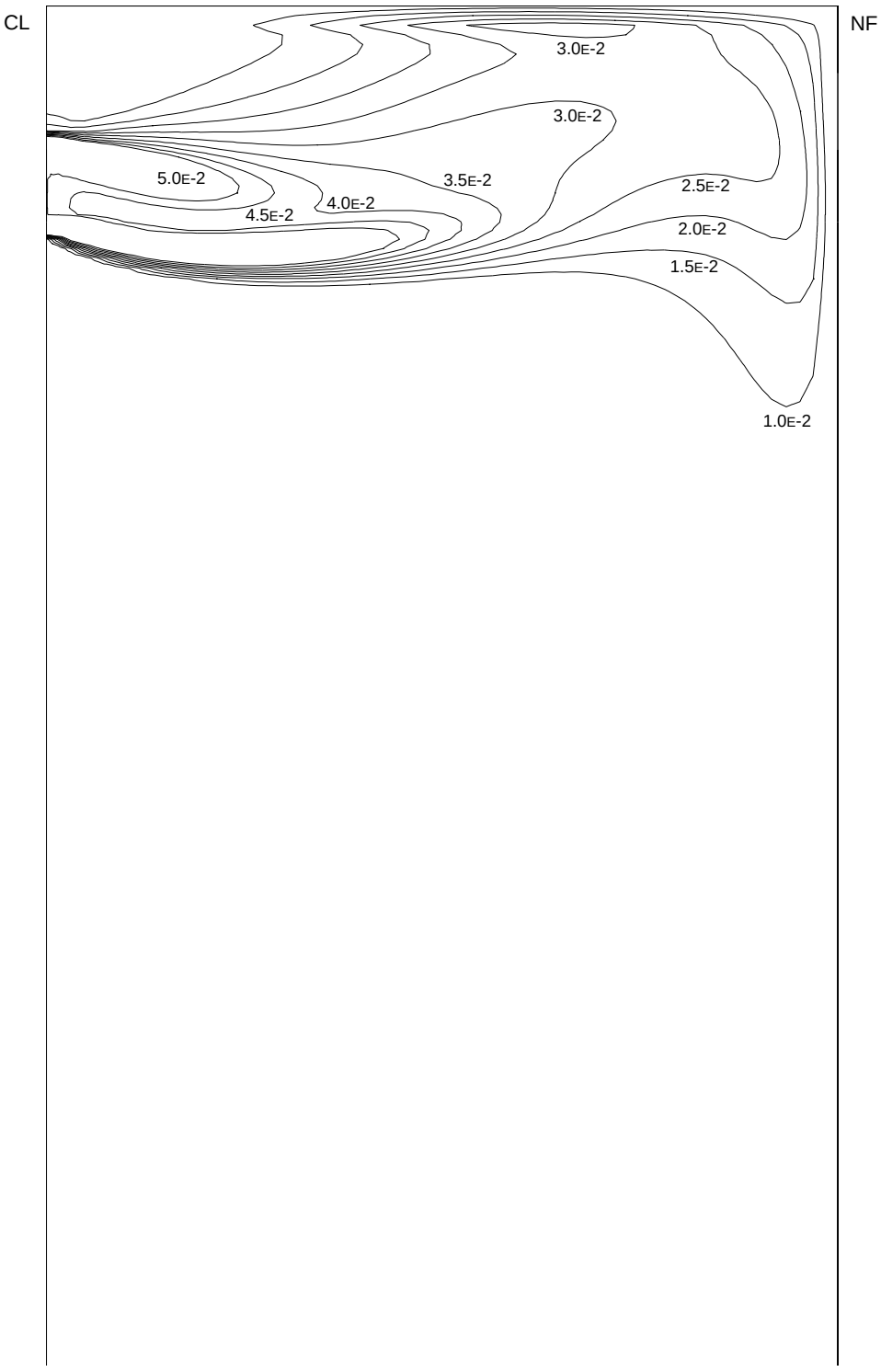

Figure 6.25. Kinetic Energy (m^2/s^2) at Centerplane Parallel to Wide Face [Case17: Submergence Depth 0.120m, 1.0 mm Bubble Diameter, 20% Gas]

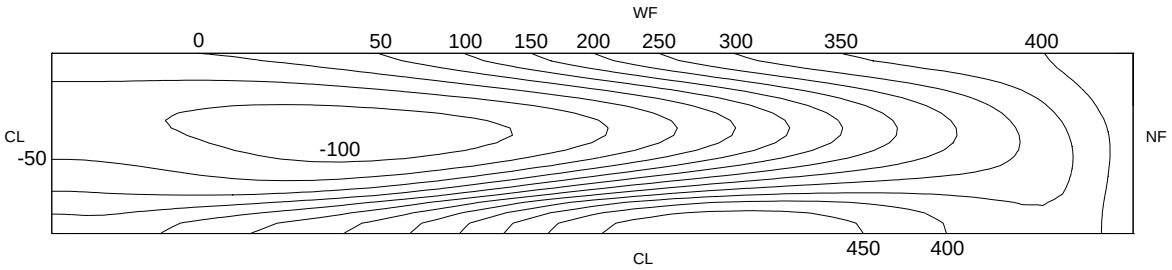

Figure 6.26. Pressure (kg/ms^2) at 1 mm Below Top Surface [Case17: Submergence Depth 0.120m, 1.0 mm Bubble Diameter, 20% Gas]

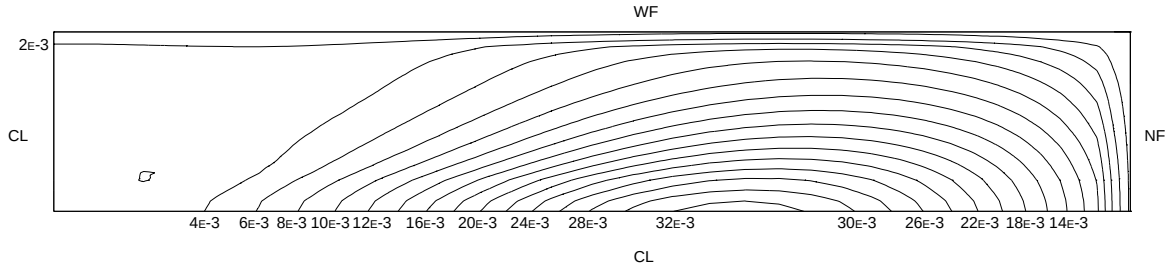

Figure 6.27. Kinetic Energy (m^2/s^2) at 1mm Below Top Surface. [Case17: Submergence Depth 0.120m, 1.0 mm Bubble Diameter, 20% Gas]

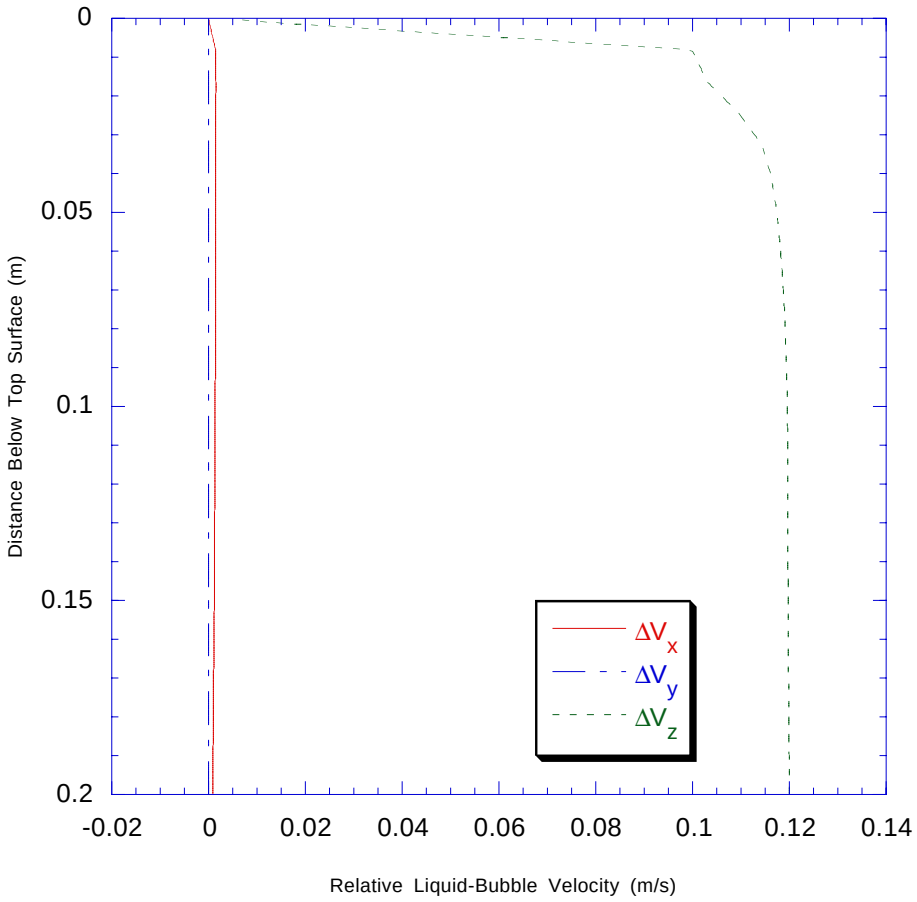

Figure 6.28. Relative Velocity of Liquid and Gas Phases

7 Conclusions

Computational models of turbulent flow, multiphase flow and heat transfer have been developed to analyze phenomena related to steel quality and to compare modeling techniques for flow in the continuous casting nozzle and strand using the CFX computational fluid dynamics package. The effects of grid size, turbulence model and boundary conditions on the heat transfer solution in the mold are compared using a combined turbulent fluid flow and heat transfer model. Models implementing three different strategies for treating the solidification of the steel shell are compared to determine the effect of the shell on flow. A parametric study is performed on a multiphase model of fluid and gas flow in the strand. The effects of gas flow rate, gas bubble diameter, casting speed, nozzle submergence depth and mold width on steel quality issues are quantified

7.1 Turbulence Model Evaluation

Turbulent heat transfer calculations are much more sensitive to the turbulence model and wall boundary conditions than the fluid flow calculation is.

The standard K-ε model using a user supplied wall law for enthalpy in CFX predicts profiles of wall heat flux which match experimental data [22]. Compared to this best model, the standard K-ε model using the default wall law for enthalpy in CFX underpredicts the total heat flux at the narrow face mold wall by 15% and the peak heat flux at the jet impingement point by 50%.

The Low K-ε model is very sensitive to grid refinement, and produces unreliable results on a coarse grid with maximum cell y^+ value at the wall of 6 or 30.

The total heat flux predicted by Low K-ε model with the $y^+<1$ grid is only 10% greater than for the user–modified K-ε model. However, the peak for the Low K-ε model is 174% higher and is only about 80 mm wide at the impingement point, while the peak for the standard K-ε model is approximately 250 mm wide. It is not known which shape is correct, but it is suspected that the user–modified K-ε model prediction is better. In real

life, the jet moves between several steady flow patterns, spreading out the region where heat is delivered. Thus, the standard K-ε model with the user-defined heat transfer wall law appears to be both the most realistic and computationally efficient method to simulate turbulent flow and heat transfer and heat transfer using CFX.

7.2 Effect of the Shell on Fluid Flow

The effects of three ways to account for the solid shell are investigated.

The model including both the shell and the mass transfer across the interface ("Porous Shell model") most closely models what actually happens in the caster.

Modelling the solid shell without accounting for the mass flux creates an acceleration of flow as the fluid moves down the mold. This occurs because the cross sectional area of the domain decreases with distance below the surface, but no fluid is removed through the walls. The flow results for this model become increasingly large below the mold, an unrealistic result. In addition, larger recirculations and eddies are found near the shell, especially at the meniscus. This is because there is no mass sink at the walls to draw the fluid towards the wall.

With no shell at all, the general flow pattern matches with the realistic Porous Shell case quite well. In water modeling, a porous shell is not feasible. Thus, it appears best to simplyignore the shell and build the domain of the water model with a straight sided strand.

7.3 Multiphase Mold Flow

A parametric study on gas flow rate, gas bubble diameter, casting speed, nozzle submergence depth and mold width is performed to quantify the relationship between flow conditions and parameters controlling steel quality.

High gas flow rates are associated with high turbulence levels and surface level fluctuations. This can cause quality problems with the surface of the shell around the

mold perimeter. There is also a higher chance of creating foam, which is bad for the process, and of trapping bubbles lower in the caster, which creates inclusions.

Large bubbles tend to split the jet, making part of it rise to the surface soon after exiting the nozzle. Small bubbles tend to stay with the jet longer, raising the impingement point. The jet will also bend above the impingement point for small bubbles, and below for large bubbles. Small bubbles also penetrate deeper into the mold than large bubbles. Bubbles that penetrate deeply into the mold can be trapped in the solidifying shell and form pencil-pipe defects.

Shallower submergence depth makes single roll flow easier to develop. Single roll flow increases the maximum surface velocity. This increases the chance that liquid flux will be entrained. When flux is entrained in the flow, the flux globules can solidify in the shell, creating inclusions. When the flow changes to a single roll pattern, gas bubbles do not penetrate as deeply into the mold. This will decrease the chance of bubble entrapment and pencil-pipe defects.

A high casting speed, the bubbles have less effect on the flow pattern so single roll flow is less likely. Increasing the casting speed increases the maximum surface velocity, surface level, and surface level fluctuations, all of which are detrimental to steel surface quality.

7.4 Future Work

The work done on turbulent heat transfer is a preliminary step in detailed models of shell solidification and freezing of steel in the meniscus corner. Modeling shell solidification can help to predict when breakouts will occur. Freezing in the meniscus, where the steel, the flux layers and the copper mold meet, creates “hook” defects. By accurately predicting the temperature in the meniscus, the flow conditions that lead to hook defects could be identified.

There are a number of casting parameters that were not looked at in this parametric study. Mold and strand curvature is an important parameter for predicting bubble entrapment.

Models of the curved strand would allow a more detailed study on bubble entrapment, and could help to establish criteria for when pencil-pipe defects will occur. Other casting parameters which have not been studied include the nozzle port angle and the jet characteristics. The jet angle has been shown to change as gas is added [20]. One way to handle this is to include the nozzle in the model, as has been done in the turbulence model and shell growth model sections.

In the real caster, a range of bubble sizes occur. The multiphase model used in this work can be extended to account for the effect of multiple bubble sizes by specifying additional gas phases, each with a different bubble diameter.

The effect of gas flow rate on maximum surface velocity has been quantified in this study, but the effect of gas on the critical surface velocity is currently unknown. By determining this relationship, a criteria for liquid flux entrainment could be developed.

Appendix A. Derivation of Wall Law for Heat Transfer

In CFX, we change a wall law with the USRWTM Fortran subroutine by specifying the turbulent multiplier, which is defined as

$$TMULT = \frac{Variable\ \ at\ \ Wall - Variable\ \ at\ \ Nearest\ \ Node}{Flux\ \ of\ \ Variable} \tag{A.1}$$

Fourier's Law of heat conduction is

$$q = -\frac{k_t}{C_p}\frac{dH}{dx} \tag{A.2}$$

where k_t is the turbulent conductivity of the fluid, H is enthalpy, and C_p is the specific heat of the fluid.

For the enthalpy equation, the turbulent multiplier becomes

$$TMULT = \frac{dH}{q} = \frac{k_t}{C_p dx} \tag{A.3}$$

The turbulent conductivity is defined as

$$k_t = \frac{C_p \mu_t}{\mathrm{Pr}_t} \tag{A.4}$$

where μ_t is the turbulent viscosity and Pr_t is the turbulent Prandtl number. The turbulent viscosity is defined as

$$\mu_t = \frac{C_\mu K^2 \rho}{\varepsilon} \tag{A.5}$$

where C_μ is the constant 0.09, K is the turbulent kinetic energy, and ε is the turbulent dissipation. Substituting for μ_t and k_t, the turbulent multiplier can be rewritten as

$$TMULT = \frac{C_\mu K^2 \rho}{\varepsilon \mathrm{Pr}_t\, dx} \tag{A.6}$$

Appendix B. User Wall Law for Heat Transfer

```
C+++++++++++++++++ USER AREA 5 ++++++++++++++++++++++++++++++++++++++++++
C
C
C-----TURBULENT WALL LAW TO CORRECT HEAT TRANSFER AT WALLS
C
C**********************************************************************
C   CREATED
C      07/01/98  DAVID T. CREECH
C
C**********************************************************************
C
      CALL IPALL('*','WALL','PATCH','CENTRES',IPT,NPT,CWORK,IWORK)
C
C  FIND VARIABLE NUMBER FOR ENTHALPY
      CALL GETVAR('USRWTM','H     ',IVAR)
C  IF ENTHALPY EQUATION SET MULTIPLIER
      IF (IVAR.EQ.IEQN) THEN
         PRANDT = PRT(IVAR,1)
      DO 120 I = 1, NPT
         INODE = IPT(I)
         IBDRY = INODE - NCELL
         LCV   = IBDRY - ISTART + 1
         INODE1 = IPNODB(IBDRY,1)
         CMU = 0.09
         DENS = DEN(INODE1,1)
         DENSQK = DEN(INODE1,1) * SQRT( TE(INODE1,1) )
         EPSILON = ED(INODE,1)
         AKE = TE(INODE1,1)
         AKK = AKE*AKE
C    CALCULATE NORMAL DISTANCE FROM NODE TO WALL
C
         DN = YWALL(LCV)
C         WRITE(NWRITE,*) YWALL(LCV)
C
C     COMPUTE MULTIPLIER
         TMULT(LCV,1) = (CMU*DENS*AKK)/(PRANDT*DN*EPSILON)
  120 CONTINUE
C
      END IF
C
C+++++++++++++++++ END OF USER AREA 5 +++++++++++++++++++++++++++++++++++
```

Appendix C. User Subroutine for Shell Model Source Term

```
      SUBROUTINE USRSRC(IEQN,ICALL,CNAME,CALIAS,AM,SP,SU,CONV
     +                 ,U,V,W,P,VFRAC,DEN,VIS,TE,ED,RS,T,H,RF,SCAL
     +                 ,XP,YP,ZP,VOL,AREA,VPOR,ARPOR,WFACT,IPT
     +                 ,IBLK,IPVERT,IPNODN,IPFACN,IPNODF,IPNODB,IPFACB
     +                 ,WORK,IWORK,CWORK)
C
C***********************************************************************
C
C   UTILITY SUBROUTINE FOR USER-SUPPLIED SOURCES
C
C   >>> IMPORTANT                                                    <<<
C   >>>                                                             <<<
C   >>> USERS MAY ONLY ADD OR ALTER PARTS OF THE SUBROUTINE WITHIN  <<<
C   >>> THE DESIGNATED USER AREAS                                   <<<
C
C***********************************************************************
C
C   THIS SUBROUTINE IS CALLED BY THE FOLLOWING SUBROUTINES
C      CUSR  SCDF  SCDS  SCED  SCENRG  SCHF  SCMOM  SCPCE  SCSCAL
C      SCTE  SCVF
C
C***********************************************************************
C   CREATED
C      08/03/90  ADB
C   MODIFIED
C      04/03/91  ADB  ALTERED ARGUMENT LIST.
C      28/08/91  IRH  NEW STRUCTURE
C      28/09/91  IRH  CHANGE EXAMPLE + ADD COMMON BLOCKS
C      10/02/92  PHA  UPDATE CALLED BY COMMENT, ADD RF ARGUMENT,
C                     CHANGE LAST DIMENSION OF RS TO 6 AND IVERS TO 2
C      03/06/92  PHA  ADD PRECISION FLAG AND CHANGE IVERS TO 3
C      23/11/93  CSH  EXPLICITLY DIMENSION IPVERT ETC.
C      07/12/93  NSW  INCLUDE CONV IN ARGUMENT LIST AND CHANGE IVERS
C                     TO 4
C      03/02/94  PHA  CHANGE FLOW3D TO CFDS-FLOW3D
C      03/03/94  FHW  CORRECTION OF SPELLING MISTAKE
C      08/03/94  NSW  CORRECT SPELLING
C      09/08/94  NSW  CORRECT SPELLING.
C                     MOVE 'IF(IUSED.EQ.0) RETURN' OUT OF USER AREA.
C                     INCLUDE COMMENT ON MASS SOURCES.
C      19/12/94  NSW  CHANGE FOR CFX-F3D
C      02/07/97  NSW  UPDATE FOR CFX-4
C
C***********************************************************************
C
C   SUBROUTINE ARGUMENTS
C
C     IEQN   - EQUATION NUMBER
C     ICALL  - SUBROUTINE CALL
C     CNAME  - EQUATION NAME
C     CALIAS - ALIAS OF EQUATION NAME
C     AM     - OFF DIAGONAL MATRIX COEFFICIENTS
C     SU     - SU IN LINEARISATION OF SOURCE TERM
C     SP     - SP IN LINEARISATION OF SOURCE TERM
C     CONV   - CONVECTION COEFFICIENTS
C     U      - U COMPONENT OF VELOCITY
C     V      - V COMPONENT OF VELOCITY
C     W      - W COMPONENT OF VELOCITY
C     P      - PRESSURE
C     VFRAC  - VOLUME FRACTION
C     DEN    - DENSITY OF FLUID
C     VIS    - VISCOSITY OF FLUID
C     TE     - TURBULENT KINETIC ENERGY
C     ED     - EPSILON
C     RS     - REYNOLD STRESSES
C     T      - TEMPERATURE
C     H      - ENTHALPY
C     RF     - REYNOLD FLUXES
C     SCAL   - SCALARS (THE FIRST 'NCONC' OF THESE ARE MASS FRACTIONS)
C     XP     - X COORDINATES OF CELL CENTRES
C     YP     - Y COORDINATES OF CELL CENTRES
```

```
C     ZP     - Z COORDINATES OF CELL CENTRES
C     VOL    - VOLUME OF CELLS
C     AREA   - AREA OF CELLS
C     VPOR   - POROUS VOLUME
C     ARPOR  - POROUS AREA
C     WFACT  - WEIGHT FACTORS
C
C     IPT    - 1D POINTER ARRAY
C     IBLK   - BLOCK SIZE INFORMATION
C     IPVERT - POINTER FROM CELL CENTERS TO 8 NEIGHBOURING VERTICES
C     IPNODN - POINTER FROM CELL CENTERS TO 6 NEIGHBOURING CELLS
C     IPFACN - POINTER FROM CELL CENTERS TO 6 NEIGHBOURING FACES
C     IPNODF - POINTER FROM CELL FACES TO 2 NEIGHBOURING CELL CENTERS
C     IPNODB - POINTER FROM BOUNDARY CENTERS TO CELL CENTERS
C     IPFACB - POINTER FROM BOUNDARY CENTERS TO BOUNDARY FACESS
C
C     WORK   - REAL WORKSPACE ARRAY
C     IWORK  - INTEGER WORKSPACE ARRAY
C     CWORK  - CHARACTER WORKSPACE ARRAY
C
C   SUBROUTINE ARGUMENTS PRECEDED WITH A '*' ARE ARGUMENTS THAT MUST
C   BE SET  BY THE USER IN THIS ROUTINE.
C
C   NOTE THAT WHEN USING MASS SOURCES, THE FLOWS THROUGH MASS FLOW
C   BOUNDARIES ARE UNCHANGED. THE USER SHOULD THEREFORE INCLUDE AT
C   LEAST ONE PRESSURE BOUNDARY FOR SUCH A CALCULATION.
C
C   NOTE THAT OTHER DATA MAY BE OBTAINED FROM CFX-4 USING THE
C   ROUTINE GETADD, FOR FURTHER DETAILS SEE THE VERSION 4
C   USER MANUAL.
C
C*********************************************************************
C
      LOGICAL LDEN,LVIS,LTURB,LTEMP,LBUOY,LSCAL,LCOMP
     +       ,LRECT,LCYN,LAXIS,LPOROS,LTRANS
C
      CHARACTER*(*) CWORK
      CHARACTER     CNAME*6, CALIAS*24
C
C+++++++++++++++++ USER AREA 1 +++++++++++++++++++++++++++++++++++++++++
C---- AREA FOR USERS EXPLICITLY DECLARED VARIABLES
C
C+++++++++++++++++ END OF USER AREA 1 +++++++++++++++++++++++++++++++++++
C
      COMMON
     + /ALL/    NBLOCK,NCELL,NBDRY,NNODE,NFACE,NVERT,NDIM
     + /ALLWRK/ NRWS,NIWS,NCWS,IWRFRE,IWIFRE,IWCFRE
     + /ADDIMS/ NPHASE,NSCAL,NVAR,NPROP
     +         ,NDVAR,NDPROP,NDXNN,NDGEOM,NDCOEF,NILIST,NRLIST,NTOPOL
     + /CHKUSR/ IVERS,IUCALL,IUSED
     + /DEVICE/ NREAD,NWRITE,NRDISK,NWDISK
     + /IDUM/   ILEN,JLEN
     + /LOGIC/  LDEN,LVIS,LTURB,LTEMP,LBUOY,LSCAL,LCOMP
     +         ,LRECT,LCYN,LAXIS,LPOROS,LTRANS
     + /MLTGRD/ MLEVEL,NLEVEL,ILEVEL
     + /SGLDBL/ IFLGPR,ICHKPR
     + /SPARM/  SMALL,SORMAX,NITER,INDPRI,MAXIT,NODREF,NODMON
     + /TRANSI/ NSTEP,KSTEP,MF,INCORE
     + /TRANSR/ TIME,DT,DTINVF,TPARM
C
C+++++++++++++++++ USER AREA 2 +++++++++++++++++++++++++++++++++++++++++
C---- AREA FOR USERS TO DECLARE THEIR OWN COMMON BLOCKS
C     THESE SHOULD START WITH THE CHARACTERS 'UC' TO ENSURE
C     NO CONFLICT WITH NON-USER COMMON BLOCKS
C
      COMMON /UCSURF/ JSURF,NSURF
      COMMON /UCFLUX/ SINKFLUX,VC
C
C+++++++++++++++++ END OF USER AREA 2 +++++++++++++++++++++++++++++++++++
C
      DIMENSION AM(NCELL,6,NPHASE),SP(NCELL,NPHASE),SU(NCELL,NPHASE)
     +,CONV(NFACE,NPHASE)
C
      DIMENSION
     + U(NNODE,NPHASE),V(NNODE,NPHASE),W(NNODE,NPHASE),P(NNODE,NPHASE)
     +,VFRAC(NNODE,NPHASE),DEN(NNODE,NPHASE),VIS(NNODE,NPHASE)
```

```
     +,TE(NNODE,NPHASE),ED(NNODE,NPHASE),RS(NNODE,NPHASE,6)
     +,T(NNODE,NPHASE),H(NNODE,NPHASE),RF(NNODE,NPHASE,4)
     +,SCAL(NNODE,NPHASE,NSCAL)
C
      DIMENSION
     + XP(NNODE),YP(NNODE),ZP(NNODE)
     +,VOL(NCELL),AREA(NFACE,3),VPOR(NCELL),ARPOR(NFACE,3)
     +,WFACT(NFACE)
     +,IPT(*),IBLK(5,NBLOCK)
     +,IPVERT(NCELL,8),IPNODN(NCELL,6),IPFACN(NCELL,6),IPNODF(NFACE,4)
     +,IPNODB(NBDRY,4),IPFACB(NBDRY)
     +,IWORK(*),WORK(*),CWORK(*)
C
C+++++++++++++++++ USER AREA 3 ++++++++++++++++++++++++++++++++++++++++
C---- AREA FOR USERS TO DIMENSION THEIR ARRAYS
C
C---- AREA FOR USERS TO DEFINE DATA STATEMENTS
C
C+++++++++++++++++ END OF USER AREA 3 +++++++++++++++++++++++++++++++++
C
C---- STATEMENT FUNCTION FOR ADDRESSING
      IP(I,J,K)=IPT((K-1)*ILEN*JLEN+(J-1)*ILEN+I)
C
C----VERSION NUMBER OF USER ROUTINE AND PRECISION FLAG
C
      IVERS=4
      ICHKPR = 1
C
C+++++++++++++++++ USER AREA 4 ++++++++++++++++++++++++++++++++++++++++
C---- TO USE THIS USER ROUTINE FIRST SET IUSED=1
C
       IUSED=1
C
C+++++++++++++++++ END OF USER AREA 4 +++++++++++++++++++++++++++++++++
C
       IF (IUSED.EQ.0) RETURN
C
C---- FRONTEND CHECKING OF USER ROUTINE
       IF (IUCALL.EQ.0) RETURN
C
C---- ADD TO SOURCE TERMS
      IF (ICALL.EQ.1) THEN
C
C+++++++++++++++++ USER AREA 5 ++++++++++++++++++++++++++++++++++++++++
C
C-----------------------------------------------------------------------
C
C     USRSRC CALCULATES THE SOURCE TERM FOR REMOVING THE SOLIDIFYING
C     FLUID FROM THE DOMAIN. THE PHASE TO BE REMOVED, THE POSITION
C     OF THE MENISCUS IN THE GEOMETRY, THE CASTING SPEED AND THE SHELL
C     GROWTH CONSTANT MUST BE SET. OTHER PARAMETERS MUST BE SET IN
C     THE USRTRN SUBROUTINE. THE SINK BOUNDARY WORKSPACE, JSURF AND
C     NSURF, IS PASSED BY THE COMMON BLOCK FROM USRTRN.
C
C-----------------------------------------------------------------------
C
C---- ADD FLUID SINK TO PATCH 'SINK'
C
C#####################################################################
C ENTER MODEL PARAMETERS
C#####################################################################
C
C SET SINK PHASE INDEX
      IPHSK= 1
C SET Z POSITION OF MENISCUS, ZM, IN M
      ZM   = .559043
C SET CASTING SPEED, VC, IN M/S
      VC   = .0254
C SET SHELL GROWTH CONSTANT, AK, IN M/SQRT(S)
      AK   = 0.00327912
C
C#####################################################################
C#####################################################################
C
C  PRESSURE
C
```

```
      IF(CALIAS.EQ.'PRESSURE') THEN
C
C      SUA = 0
C      SUB = 0
C  LOOP OVER PATCH
       TOTAL = 0.0
       DO 101 I=1,NSURF
         INODE = IWORK(JSURF+I-1)
         IBDRY = INODE-NCELL
         INODE1= IPNODB(IBDRY,1)
         IFACE = IPFACB(IBDRY)
         AREAM = SQRT ( AREA(IFACE,1)*AREA(IFACE,1)
     +                 +AREA(IFACE,2)*AREA(IFACE,2)
     +                 +AREA(IFACE,3)*AREA(IFACE,3) )
         DENST = DEN(INODE1,1)
         VN    = VC/SQRT(1+(4*VC*(ZP(INODE1)-ZM))/(AK*AK))
         FLUX  = DENST*AREAM*VN
         SU(INODE1,1)=SU(INODE1,IPHSK)-FLUX
         TOTAL = TOTAL+FLUX
 101   CONTINUE
C
       SINKFLUX = TOTAL
C
       ENDIF
C
C-----------------------------------------------------------------
C  U VELOCITY
C
       IF(CALIAS.EQ.'U VELOCITY') THEN
C
C      SUA = 0
C      SUB = 0
C  LOOP OVER PATCH
       TOTAL = 0.0
       DO 201 I=1,NSURF
         INODE = IWORK(JSURF+I-1)
         IBDRY = INODE-NCELL
         INODE1= IPNODB(IBDRY,1)
         IFACE = IPFACB(IBDRY)
         AREAM = SQRT ( AREA(IFACE,1)*AREA(IFACE,1)
     +                 +AREA(IFACE,2)*AREA(IFACE,2)
     +                 +AREA(IFACE,3)*AREA(IFACE,3) )
         DENST = DEN(INODE1,1)
         VN    = VC/SQRT(1+(4*VC*(ZP(INODE1)-ZM))/(AK*AK))
         FLUX  = DENST*AREAM*VN
         SP(INODE1,1)=SP(INODE1,IPHSK)-FLUX
         TOTAL = TOTAL+FLUX
 201   CONTINUE
C
       ENDIF
C
C-----------------------------------------------------------------
C  V VELOCITY
C
       IF(CALIAS.EQ.'V VELOCITY') THEN
C
C      SUA = 0
C      SUB = 0
C  LOOP OVER PATCH
       TOTAL = 0.0
       DO 301 I=1,NSURF
         INODE = IWORK(JSURF+I-1)
         IBDRY = INODE-NCELL
         INODE1= IPNODB(IBDRY,1)
         IFACE = IPFACB(IBDRY)
         AREAM = SQRT ( AREA(IFACE,1)*AREA(IFACE,1)
     +                 +AREA(IFACE,2)*AREA(IFACE,2)
     +                 +AREA(IFACE,3)*AREA(IFACE,3) )
         DENST = DEN(INODE1,1)
         VN    = VC/SQRT(1+(4*VC*(ZP(INODE1)-ZM))/(AK*AK))
         FLUX  = DENST*AREAM*VN
         SP(INODE1,1)=SP(INODE1,IPHSK)-FLUX
         TOTAL = TOTAL+FLUX
 301   CONTINUE
C
       ENDIF
```

```
C
C-------------------------------------------------------------
C  W VELOCITY
C
      IF(CALIAS.EQ.'W VELOCITY') THEN
C
C      SUA = 0
C      SUB = 0
C  LOOP OVER PATCH
       TOTAL = 0.0
       DO 401 I=1,NSURF
         INODE = IWORK(JSURF+I-1)
         IBDRY = INODE-NCELL
         INODE1= IPNODB(IBDRY,1)
         IFACE = IPFACB(IBDRY)
         AREAM = SQRT ( AREA(IFACE,1)*AREA(IFACE,1)
     +                 +AREA(IFACE,2)*AREA(IFACE,2)
     +                 +AREA(IFACE,3)*AREA(IFACE,3) )
         DENST = DEN(INODE1,1)
         VN    = VC/SQRT(1+(4*VC*(ZP(INODE1)-ZM))/(AK*AK))
         FLUX  = DENST*AREAM*VN
         SP(INODE1,1)=SP(INODE1,IPHSK)-FLUX
         TOTAL = TOTAL+FLUX
 401   CONTINUE
C
       ENDIF
C
C-------------------------------------------------------------
C-------------------------------------------------------------
C
C---- END
C
C+++++++++++++++++ END OF USER AREA 5 +++++++++++++++++++++++++++++++++
       ENDIF
C
C---- OVERWRITE SOURCE TERMS
       IF (ICALL.EQ.2) THEN
C
C+++++++++++++++++ USER AREA 6 +++++++++++++++++++++++++++++++++++++++
C
C+++++++++++++++++ END OF USER AREA 6 +++++++++++++++++++++++++++++++++
C
       ENDIF
       RETURN
       END
C
       SUBROUTINE USRTRN(U,V,W,P,VFRAC,DEN,VIS,TE,ED,RS,T,H,RF,SCAL,
     +                  XP,YP,ZP,VOL,AREA,VPOR,ARPOR,WFACT,CONV,IPT,
     +                  IBLK,IPVERT,IPNODN,IPFACN,IPNODF,IPNODB,IPFACB,
     +                  WORK,IWORK,CWORK)
C
C**********************************************************************
C
C   USER SUBROUTINE TO ALLOW USERS TO MODIFY OR MONITOR THE SOLUTION AT
C   THE END OF EACH TIME STEP
C   THIS SUBROUTINE IS CALLED BEFORE THE START OF THE RUN AS WELL AS AT
C   THE END OF EACH TIME STEP
C
C   >>> IMPORTANT                                                  <<<
C   >>>                                                           <<<
C   >>> USERS MAY ONLY ADD OR ALTER PARTS OF THE SUBROUTINE WITHIN  <<<
C   >>> THE DESIGNATED USER AREAS                                  <<<
C
C**********************************************************************
C
C   THIS SUBROUTINE IS CALLED BY THE FOLLOWING SUBROUTINES
C      CUSR  TRNMOD
C
C**********************************************************************
C   CREATED
C      27/04/90  ADB
C   MODIFIED
C      05/08/91  IRH  NEW STRUCTURE
C      01/10/91  DSC  REDUCE COMMENT LINE GOING OVER COLUMN 72.
C      29/11/91  PHA  UPDATE CALLED BY COMMENT, ADD RF ARGUMENT,
C                     CHANGE LAST DIMENSION OF RS TO 6 AND IVERS TO 2
```

```
C      05/06/92  PHA  ADD PRECISION FLAG AND CHANGE IVERS TO 3
C      03/07/92  DSC  CORRECT COMMON MLTGRD.
C      23/11/93  CSH  EXPLICITLY DIMENSION IPVERT ETC.
C      03/02/94  PHA  CHANGE FLOW3D TO CFDS-FLOW3D
C      22/08/94  NSW  MOVE 'IF(IUSED.EQ.0) RETURN' OUT OF USER AREA
C      19/12/94  NSW  CHANGE FOR CFX-F3D
C      02/07/97  NSW  UPDATE FOR CFX-4
C
C*********************************************************************
C
C   SUBROUTINE ARGUMENTS
C
C     U      - U COMPONENT OF VELOCITY
C     V      - V COMPONENT OF VELOCITY
C     W      - W COMPONENT OF VELOCITY
C     P      - PRESSURE
C     VFRAC  - VOLUME FRACTION
C     DEN    - DENSITY OF FLUID
C     VIS    - VISCOSITY OF FLUID
C     TE     - TURBULENT KINETIC ENERGY
C     ED     - EPSILON
C     RS     - REYNOLD STRESSES
C     T      - TEMPERATURE
C     H      - ENTHALPY
C     RF     - REYNOLD FLUXES
C     SCAL   - SCALARS (THE FIRST 'NCONC' OF THESE ARE MASS FRACTIONS)
C     XP     - X COORDINATES OF CELL CENTRES
C     YP     - Y COORDINATES OF CELL CENTRES
C     ZP     - Z COORDINATES OF CELL CENTRES
C     VOL    - VOLUME OF CELLS
C     AREA   - AREA OF CELLS
C     VPOR   - POROUS VOLUME
C     ARPOR  - POROUS AREA
C     WFACT  - WEIGHT FACTORS
C     CONV   - CONVECTION COEFFICIENTS
C
C     IPT    - 1D POINTER ARRAY
C     IBLK   - BLOCK SIZE INFORMATION
C     IPVERT - POINTER FROM CELL CENTERS TO 8 NEIGHBOURING VERTICES
C     IPNODN - POINTER FROM CELL CENTERS TO 6 NEIGHBOURING CELLS
C     IPFACN - POINTER FROM CELL CENTERS TO 6 NEIGHBOURING FACES
C     IPNODF - POINTER FROM CELL FACES TO 2 NEIGHBOURING CELL CENTERS
C     IPNODB - POINTER FROM BOUNDARY CENTERS TO CELL CENTERS
C     IPFACB - POINTER FROM BOUNDARY CENTERS TO BOUNDARY FACESS
C
C     WORK   - REAL WORKSPACE ARRAY
C     IWORK  - INTEGER WORKSPACE ARRAY
C     CWORK  - CHARACTER WORKSPACE ARRAY
C
C   SUBROUTINE ARGUMENTS PRECEDED WITH A '*' ARE ARGUMENTS THAT MUST
C   BE SET  BY THE USER IN THIS ROUTINE.
C
C   NOTE THAT OTHER DATA MAY BE OBTAINED FROM CFX-4 USING THE
C   ROUTINE GETADD, FOR FURTHER DETAILS SEE THE VERSION 4
C   USER MANUAL.
C
C*********************************************************************
C
C
      LOGICAL LDEN,LVIS,LTURB,LTEMP,LBUOY,LSCAL,LCOMP
     +       ,LRECT,LCYN,LAXIS,LPOROS,LTRANS
C
      CHARACTER*(*) CWORK
C
C+++++++++++++++++ USER AREA 1 ++++++++++++++++++++++++++++++++++++++++
C---- AREA FOR USERS EXPLICITLY DECLARED VARIABLES
C
C+++++++++++++++++ END OF USER AREA 1 +++++++++++++++++++++++++++++++++
C
      COMMON
     + /ALL/    NBLOCK,NCELL,NBDRY,NNODE,NFACE,NVERT,NDIM
     + /ALLWRK/ NRWS,NIWS,NCWS,IWRFRE,IWIFRE,IWCFRE
     + /ADDIMS/ NPHASE,NSCAL,NVAR,NPROP
     +         ,NDVAR,NDPROP,NDXNN,NDGEOM,NDCOEF,NILIST,NRLIST,NTOPOL
     + /CHKUSR/ IVERS,IUCALL,IUSED
     + /CONC/   NCONC
```

```
     + /DEVICE/ NREAD,NWRITE,NRDISK,NWDISK
     + /IDUM/   ILEN,JLEN
     + /LOGIC/  LDEN,LVIS,LTURB,LTEMP,LBUOY,LSCAL,LCOMP
     +         ,LRECT,LCYN,LAXIS,LPOROS,LTRANS
     + /MLTGRD/ MLEVEL,NLEVEL,ILEVEL
     + /SGLDBL/ IFLGPR,ICHKPR
     + /SPARM/  SMALL,SORMAX,NITER,INDPRI,MAXIT,NODREF,NODMON
     + /TIMUSR/ DTUSR
     + /TRANSI/ NSTEP,KSTEP,MF,INCORE
     + /TRANSR/ TIME,DT,DTINVF,TPARM
C
C+++++++++++++++++ USER AREA 2 ++++++++++++++++++++++++++++++++++++++++
C---- AREA FOR USERS TO DECLARE THEIR OWN COMMON BLOCKS
C     THESE SHOULD START WITH THE CHARACTERS 'UC' TO ENSURE
C     NO CONFLICT WITH NON-USER COMMON BLOCKS
C
      COMMON /UCSURF/  JSURF,NSURF
      COMMON /UCFLUX/  SINKFLUX,VC
C
C+++++++++++++++++ END OF USER AREA 2 +++++++++++++++++++++++++++++++++++
C
      DIMENSION
     + U(NNODE,NPHASE),V(NNODE,NPHASE),W(NNODE,NPHASE),P(NNODE,NPHASE)
     +,VFRAC(NNODE,NPHASE),DEN(NNODE,NPHASE),VIS(NNODE,NPHASE)
     +,TE(NNODE,NPHASE),ED(NNODE,NPHASE),RS(NNODE,NPHASE,6)
     +,T(NNODE,NPHASE),H(NNODE,NPHASE),RF(NNODE,NPHASE,4)
     +,SCAL(NNODE,NPHASE,NSCAL)
      DIMENSION
     + XP(NNODE),YP(NNODE),ZP(NNODE)
     +,VOL(NCELL),AREA(NFACE,3),VPOR(NCELL),ARPOR(NFACE,3)
     +,WFACT(NFACE),CONV(NFACE,NPHASE)
     +,IPT(*),IBLK(5,NBLOCK)
     +,IPVERT(NCELL,8),IPNODN(NCELL,6),IPFACN(NCELL,6),IPNODF(NFACE,4)
     +,IPNODB(NBDRY,4),IPFACB(NBDRY)
     +,IWORK(*),WORK(*),CWORK(*)
C
C+++++++++++++++++ USER AREA 3 ++++++++++++++++++++++++++++++++++++++++
C---- AREA FOR USERS TO DIMENSION THEIR ARRAYS
C
C---- AREA FOR USERS TO DEFINE DATA STATEMENTS
C
C+++++++++++++++++ END OF USER AREA 3 +++++++++++++++++++++++++++++++++++
C
C---- STATEMENT FUNCTION FOR ADDRESSING
      IP(I,J,K)=IPT((K-1)*ILEN*JLEN+(J-1)*ILEN+I)
C
C----VERSION NUMBER OF USER ROUTINE AND PRECISION FLAG
C
      IVERS=3
      ICHKPR = 1
C
C+++++++++++++++++ USER AREA 4 ++++++++++++++++++++++++++++++++++++++++
C---- TO USE THIS USER ROUTINE FIRST SET IUSED=1
C
       IUSED=1
C
C+++++++++++++++++ END OF USER AREA 4 +++++++++++++++++++++++++++++++++++
C
       IF (IUSED.EQ.0) RETURN
C
C---- FRONTEND CHECKING OF USER ROUTINE
       IF (IUCALL.EQ.0) RETURN
C
C+++++++++++++++++ USER AREA 5 ++++++++++++++++++++++++++++++++++++++++
C
      IF (KSTEP.EQ.0) THEN
C
C---------------------------------------------------------------------
C
C     USRTRN LOADS THE INLET, OUTLET AND SINK BOUNDARIES INTO WORKSPACE
C     SO THAT THEY MAY BE USED IN USRSRC AND FOR CALCULATING THE MASS
C     BALANCE. THE CORRECT PATCH NAMES MUST BE ENTERED, DEPENDING ON WHAT
C     THEY ARE NAMED IN THE GEOMETRY. THE DEFAULT NAMES ARE 'NOZZLE INLET',
C     'MOLD OUTLET' AND 'SINK'.
C
C---------------------------------------------------------------------
```

```
C
C-----SINK BOUNDARY LOCATIONS
C
C#####################################################################
C ENTER SINK PATCH NAME
C#####################################################################
C
      CALL IPALL('SINK','*','PATCH','CENTRES',IPT,NPT,
     +           CWORK,IWORK)
C
C#####################################################################
C#####################################################################
C
      NSURF=NPT
C     SET SINK BOUNDARY LIST INTO INTERGER WORK SPACE
      CALL SETPER('USRTRN','IWORK ','ISURF ',NSURF,JSURF)
C
      DO 10 I=1,NSURF
        IWORK(JSURF+I-1)=IPT(I)
 10   CONTINUE
      WRITE(NWRITE,*) ' NSURF=',NSURF,' JSURF=',JSURF
      WRITE(NWRITE,*) ' IWORK(JSURF)=',IWORK(JSURF)
      WRITE(NWRITE,*) ' IWORK(JSURF+NSURF-1)=',IWORK(JSURF+NSURF-1)
C
      ENDIF
C
C---------------------------------------------------------------------
C     END OPERATION
C
      IF(KSTEP.EQ.NSTEP) THEN
C
C
C---------------------------------------------------------------------
C
C     CHECK MASS BALANCE. THE VARIABLES SINKFLUX AND VC ARE PASSED FROM
C     THE USRSRC SUBROUTINE THROUGH THE COMMON BLOCK.
C
C---------------------------------------------------------------------
C
C
C#####################################################################
C ENTER INLET PATCH NAME
C#####################################################################
C
      CALL IPALL('NOZZLE INLET','*','PATCH','CENTRES',IPT,NPT,
     +           CWORK,IWORK)
C
C#####################################################################
C#####################################################################
C
      WATIN = 0.0
      DO 115 I=1,NPT
        INODE = IPT(I)
        IBDRY = INODE-NCELL
        IFACE = IPFACB(IBDRY)
        WATIN = WATIN+CONV(IFACE,1)
 115  CONTINUE
C
C
C#####################################################################
C ENTER OUTLET PATCH NAME
C#####################################################################
C
      CALL IPALL('MOLD OUTLET','*','PATCH','CENTRES',IPT,NPT,
     +           CWORK,IWORK)
C
C#####################################################################
C#####################################################################
C
      WATOUT = 0.0
      WVELSUM = 0.0
      AREASUM = 0.0
C
C.....SINKFLUX INITIALISED IN USRSRC
      DO 125 I=1,NPT
        INODE = IPT(I)
```

```
         IBDRY = INODE-NCELL
         INODE1= IPNODB(IBDRY,1)
         IFACE = IPFACB(IBDRY)
         AREAM = SQRT ( AREA(IFACE,1)*AREA(IFACE,1)
     +                 +AREA(IFACE,2)*AREA(IFACE,2)
     +                 +AREA(IFACE,3)*AREA(IFACE,3) )
         WATOUT = WATOUT+CONV(IFACE,1)
         AREASUM = AREASUM + AREAM
         WVELSUM = WVELSUM+W(INODE1,1)*AREAM
 125  CONTINUE
      WVELAVG = WVELSUM/AREASUM
      WRITE(NWRITE,*) NPT
C
C
      WRITE(NWRITE,*) ' *** MASS BALANCE ***'
      WRITE(NWRITE,*) ' '
      WRITE(NWRITE,*) ' LIQUID'
      WRITE(NWRITE,*) '   INFLOW  (kg/s) =',WATIN
      WRITE(NWRITE,*) '   OUTFLOW (kg/s) =',WATOUT
      WRITE(NWRITE,*) '   SINK    (kg/s) =',SINKFLUX
      WATERR=(WATOUT+SINKFLUX-WATIN)*100.0/WATIN
      WRITE(NWRITE,*) '   % ERROR        =',WATERR
      WRITE(NWRITE,*) ' '
C      WRITE(NWRITE,*) '   SUM OF  W VEL  =',WVELSUM
      WRITE(NWRITE,*) '   OUTLET AREA    =',AREASUM
      WRITE(NWRITE,*) '   AVERAGE W VEL  =',WVELAVG
      WRITE(NWRITE,*) '   CASTING SPEED  =',VC
      OUTERR=(WVELAVG-VC)*100/VC
      WRITE(NWRITE,*) '   % ERROR        =',OUTERR
C
      ENDIF
C
C+++++++++++++++++ END OF USER AREA 5 +++++++++++++++++++++++++++++++++++
C
      RETURN
      END
```

Appendix D. User Subroutine for Gas Injection and Removal

```
      SUBROUTINE USRSRC(IEQN,ICALL,CNAME,CALIAS,AM,SP,SU,CONV
     +                 ,U,V,W,P,VFRAC,DEN,VIS,TE,ED,RS,T,H,RF,SCAL
     +                 ,XP,YP,ZP,VOL,AREA,VPOR,ARPOR,WFACT,IPT
     +                 ,IBLK,IPVERT,IPNODN,IPFACN,IPNODF,IPNODB,IPFACB
     +                 ,WORK,IWORK,CWORK)
C
C***********************************************************************
C
C   UTILITY SUBROUTINE FOR USER-SUPPLIED SOURCES
C
C   >>> IMPORTANT                                                   <<<
C   >>>                                                            <<<
C   >>> USERS MAY ONLY ADD OR ALTER PARTS OF THE SUBROUTINE WITHIN  <<<
C   >>> THE DESIGNATED USER AREAS                                  <<<
C
C***********************************************************************
C
C   THIS SUBROUTINE IS CALLED BY THE FOLLOWING SUBROUTINES
C      CUSR  SCDF  SCDS  SCED  SCENRG  SCHF  SCMOM  SCPCE  SCSCAL
C      SCTE  SCVF
C
C***********************************************************************
C   CREATED
C      08/03/90  ADB
C   MODIFIED
C      04/03/91  ADB  ALTERED ARGUMENT LIST.
C      28/08/91  IRH  NEW STRUCTURE
C      28/09/91  IRH  CHANGE EXAMPLE + ADD COMMON BLOCKS
C      10/02/92  PHA  UPDATE CALLED BY COMMENT, ADD RF ARGUMENT,
C                     CHANGE LAST DIMENSION OF RS TO 6 AND IVERS TO 2
C      03/06/92  PHA  ADD PRECISION FLAG AND CHANGE IVERS TO 3
C      23/11/93  CSH  EXPLICITLY DIMENSION IPVERT ETC.
C      07/12/93  NSW  INCLUDE CONV IN ARGUMENT LIST AND CHANGE IVERS
C                     TO 4
C      03/02/94  PHA  CHANGE FLOW3D TO CFDS-FLOW3D
C      03/03/94  FHW  CORRECTION OF SPELLING MISTAKE
C      08/03/94  NSW  CORRECT SPELLING
C
C***********************************************************************
C
C   SUBROUTINE ARGUMENTS
C
C     IEQN   - EQUATION NUMBER
C     ICALL  - SUBROUTINE CALL
C     CNAME  - EQUATION NAME
C     CALIAS - ALIAS OF EQUATION NAME
C     AM     - OFF DIAGONAL MATRIX COEFFICIENTS
C     SU     - SU IN LINEARISATION OF SOURCE TERM
C     SP     - SP IN LINEARISATION OF SOURCE TERM
C     CONV   - CONVECTION COEFFICIENTS
C     U      - U COMPONENT OF VELOCITY
C     V      - V COMPONENT OF VELOCITY
C     W      - W COMPONENT OF VELOCITY
C     P      - PRESSURE
C     VFRAC  - VOLUME FRACTION
C     DEN    - DENSITY OF FLUID
C     VIS    - VISCOSITY OF FLUID
C     TE     - TURBULENT KINETIC ENERGY
C     ED     - EPSILON
C     RS     - REYNOLD STRESSES
C     T      - TEMPERATURE
C     H      - ENTHALPY
C     RF     - REYNOLD FLUXES
C     SCAL   - SCALARS (THE FIRST 'NCONC' OF THESE ARE MASS FRACTIONS)
C     XP     - X COORDINATES OF CELL CENTRES
C     YP     - Y COORDINATES OF CELL CENTRES
C     ZP     - Z COORDINATES OF CELL CENTRES
C     VOL    - VOLUME OF CELLS
C     AREA   - AREA OF CELLS
C     VPOR   - POROUS VOLUME
C     ARPOR  - POROUS AREA
```

```
C     WFACT  - WEIGHT FACTORS
C
C     IPT    - 1D POINTER ARRAY
C     IBLK   - BLOCK SIZE INFORMATION
C     IPVERT - POINTER FROM CELL CENTERS TO 8 NEIGHBOURING VERTICES
C     IPNODN - POINTER FROM CELL CENTERS TO 6 NEIGHBOURING CELLS
C     IPFACN - POINTER FROM CELL CENTERS TO 6 NEIGHBOURING FACES
C     IPNODF - POINTER FROM CELL FACES TO 2 NEIGHBOURING CELL CENTERS
C     IPNODB - POINTER FROM BOUNDARY CENTERS TO CELL CENTERS
C     IPFACB - POINTER FROM BOUNDARY CENTERS TO BOUNDARY FACESS
C
C     WORK   - REAL WORKSPACE ARRAY
C     IWORK  - INTEGER WORKSPACE ARRAY
C     CWORK  - CHARACTER WORKSPACE ARRAY
C
C   SUBROUTINE ARGUMENTS PRECEDED WITH A '*' ARE ARGUMENTS THAT MUST
C   BE SET  BY THE USER IN THIS ROUTINE.
C
C   NOTE THAT OTHER DATA MAY BE OBTAINED FROM CFDS-FLOW3D USING THE
C   ROUTINE GETADD, FOR FURTHER DETAILS SEE THE RELEASE 3
C   USER MANUAL.
C
C*********************************************************************
C
      LOGICAL LDEN,LVIS,LTURB,LTEMP,LBUOY,LSCAL,LCOMP
     +       ,LRECT,LCYN,LAXIS,LPOROS,LTRANS
C
      CHARACTER*(*) CWORK
      CHARACTER     CNAME*6, CALIAS*24
C
C+++++++++++++++++ USER AREA 1 ++++++++++++++++++++++++++++++++++++++++
C---- AREA FOR USERS EXPLICITLY DECLARED VARIABLES
C
C+++++++++++++++++ END OF USER AREA 1 ++++++++++++++++++++++++++++++++++
C
      COMMON
     + /ALL/    NBLOCK,NCELL,NBDRY,NNODE,NFACE,NVERT,NDIM
     + /ALLWRK/ NRWS,NIWS,NCWS,IWRFRE,IWIFRE,IWCFRE
     + /ADDIMS/ NPHASE,NSCAL,NVAR,NPROP
     +         ,NDVAR,NDPROP,NDXNN,NDGEOM,NDCOEF,NILIST,NRLIST,NTOPOL
     + /CHKUSR/ IVERS,IUCALL,IUSED
     + /DEVICE/ NREAD,NWRITE,NRDISK,NWDISK
     + /IDUM/   ILEN,JLEN
     + /LOGIC/  LDEN,LVIS,LTURB,LTEMP,LBUOY,LSCAL,LCOMP
     +         ,LRECT,LCYN,LAXIS,LPOROS,LTRANS
     + /MLTGRD/ MLEVEL,NLEVEL,ILEVEL
     + /SGLDBL/ IFLGPR,ICHKPR
     + /SPARM/  SMALL,SORMAX,NITER,INDPRI,MAXIT,NODREF,NODMON
     + /TRANSI/ NSTEP,KSTEP,MF,INCORE
     + /TRANSR/ TIME,DT,DTINVF,TPARM
C
C+++++++++++++++++ USER AREA 2 ++++++++++++++++++++++++++++++++++++++++
C---- AREA FOR USERS TO DECLARE THEIR OWN COMMON BLOCKS
C     THESE SHOULD START WITH THE CHARACTERS 'UC' TO ENSURE
C     NO CONFLICT WITH NON-USER COMMON BLOCKS
C
      COMMON /UCSURF/ JISURF,NISURF,JDSURF,NDSURF
      COMMON /UCINJR/ FINJ2,UGASIN,VGASIN,WGASIN
      COMMON /UCFLUX/ GASIN,GASOUT
C
C+++++++++++++++++ END OF USER AREA 2 ++++++++++++++++++++++++++++++++++
C
      DIMENSION AM(NCELL,6,NPHASE),SP(NCELL,NPHASE),SU(NCELL,NPHASE)
     +,CONV(NFACE,NPHASE)
C
      DIMENSION
     + U(NNODE,NPHASE),V(NNODE,NPHASE),W(NNODE,NPHASE),P(NNODE,NPHASE)
     +,VFRAC(NNODE,NPHASE),DEN(NNODE,NPHASE),VIS(NNODE,NPHASE)
     +,TE(NNODE,NPHASE),ED(NNODE,NPHASE),RS(NNODE,NPHASE,6)
     +,T(NNODE,NPHASE),H(NNODE,NPHASE),RF(NNODE,NPHASE,4)
     +,SCAL(NNODE,NPHASE,NSCAL)
C
      DIMENSION
     + XP(NNODE),YP(NNODE),ZP(NNODE)
     +,VOL(NCELL),AREA(NFACE,3),VPOR(NCELL),ARPOR(NFACE,3)
     +,WFACT(NFACE)
```

```
     +,IPT(*),IBLK(5,NBLOCK)
     +,IPVERT(NCELL,8),IPNODN(NCELL,6),IPFACN(NCELL,6),IPNODF(NFACE,4)
     +,IPNODB(NBDRY,4),IPFACB(NBDRY)
     +,IWORK(*),WORK(*),CWORK(*)
C
C+++++++++++++++++ USER AREA 3 ++++++++++++++++++++++++++++++++++++++++
C---- AREA FOR USERS TO DIMENSION THEIR ARRAYS
C
C---- AREA FOR USERS TO DEFINE DATA STATEMENTS
C
C+++++++++++++++++ END OF USER AREA 3 +++++++++++++++++++++++++++++++++
C
C---- STATEMENT FUNCTION FOR ADRESSING
      IP(I,J,K)=IPT((K-1)*ILEN*JLEN+(J-1)*ILEN+I)
C
C----VERSION NUMBER OF USER ROUTINE AND PRECISION FLAG
C
      IVERS=4
      ICHKPR = 1
C
C+++++++++++++++++ USER AREA 4 ++++++++++++++++++++++++++++++++++++++++
C---- TO USE THIS USER ROUTINE FIRST SET IUSED=1
C
       IUSED=1
       IF (IUSED.EQ.0) RETURN
C
C+++++++++++++++++ END OF USER AREA 4 +++++++++++++++++++++++++++++++++
C
C---- FRONTEND CHECKING OF USER ROUTINE
       IF (IUCALL.EQ.0) RETURN
C
C---- ADD TO SOURCE TERMS
      IF (ICALL.EQ.1) THEN
C
C+++++++++++++++++ USER AREA 5 ++++++++++++++++++++++++++++++++++++++++
C
C     CALCULATE SOURCE TERMS, SU AND SP, TO INJECT GAS AT INLET AND REMOVE
C     GAS AT TOP SURFACE. SUBROUTINE INJGAS CALCULATES THE SP SOURCE TERM
C     FOR THE INLET, DEGAS CALCULATES THE LINEARIZED SOURCE TERM, SU,
C     FOR THE REMOVAL AT THE TOP SURFACE. THE SUBROUTINES ARE CALLED FOR
C     EACH EQUATION. THE INJECTION AND REMOVAL RATES ARE SET IN USRTRN,
C     AND ARE PASSED TO INJGAS AND DEGAS BY COMMON BLOCKS.
C
C-----------------------------------------------------------------
C  VOLUME FRACTION [M]/[T]
C
      IF(CALIAS.EQ.'VOLUME FRACTION') THEN
C
C.......SOURCE AT INJECTOR
        CALL INJGAS(CALIAS,SU,U,VFRAC,DEN,AREA,IWORK(JISURF),NISURF
     +             ,IPNODB,IPFACB,TOTAL,XP,YP,ZP)
C
C.......SINK AT TOP
        CALL DEGAS(CALIAS,SP,U,VFRAC,DEN,AREA,IWORK(JDSURF),NDSURF
     +             ,IPNODB,IPFACB,TOTAL)
C        WRITE(NWRITE,*) ' VF :',TOTAL
C
      ENDIF
C
C-----------------------------------------------------------------
C  PRESSURE [M]/[T]
C
      IF(CALIAS.EQ.'PRESSURE') THEN
C
C.......SOURCE AT INJECTOR
        CALL INJGAS(CALIAS,SU,U,VFRAC,DEN,AREA,IWORK(JISURF),NISURF
     +             ,IPNODB,IPFACB,TOTAL,XP,YP,ZP)
        GASIN = TOTAL
C
C.......SINK AT TOP
        CALL DEGAS(CALIAS,SU,U,VFRAC,DEN,AREA,IWORK(JDSURF),NDSURF
     +             ,IPNODB,IPFACB,TOTAL)
        GASOUT = TOTAL
C        WRITE(NWRITE,*) ' PP :',TOTAL
C
      ENDIF
```

```
C
C---------------------------------------------------------------
C  U VELOCITY [M][L]/[T]^2
C
      IF(CALIAS.EQ.'U VELOCITY') THEN
C
C.......SOURCE AT INJECTOR
C        SU(IPTINJ,2)=SU(IPTINJ,2)+FINJ2*VJET
        CALL INJGAS(CALIAS,SU,U,VFRAC,DEN,AREA,IWORK(JISURF),NISURF
     +             ,IPNODB,IPFACB,TOTAL,XP,YP,ZP)
C
C.......SINK AT TOP
        CALL DEGAS(CALIAS,SP,U,VFRAC,DEN,AREA,IWORK(JDSURF),NDSURF
     +             ,IPNODB,IPFACB,TOTAL)
C        WRITE(NWRITE,*) ' U :',TOTAL
C
C.......SET MINIMUM VOID FRACTION
        VFMIN=1.0E-8
        DO 101 INODE=1,NNODE
          VFRAC(INODE,2)=MAX(VFRAC(INODE,2),VFMIN)
 101    CONTINUE
C
      ENDIF
C
C---------------------------------------------------------------
C  V VELOCITY [M][L]/[T]^2
C
      IF(CALIAS.EQ.'V VELOCITY') THEN
C
C.......SOURCE AT INJECTOR
        CALL INJGAS(CALIAS,SU,U,VFRAC,DEN,AREA,IWORK(JISURF),NISURF
     +             ,IPNODB,IPFACB,TOTAL,XP,YP,ZP)
C
C.......SINK AT TOP
        CALL DEGAS(CALIAS,SP,U,VFRAC,DEN,AREA,IWORK(JDSURF),NDSURF
     +             ,IPNODB,IPFACB,TOTAL)
C        WRITE(NWRITE,*) ' V :',TOTAL
C
C
C.......SET MINIMUM VOID FRACTION
        VFMIN=1.0E-8
        DO 201 INODE=1,NNODE
          VFRAC(INODE,2)=MAX(VFRAC(INODE,2),VFMIN)
 201    CONTINUE
C
      ENDIF
C
C---------------------------------------------------------------
C  W VELOCITY [M][L]/[T]^2
C
      IF(CALIAS.EQ.'W VELOCITY') THEN
C
C.......SOURCE AT INJECTOR
        CALL INJGAS(CALIAS,SU,U,VFRAC,DEN,AREA,IWORK(JISURF),NISURF
     +             ,IPNODB,IPFACB,TOTAL,XP,YP,ZP)
C
C.......SINK AT TOP
        CALL DEGAS(CALIAS,SP,U,VFRAC,DEN,AREA,IWORK(JDSURF),NDSURF
     +             ,IPNODB,IPFACB,TOTAL)
C        WRITE(NWRITE,*) ' W :',TOTAL
C
C.......SET MINIMUM VOID FRACTION
        VFMIN=1.0E-8
        DO 301 INODE=1,NNODE
          VFRAC(INODE,2)=MAX(VFRAC(INODE,2),VFMIN)
 301    CONTINUE
C
      ENDIF
C
C+++++++++++++++++ END OF USER AREA 5 +++++++++++++++++++++++++++++++++
      ENDIF
C
C---- OVERWRITE SOURCE TERMS
      IF (ICALL.EQ.2) THEN
C
C+++++++++++++++++ USER AREA 6 +++++++++++++++++++++++++++++++++++++++
```

```
C
C+++++++++++++++++ END OF USER AREA 6 +++++++++++++++++++++++++++++++++
C
      ENDIF
      RETURN
      END
C
C-----------------------------------------------------------------
C
      SUBROUTINE INJGAS(CALIAS,SUU,U,VFRAC,DEN,AREA,IPTSRF,NISURF
     +                 ,IPNODB,IPFACB,TOTAL,XP,YP,ZP)
C
C**********************************************************************
C
C   UTILITY SUBROUTINE FOR USER-SUPPLIED GAS INJECTION
C
C**********************************************************************
C
C   THIS SUBROUTINE IS CALLED BY THE FOLLOWING SUBROUTINES
C      USRSRC
C
C**********************************************************************
C   CREATED
C      03/05/94  SML
C   MODIFIED
C      02/06/98  DTC  MODIFIED DEGAS FOR GAS INJECTION
C**********************************************************************
C
C   SUBROUTINE ARGUMENTS
C
C     CALIAS - ALIAS OF EQUATION NAME
C     SUU    - SU IN LINEARISATION OF SOURCE TERM
C     U      - VELOCITY COMPONENT FOR DEGASSING
C     VFRAC  - VOLUME FRACTION
C     DEN    - DENSITY OF FLUID
C     AREA   - AREA OF CELLS
C     IPTSRF - 1D POINTER ARRAY
C     NISURF - NUMBER OF SURFACE NODE
C     IPNODB - POINTER FROM BOUNDARY CENTERS TO CELL CENTERS
C     IPFACB - POINTER FROM BOUNDARY CENTERS TO BOUNDARY FACES
C     TOTAL  - TOTAL OF SOURCE ADDED
C     XP     - X COORDINATE OF NODE LOCATIONS
C     YP     - Y COORDINATE OF NODE LOCATIONS
C     ZP     - Z COORDINATE OF NODE LOCATIONS
C     FINJ2  - MASS FLOW RATE OF INJECTED GAS
C     UGASIN - U VELOCITY OF INJECTED GAS
C     VGASIN - V VELOCITY OF INJECTED GAS
C     WGASIN - W VELOCITY OF INJECTED GAS
C
C**********************************************************************
C
      CHARACTER     CALIAS*24
C
C+++++++++++++++++ USER AREA 1 +++++++++++++++++++++++++++++++++++++++++
C---- AREA FOR USERS EXPLICITLY DECLARED VARIABLES
C
C+++++++++++++++++ END OF USER AREA 1 +++++++++++++++++++++++++++++++++
C
      COMMON
     + /ALL/    NBLOCK,NCELL,NBDRY,NNODE,NFACE,NVERT,NDIM
     + /ALLWRK/ NRWS,NIWS,NCWS,IWRFRE,IWIFRE,IWCFRE
     + /ADDIMS/ NPHASE,NSCAL,NVAR,NPROP
     +         ,NDVAR,NDPROP,NDXNN,NDGEOM,NDCOEF,NILIST,NRLIST,NTOPOL
     + /DEVICE/ NREAD,NWRITE,NRDISK,NWDISK
C
C+++++++++++++++++ USER AREA 2 +++++++++++++++++++++++++++++++++++++++++
C---- AREA FOR USERS TO DECLARE THEIR OWN COMMON BLOCKS
C     THESE SHOULD START WITH THE CHARACTERS 'UC' TO ENSURE
C     NO CONFLICT WITH NON-USER COMMON BLOCKS
      COMMON /UCINJR/ FINJ2,UGASIN,VGASIN,WGASIN
C
C+++++++++++++++++ END OF USER AREA 2 +++++++++++++++++++++++++++++++++
C
      DIMENSION SUU(NCELL,NPHASE)
     +,U(NNODE,NPHASE),VFRAC(NNODE,NPHASE),DEN(NNODE,NPHASE)
     +,AREA(NFACE,3),IPTSRF(NISURF),IPNODB(NBDRY,4),IPFACB(NBDRY)
```

```
C
C+++++++++++++++++ USER AREA 3 ++++++++++++++++++++++++++++++++++++++++
C---- AREA FOR USERS TO DIMENSION THEIR ARRAYS
      DIMENSION
     + XP(NNODE),YP(NNODE),ZP(NNODE)
C
C---- AREA FOR USERS TO DEFINE DATA STATEMENTS
C
C+++++++++++++++++ END OF USER AREA 3 +++++++++++++++++++++++++++++++++
C
C---- STATEMENT FUNCTION FOR ADRESSING
C       IP(I,J,K)=IPT((K-1)*ILEN*JLEN+(J-1)*ILEN+I)
C
C+++++++++++++++++ USER AREA 4 ++++++++++++++++++++++++++++++++++++++++
C
C+++++++++++++++++ END OF USER AREA 4 +++++++++++++++++++++++++++++++++
C
C+++++++++++++++++ USER AREA 5 ++++++++++++++++++++++++++++++++++++++++
C
C     SUBROUTINE INJGAS CALCULATES THE SOURCE TERM SU TO ACCOUNT FOR
C     GAS INJECTION AT THE INLET. THE AMOUNT OF GAS INJECTED AND THE
C     VELOCITY OF THE GAS JET ARE SET IN THE USRTRN ROUTINE.
C
C
C
C-----------------------------------------------------------------
C
C-----INJECTION PHASE INDEX. THE PHASE TO INJECT, AS SET IN THE
C     COMMAND FILE. FOR THIS PROBLEM, 1 = LIQUID PHASE, 2 = GAS PHASE.
C
      IPHINJ=2
C
C-----------------------------------------------------------------
C  VOLUME FRACTION AND PRESSURE
C
      IF((CALIAS.EQ.'VOLUME FRACTION').OR.
     +                    (CALIAS.EQ.'PRESSURE')) THEN
C
      TOTAL = 0.0
      TOTALA = 0.0
      DO 101 I=1,NISURF
        INODE = IPTSRF(I)
        IBDRY = INODE-NCELL
        INODE1= IPNODB(IBDRY,1)
        IFACE = IPFACB(IBDRY)
        AREAM = SQRT ( AREA(IFACE,1)*AREA(IFACE,1)
     +                +AREA(IFACE,2)*AREA(IFACE,2)
     +                +AREA(IFACE,3)*AREA(IFACE,3) )
        FLUX  = FINJ2*AREAM
        SUU(INODE1,IPHINJ)=SUU(INODE1,IPHINJ)+FLUX
        TOTAL = TOTAL+FLUX
        TOTALA = TOTALA+AREAM
C        WRITE(NWRITE,*) ' FLUX=',FLUX
C        WRITE(NWRITE,*) ' X,Y,Z=',XP(INODE1),YP(INODE1),ZP(INODE1)
 101  CONTINUE
C        WRITE(NWRITE,*) 'TOTAL GAS FLUX=',TOTAL,'TOTAL AREA=',TOTALA
C
C-----------------------------------------------------------------
C  U VELOCITY
C
      ELSE IF(CALIAS.EQ.'U VELOCITY') THEN
C
      TOTAL = 0.0
      DO 201 I=1,NISURF
        INODE = IPTSRF(I)
        IBDRY = INODE-NCELL
        INODE1= IPNODB(IBDRY,1)
        IFACE = IPFACB(IBDRY)
        AREAM = SQRT ( AREA(IFACE,1)*AREA(IFACE,1)
     +                +AREA(IFACE,2)*AREA(IFACE,2)
     +                +AREA(IFACE,3)*AREA(IFACE,3) )
        FLUX  = FINJ2*AREAM*UGASIN
        SUU(INODE1,IPHINJ)=SUU(INODE1,IPHINJ)+FLUX
        TOTAL = TOTAL+FLUX
C        WRITE(NWRITE,*) ' FLUX=',FLUX
 201  CONTINUE
```

```
C
C
C-----------------------------------------------------------
C  V VELOCITY
C
      ELSE IF(CALIAS.EQ.'V VELOCITY') THEN
C
      TOTAL = 0.0
      DO 301 I=1,NISURF
        INODE = IPTSRF(I)
        IBDRY = INODE-NCELL
        INODE1= IPNODB(IBDRY,1)
        IFACE = IPFACB(IBDRY)
        AREAM = SQRT ( AREA(IFACE,1)*AREA(IFACE,1)
     +               +AREA(IFACE,2)*AREA(IFACE,2)
     +               +AREA(IFACE,3)*AREA(IFACE,3) )
        FLUX  = FINJ2*AREAM*VGASIN
        SUU(INODE1,IPHINJ)=SUU(INODE1,IPHINJ)+FLUX
        TOTAL = TOTAL+FLUX
C        WRITE(NWRITE,*) ' FLUX=',FLUX
 301  CONTINUE
C
C
C-----------------------------------------------------------
C  W VELOCITY
C
      ELSE IF(CALIAS.EQ.'W VELOCITY') THEN
C
      TOTAL = 0.0
      DO 401 I=1,NISURF
        INODE = IPTSRF(I)
        IBDRY = INODE-NCELL
        INODE1= IPNODB(IBDRY,1)
        IFACE = IPFACB(IBDRY)
        AREAM = SQRT ( AREA(IFACE,1)*AREA(IFACE,1)
     +               +AREA(IFACE,2)*AREA(IFACE,2)
     +               +AREA(IFACE,3)*AREA(IFACE,3) )
        FLUX  = FINJ2*AREAM*WGASIN
        SUU(INODE1,IPHINJ)=SUU(INODE1,IPHINJ)+FLUX
        TOTAL = TOTAL+FLUX
C        WRITE(NWRITE,*) ' FLUX=',FLUX
 401  CONTINUE
C
      ENDIF
C
      RETURN
      END
C
C-----------------------------------------------------------
C
      SUBROUTINE DEGAS(CALIAS,SUP,U,VFRAC,DEN,AREA,IPTSRF,NDSURF
     +                ,IPNODB,IPFACB,TOTAL)
C
C*********************************************************************
C
C   UTILITY SUBROUTINE FOR USER-SUPPLIED FREE SURFACE DEGASSING
C
C*********************************************************************
C
C   THIS SUBROUTINE IS CALLED BY THE FOLLOWING SUBROUTINES
C      USRSRC
C
C*********************************************************************
C   CREATED
C      03/05/94  SML
C   MODIFIED
C      02/06/98  DTC  MODIFIED DEGAS FOR CONTINUOUS CASTING MODEL
C*********************************************************************
C
C   SUBROUTINE ARGUMENTS
C
C     CALIAS - ALIAS OF EQUATION NAME
C     SUP    - SP IN LINEARISATION OF SOURCE TERM
C     U      - VELOCITY COMPONENT FOR DEGASSING
C     VFRAC  - VOLUME FRACTION
C     DEN    - DENSITY OF FLUID
```

```
C     AREA   - AREA OF CELLS
C     IPTSRF - 1D POINTER ARRAY
C     NDSURF - NUMBER OF SURFACE NODES
C     IPNODB - POINTER FROM BOUNDARY CENTERS TO CELL CENTERS
C     IPFACB - POINTER FROM BOUNDARY CENTERS TO BOUNDARY FACES
C     TOTAL  - TOTAL OF SOURCE ADDED
C     XP     - X COORDINATE OF NODE LOCATIONS
C     YP     - Y COORDINATE OF NODE LOCATIONS
C     ZP     - Z COORDINATE OF NODE LOCATIONS
C     FINJ2  - MASS FLOW RATE OF INJECTED GAS
C     UGASIN - U VELOCITY OF INJECTED GAS
C     VGASIN - V VELOCITY OF INJECTED GAS
C     WGASIN - W VELOCITY OF INJECTED GAS
C
C*********************************************************************
C
      CHARACTER     CALIAS*24
C
C+++++++++++++++++ USER AREA 1 +++++++++++++++++++++++++++++++++++++++
C---- AREA FOR USERS EXPLICITLY DECLARED VARIABLES
C
C+++++++++++++++++ END OF USER AREA 1 +++++++++++++++++++++++++++++++++
C
      COMMON
     + /ALL/    NBLOCK,NCELL,NBDRY,NNODE,NFACE,NVERT,NDIM
     + /ALLWRK/ NRWS,NIWS,NCWS,IWRFRE,IWIFRE,IWCFRE
     + /ADDIMS/ NPHASE,NSCAL,NVAR,NPROP
     +         ,NDVAR,NDPROP,NDXNN,NDGEOM,NDCOEF,NILIST,NRLIST,NTOPOL
     + /DEVICE/ NREAD,NWRITE,NRDISK,NWDISK
C
C+++++++++++++++++ USER AREA 2 +++++++++++++++++++++++++++++++++++++++
C---- AREA FOR USERS TO DECLARE THEIR OWN COMMON BLOCKS
C     THESE SHOULD START WITH THE CHARACTERS 'UC' TO ENSURE
C     NO CONFLICT WITH NON-USER COMMON BLOCKS
C
C+++++++++++++++++ END OF USER AREA 2 +++++++++++++++++++++++++++++++++
C
      DIMENSION SUP(NCELL,NPHASE)
     +,U(NNODE,NPHASE),VFRAC(NNODE,NPHASE),DEN(NNODE,NPHASE)
     +,AREA(NFACE,3),IPTSRF(NDSURF),IPNODB(NBDRY,4),IPFACB(NBDRY)
C
C+++++++++++++++++ USER AREA 3 +++++++++++++++++++++++++++++++++++++++
C---- AREA FOR USERS TO DIMENSION THEIR ARRAYS
C
C---- AREA FOR USERS TO DEFINE DATA STATEMENTS
C
C+++++++++++++++++ END OF USER AREA 3 +++++++++++++++++++++++++++++++++
C
C---- STATEMENT FUNCTION FOR ADRESSING
C       IP(I,J,K)=IPT((K-1)*ILEN*JLEN+(J-1)*ILEN+I)
C
C+++++++++++++++++ USER AREA 4 +++++++++++++++++++++++++++++++++++++++
C
C+++++++++++++++++ END OF USER AREA 4 +++++++++++++++++++++++++++++++++
C
C+++++++++++++++++ USER AREA 5 +++++++++++++++++++++++++++++++++++++++
C

C     SUBROUTINE DEGAS CALCULATES THE LINEARIZED SOURCE TERM SP
C     TO ACCOUNT FOR GAS REMOVAL AT THE TOP SURFACE. THE AMOUNT
C     OF GAS REMOVED DEPENDS ON THE UPWARDS VELOCITY OF THE GAS
C     PHASE AT EACH LOCATION ON THE TOP SURFACE.
C
C
C
C-----------------------------------------------------------------
C
C-----DEGASSING PHASE INDEX. THE PHASE TO REMOVE, AS SET IN THE
C     COMMAND FILE. FOR THIS PROBLEM, 1 = LIQUID PHASE, 2 = GAS PHASE.
C
      IPHDG=2
C
C-----------------------------------------------------------------
C  VOLUME FRACTION
C
      IF(CALIAS.EQ.'VOLUME FRACTION') THEN
```

```
C
      TOTAL = 0.0
      DO 101 I=1,NDSURF
        INODE = IPTSRF(I)
        IBDRY = INODE-NCELL
        INODE1= IPNODB(IBDRY,1)
        IFACE = IPFACB(IBDRY)
        AREAM = SQRT ( AREA(IFACE,1)*AREA(IFACE,1)
     +               +AREA(IFACE,2)*AREA(IFACE,2)
     +               +AREA(IFACE,3)*AREA(IFACE,3) )
        FLUX  = DEN(INODE1,IPHDG)*
     +           AREAM*MAX(W(INODE1,IPHDG),0.0)
        SUP(INODE1,IPHDG)=SUP(INODE1,IPHDG)-FLUX
        TOTAL = TOTAL+FLUX
C        WRITE(NWRITE,*) ' FLUX=',FLUX
 101  CONTINUE
C
C-----------------------------------------------------------------
C  ALL OTHER VARIABLES
C
      ELSE
C
      TOTAL = 0.0
      DO 201 I=1,NDSURF
        INODE = IPTSRF(I)
        IBDRY = INODE-NCELL
        INODE1= IPNODB(IBDRY,1)
        IFACE = IPFACB(IBDRY)
        AREAM = SQRT ( AREA(IFACE,1)*AREA(IFACE,1)
     +               +AREA(IFACE,2)*AREA(IFACE,2)
     +               +AREA(IFACE,3)*AREA(IFACE,3) )
        FLUX  = VFRAC(INODE1,IPHDG)*DEN(INODE1,IPHDG)
     +           *AREAM*MAX(U(INODE1,IPHDG),0.0)
        SUP(INODE1,IPHDG)=SUP(INODE1,IPHDG)-FLUX
        TOTAL = TOTAL+FLUX
C        WRITE(NWRITE,*) ' FLUX=',FLUX
 201  CONTINUE
C
      ENDIF
C
      RETURN
      END
C
C-----------------------------------------------------------------
C
      SUBROUTINE USRTRN(U,V,W,P,VFRAC,DEN,VIS,TE,ED,RS,T,H,RF,SCAL,
     +                  XP,YP,ZP,VOL,AREA,VPOR,ARPOR,WFACT,CONV,IPT,
     +                  IBLK,IPVERT,IPNODN,IPFACN,IPNODF,IPNODB,IPFACB,
     +                  WORK,IWORK,CWORK)
C
C**********************************************************************
C
C   USER SUBROUTINE TO ALLOW USERS TO MODIFY OR MONITOR THE SOLUTION AT
C   THE END OF EACH TIME STEP
C   THIS SUBROUTINE IS CALLED BEFORE THE START OF THE RUN AS WELL AS AT
C   THE END OF EACH TIME STEP
C
C   >>> IMPORTANT                                                  <<<
C   >>>                                                           <<<
C   >>> USERS MAY ONLY ADD OR ALTER PARTS OF THE SUBROUTINE WITHIN  <<<
C   >>> THE DESIGNATED USER AREAS                                  <<<
C
C**********************************************************************
C
C   THIS SUBROUTINE IS CALLED BY THE FOLLOWING SUBROUTINES
C      CUSR  TRNMOD
C
C**********************************************************************
C   CREATED
C      27/04/90  ADB
C   MODIFIED
C      05/08/91  IRH  NEW STRUCTURE
C      01/10/91  DSC  REDUCE COMMENT LINE GOING OVER COLUMN 72.
C      29/11/91  PHA  UPDATE CALLED BY COMMENT, ADD RF ARGUMENT,
C                     CHANGE LAST DIMENSION OF RS TO 6 AND IVERS TO 2
C      05/06/92  PHA  ADD PRECISION FLAG AND CHANGE IVERS TO 3
```

```
C      03/07/92  DSC  CORRECT COMMON MLTGRD.
C      23/11/93  CSH  EXPLICITLY DIMENSION IPVERT ETC.
C      03/02/94  PHA  CHANGE FLOW3D TO CFDS-FLOW3D
C
C***********************************************************************
C
C   SUBROUTINE ARGUMENTS
C
C     U       - U COMPONENT OF VELOCITY
C     V       - V COMPONENT OF VELOCITY
C     W       - W COMPONENT OF VELOCITY
C     P       - PRESSURE
C     VFRAC   - VOLUME FRACTION
C     DEN     - DENSITY OF FLUID
C     VIS     - VISCOSITY OF FLUID
C     TE      - TURBULENT KINETIC ENERGY
C     ED      - EPSILON
C     RS      - REYNOLD STRESSES
C     T       - TEMPERATURE
C     H       - ENTHALPY
C     RF      - REYNOLD FLUXES
C     SCAL    - SCALARS (THE FIRST 'NCONC' OF THESE ARE MASS FRACTIONS)
C     XP      - X COORDINATES OF CELL CENTRES
C     YP      - Y COORDINATES OF CELL CENTRES
C     ZP      - Z COORDINATES OF CELL CENTRES
C     VOL     - VOLUME OF CELLS
C     AREA    - AREA OF CELLS
C     VPOR    - POROUS VOLUME
C     ARPOR   - POROUS AREA
C     WFACT   - WEIGHT FACTORS
C     CONV    - CONVECTION COEFFICIENTS
C
C     IPT     - 1D POINTER ARRAY
C     IBLK    - BLOCK SIZE INFORMATION
C     IPVERT  - POINTER FROM CELL CENTERS TO 8 NEIGHBOURING VERTICES
C     IPNODN  - POINTER FROM CELL CENTERS TO 6 NEIGHBOURING CELLS
C     IPFACN  - POINTER FROM CELL CENTERS TO 6 NEIGHBOURING FACES
C     IPNODF  - POINTER FROM CELL FACES TO 2 NEIGHBOURING CELL CENTERS
C     IPNODB  - POINTER FROM BOUNDARY CENTERS TO CELL CENTERS
C     IPFACB  - POINTER FROM BOUNDARY CENTERS TO BOUNDARY FACESS
C
C     WORK    - REAL WORKSPACE ARRAY
C     IWORK   - INTEGER WORKSPACE ARRAY
C     CWORK   - CHARACTER WORKSPACE ARRAY
C
C   SUBROUTINE ARGUMENTS PRECEDED WITH A '*' ARE ARGUMENTS THAT MUST
C   BE SET  BY THE USER IN THIS ROUTINE.
C
C   NOTE THAT OTHER DATA MAY BE OBTAINED FROM CFDS-FLOW3D USING THE
C   ROUTINE GETADD, FOR FURTHER DETAILS SEE THE RELEASE 3
C   USER MANUAL.
C
C***********************************************************************
C
C
      LOGICAL LDEN,LVIS,LTURB,LTEMP,LBUOY,LSCAL,LCOMP
     +       ,LRECT,LCYN,LAXIS,LPOROS,LTRANS
C
      CHARACTER*(*) CWORK
C
C+++++++++++++++++ USER AREA 1 ++++++++++++++++++++++++++++++++++++++++
C---- AREA FOR USERS EXPLICITLY DECLARED VARIABLES
C
C+++++++++++++++++ END OF USER AREA 1 +++++++++++++++++++++++++++++++++
C
      COMMON
     + /ALL/    NBLOCK,NCELL,NBDRY,NNODE,NFACE,NVERT,NDIM
     + /ALLWRK/ NRWS,NIWS,NCWS,IWRFRE,IWIFRE,IWCFRE
     + /ADDIMS/ NPHASE,NSCAL,NVAR,NPROP
     +         ,NDVAR,NDPROP,NDXNN,NDGEOM,NDCOEF,NILIST,NRLIST,NTOPOL
     + /CHKUSR/ IVERS,IUCALL,IUSED
     + /CONC/   NCONC
     + /DEVICE/ NREAD,NWRITE,NRDISK,NWDISK
     + /IDUM/   ILEN,JLEN
     + /LOGIC/  LDEN,LVIS,LTURB,LTEMP,LBUOY,LSCAL,LCOMP
     +         ,LRECT,LCYN,LAXIS,LPOROS,LTRANS
```

```
     + /MLTGRD/ MLEVEL,NLEVEL,ILEVEL
     + /SGLDBL/ IFLGPR,ICHKPR
     + /SPARM/  SMALL,SORMAX,NITER,INDPRI,MAXIT,NODREF,NODMON
     + /TIMUSR/ DTUSR
     + /TRANSI/ NSTEP,KSTEP,MF,INCORE
     + /TRANSR/ TIME,DT,DTINVF,TPARM
C
C+++++++++++++++++ USER AREA 2 ++++++++++++++++++++++++++++++++++++++++
C---- AREA FOR USERS TO DECLARE THEIR OWN COMMON BLOCKS
C     THESE SHOULD START WITH THE CHARACTERS 'UC' TO ENSURE
C     NO CONFLICT WITH NON-USER COMMON BLOCKS
C
      COMMON /UCSURF/ JISURF,NISURF,JDSURF,NDSURF
      COMMON /UCINJR/ FINJ2,UGASIN,VGASIN,WGASIN
      COMMON /UCFLUX/ GASIN,GASOUT
C
C+++++++++++++++++ END OF USER AREA 2 ++++++++++++++++++++++++++++++++++
C
      DIMENSION
     + U(NNODE,NPHASE),V(NNODE,NPHASE),W(NNODE,NPHASE),P(NNODE,NPHASE)
     +,VFRAC(NNODE,NPHASE),DEN(NNODE,NPHASE),VIS(NNODE,NPHASE)
     +,TE(NNODE,NPHASE),ED(NNODE,NPHASE),RS(NNODE,NPHASE,6)
     +,T(NNODE,NPHASE),H(NNODE,NPHASE),RF(NNODE,NPHASE,4)
     +,SCAL(NNODE,NPHASE,NSCAL)
      DIMENSION
     + XP(NNODE),YP(NNODE),ZP(NNODE)
     +,VOL(NCELL),AREA(NFACE,3),VPOR(NCELL),ARPOR(NFACE,3)
     +,WFACT(NFACE),CONV(NFACE,NPHASE)
     +,IPT(*),IBLK(5,NBLOCK)
     +,IPVERT(NCELL,8),IPNODN(NCELL,6),IPFACN(NCELL,6),IPNODF(NFACE,4)
     +,IPNODB(NBDRY,4),IPFACB(NBDRY)
     +,IWORK(*),WORK(*),CWORK(*)
C
C+++++++++++++++++ USER AREA 3 ++++++++++++++++++++++++++++++++++++++++
C---- AREA FOR USERS TO DIMENSION THEIR ARRAYS
C
C---- AREA FOR USERS TO DEFINE DATA STATEMENTS
C
C+++++++++++++++++ END OF USER AREA 3 ++++++++++++++++++++++++++++++++++
C
C---- STATEMENT FUNCTION FOR ADDRESSING
      IP(I,J,K)=IPT((K-1)*ILEN*JLEN+(J-1)*ILEN+I)
C
C----VERSION NUMBER OF USER ROUTINE AND PRECISION FLAG
C
      IVERS=3
      ICHKPR = 1
C
C+++++++++++++++++ USER AREA 4 ++++++++++++++++++++++++++++++++++++++++
C---- TO USE THIS USER ROUTINE FIRST SET IUSED=1
C
       IUSED=1
       IF (IUSED.EQ.0) RETURN
C+++++++++++++++++ END OF USER AREA 4 ++++++++++++++++++++++++++++++++++
C
C---- FRONTEND CHECKING OF USER ROUTINE
       IF (IUCALL.EQ.0) RETURN
C
C+++++++++++++++++ USER AREA 5 ++++++++++++++++++++++++++++++++++++++++
C
      IF (KSTEP.EQ.0) THEN
C
C-----INJECTION BOUNDARY LOCATIONS
C
      CALL IPALL('NOZZLE INLET','*','PATCH','CENTRES',IPT,NPT,
     +           CWORK,IWORK)
C
      NISURF=NPT
C     SET INJECTION BOUNDARY LIST INTO INTERGER WORK SPACE
      CALL SETPER('USRTRN','IWORK ','ISURF ',NISURF,JISURF)
C
      DO 101 I=1,NISURF
        IWORK(JISURF+I-1)=IPT(I)
 101  CONTINUE
      WRITE(NWRITE,*) '  '
      WRITE(NWRITE,*) '******** USRTRN - INLET **********'
```

```
      WRITE(NWRITE,*) '  NISURF=',NISURF,' JISURF=',JISURF
      WRITE(NWRITE,*) '  IWORK(JISURF)=',IWORK(JISURF)
      WRITE(NWRITE,*) '  IWORK(JISURF+NISURF-1)=',IWORK(JISURF+NISURF-1)
C
C-----INJECTION RATES: MASS FLUX IN kg/s, VELOCITY IN m/s
      FGASIN = 0.0000001
      UGASIN = 1.062
      VGASIN = 0.1
      WGASIN = -0.427
C
C-----DETERMINE TOTAL AREA OF INLET BOUNDARY AND MASS FLUX PER AREA
      TOTALA = 0.0
      DO 201 I=1,NISURF
        INODE = IWORK(JISURF+I-1)
        IBDRY = INODE-NCELL
        IFACE = IPFACB(IBDRY)
        AREAM = SQRT ( AREA(IFACE,1)*AREA(IFACE,1)
     +               +AREA(IFACE,2)*AREA(IFACE,2)
     +               +AREA(IFACE,3)*AREA(IFACE,3) )
        TOTALA = TOTALA+AREAM
 201  CONTINUE
C
      WRITE(NWRITE,*) '  TOTAL AREA OF INLET =',TOTALA
      FINJ2 = FGASIN/TOTALA
C
      WRITE(NWRITE,*) ' INJECTOR '
      WRITE(NWRITE,*) '  AIR  FLOW RATE  (kg/s)=    ',FGASIN
      WRITE(NWRITE,*) '  AIR  FLOW RATE  (kg/m^2*s)=',FINJ2
      WRITE(NWRITE,*) '  JET  VELOCITY    (m/s)=',UGASIN,VGASIN,WGASIN
C
C
C-----DEGASSING BOUNDARY LOCATIONS
C
      CALL IPALL('TOP SURFACE','*','PATCH','CENTRES',IPT,NPT,
     +           CWORK,IWORK)
C
      NDSURF=NPT
C     SET DEGASSING BOUNDARY LIST INTO INTERGER WORK SPACE
      CALL SETPER('USRTRN','IWORK ','DSURF ',NDSURF,JDSURF)
C
      DO 401 I=1,NDSURF
        IWORK(JDSURF+I-1)=IPT(I)
 401  CONTINUE
      WRITE(NWRITE,*) '  '
      WRITE(NWRITE,*) '******** USRTRN - OUTLET *********'
      WRITE(NWRITE,*) ' NDSURF=',NDSURF,' JDSURF=',JDSURF
      WRITE(NWRITE,*) ' IWORK(JDSURF)=',IWORK(JDSURF)
      WRITE(NWRITE,*) ' IWORK(JDSURF+NDSURF-1)=',IWORK(JDSURF+NDSURF-1)
C
      ENDIF
C
C-----------------------------------------------------------------------
C     END OPERATION
C
      IF(KSTEP.EQ.NSTEP) THEN
C
C=====CHECK MASS BALANCE
C
C.....INLET
      CALL IPALL('NOZZLE INLET','*','PATCH','CENTRES',IPT,NPT,
     +           CWORK,IWORK)
C
      WATIN = 0.0
C.....GASIN INITIALISED IN USRSRC
      DO 501 I=1,NPT
        INODE = IPT(I)
        IBDRY = INODE-NCELL
        IFACE = IPFACB(IBDRY)
        WATIN = WATIN+CONV(IFACE,1)
        GASIN = GASIN+CONV(IFACE,2)
 501  CONTINUE
C
C.....OUTLET
      CALL IPALL('OUTLET','*','PATCH','CENTRES',IPT,NPT,
     +           CWORK,IWORK)
C
```

```
      WATOUT = 0.0
C.....GASOUT INITIALISED IN USRSRC
      DO 601 I=1,NPT
        INODE = IPT(I)
        IBDRY = INODE-NCELL
        IFACE = IPFACB(IBDRY)
        WATOUT = WATOUT+CONV(IFACE,1)
        GASOUT = GASOUT+CONV(IFACE,2)
 601  CONTINUE
C
      WRITE(NWRITE,*) ' *** MASS BALANCE ***'
      WRITE(NWRITE,*) ' '
      WRITE(NWRITE,*) ' AIR'
      WRITE(NWRITE,*) '   INFLOW  (kg/s) =',GASIN
      WRITE(NWRITE,*) '   OUTFLOW (kg/s) =',GASOUT
      GASERR=(GASOUT-GASIN)*100.0/GASIN
      WRITE(NWRITE,*) '   % ERROR         =',GASERR
      WRITE(NWRITE,*) ' '
      WRITE(NWRITE,*) ' WATER'
      WRITE(NWRITE,*) '   INFLOW  (kg/s) =',WATIN
      WRITE(NWRITE,*) '   OUTFLOW (kg/s) =',WATOUT
      WATERR=(WATOUT-WATIN)*100.0/WATIN
      WRITE(NWRITE,*) '   % ERROR         =',WATERR
      WRITE(NWRITE,*) ' '
C
C.....SET IPLT=1 TO CLEAN UP VELOCITY FOR PLOTTING
C*****NOTE THAT THIS OPERATION WILL SLIGHTLY ALTER THE VELOCITY FIELD
C     HENCE THE DUMP FILE GENERATED SHOULD BE USED FOR PLOTTING ONLY
C     NOT FOR RESTART.
C
        IPLT=0
C
C.....FILTER OUT VELOCITY WITH SMALL VOLUME FRACTION
        IF(IPLT.EQ.1) THEN
          DO 701 INODE=1,NNODE
            FILTER=1.0-EXP(-3.0*VFRAC(INODE,2)/1.E-4)
            U(INODE,2)=U(INODE,2)*FILTER
            V(INODE,2)=V(INODE,2)*FILTER
            W(INODE,2)=W(INODE,2)*FILTER
 701      CONTINUE
C
        ENDIF
C
      ENDIF
C
C+++++++++++++++++ END OF USER AREA 5 +++++++++++++++++++++++++++++++++++
C
      RETURN
      END
```

Appendix E. Parametric Study Results

For each case in the multiphase parametric study, plots of velocity at the centerplane, wide face and top surface, plots of pressure at the centerplane and top surface, and plots of turbulence kinetic energy (K) are given.

Centerplane velocity is plotted on the centerplane parallel to the wide face. Wide face velocity is plotted at 1 mm from the wide face boundary. Top surface velocity is plotted at 1 mm below the top surface of the domain.

Centerplane pressure is plotted on the centerplane parallel to the wide face
Top surface pressure is plotted at 1 mm below the top surface, where the gradient of p is small.

Centerplane K is plotted on the centerplane parallel to the wide face. Top surface K is plotted at 16 mm below the top surface (2 nodes from the top surface boundary) where the gradient of K is small.

All centerplane and wide face velocity figures show the top 1.75 m of the domain.

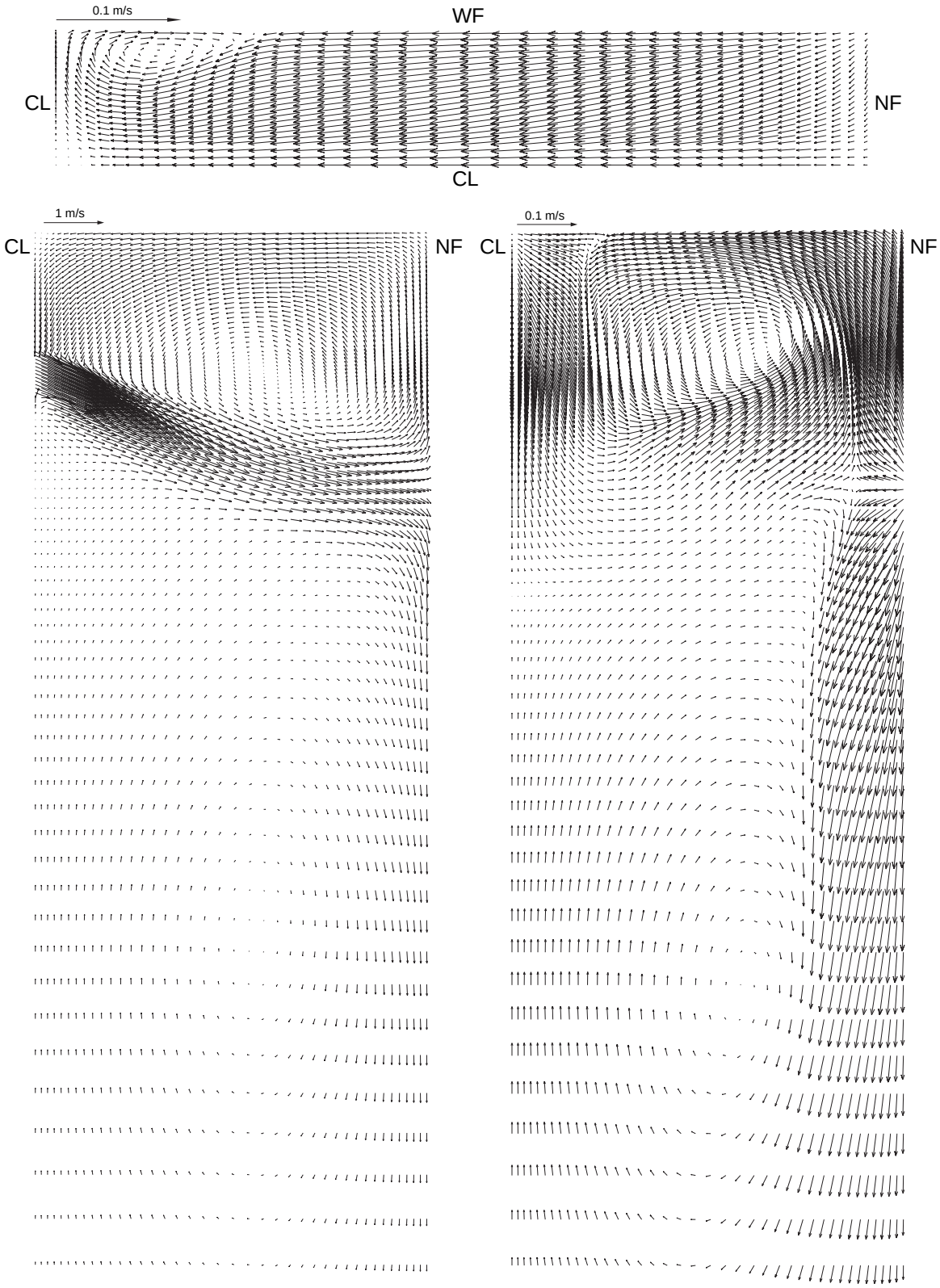

Figure E.1. Case 1. Centerplane (left), Wide Face (right) and Top Surface (top) Velocity. Standard Conditions, 0% Gas.

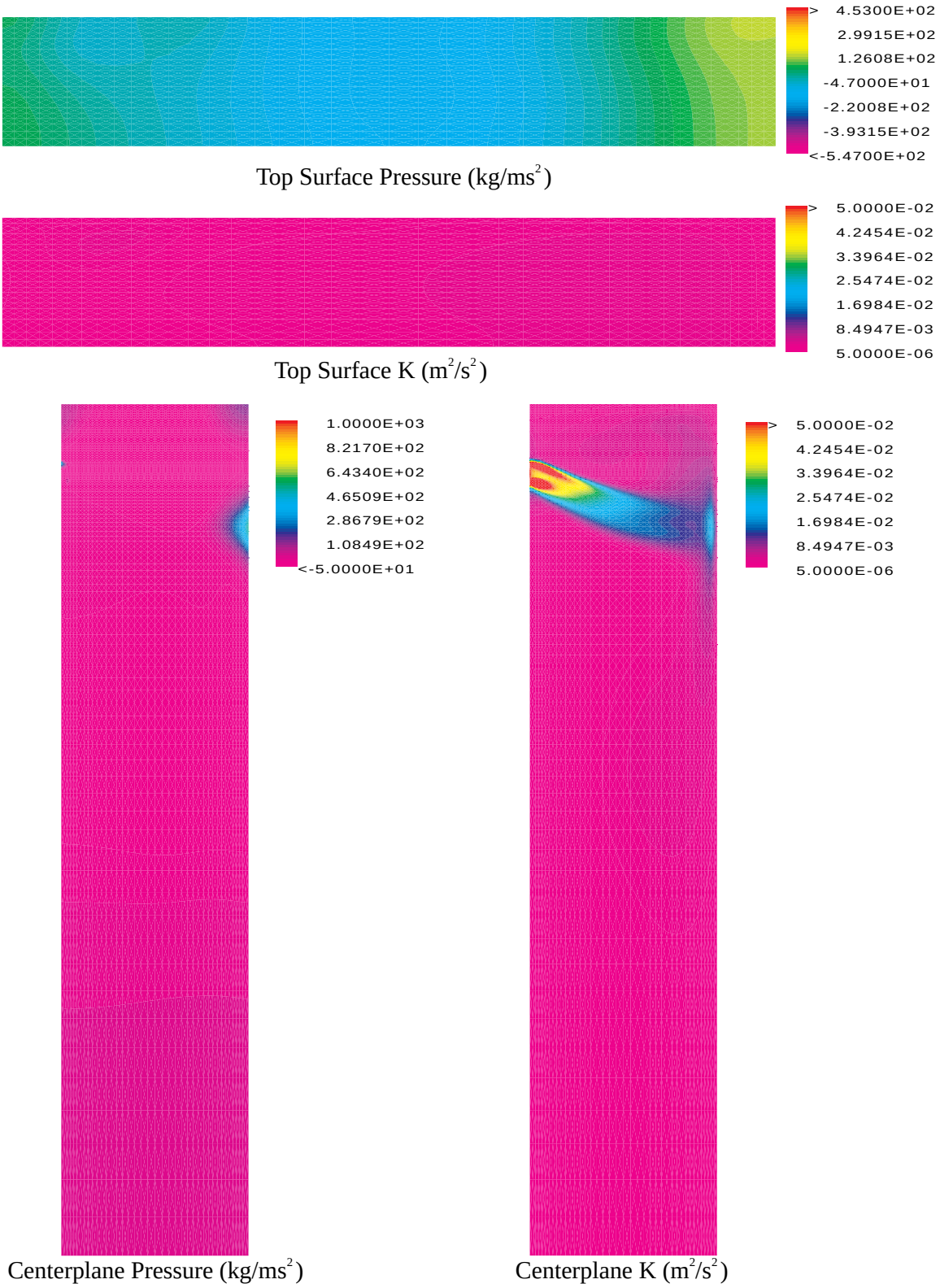

Figure E.2. Case 1. Standard Conditions, 0% Gas.

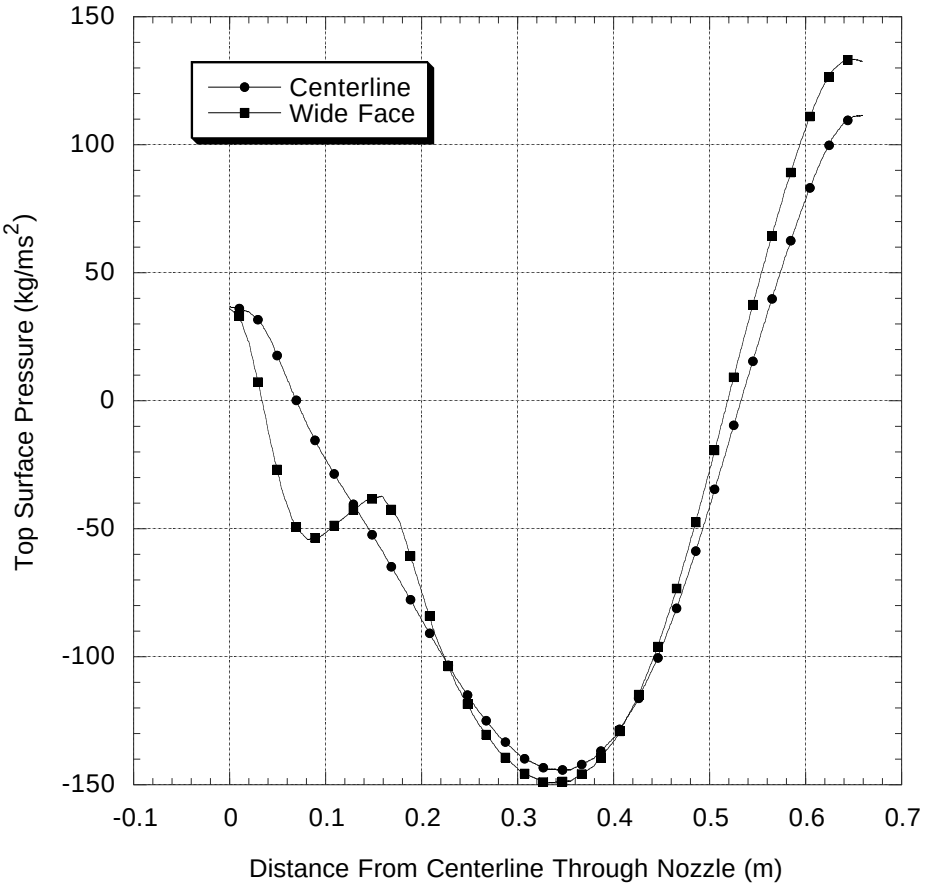

Figure E.3. Case 1. Centerplane and Wide Face Top Surface Pressure. Standard Conditions, 0% Gas.

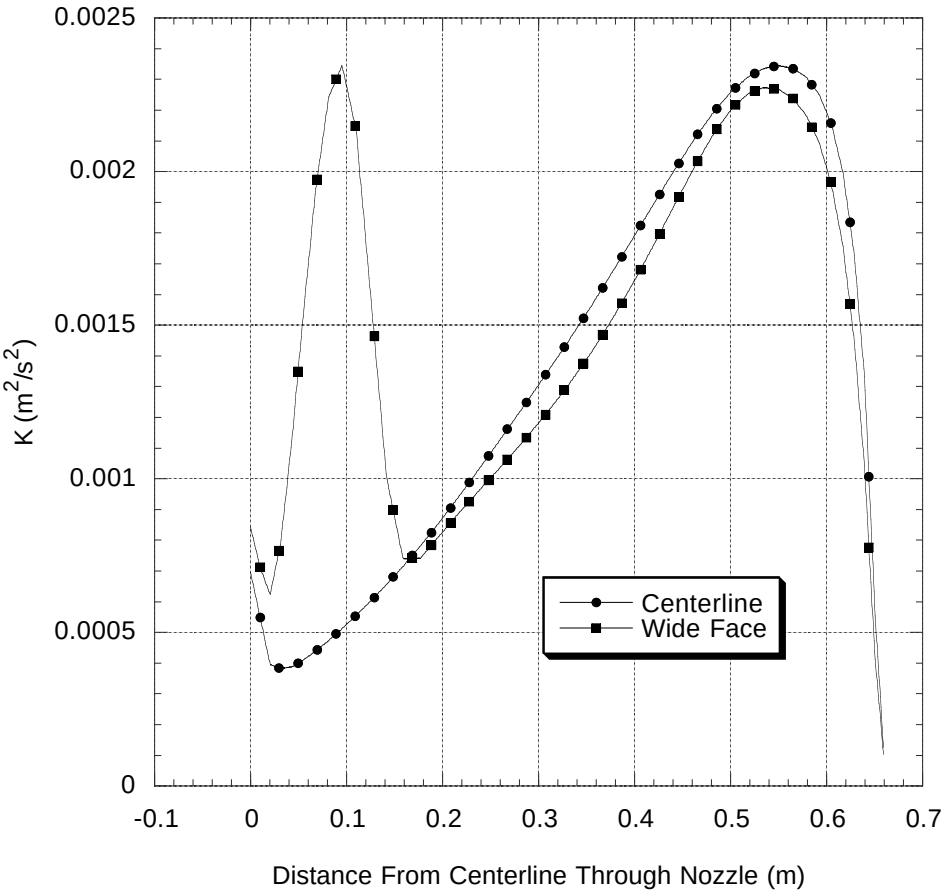

Figure E.4. Case 1. Centerplane and Wide Face Turbulent Kinetic Energy (K). Standard Conditions, 0% Gas.

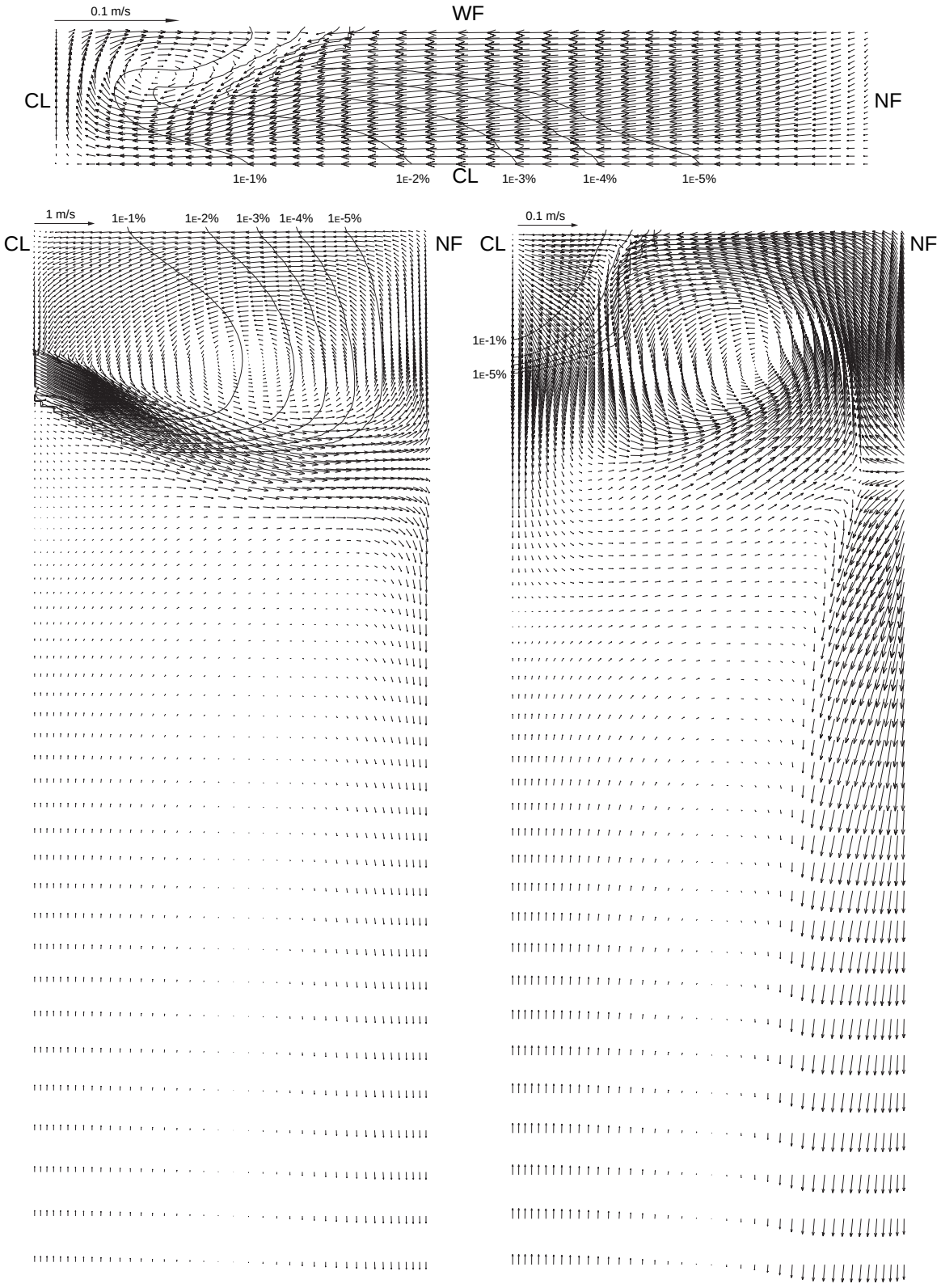

Figure E.5. Case 2. Centerplane (left), Wide Face (right) and Top Surface (top) Velocity. Standard Conditions, 1.0 mm Bubble Diameter, 6% Gas.

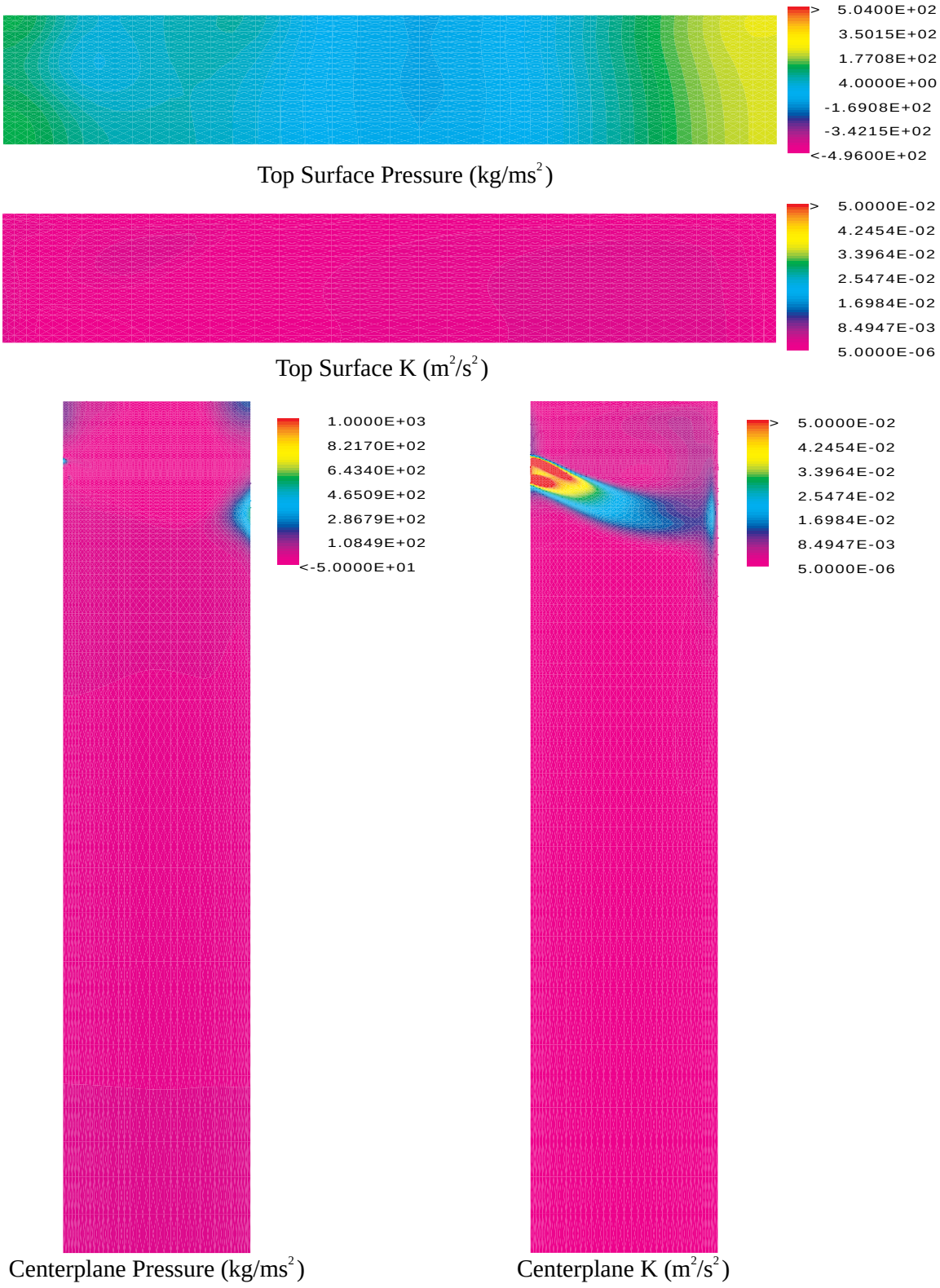

Figure E.6. Case 2. Standard Conditions, 1.0 mm Bubble Diameter, 6% Gas.

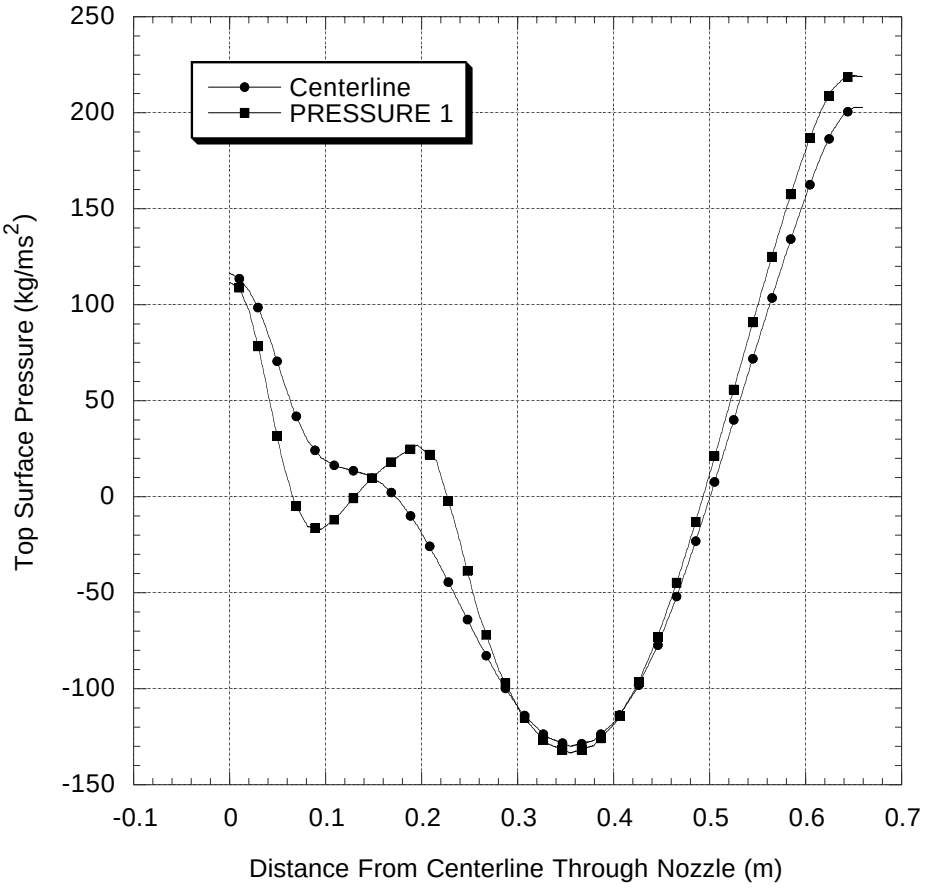

Figure E.7. Case 2. Centerplane and Wide Face Top Surface Pressure. Standard Conditions, 1.0 mm Bubble Diameter, 6% Gas.

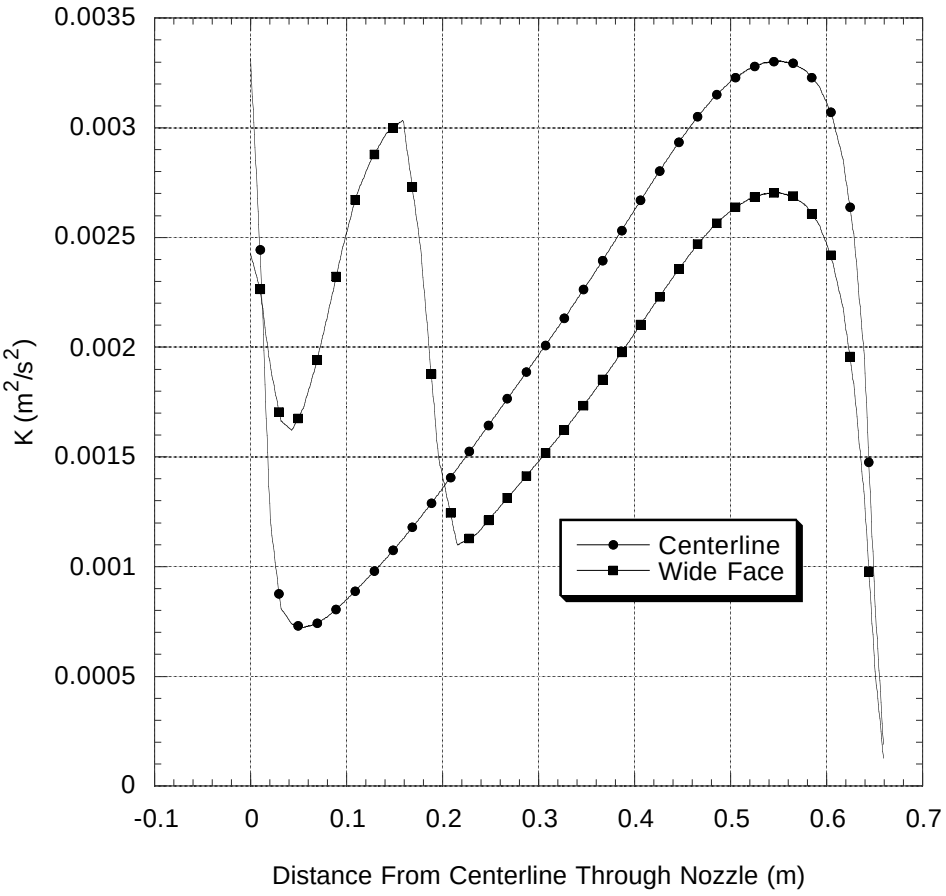

Figure E.8. Case 2. Centerplane and Wide Face Turbulent Kinetic Energy (K). Standard Conditions, 1.0 mm Bubble Diameter, 6% Gas.

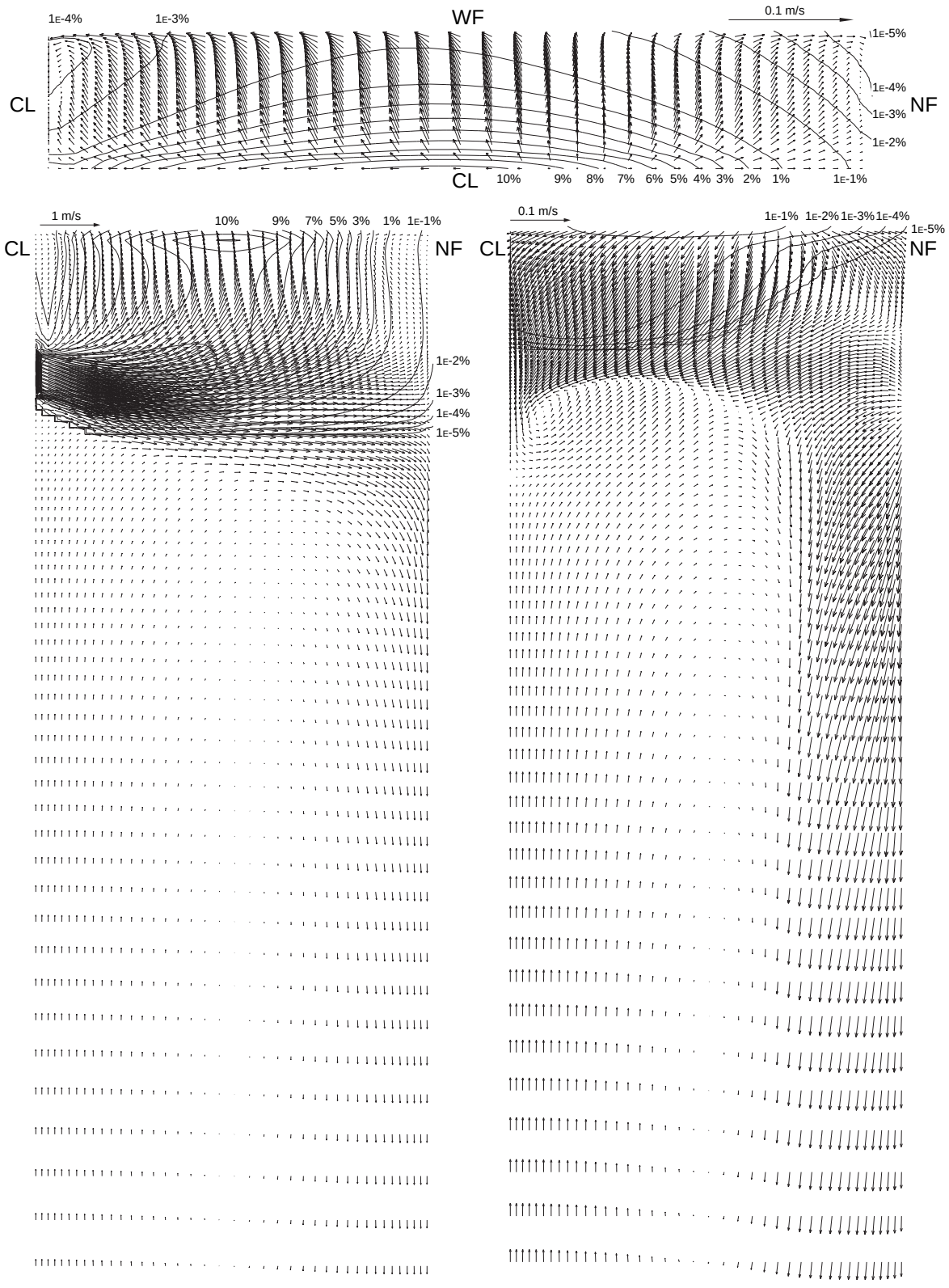

Figure E.9. Case 3. Centerplane (left), Wide Face (right) and Top Surface (top) Velocity. Standard Conditions, 1.0 mm Bubble Diameter, 20% Gas.

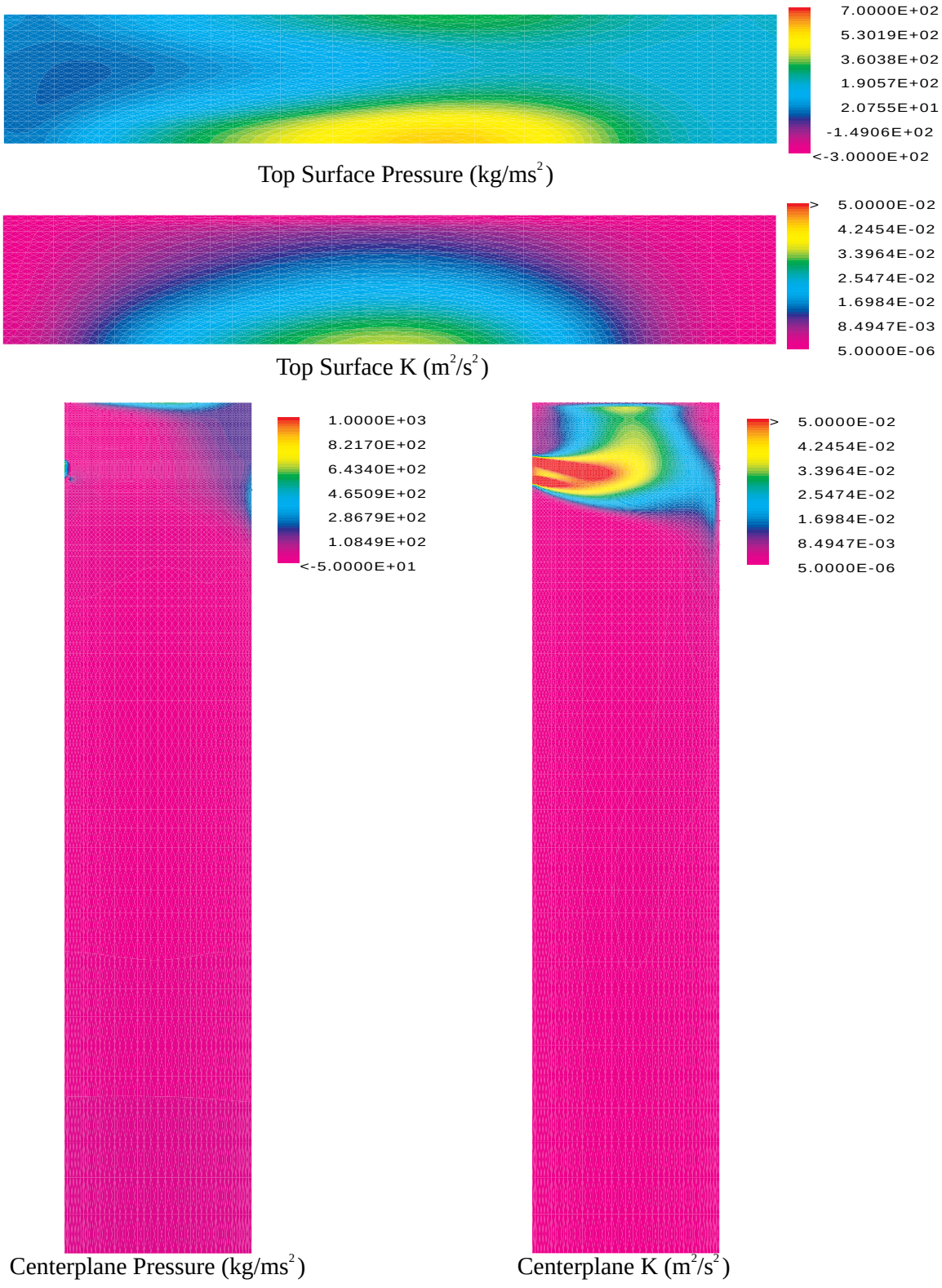

Figure E.10. Case 3. Standard Conditions, 1.0 mm Bubble Diameter, 20% Gas.

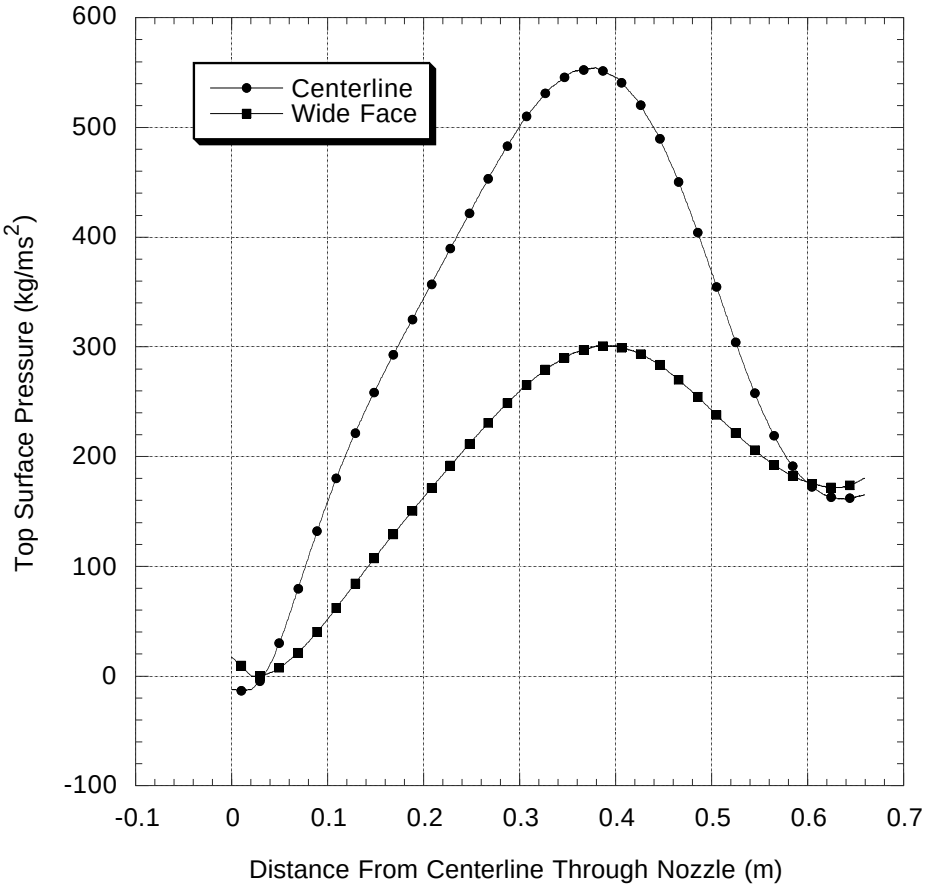

Figure E.11. Case 3. Centerplane and Wide Face Top Surface Pressure. Standard Conditions, 1.0 mm Bubble Diameter, 20% Gas.

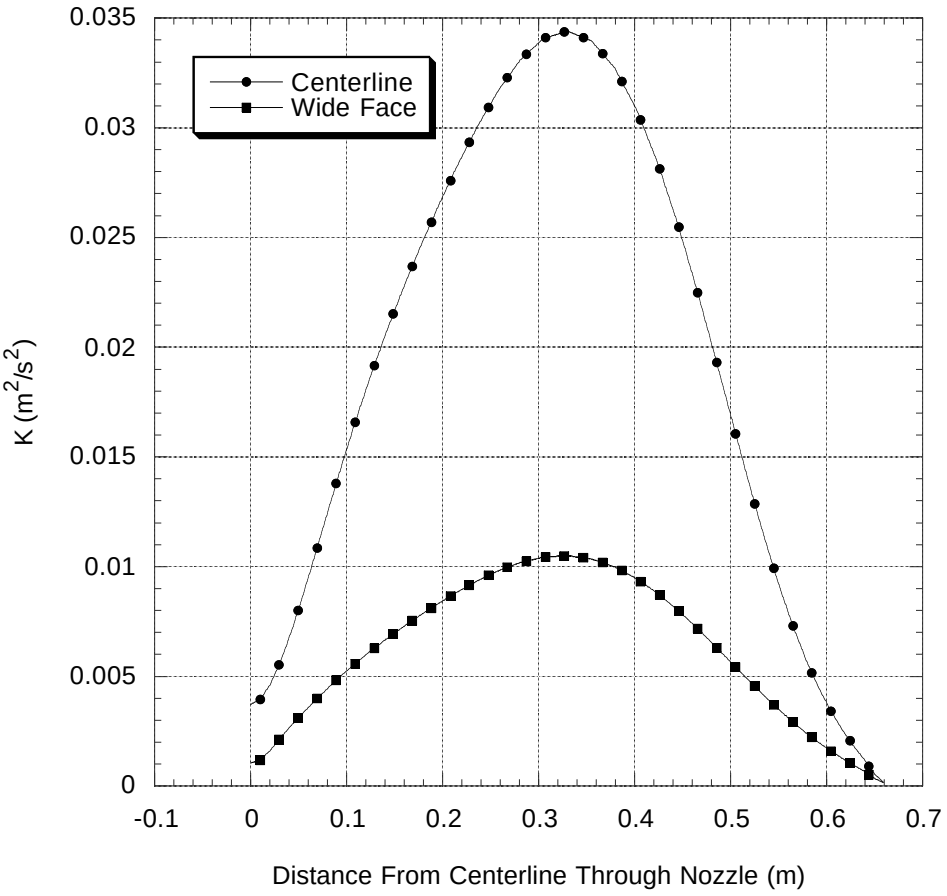

Figure E.12. Case 3. Centerplane and Wide Face Turbulent Kinetic Energy (K). Standard Conditions, 1.0 mm Bubble Diameter, 20% Gas.

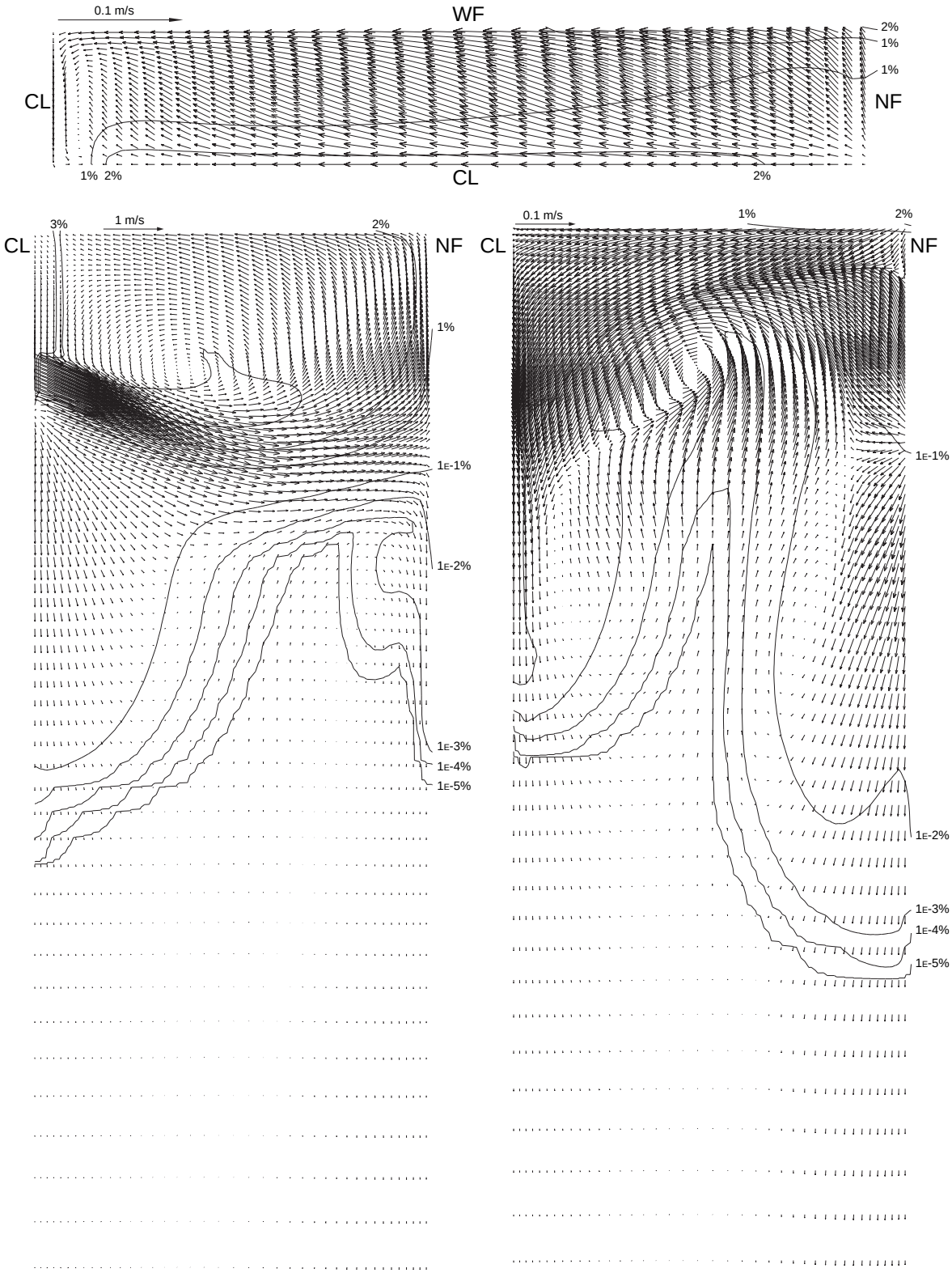

Figure E.13. Case 4. Centerplane (left), Wide Face (right) and Top Surface (top) Velocity. Standard Conditions, 0.5 mm Bubble Diameter, 6% Gas.

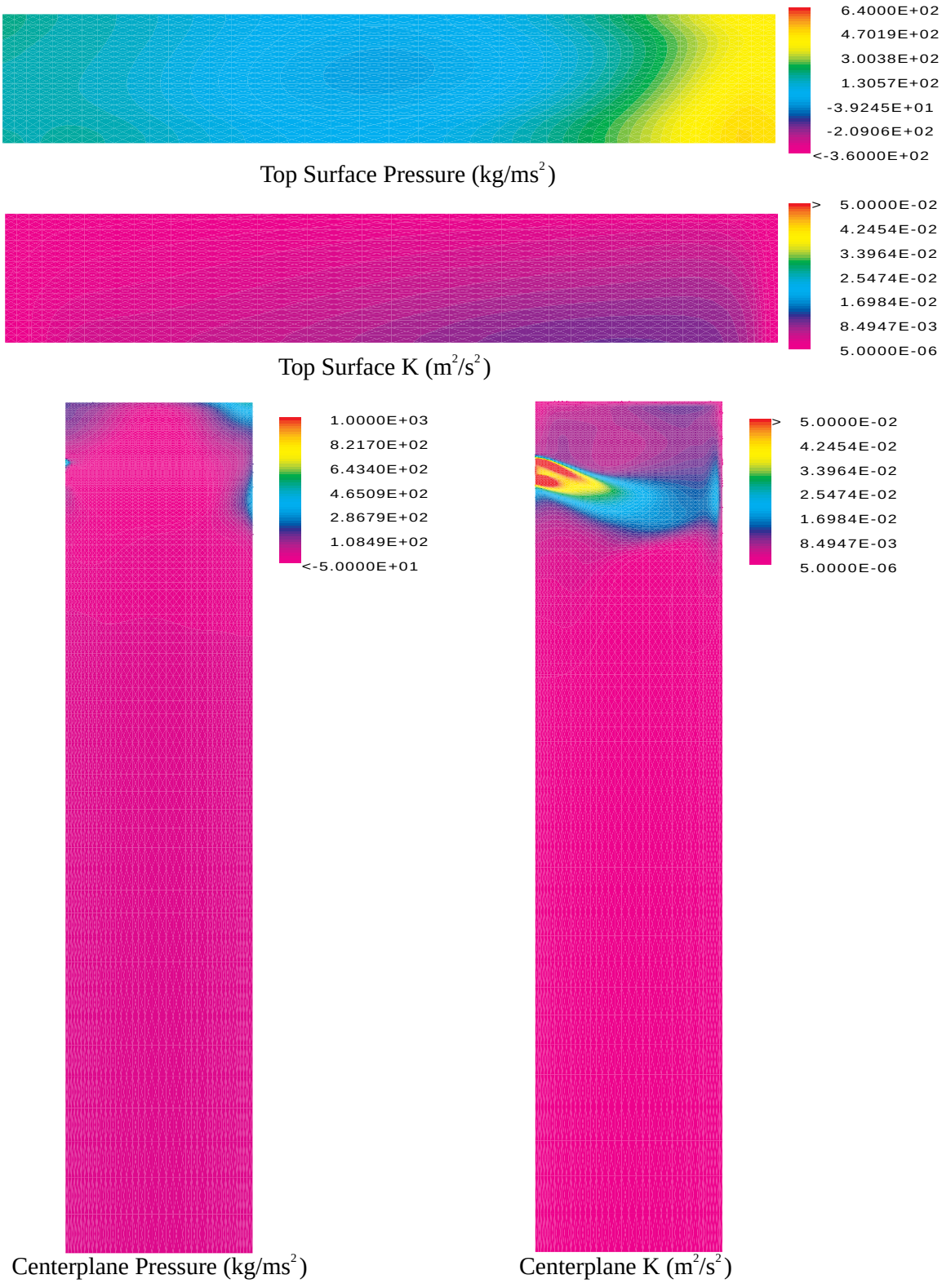

Figure E.14. Case 4. Standard Conditions, 0.5 mm Bubble Diameter, 6% Gas.

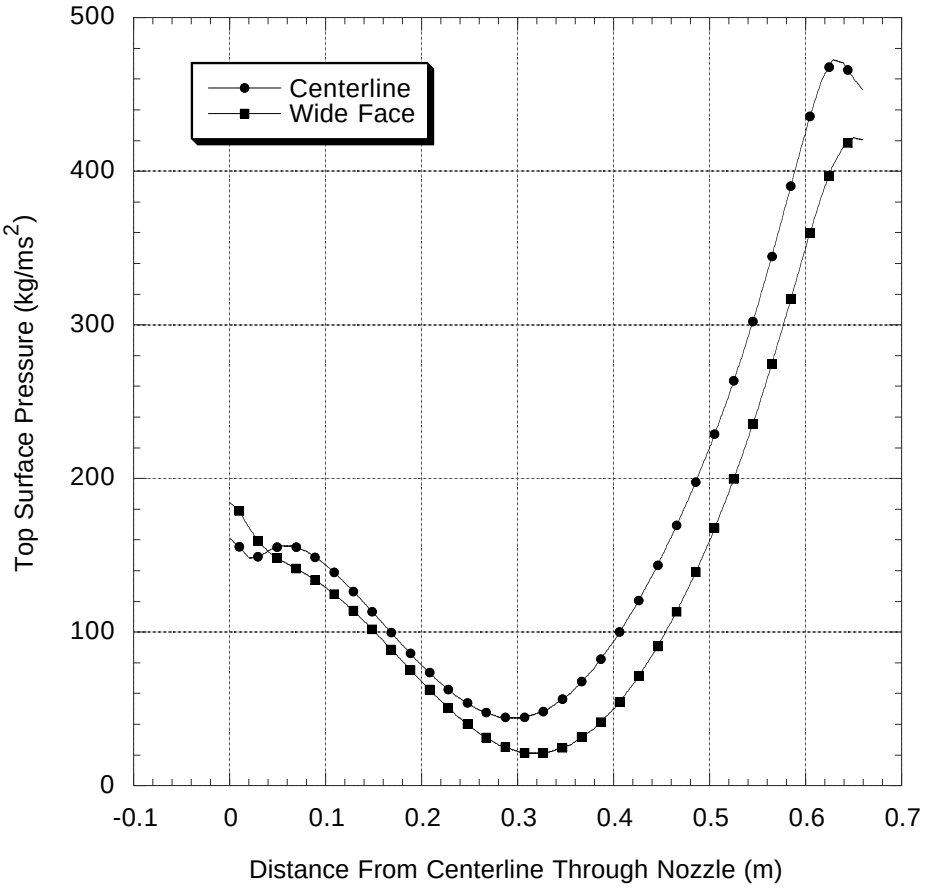

Figure E.15. Case 4. Centerplane and Wide Face Top Surface Pressure. Standard Conditions, 0.5 mm Bubble Diameter, 6% Gas.

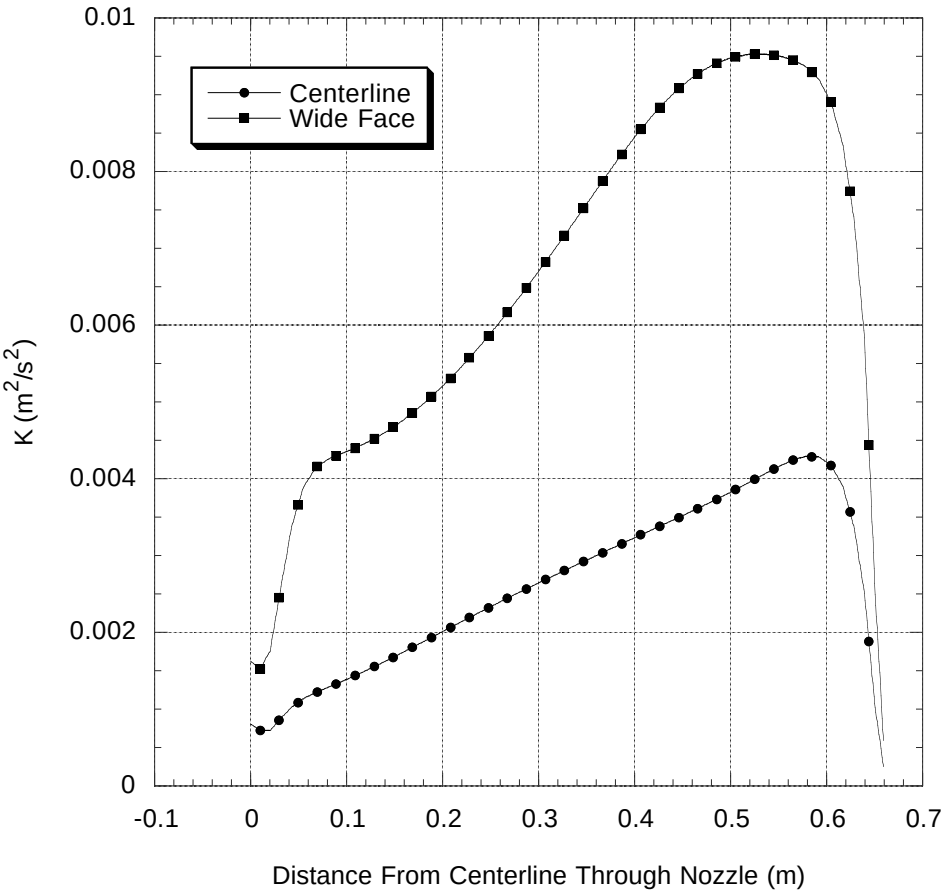

Figure E.16. Case 4. Centerplane and Wide Face Turbulent Kinetic Energy (K). Standard Conditions, 0.5 mm Bubble Diameter, 6% Gas.

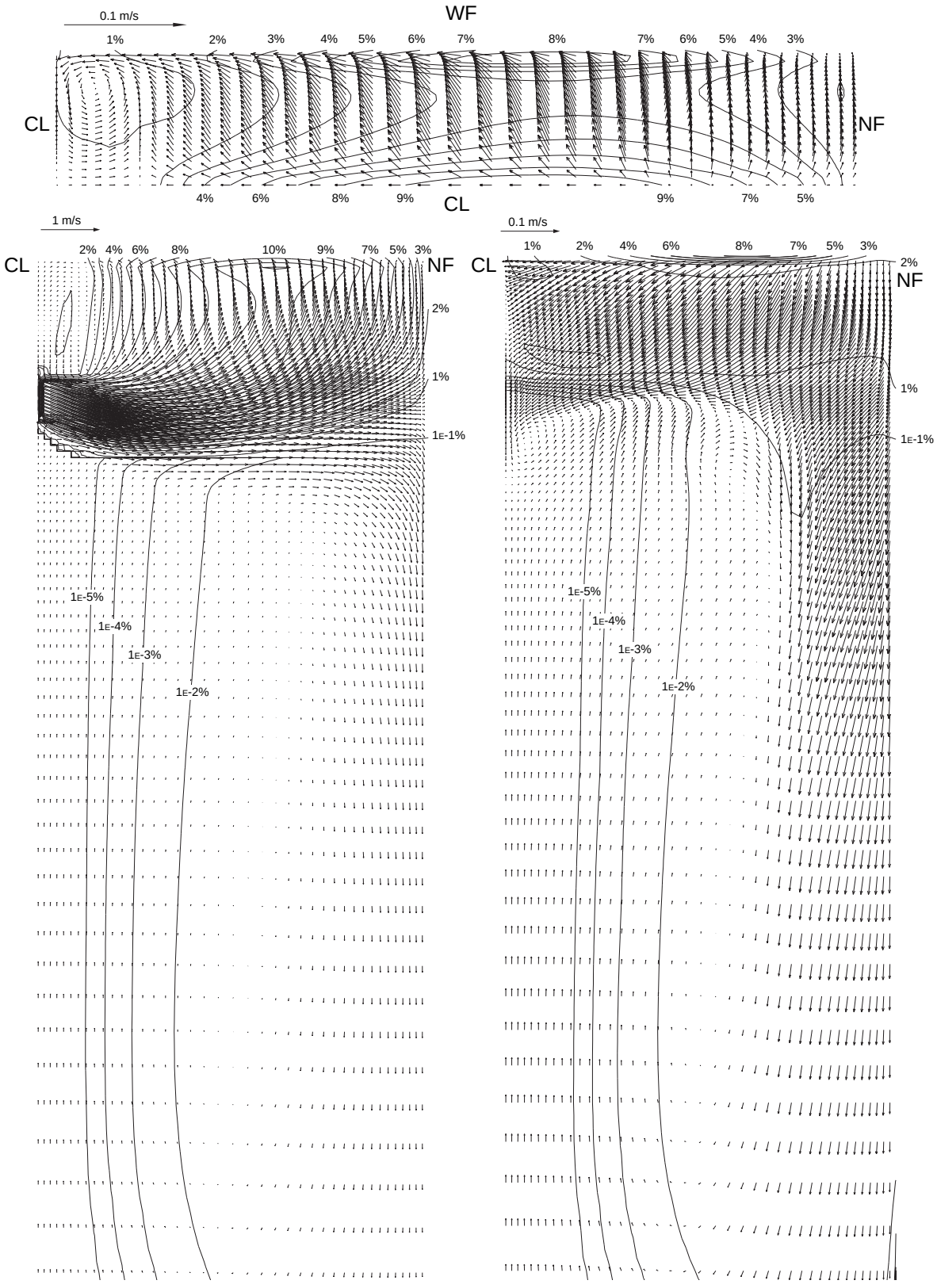

Figure E.17. Case 5. Centerplane (left), Wide Face (right) and Top Surface (top) Velocity. Standard Conditions, 0.5 mm Bubble Diameter, 20% Gas.

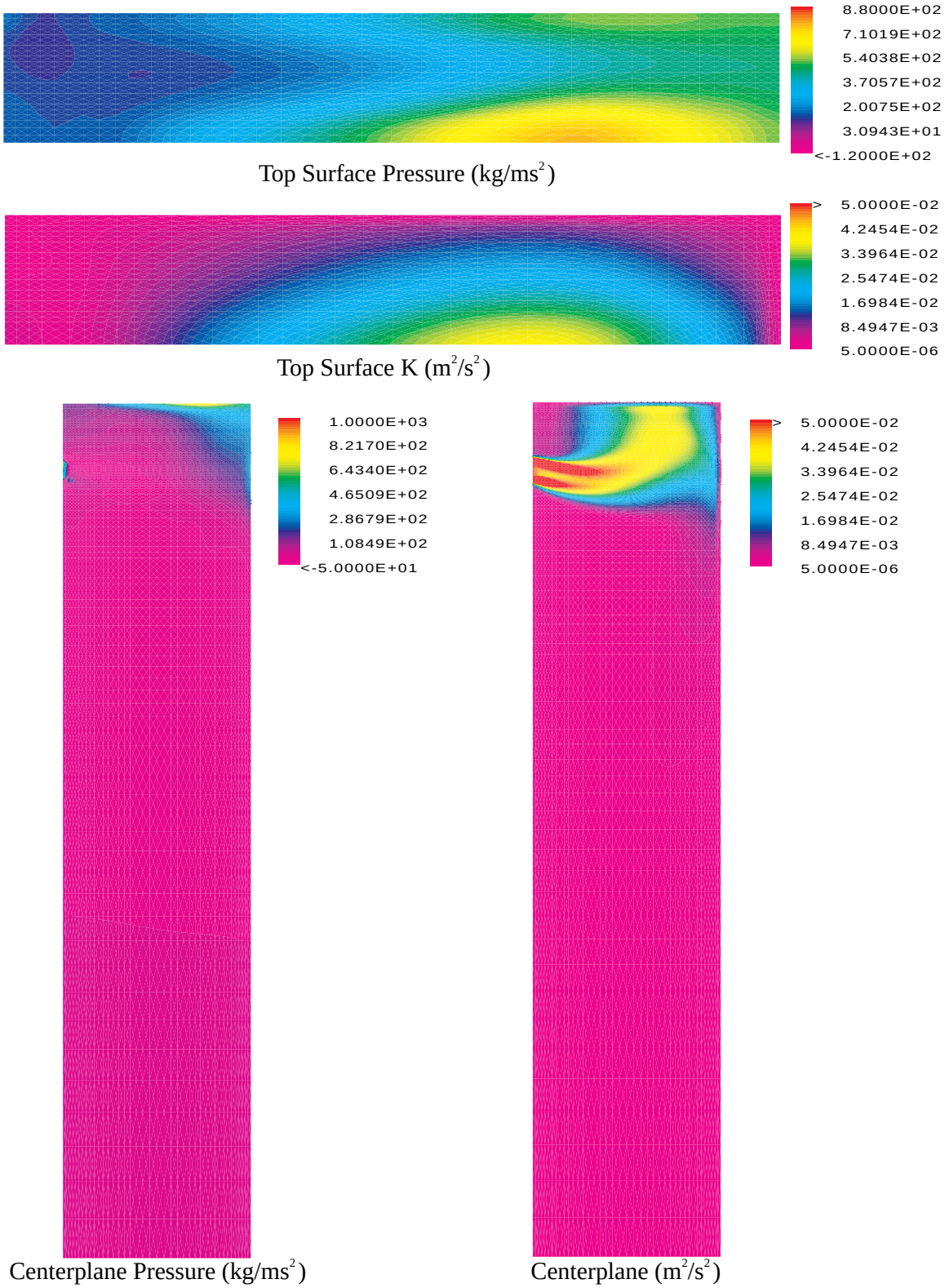

Figure E.18. Case 5. Standard Conditions, 0.5 mm Bubble Diameter, 20% Gas.

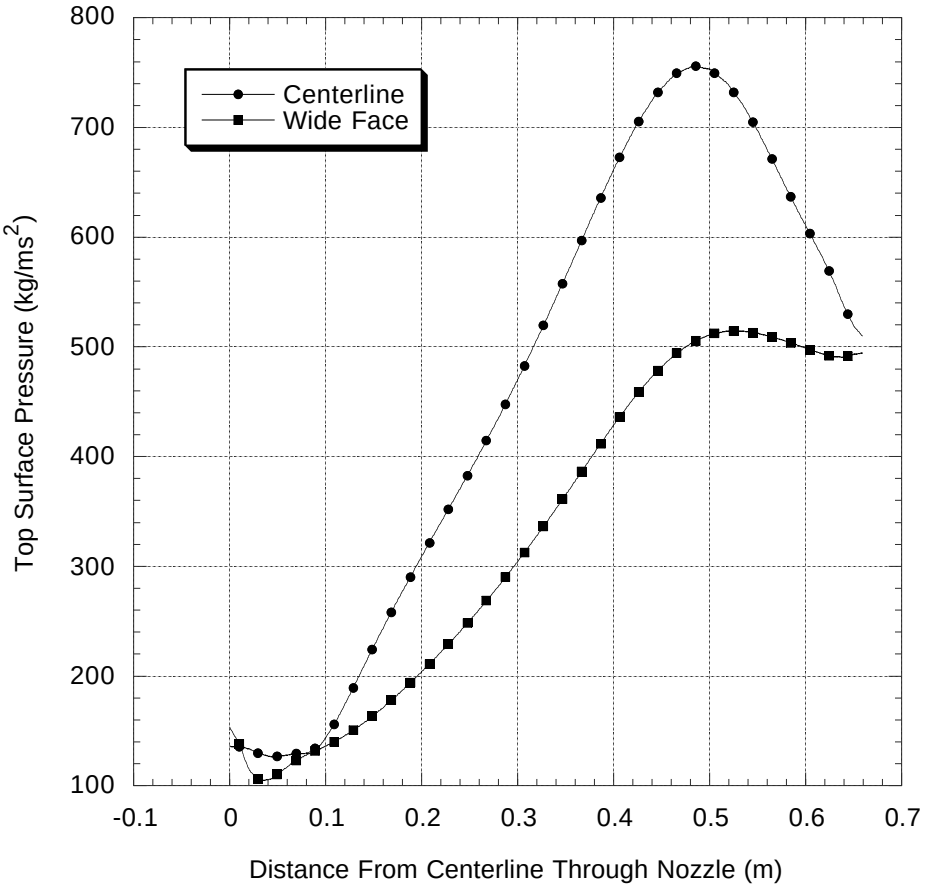

Figure E.19. Case 5. Centerplane and Wide Face Top Surface Pressure. Standard Conditions, 0.5 mm Bubble Diameter, 20% Gas.

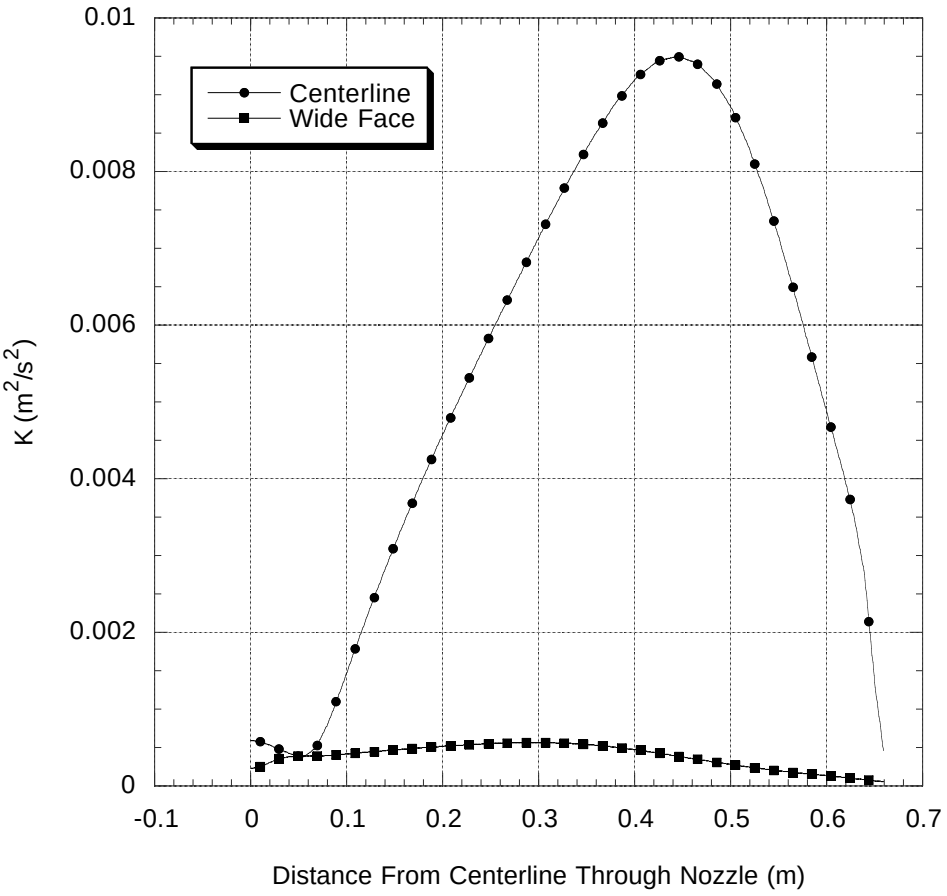

Figure E.20. Case 5. Centerplane and Wide Face Turbulent Kinetic Energy (K). Standard Conditions, 0.5 mm Bubble Diameter, 20% Gas.

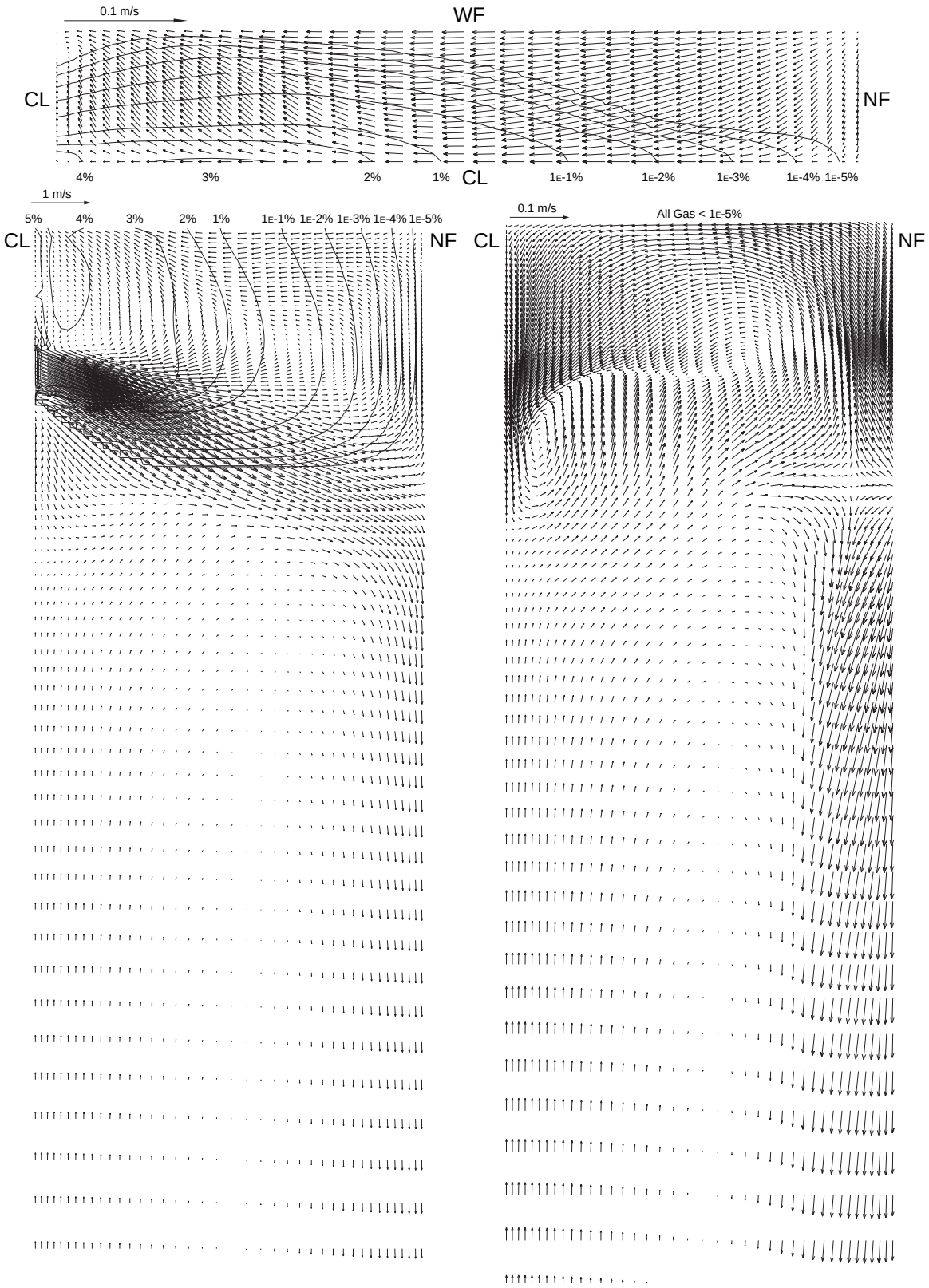

Figure E.21. Case 6. Centerplane (left), Wide Face (right) and Top Surface (top) Velocity. Standard Conditions, 2.0 mm Bubble Diameter, 6% Gas.

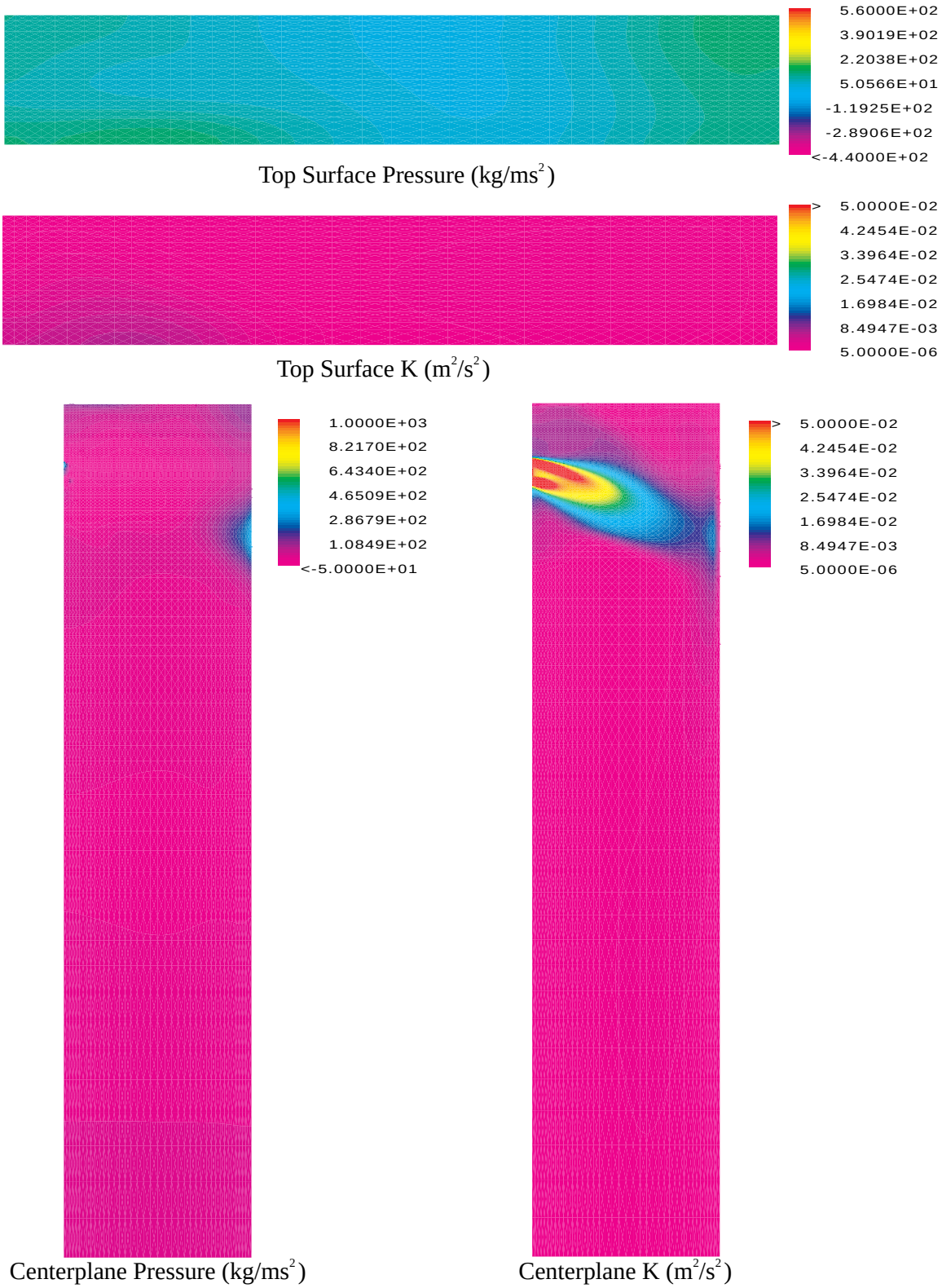

Figure E.22. Case 6. Standard Conditions, 2.0 mm Bubble Diameter, 6% Gas.

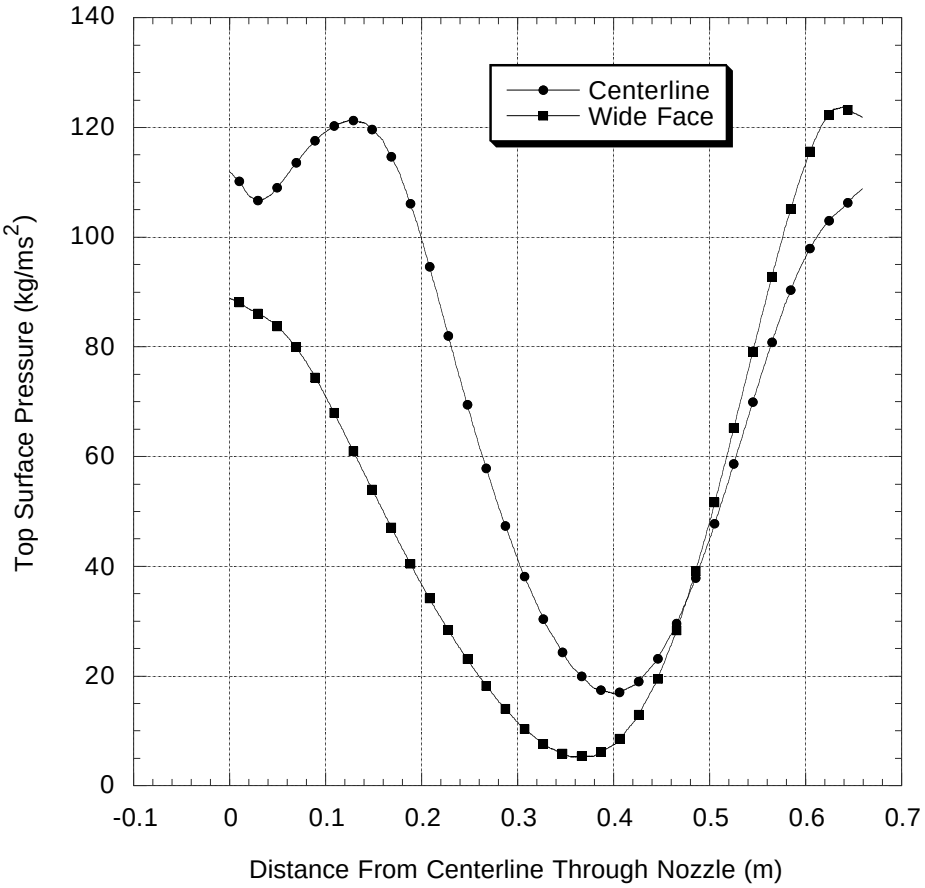

Figure E.23. Case 6. Centerplane and Wide Face Top Surface Pressure. Standard Conditions, 2.0 mm Bubble Diameter, 6% Gas.

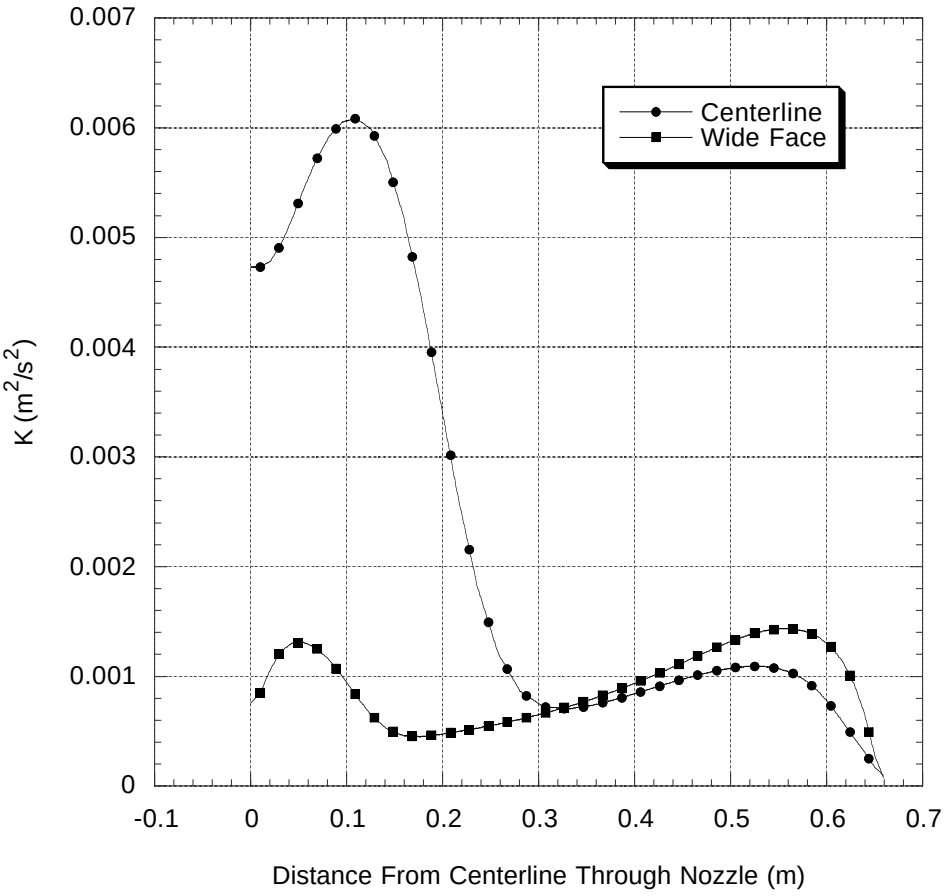

Figure E.24. Case 6. Centerplane and Wide Face Turbulent Kinetic Energy (K). Standard Conditions, 2.0 mm Bubble Diameter, 6% Gas.

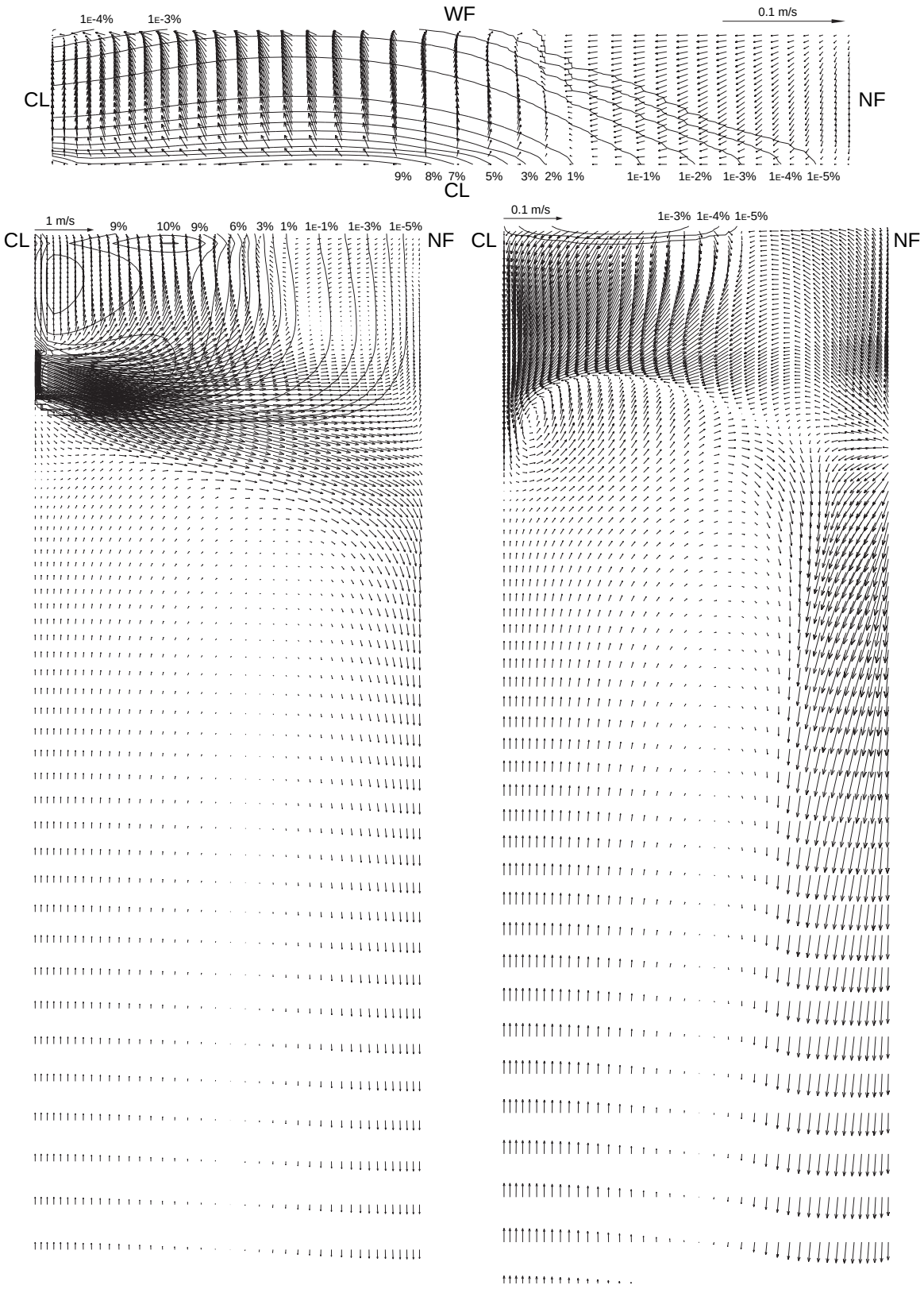

Figure E.25. Case 7. Centerplane (left), Wide Face (right) and Top Surface (top) Velocity. Standard Conditions, 2.0 mm Bubble Diameter, 20% Gas.

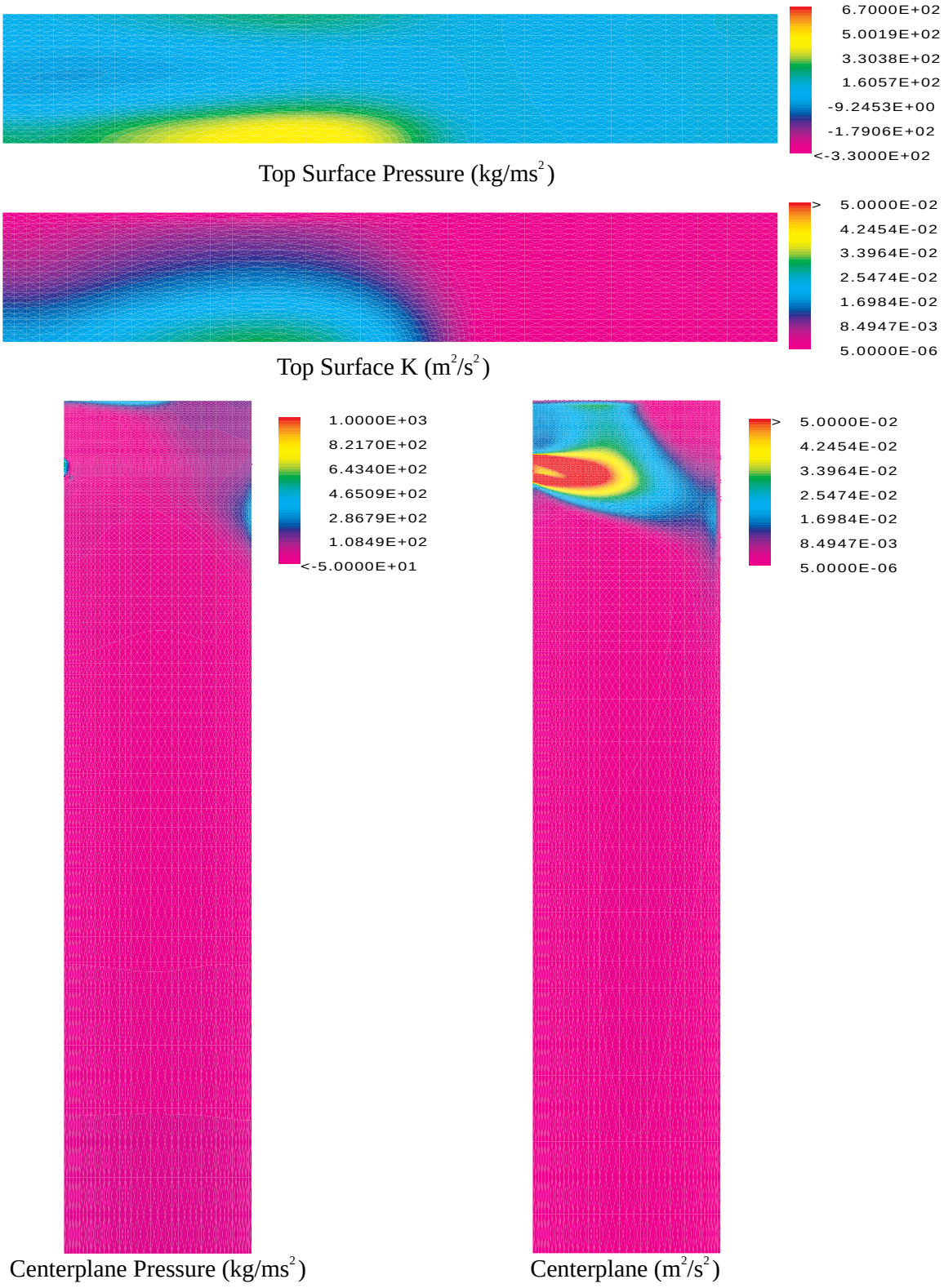

Figure E.26. Case 7. Standard Conditions, 2.0 mm Bubble Diameter, 20% Gas.

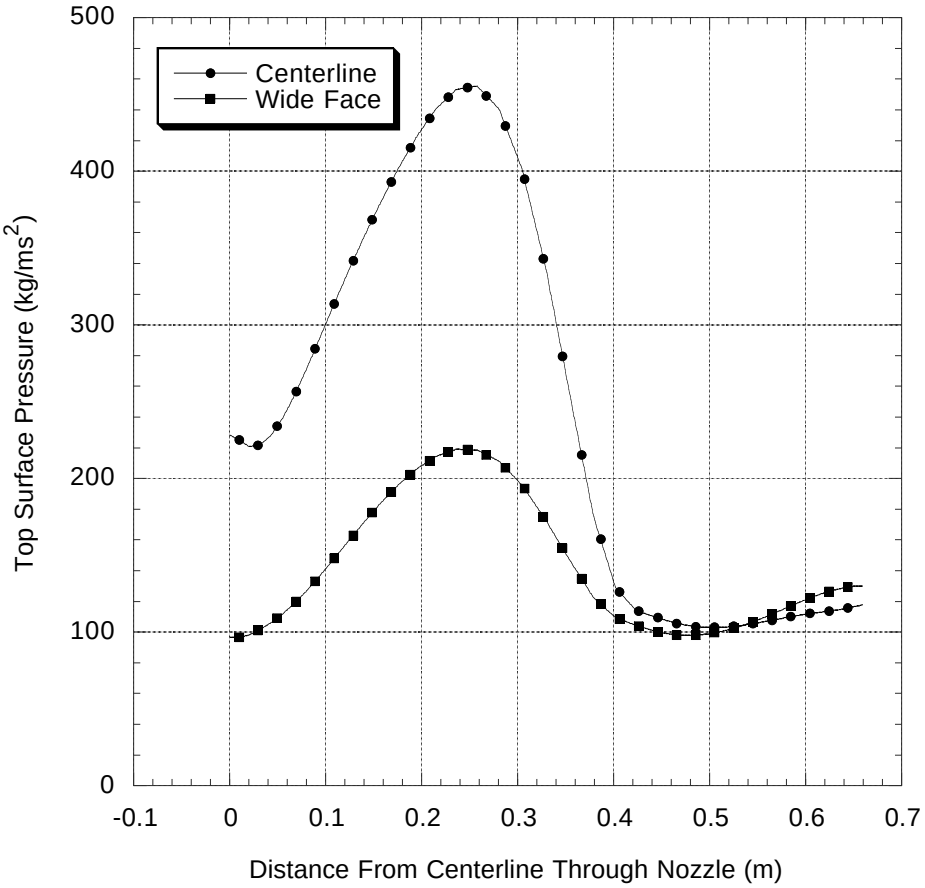

Figure E.27. Case 7. Centerplane and Wide Face Top Surface Pressure. Standard Conditions, 2.0 mm Bubble Diameter, 20% Gas.

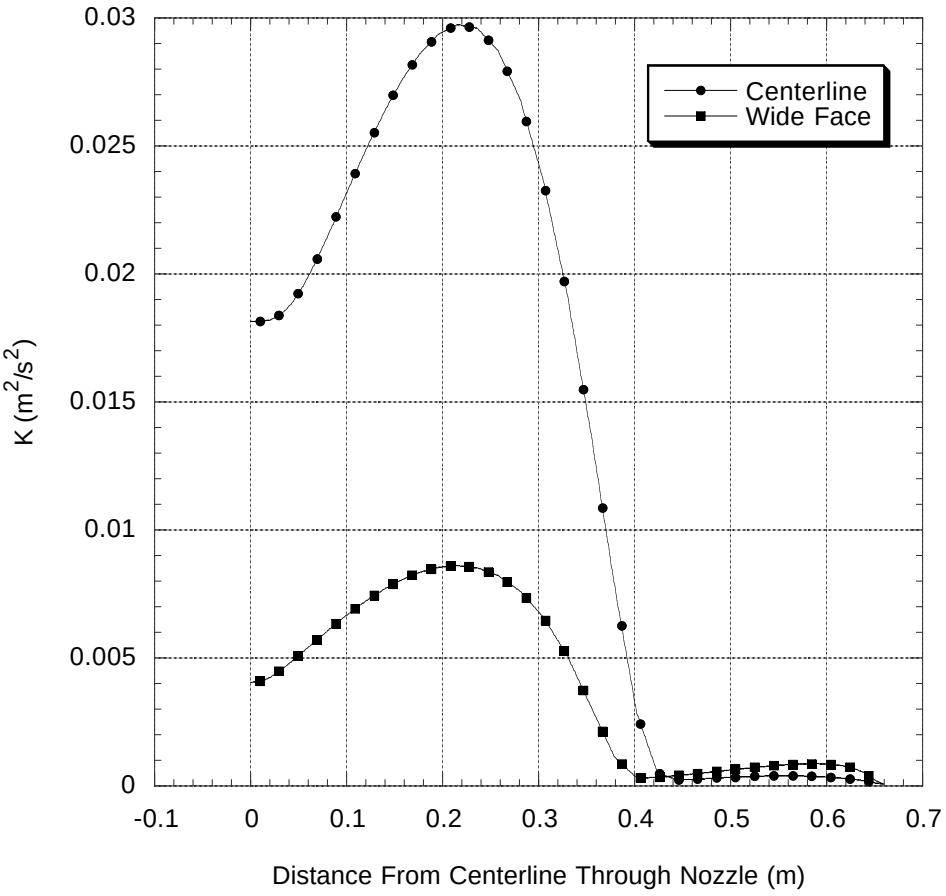

Figure E.28. Case 7. Centerplane and Wide Face Turbulent Kinetic Energy (K). Standard Conditions, 2.0 mm Bubble Diameter, 20% Gas.

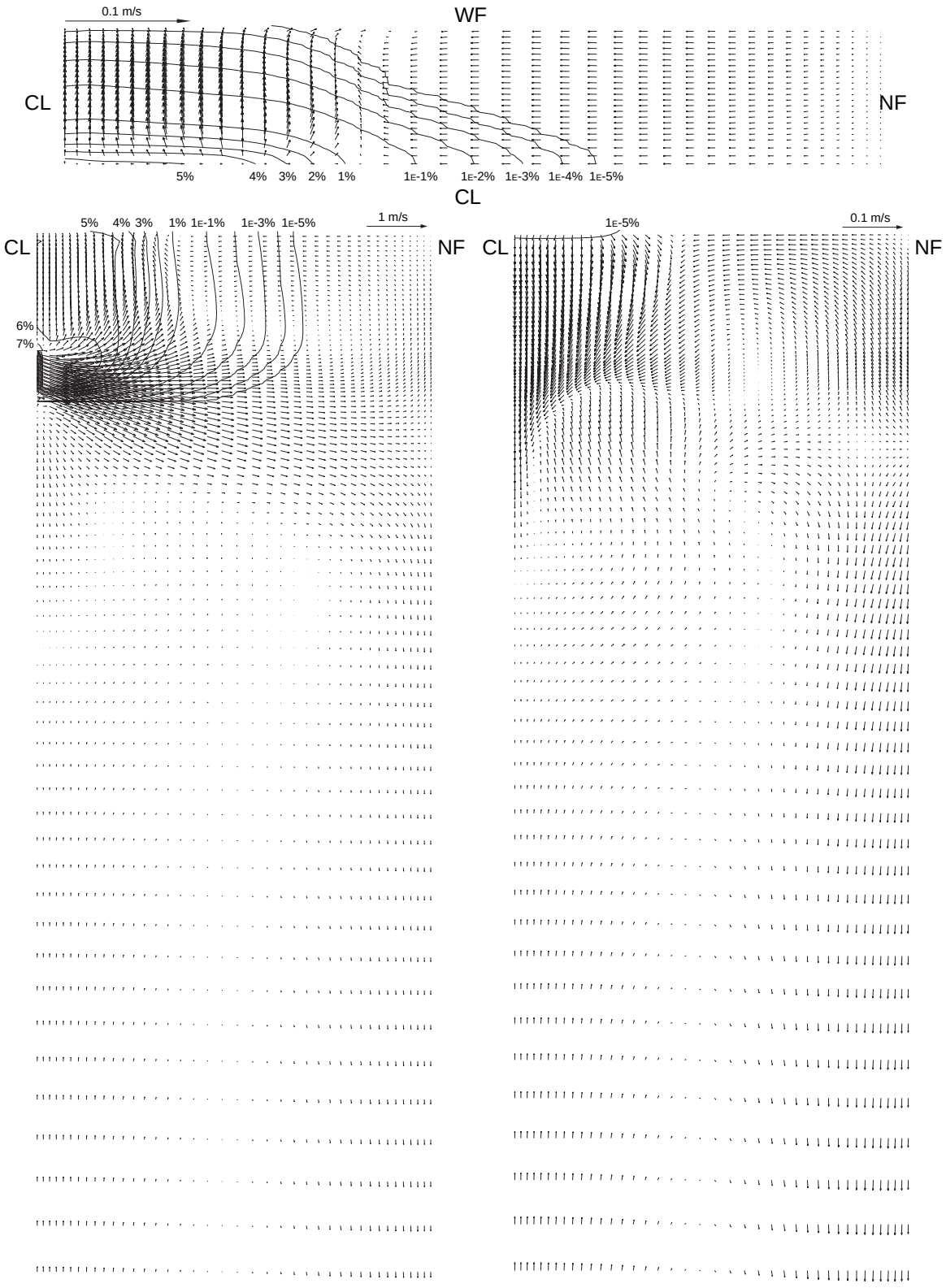

Figure E.29. Case 8. Centerplane (left), Wide Face (right) and Top Surface (top) Velocity. Casting Speed 8.35 m/s, 2.0 mm Bubble Diameter, 6% Gas.

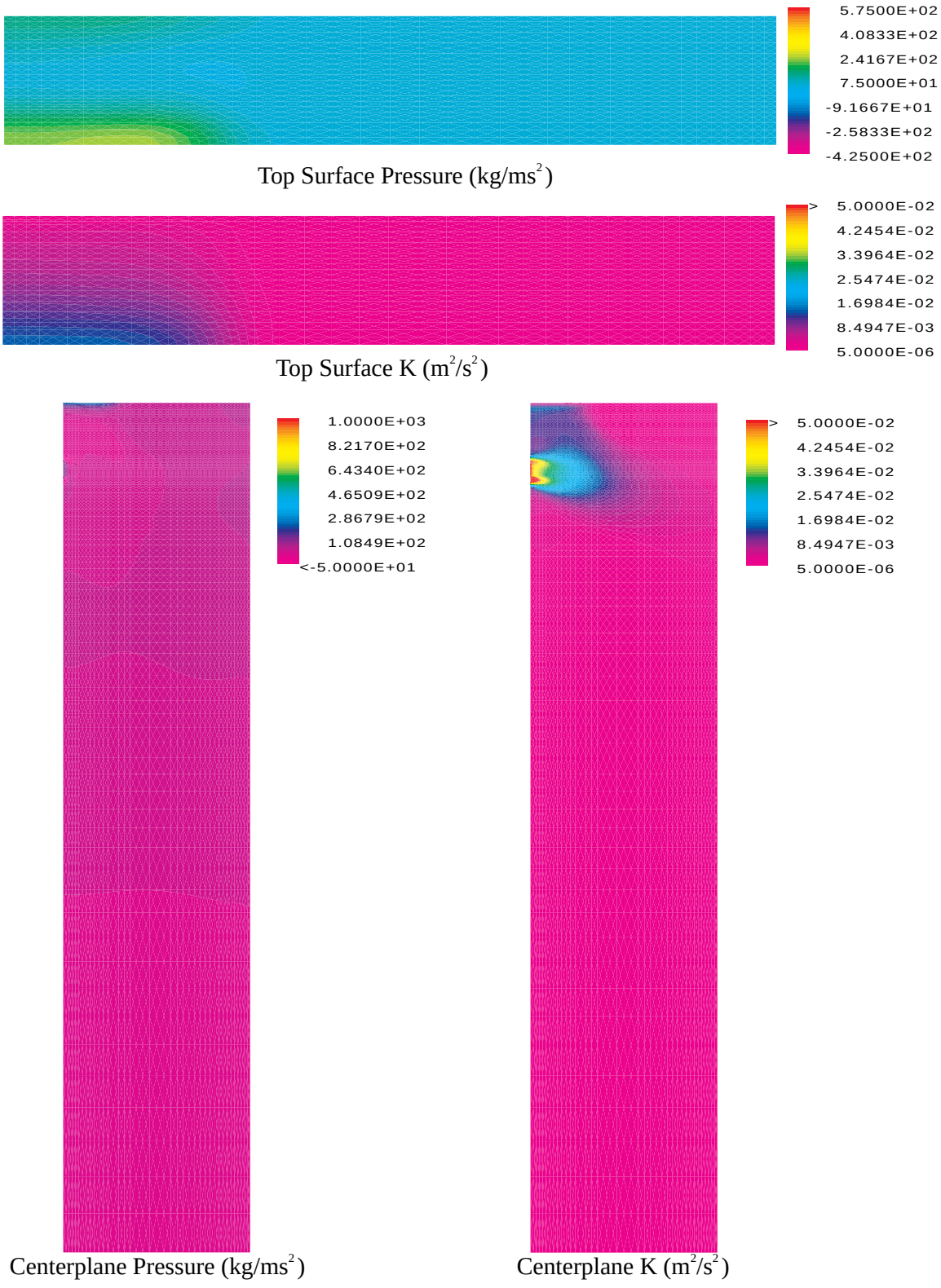

Figure E.30. Case 8. Casting Speed 8.35 m/s, 2.0 mm Bubble Diameter, 6% Gas.

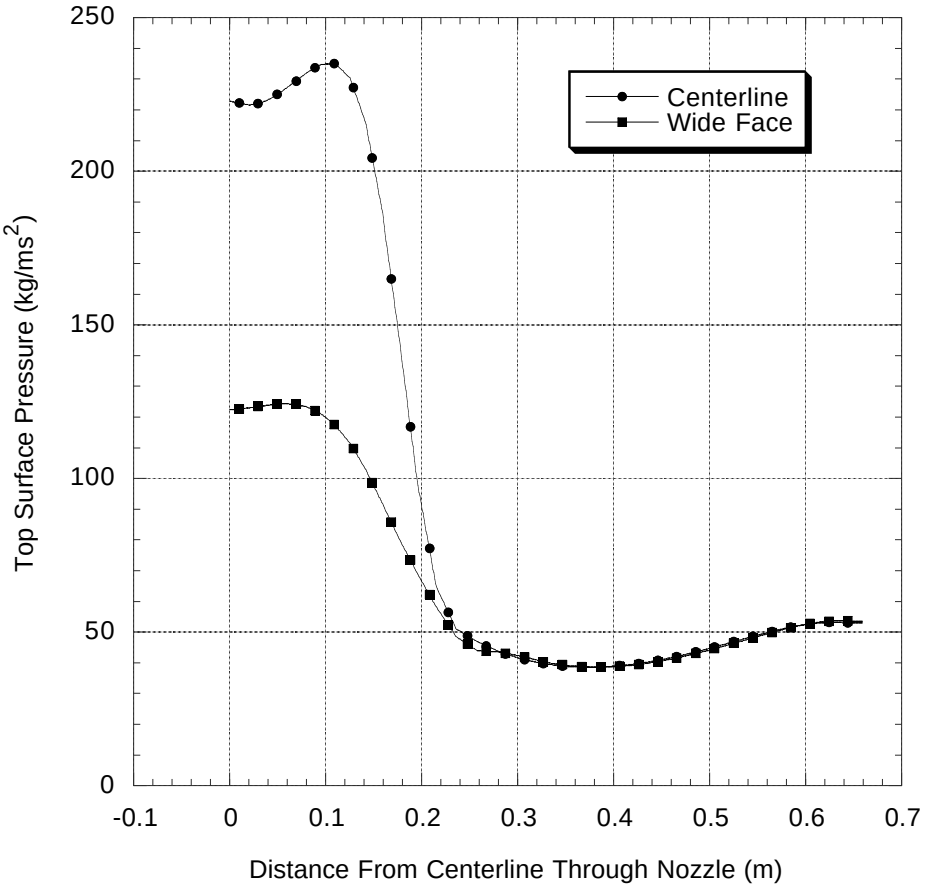

Figure E.31. Case 8. Centerplane and Wide Face Top Surface Pressure. Casting Speed 8.35 m/s, 2.0 mm Bubble Diameter, 6% Gas.

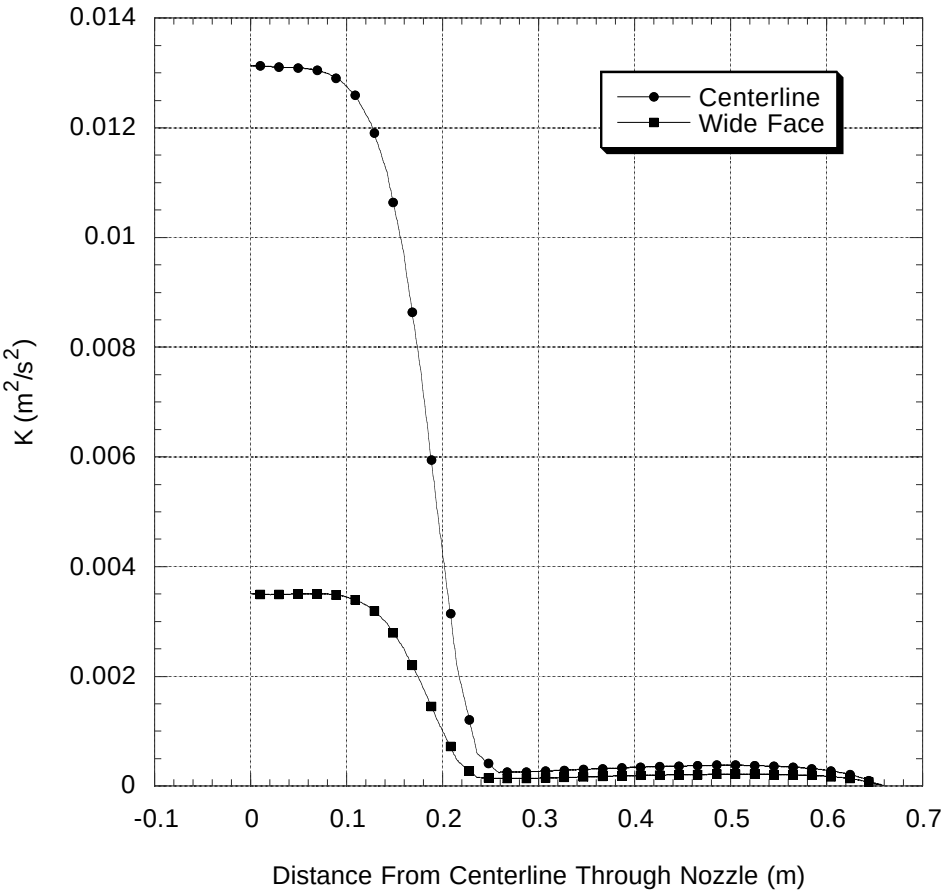

Figure E.32. Case 8. Centerplane and Wide Face Turbulent Kinetic Energy (K). Casting Speed 8.35 m/s, 2.0 mm Bubble Diameter, 6% Gas.

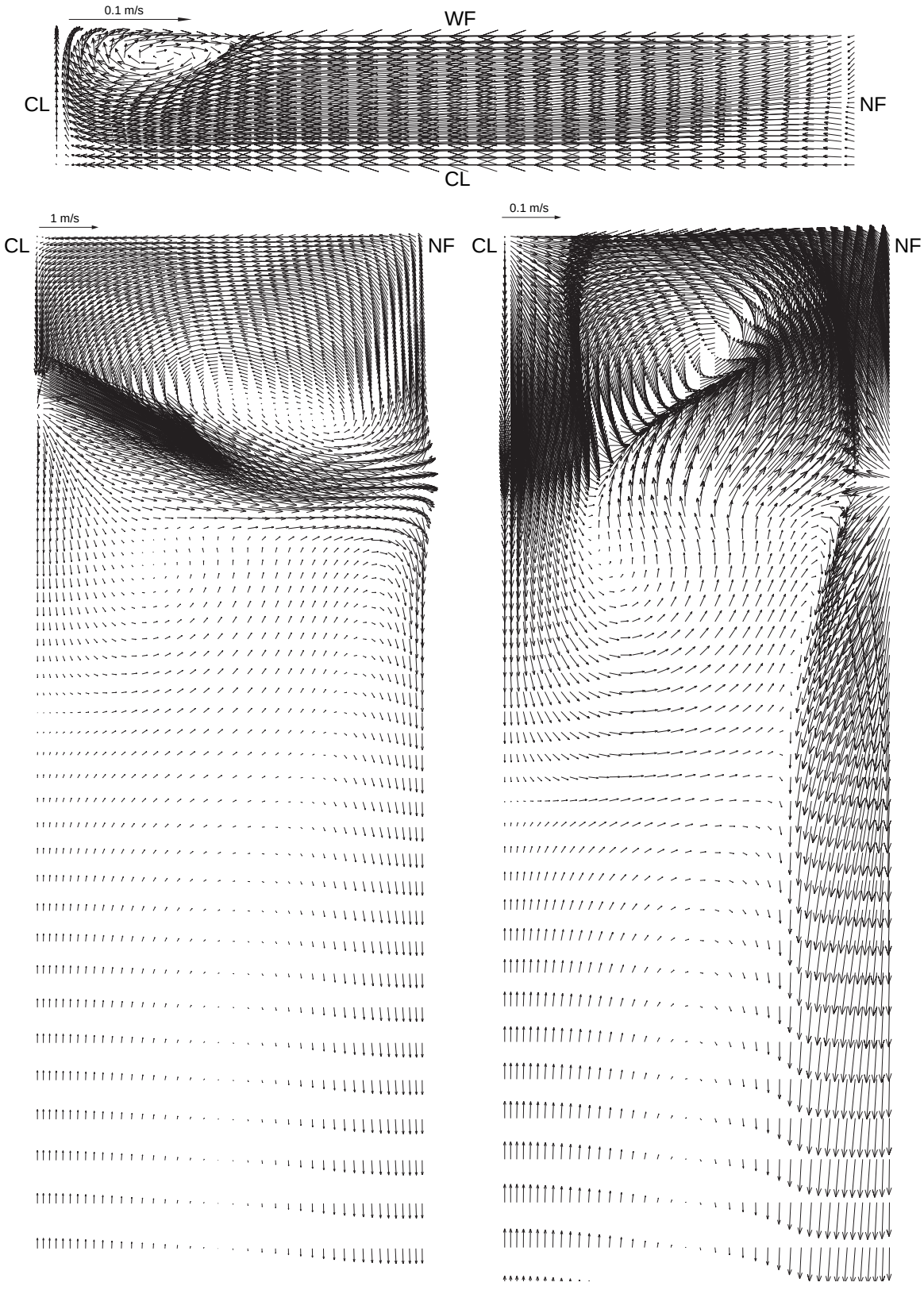

Figure E.33. Case 9. Centerplane (left), Wide Face (right) and Top Surface (top) Velocity. Casting Speed 41.75 m/s, 0% Gas.

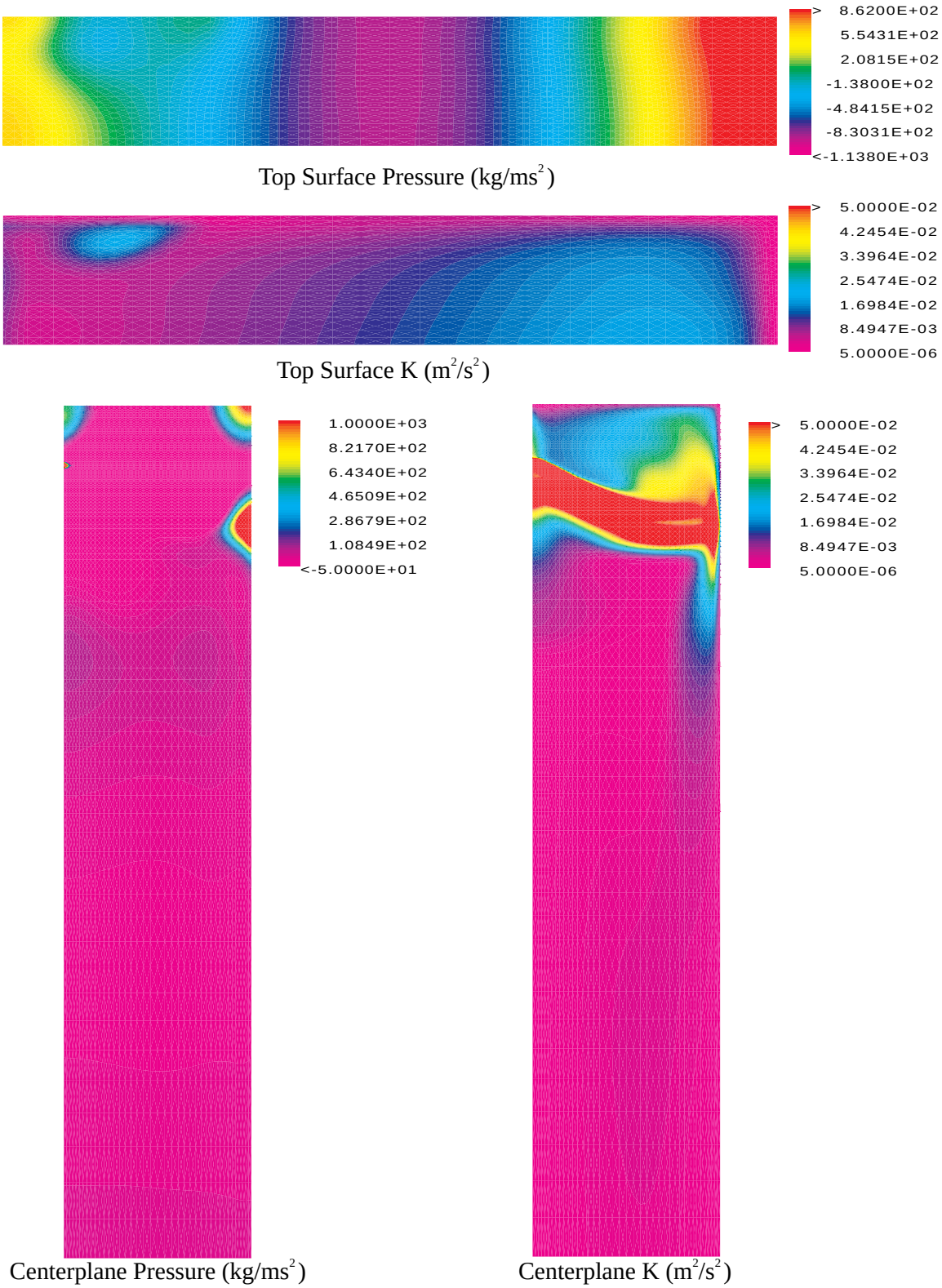

Figure E.34. Case 9. Casting Speed 41.75 m/s, 0% Gas.

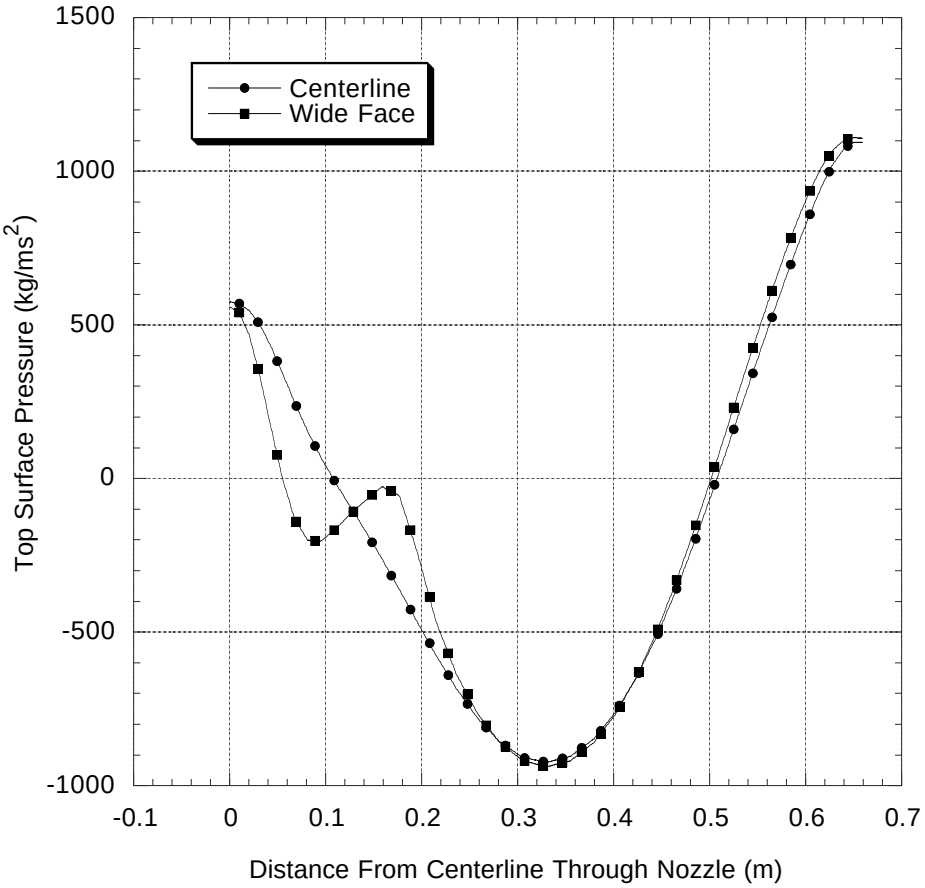

Figure E.35. Case 9. Centerplane and Wide Face Top Surface Pressure. Casting Speed 41.75 m/s, 0% Gas.

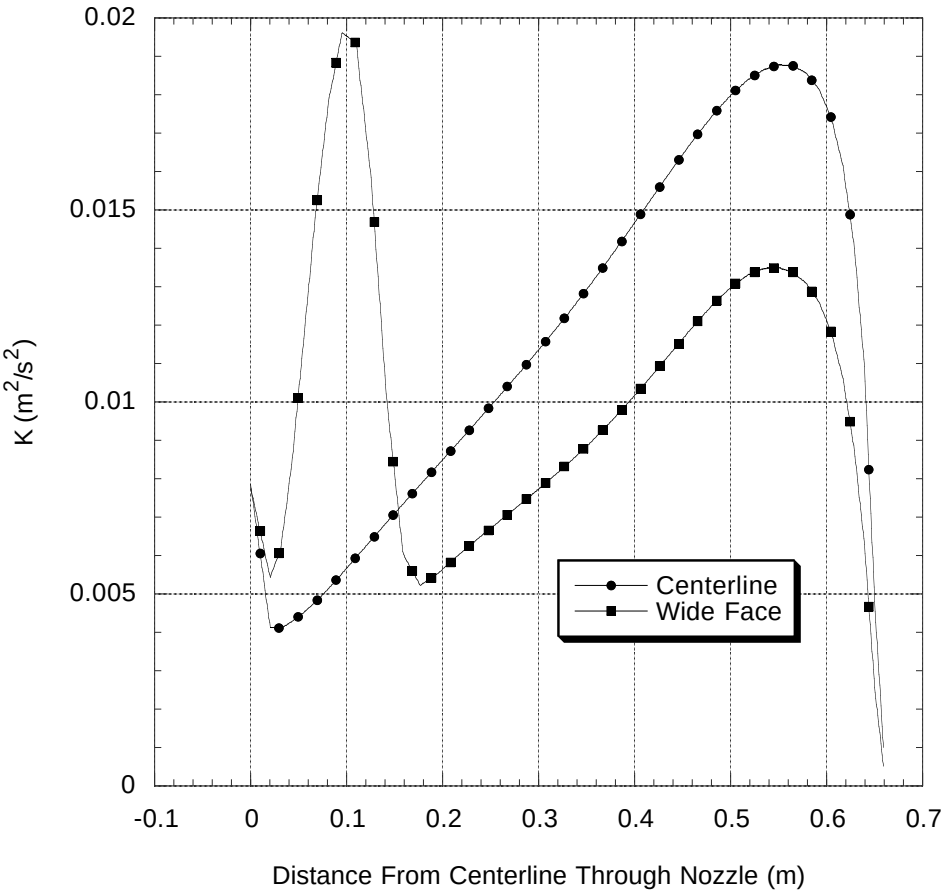

Figure E.36. Case 9. Centerplane and Wide Face Turbulent Kinetic Energy (K). Casting Speed 41.75 m/s, 0% Gas.

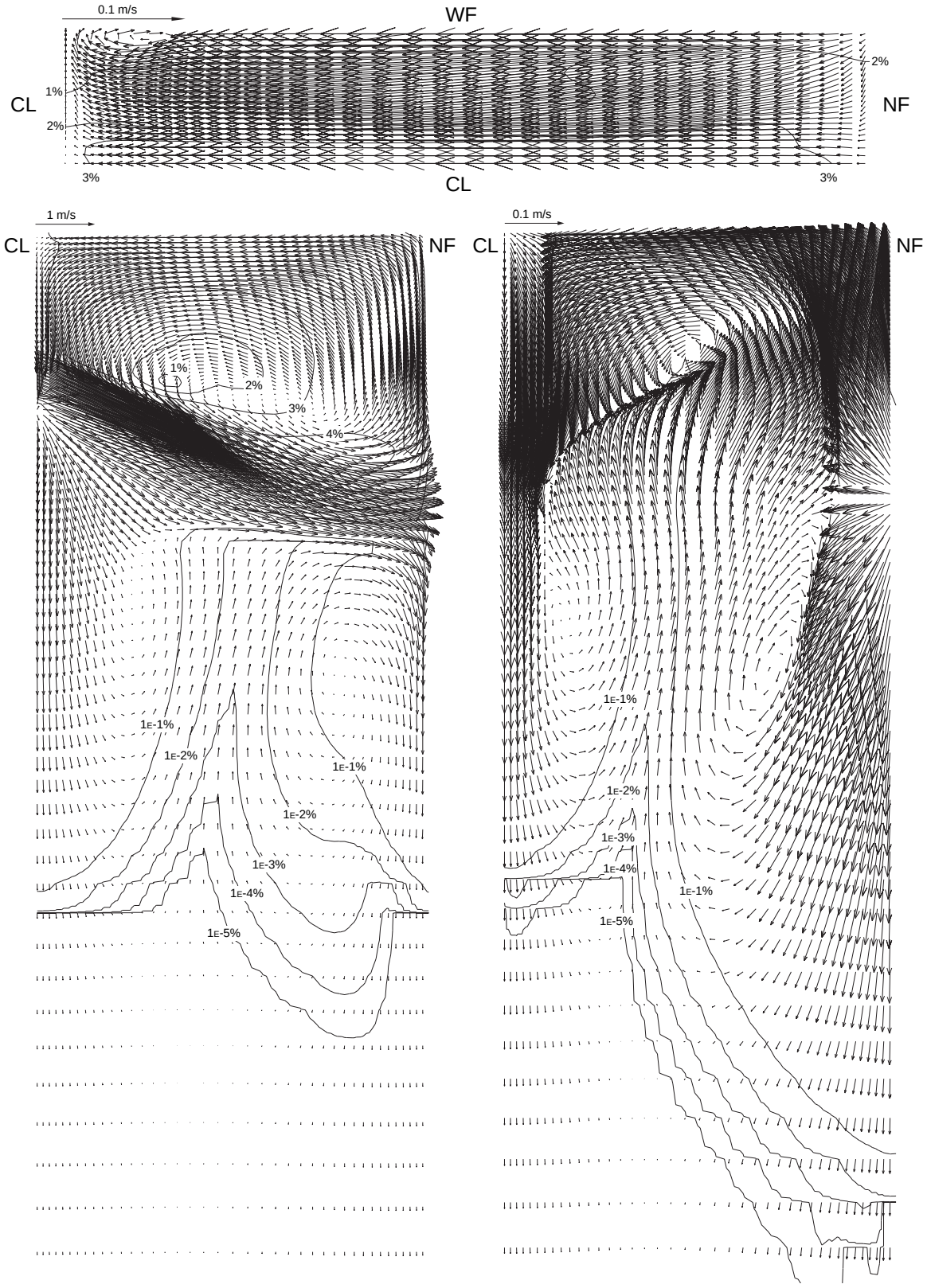

Figure E.37. Case 10. Centerplane (left), Wide Face (right) and Top Surface (top) Velocity. Casting Speed 41.75 m/s, 1.0 mm Bubble Diameter, 20% Gas.

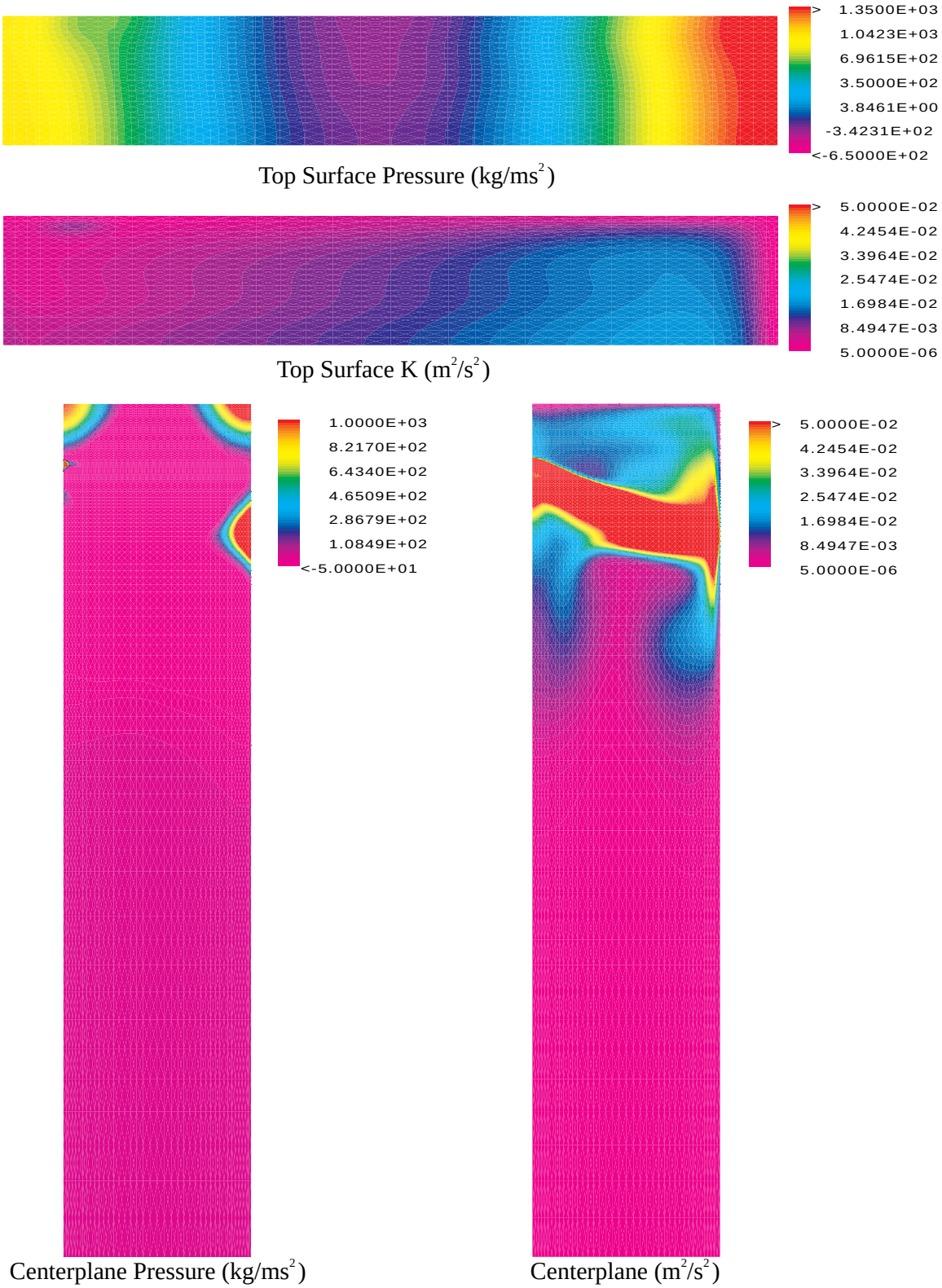

Figure E.38. Case 10. Casting Speed 41.75 m/s, 1.0 mm Bubble Diameter, 20% Gas.

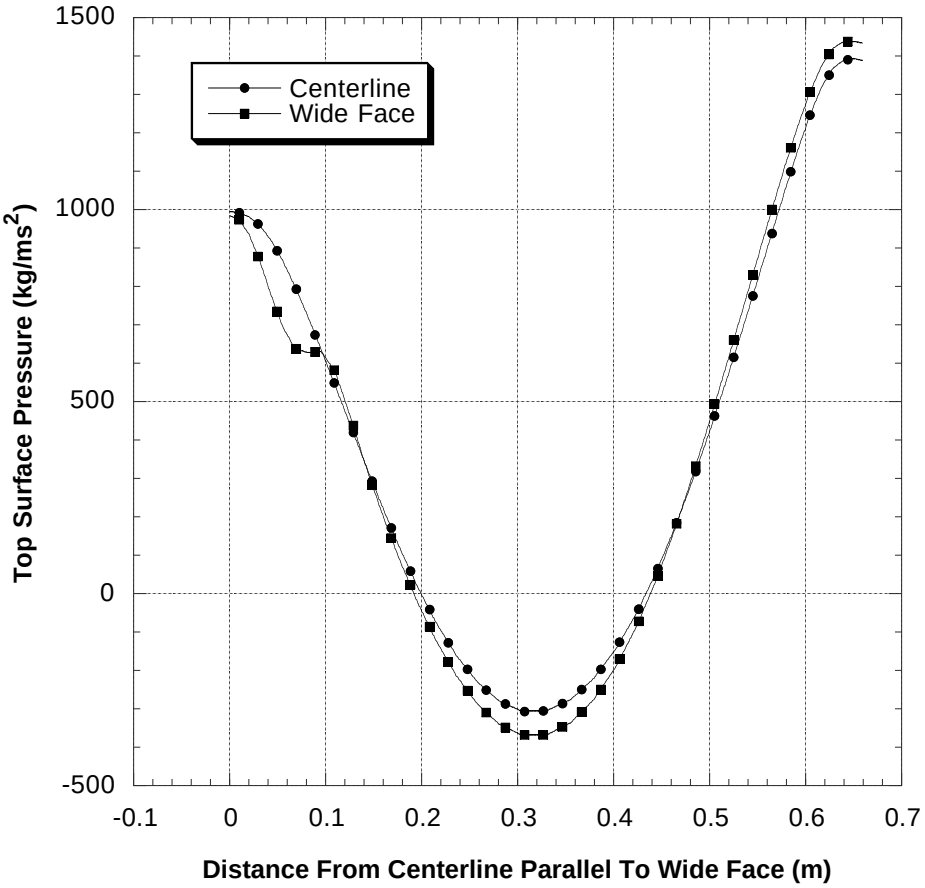

Figure E.39. Case 10. Centerplane and Wide Face Top Surface Pressure. Casting Speed 41.75 m/s, 1.0 mm Bubble Diameter, 20% Gas.

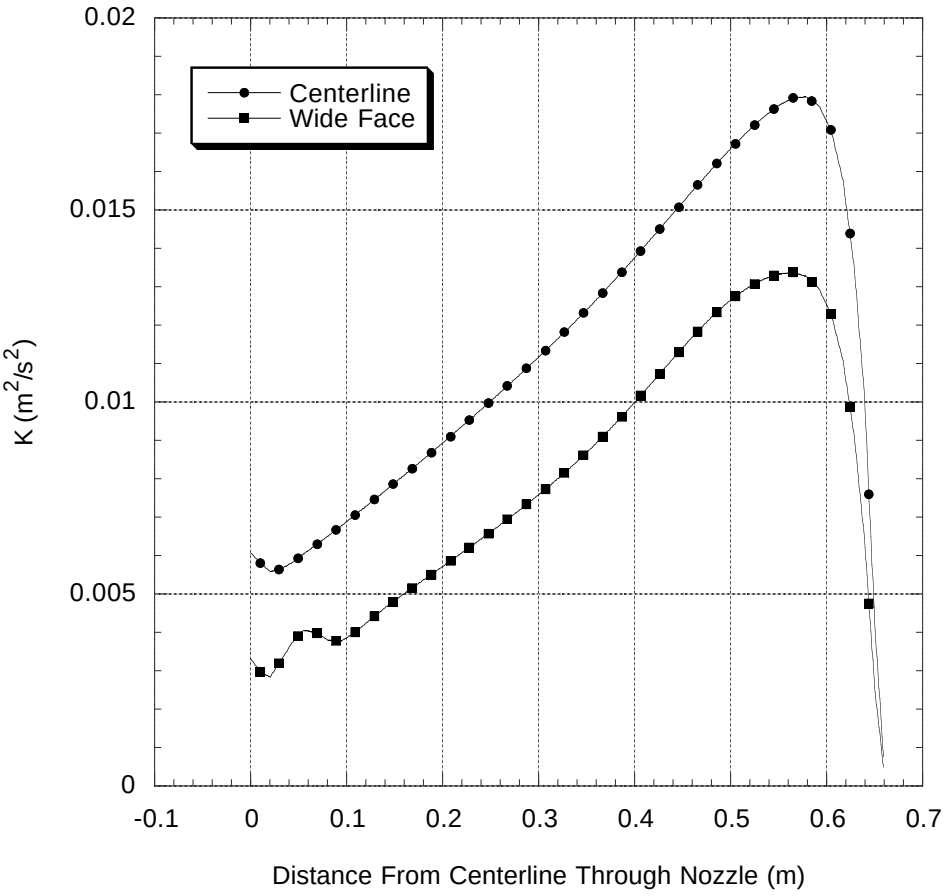

Figure E.40. Case 10. Centerplane and Wide Face Turbulent Kinetic Energy (K). Casting Speed 41.75 m/s, 1.0 mm Bubble Diameter, 20% Gas.

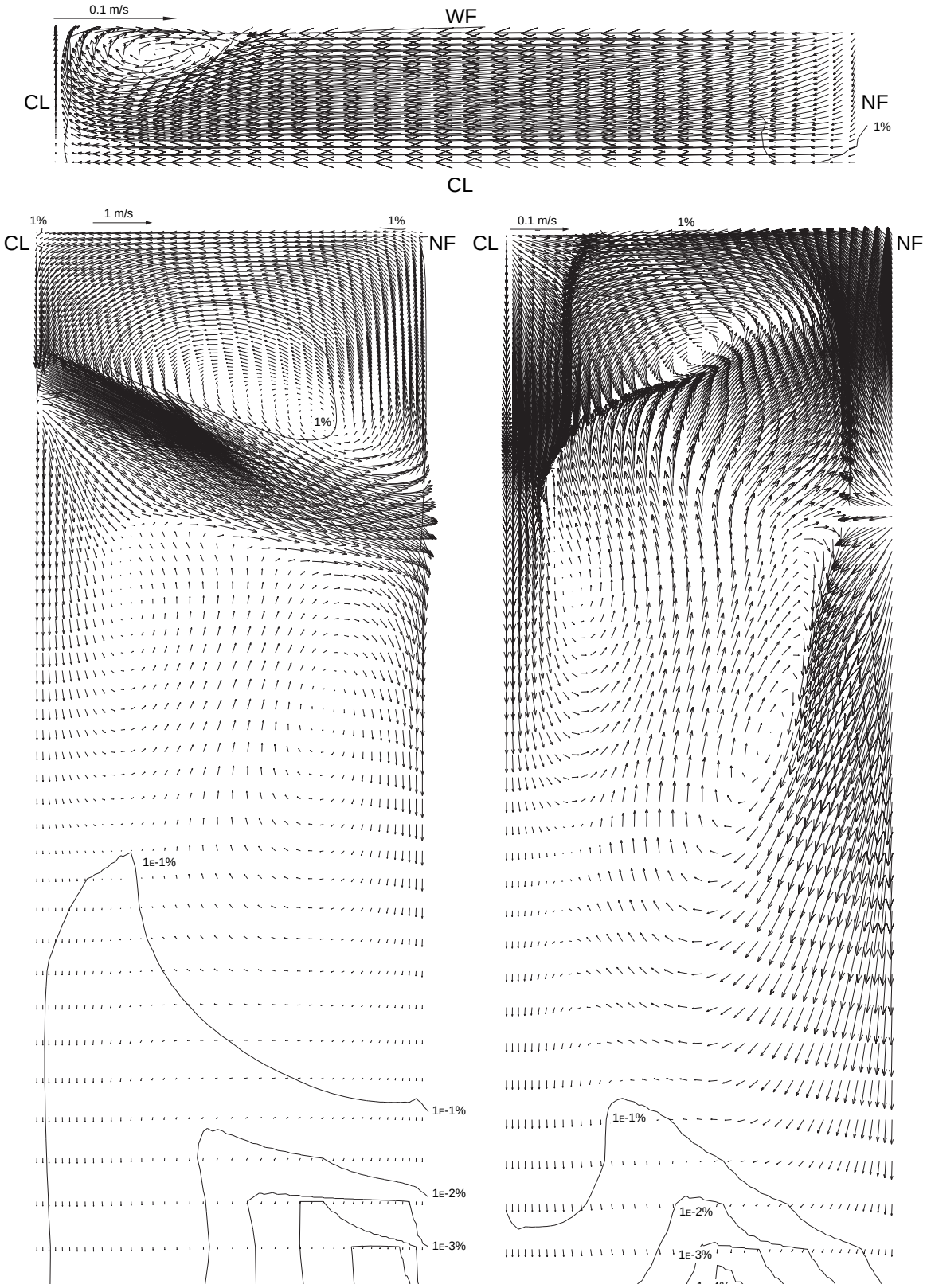

Figure E.41. Case 11. Centerplane (left), Wide Face (right) and Top Surface (top) Velocity. Casting Speed 41.75 m/s, 0.5 mm Bubble Diameter, 6% Gas.

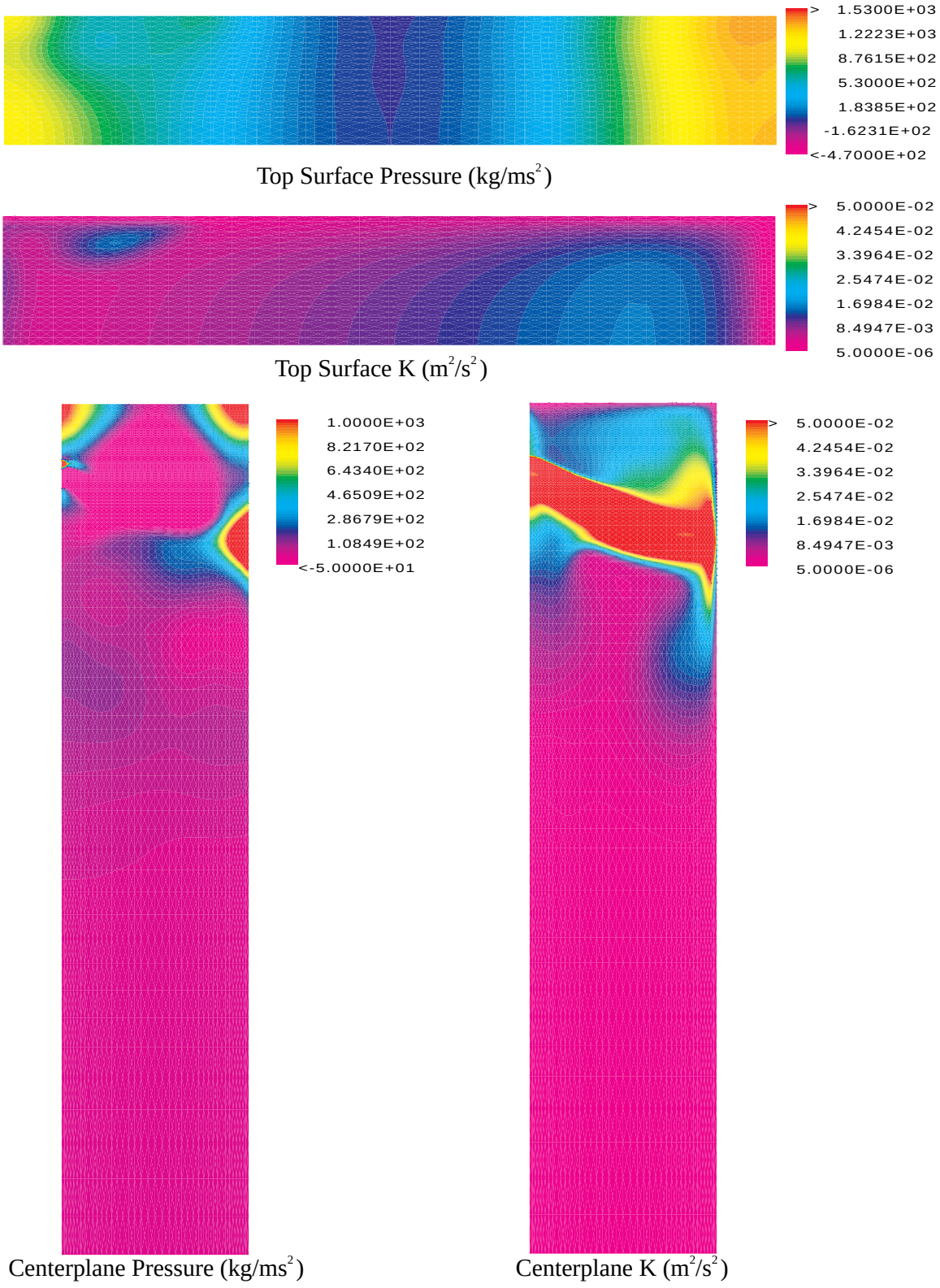

Figure E.42. Case 11. Casting Speed 41.75 m/s, 0.5 mm Bubble Diameter, 6% Gas.

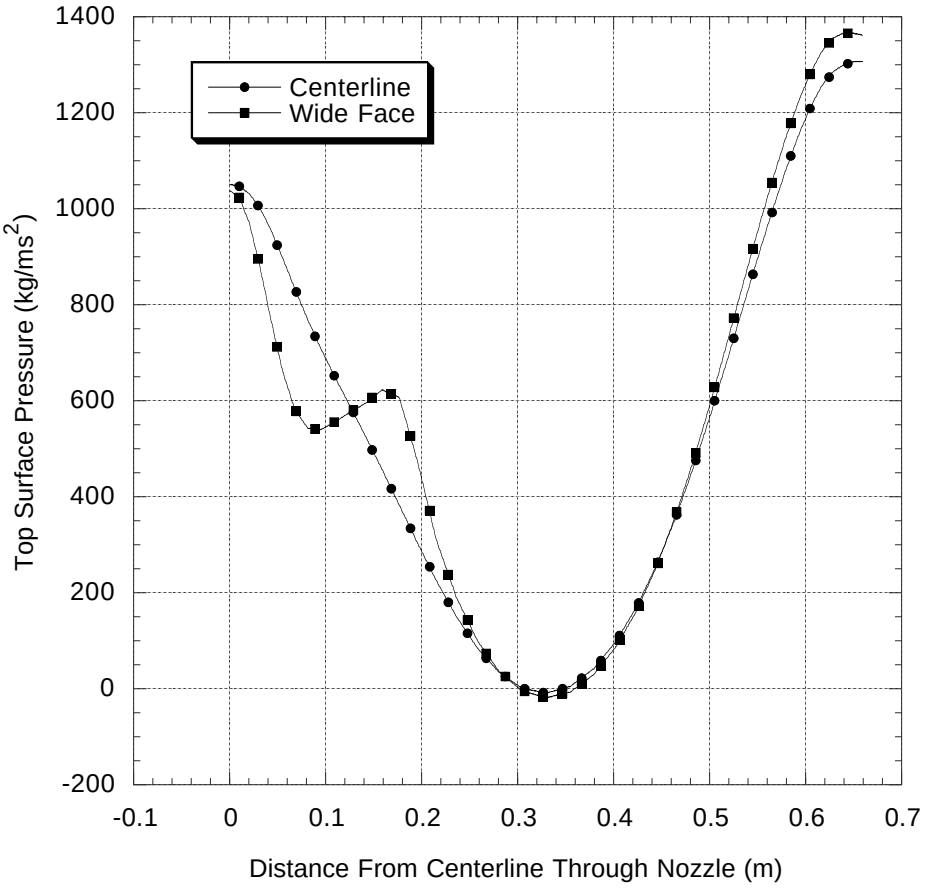

Figure E.43. Case 11. Centerplane and Wide Face Top Surface Pressure. Casting Speed 41.75 m/s, 0.5 mm Bubble Diameter, 6% Gas.

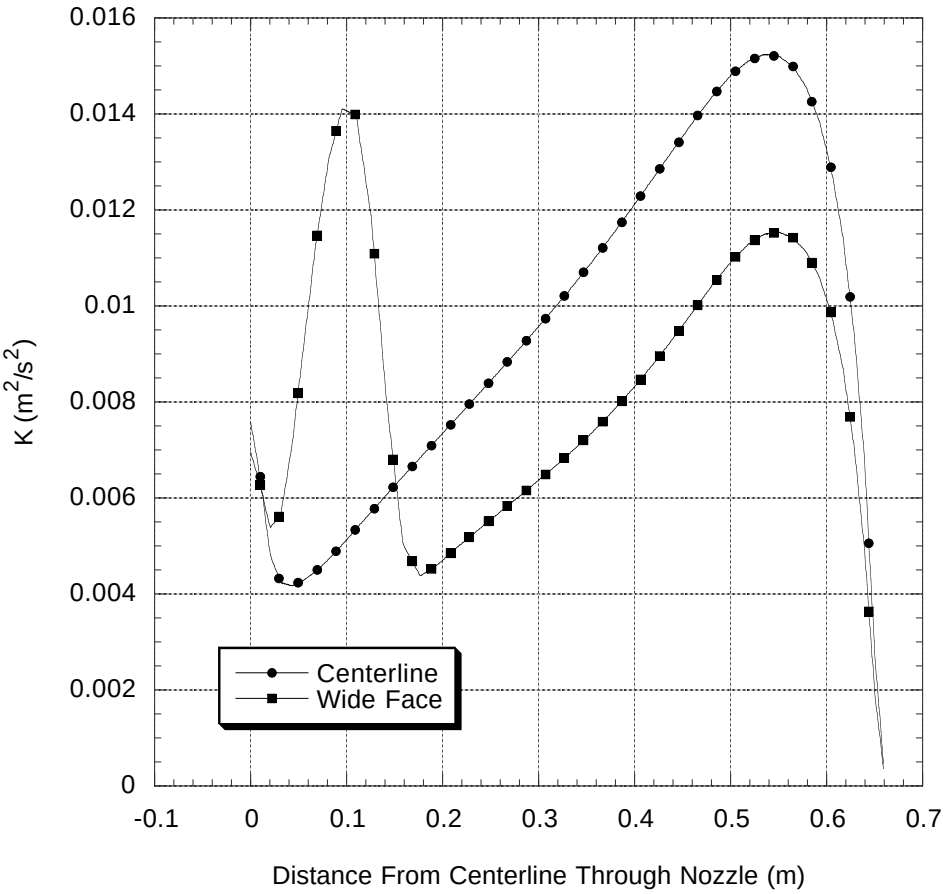

Figure E.44. Case 11. Centerplane and Wide Face Turbulent Kinetic Energy (K). Casting Speed 41.75 m/s, 0.5 mm Bubble Diameter, 6% Gas.

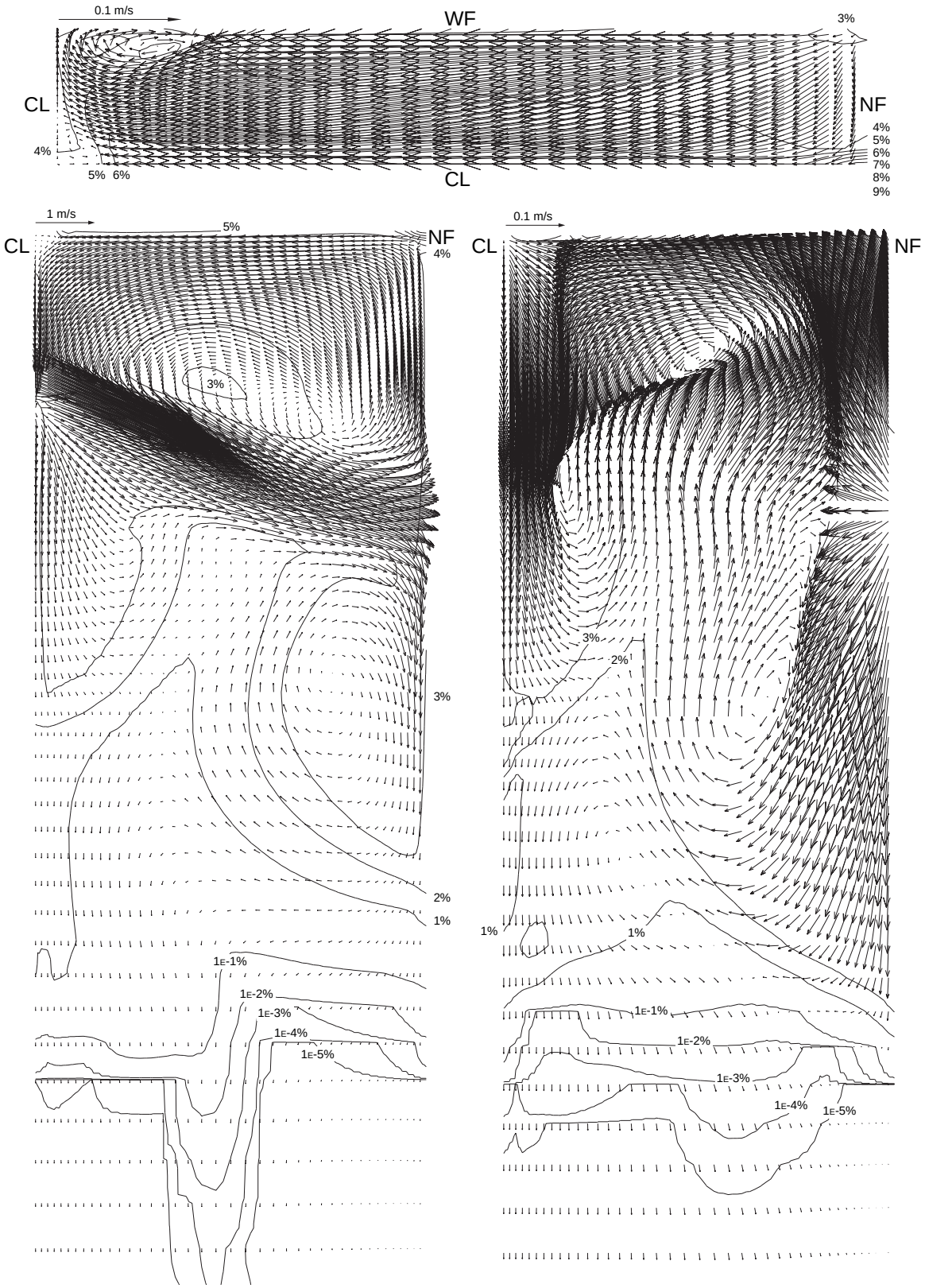

Figure E.45. Case 12. Centerplane (left), Wide Face (right) and Top Surface (top) Velocity. Casting Speed 41.75 m/s, 0.5 mm Bubble Diameter, 20% Gas.

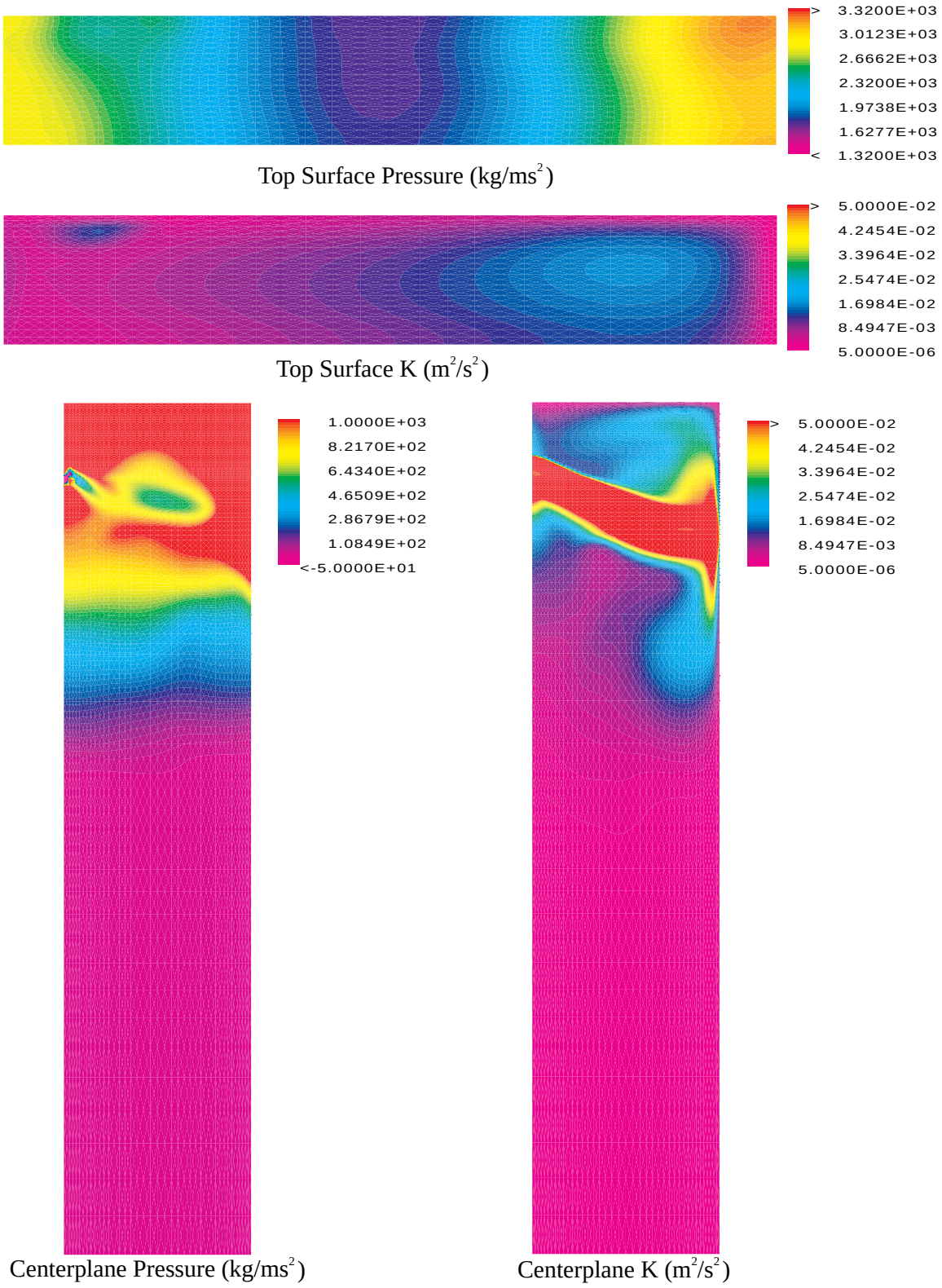

Figure E.46. Case 12. Casting Speed 41.75 m/s, 0.5 mm Bubble Diameter, 20% Gas.

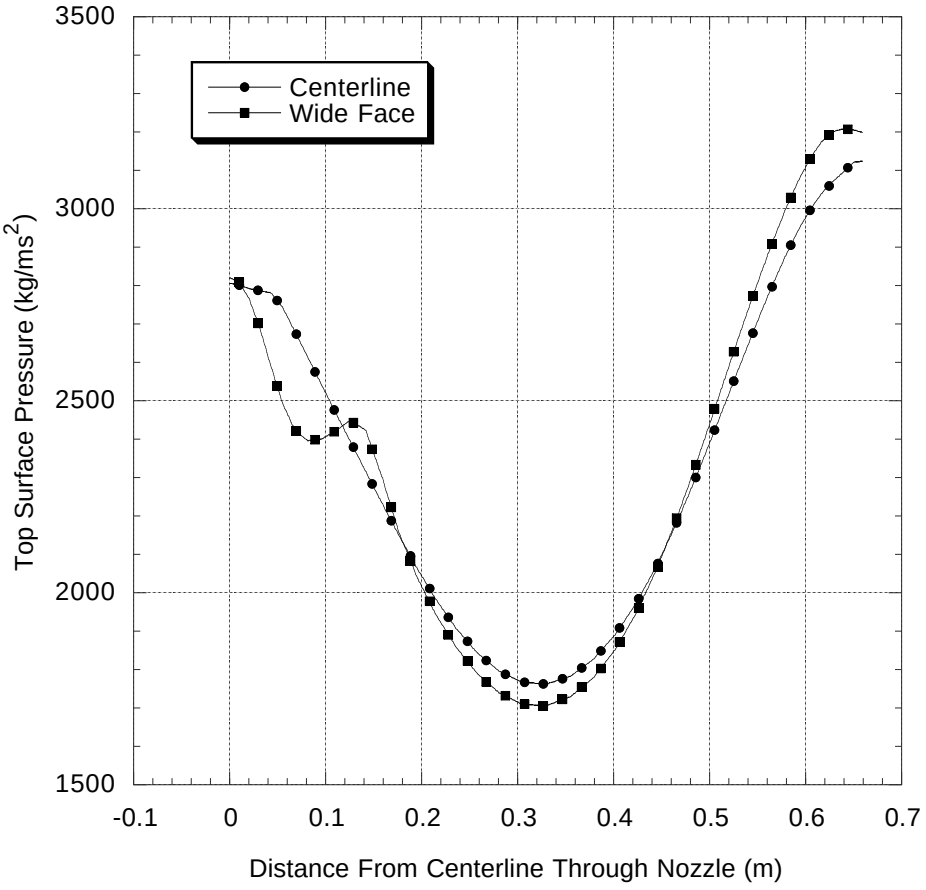

Figure E.47. Case 12. Centerplane and Wide Face Top Surface Pressure. Casting Speed 41.75 m/s, 0.5 mm Bubble Diameter, 20% Gas.

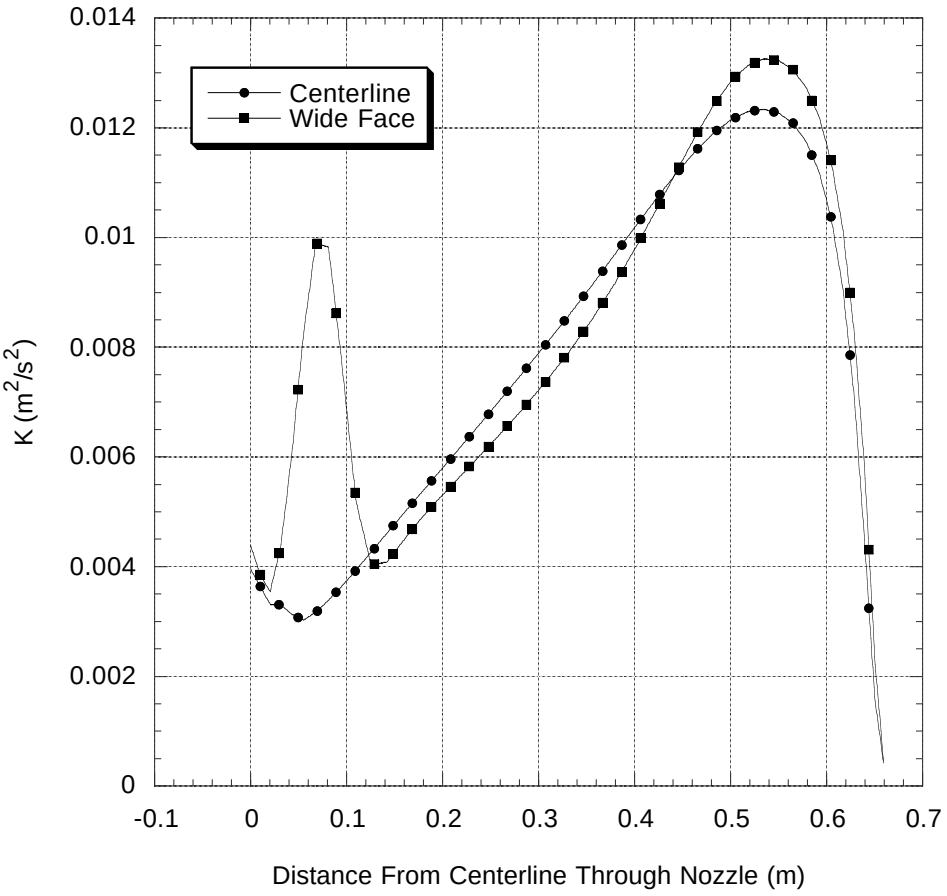

Figure E.48. Case 12. Centerplane and Wide Face Turbulent Kinetic Energy (K). Casting Speed 41.75 m/s, 0.5 mm Bubble Diameter, 20% Gas.

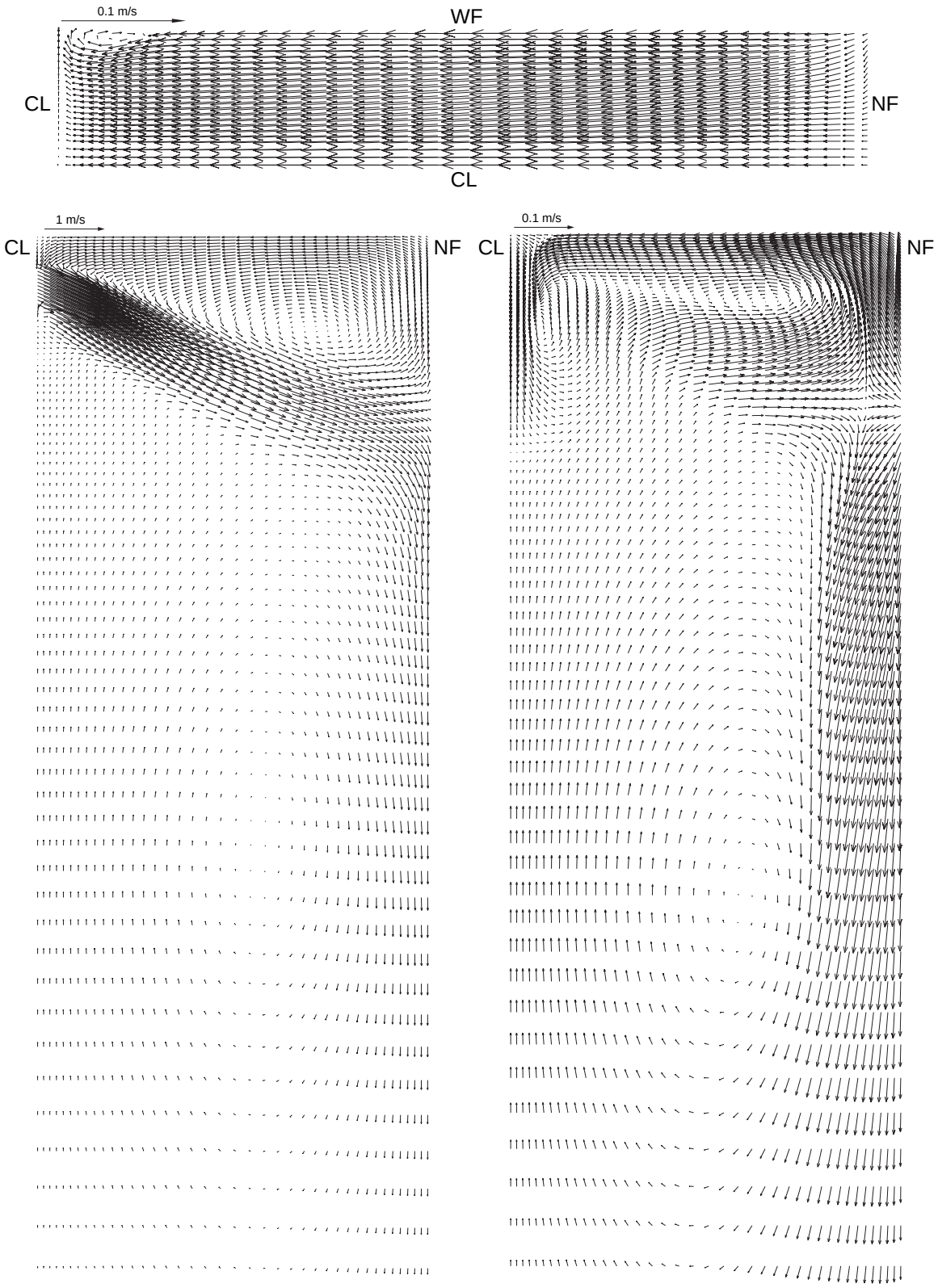

Figure E.49. Case 13. Centerplane (left), Wide Face (right) and Top Surface (top) Velocity. Submergence Depth 0.050 m, 0% Gas.

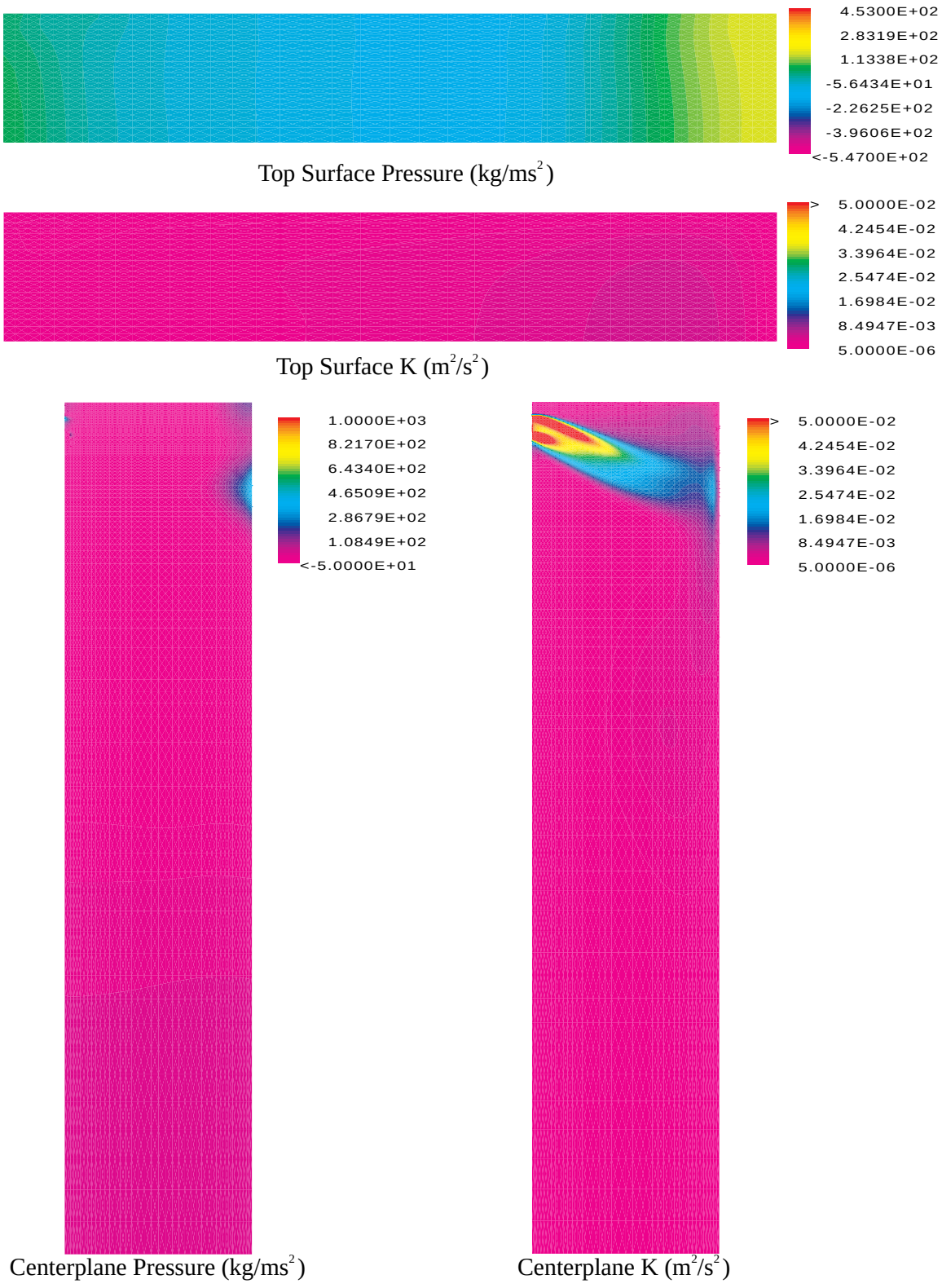

Figure E.50. Case 13. Submergence Depth 0.050 m, 0% Gas.

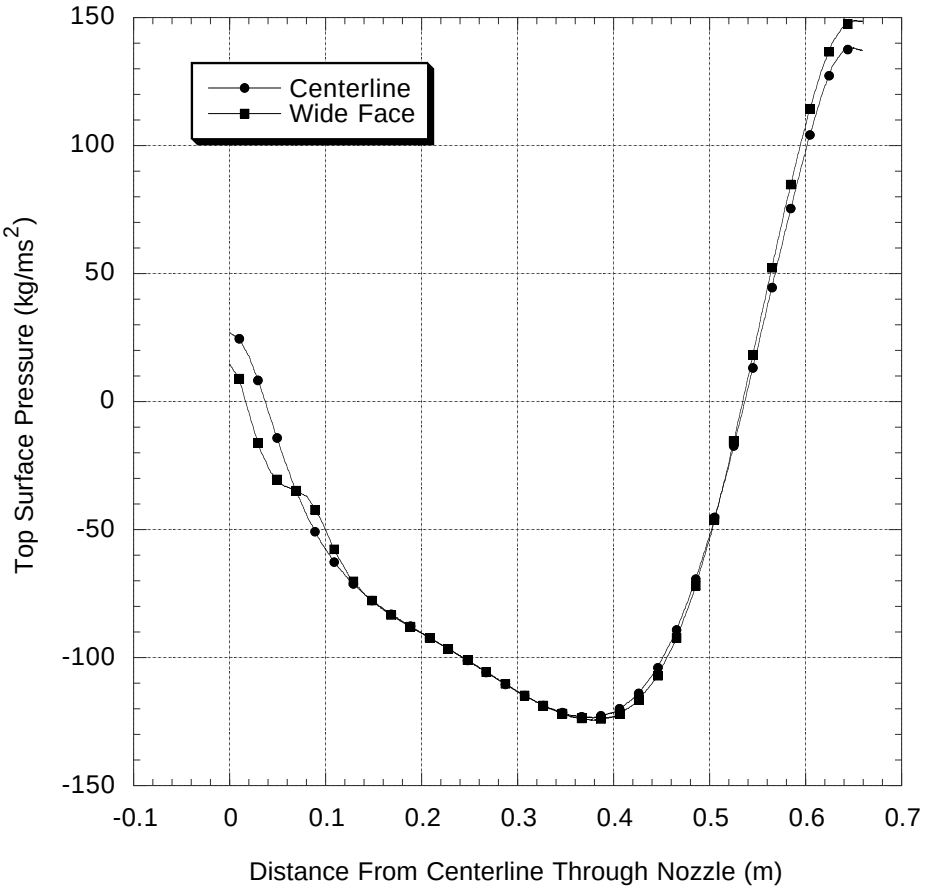

Figure E.51. Case 13. Centerplane and Wide Face Top Surface Pressure. Submergence Depth 0.050 m, 0% Gas.

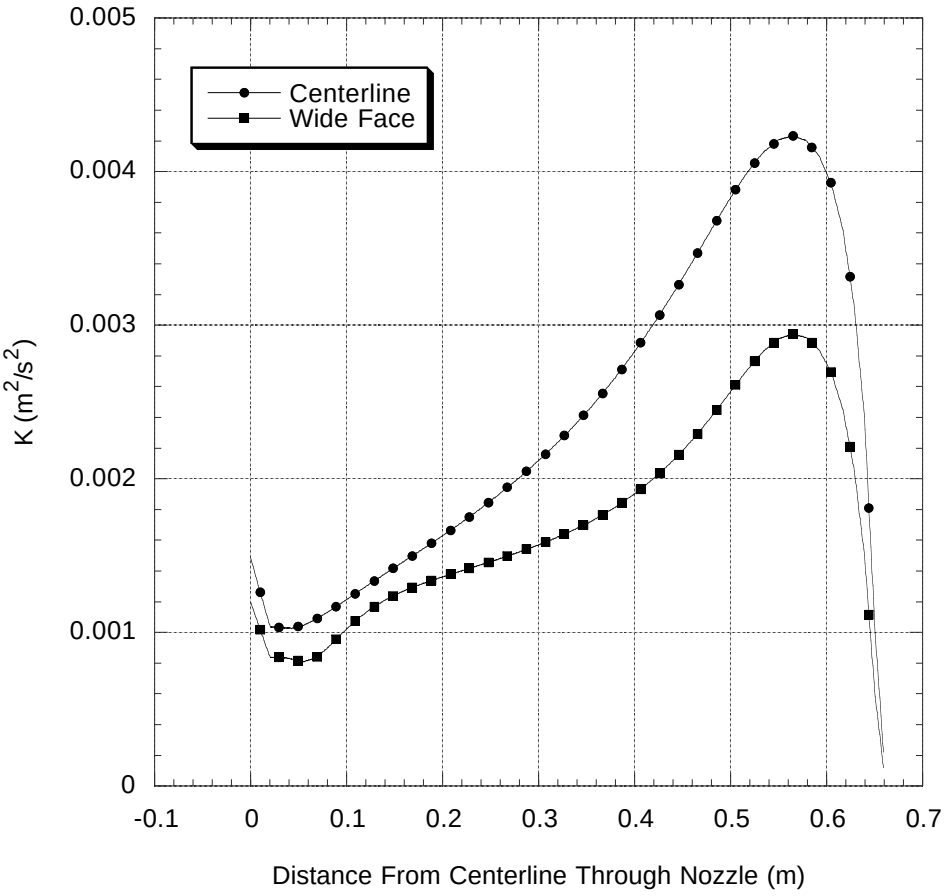

Figure E.52. Case 13. Centerplane and Wide Face Turbulent Kinetic Energy (K). Submergence Depth 0.050 m, 0% Gas.

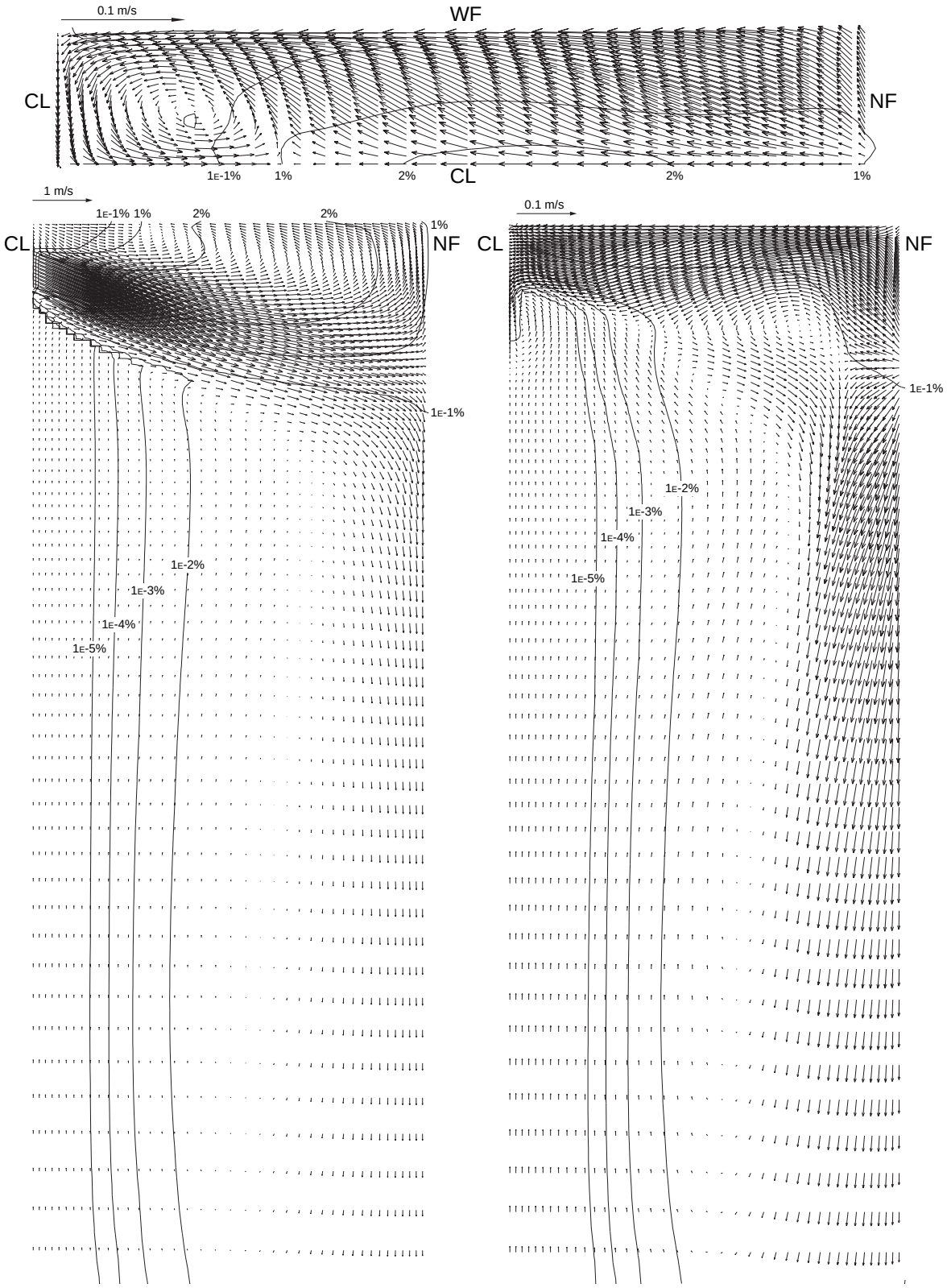

Figure E.53. Case 14. Centerplane (left), Wide Face (right) and Top Surface (top) Velocity. Submergence Depth 0.050 m, 0.5 mm Bubble Diameter, 4% Gas.

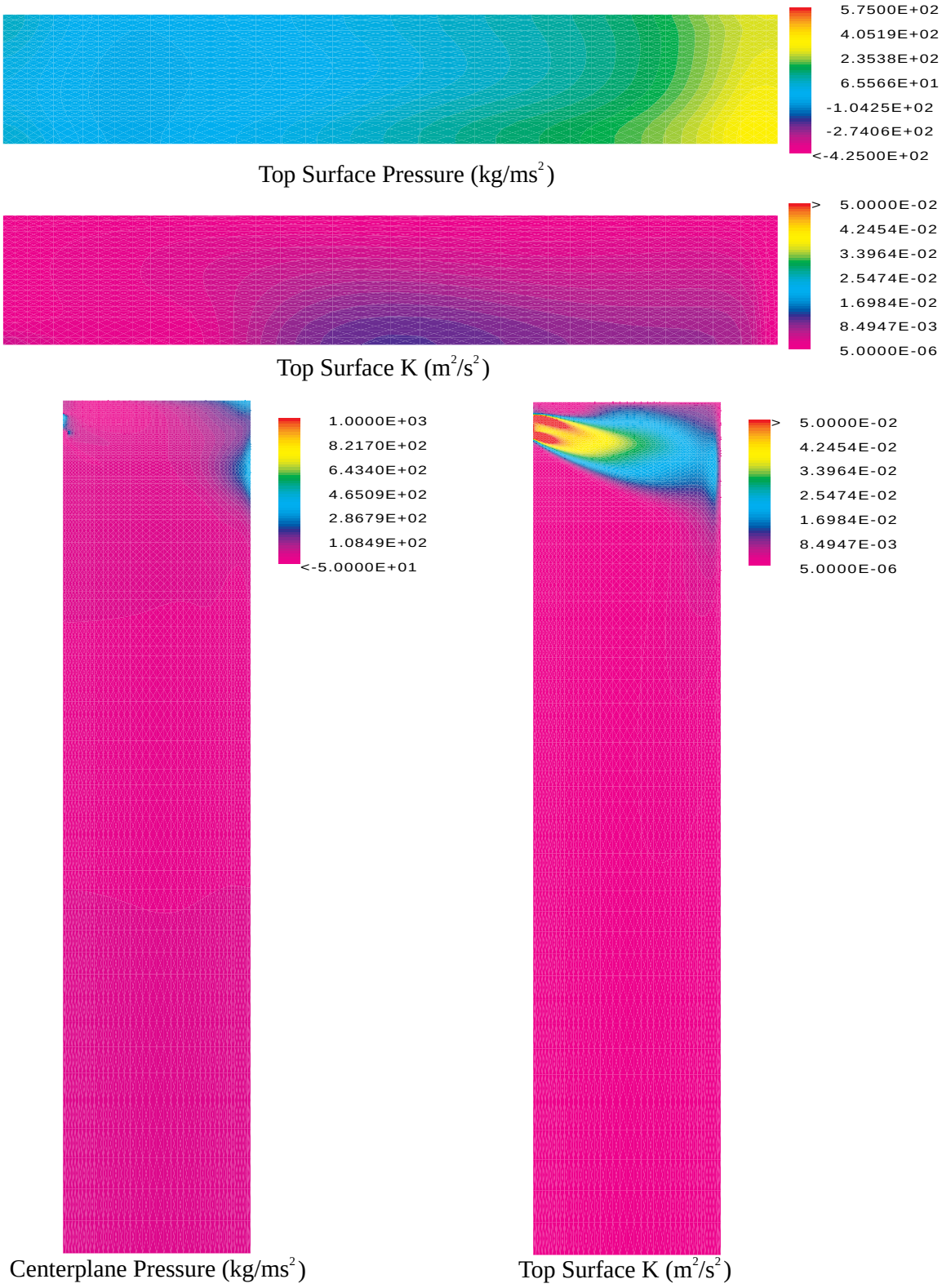

Figure E.54. Case 14. Submergence Depth 0.050 m, 0.5 mm Bubble Diameter, 4% Gas.

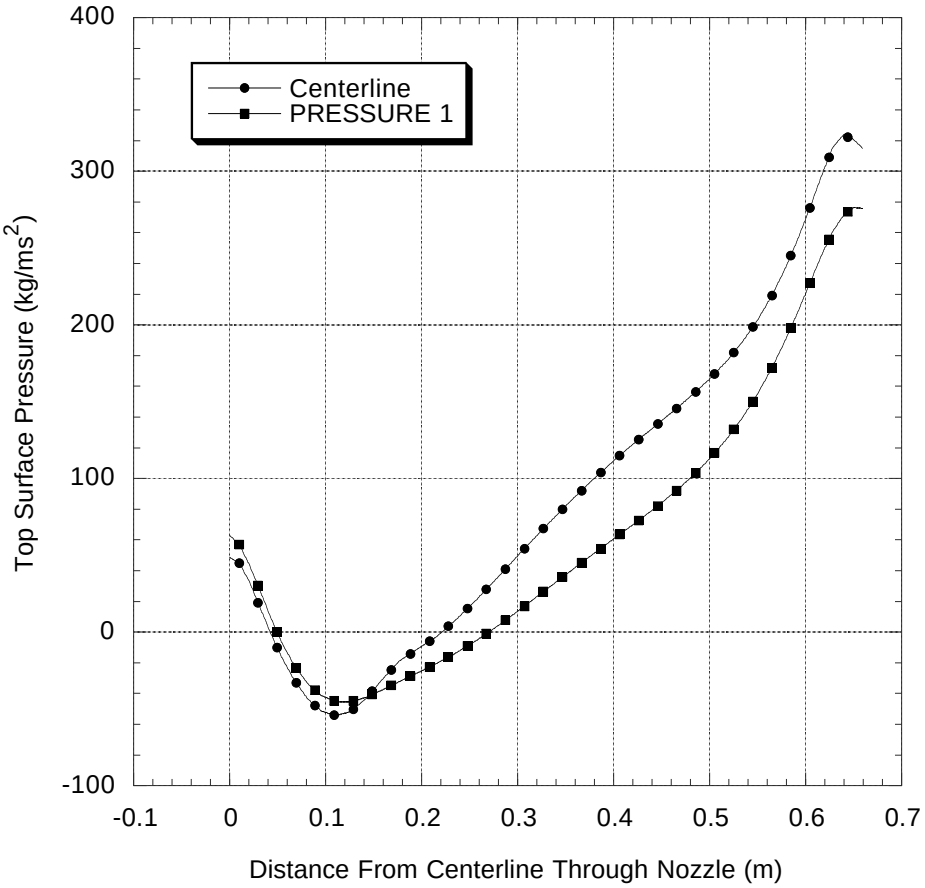

Figure E.55. Case 14. Centerplane and Wide Face Top Surface Pressure. Submergence Depth 0.050 m, 0.5 mm Bubble Diameter, 4% Gas.

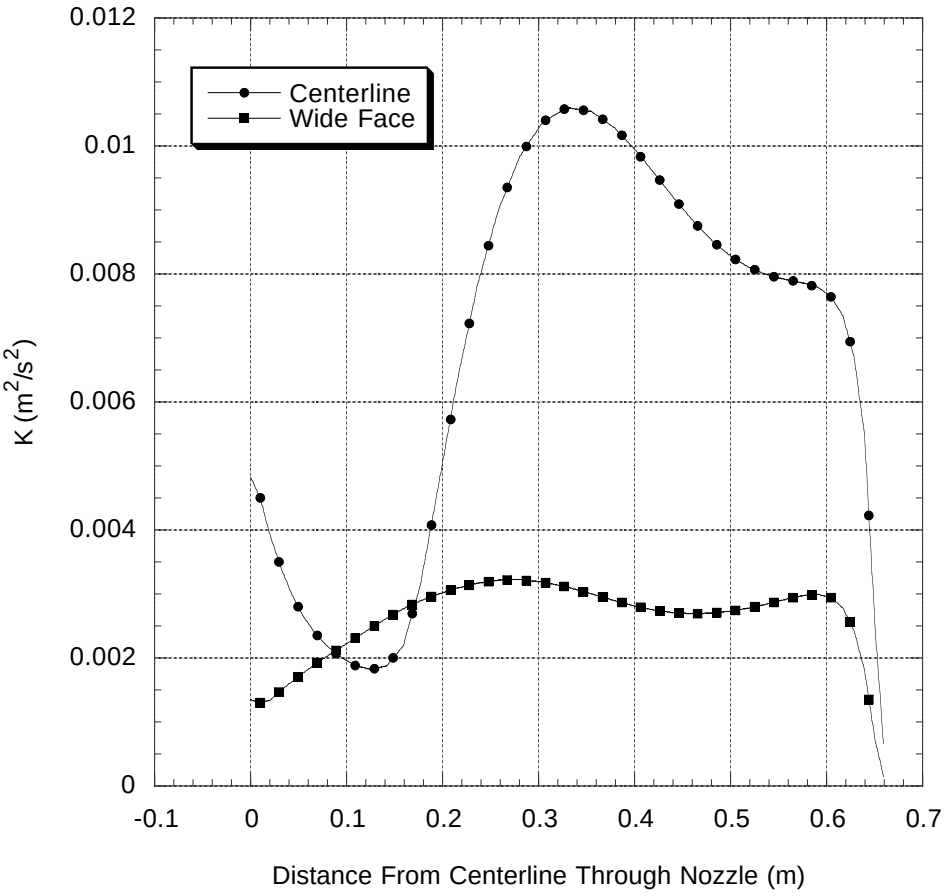

Figure E.56. Case 14. Centerplane and Wide Face Turbulent Kinetic Energy (K). Submergence Depth 0.050 m, 0.5 mm Bubble Diameter, 4% Gas.

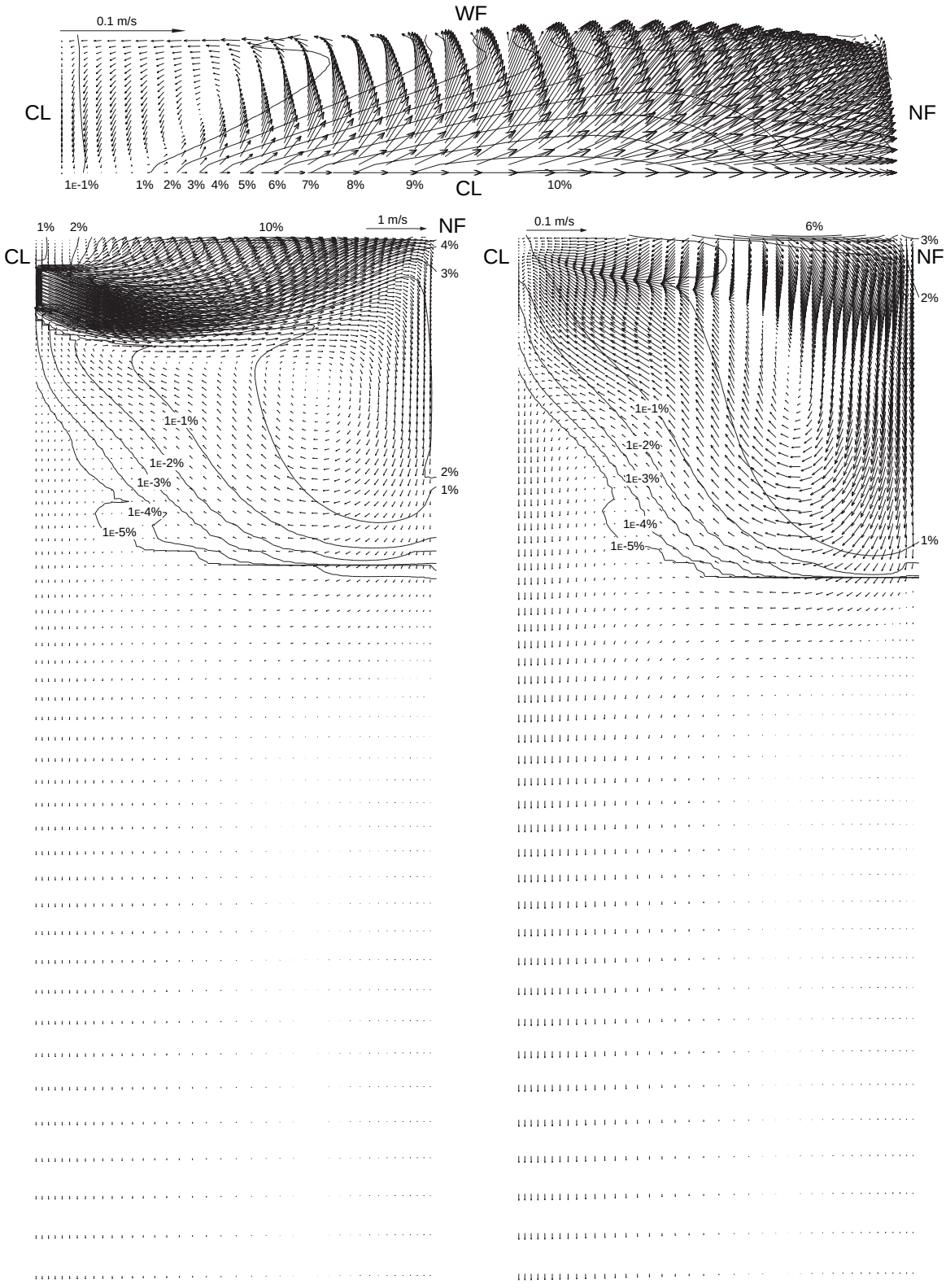

Figure E.57. Case 15. Centerplane (left), Wide Face (right) and Top Surface (top) Velocity. Submergence Depth 0.050 m, 0.5 mm Bubble Diameter, 20% Gas.

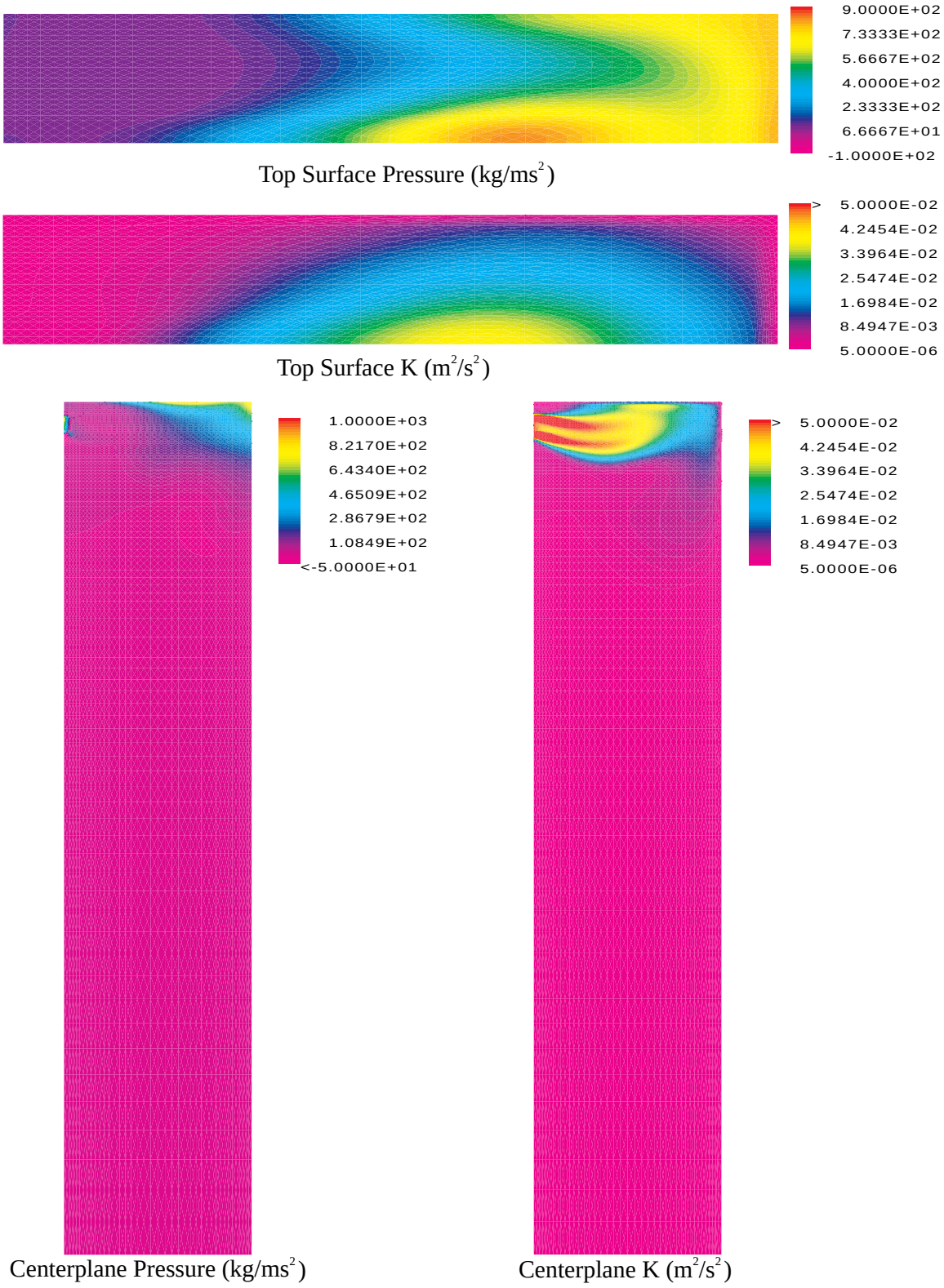

Figure E.58. Case 15. Submergence Depth 0.050 m, 0.5 mm Bubble Diameter, 20% Gas.

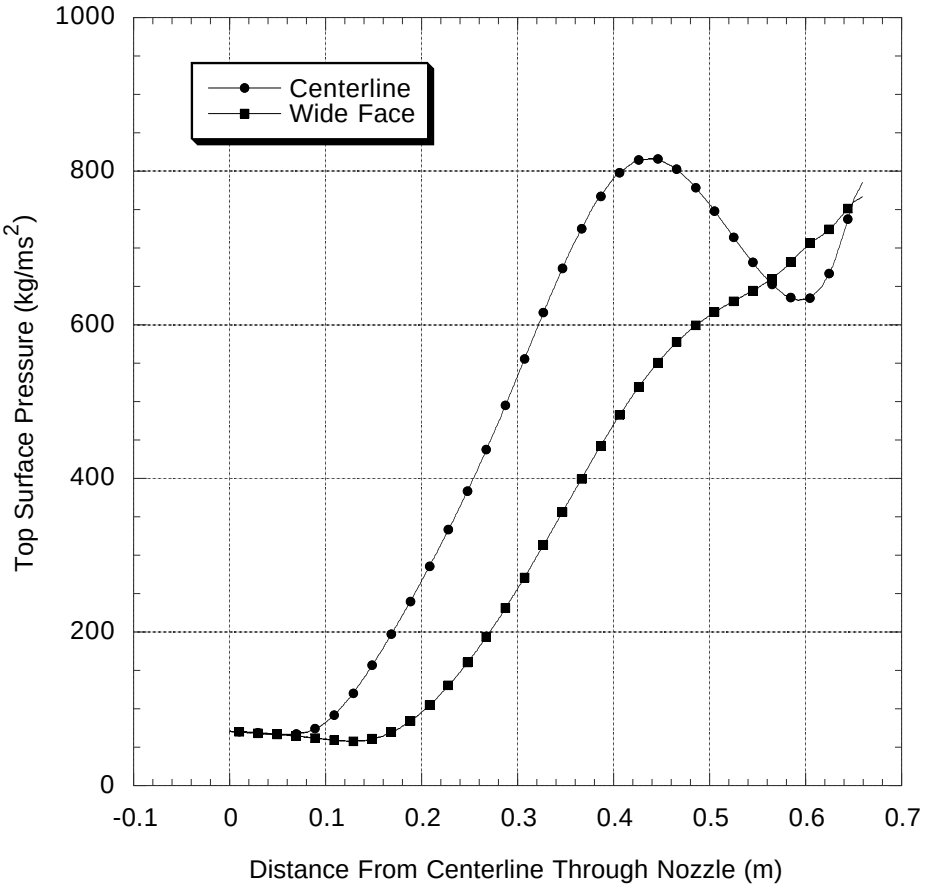

Figure E.59. Case 15. Centerplane and Wide Face Top Surface Pressure. Submergence Depth 0.050 m, 0.5 mm Bubble Diameter, 20% Gas.

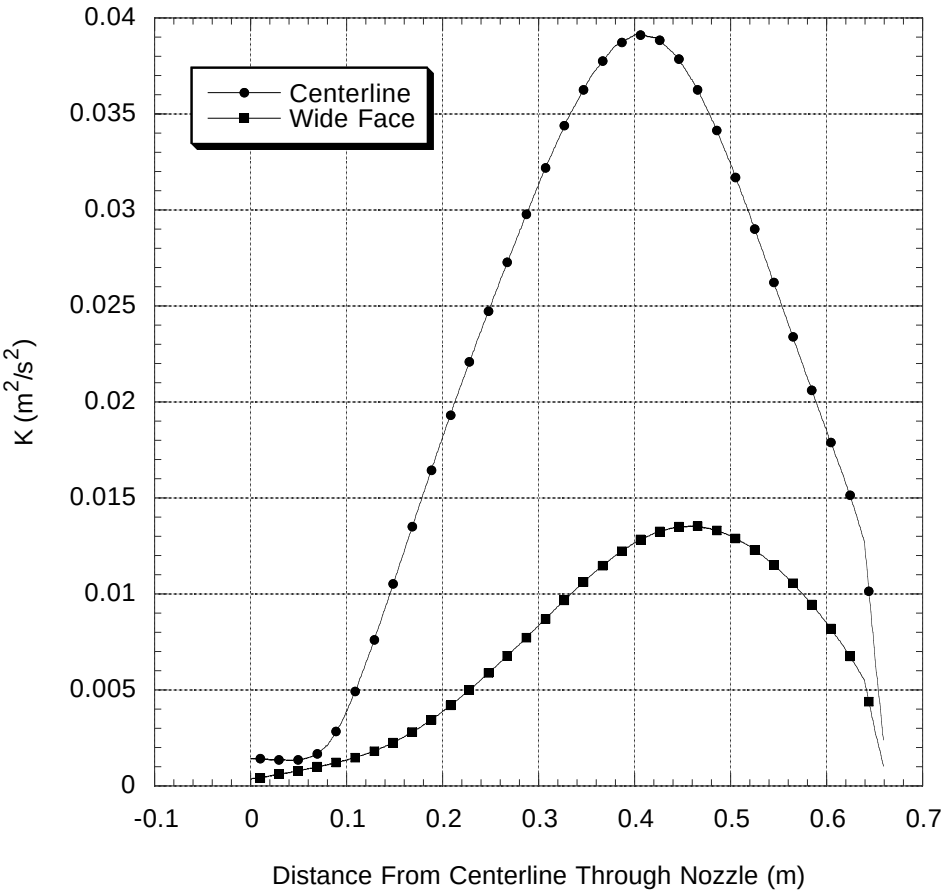

Figure E.60. Case 15. Centerplane and Wide Face Turbulent Kinetic Energy (K). Submergence Depth 0.050 m, 0.5 mm Bubble Diameter, 20% Gas.

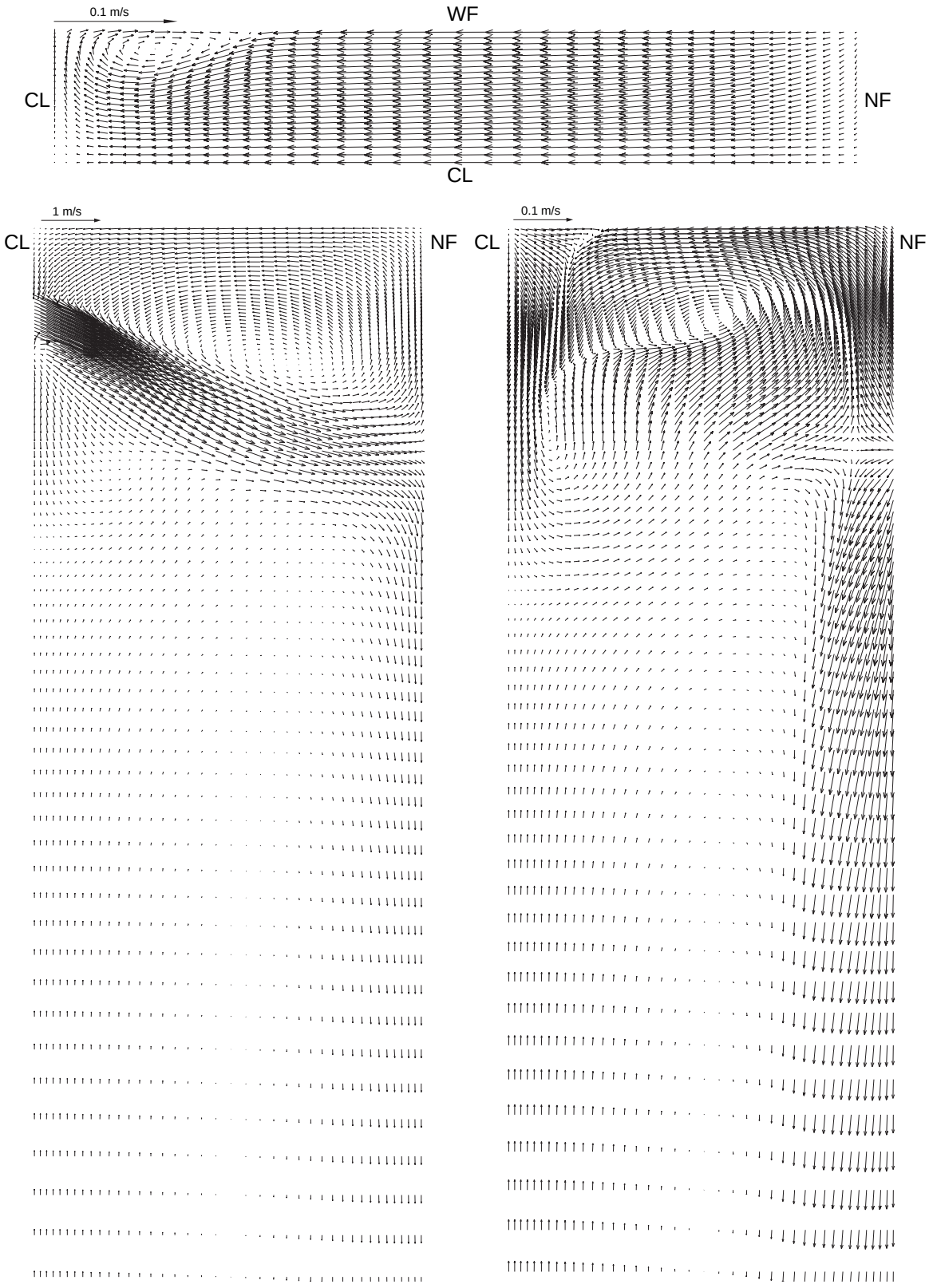

Figure E.61. Case 16. Centerplane (left), Wide Face (right) and Top Surface (top) Velocity. Submergence Depth 0.120 m, 0% Gas.

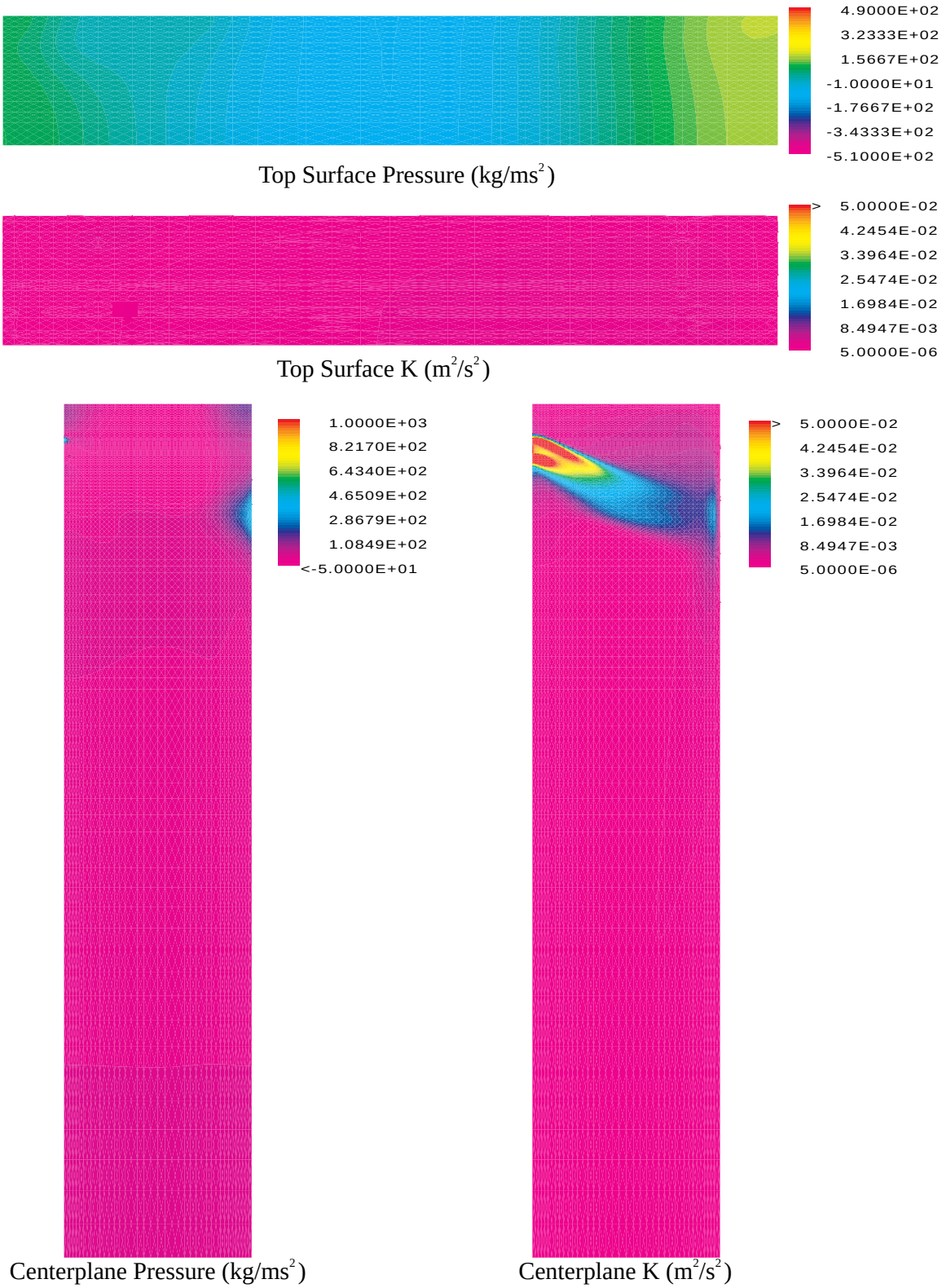

Figure E.62. Case 16. Submergence Depth 0.120 m, 0% Gas.

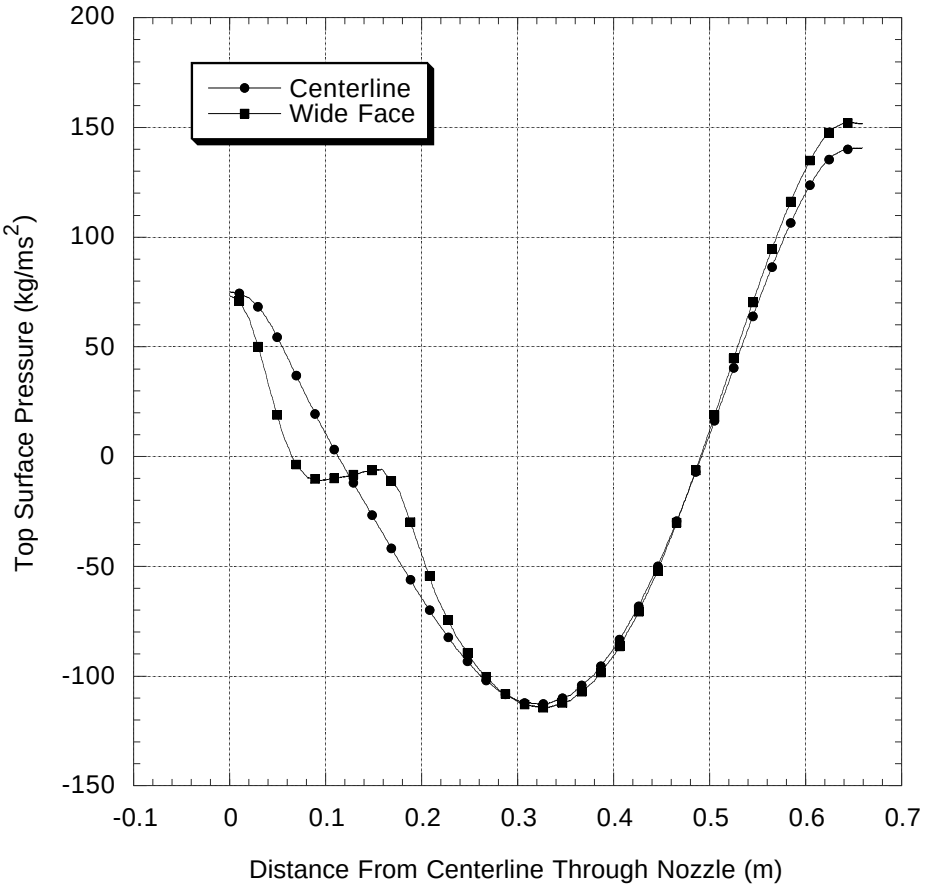

Figure E.63. Case 16. Centerplane and Wide Face Top Surface Pressure. Submergence Depth 0.120 m, 0% Gas.

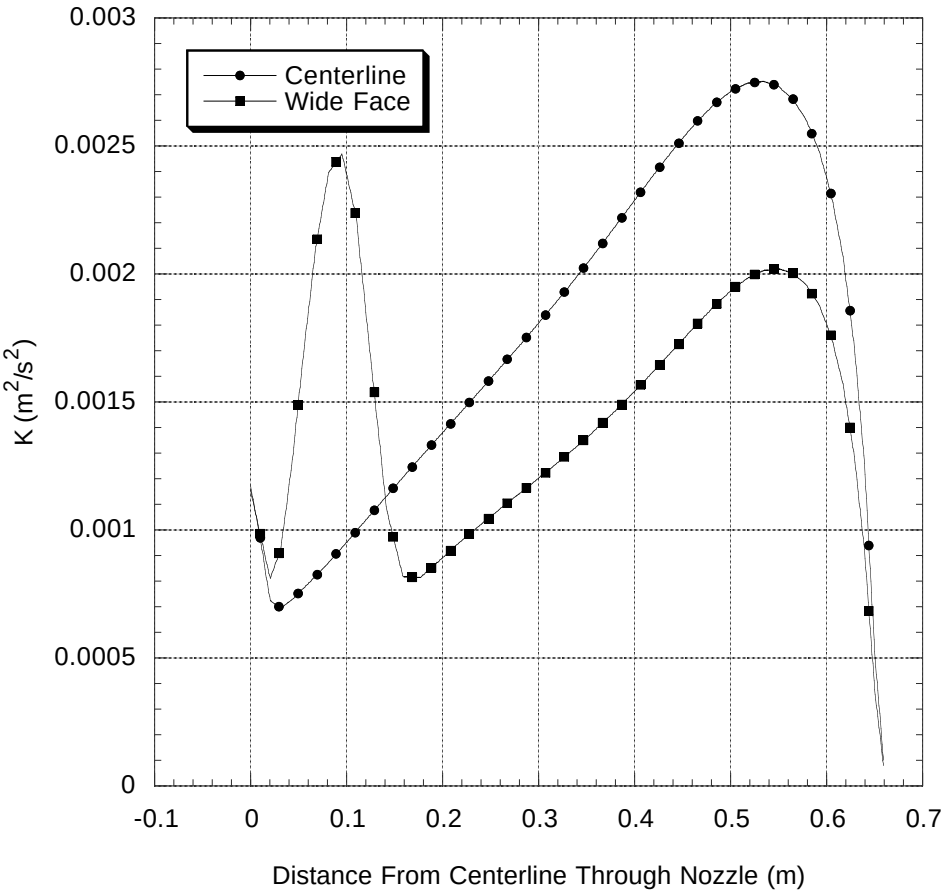

Figure E.64. Case 16. Centerplane and Wide Face Turbulent Kinetic Energy (K). Submergence Depth 0.120 m, 0% Gas.

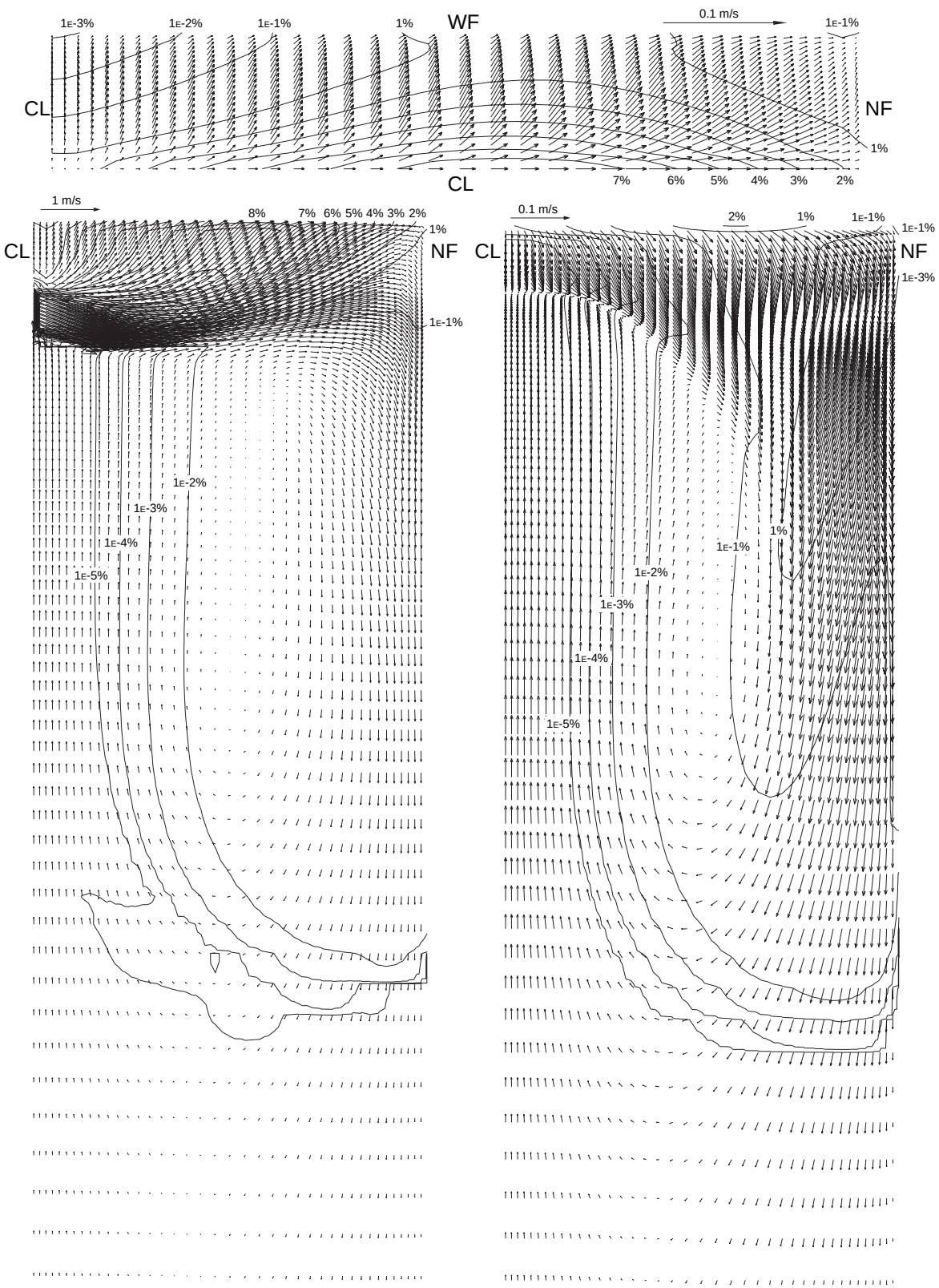

Figure E.65. Case 17. Centerplane (left), Wide Face (right) and Top Surface (top) Velocity. Submergence Depth 0.120 m, 1.0 mm Bubble Diameter, 20% Gas.

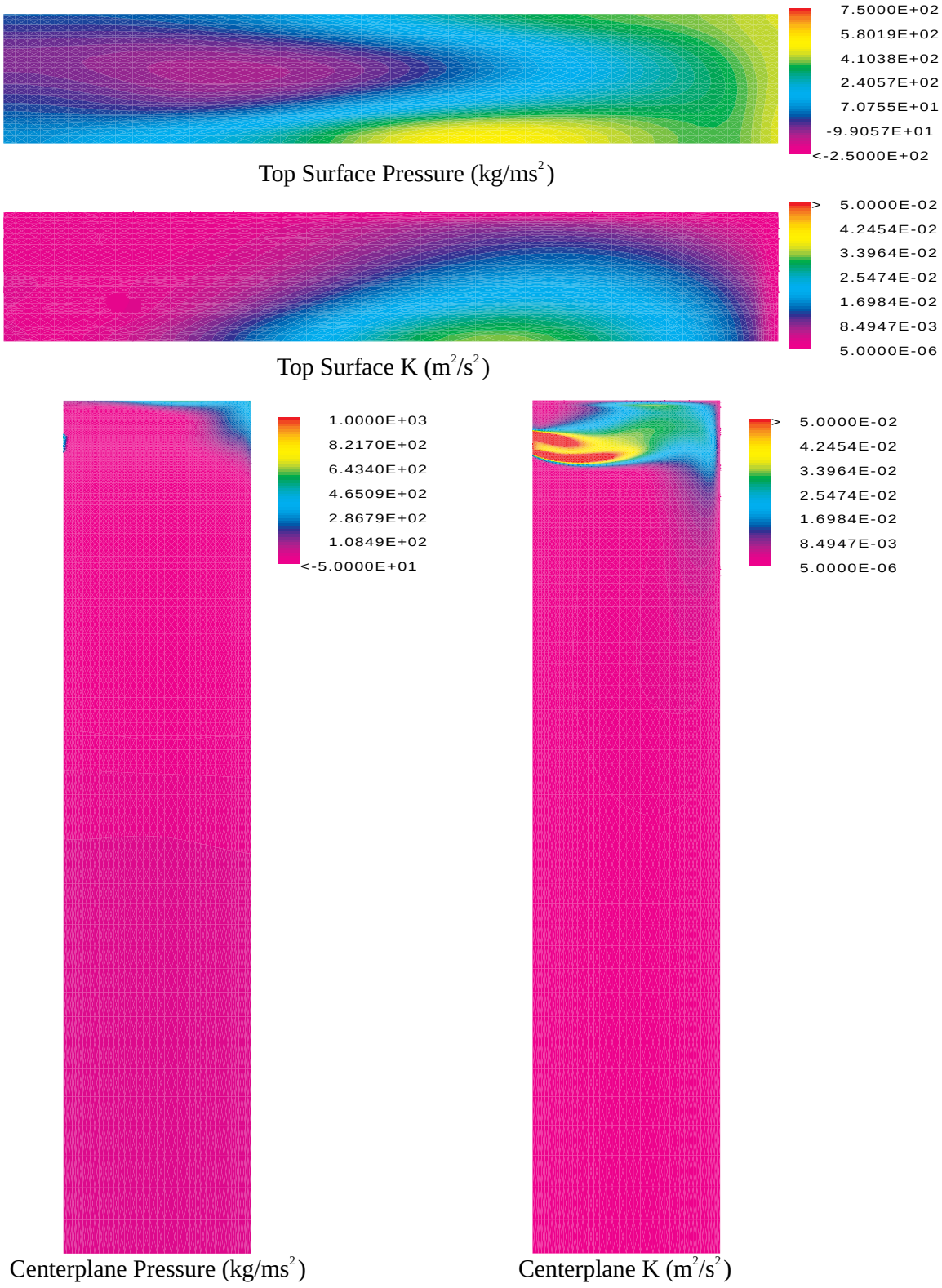

Figure E.66. Case 17. Submergence Depth 0.120 m, 1.0 mm Bubble Diameter, 20% Gas.

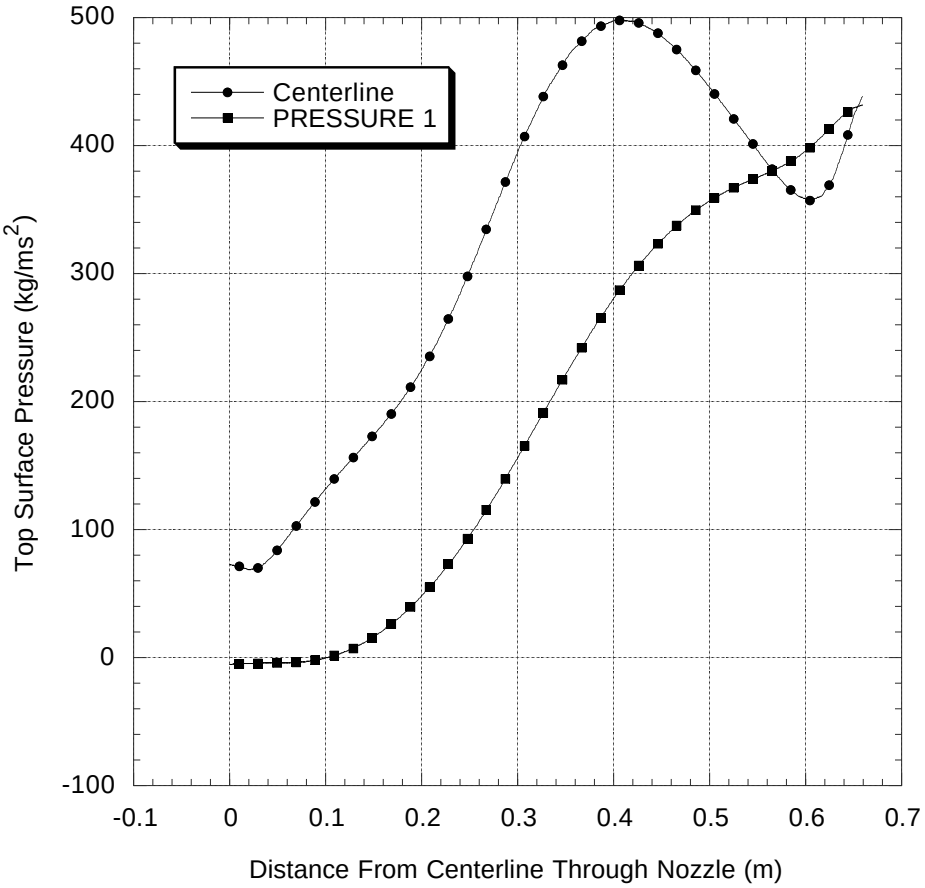

Figure E.67. Case 17. Centerplane and Wide Face Top Surface Pressure. Submergence Depth 0.120 m, 1.0 mm Bubble Diameter, 20% Gas.

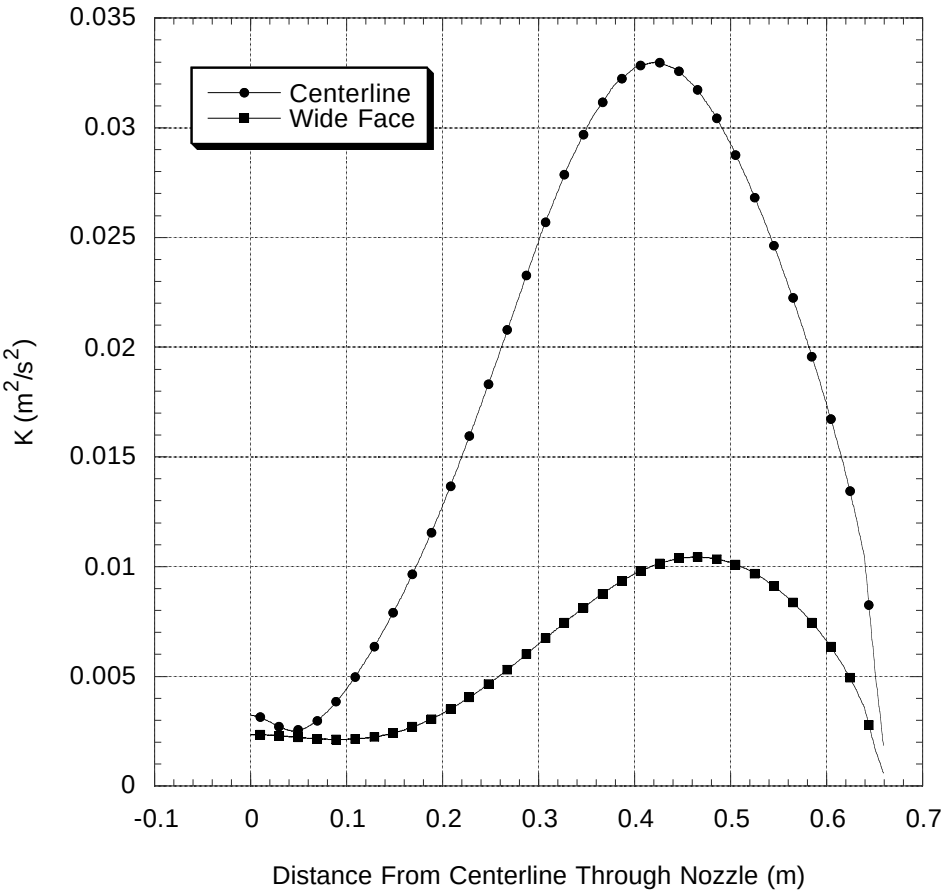

Figure E.68. Case 17. Centerplane and Wide Face Turbulent Kinetic Energy (K). Submergence Depth 0.120 m, 1.0 mm Bubble Diameter, 20% Gas.

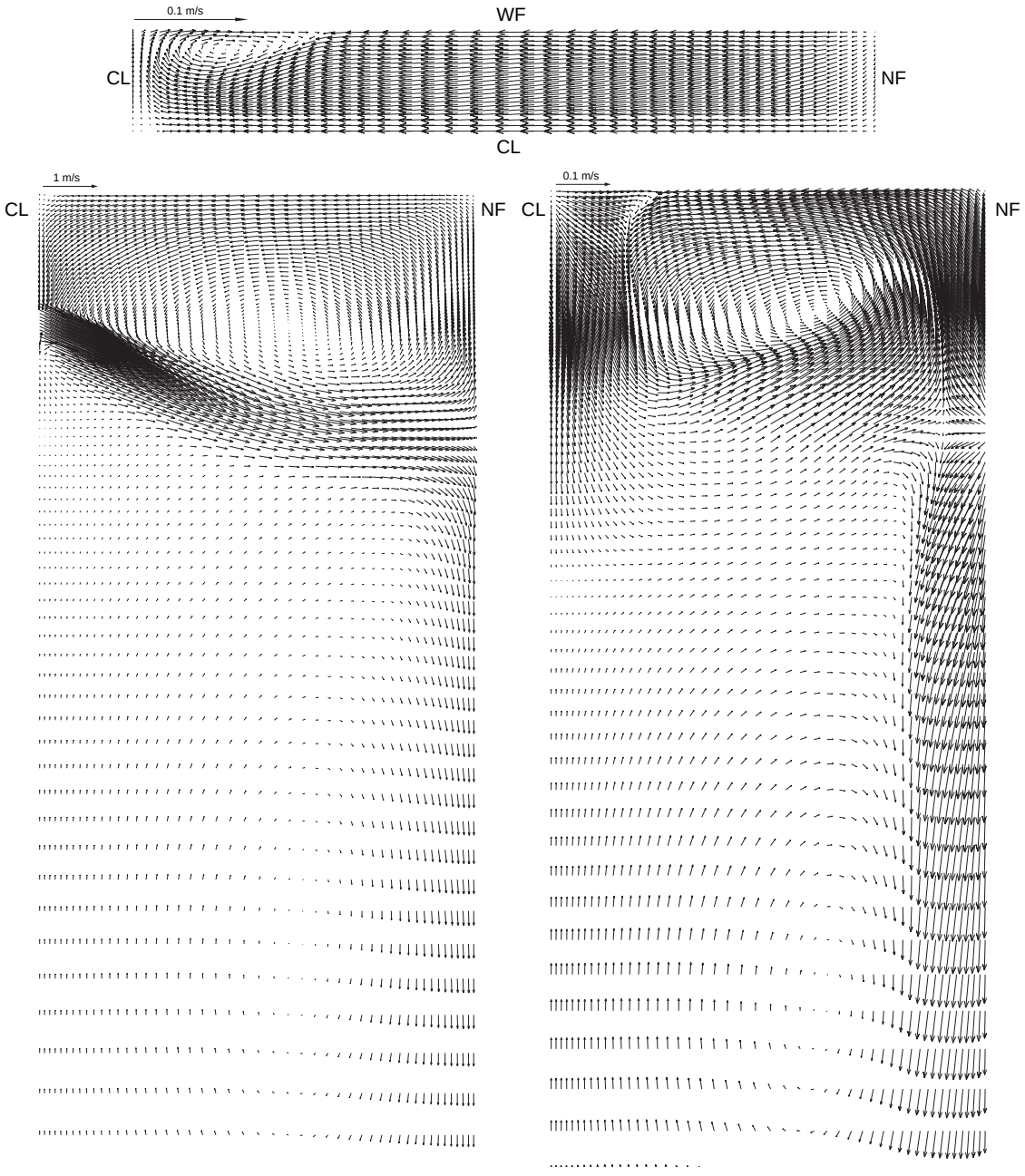

Figure E.69. Case 18. Centerplane (left), Wide Face (right) and Top Surface (top) Velocity. Width 1.60 m, 0% Gas.

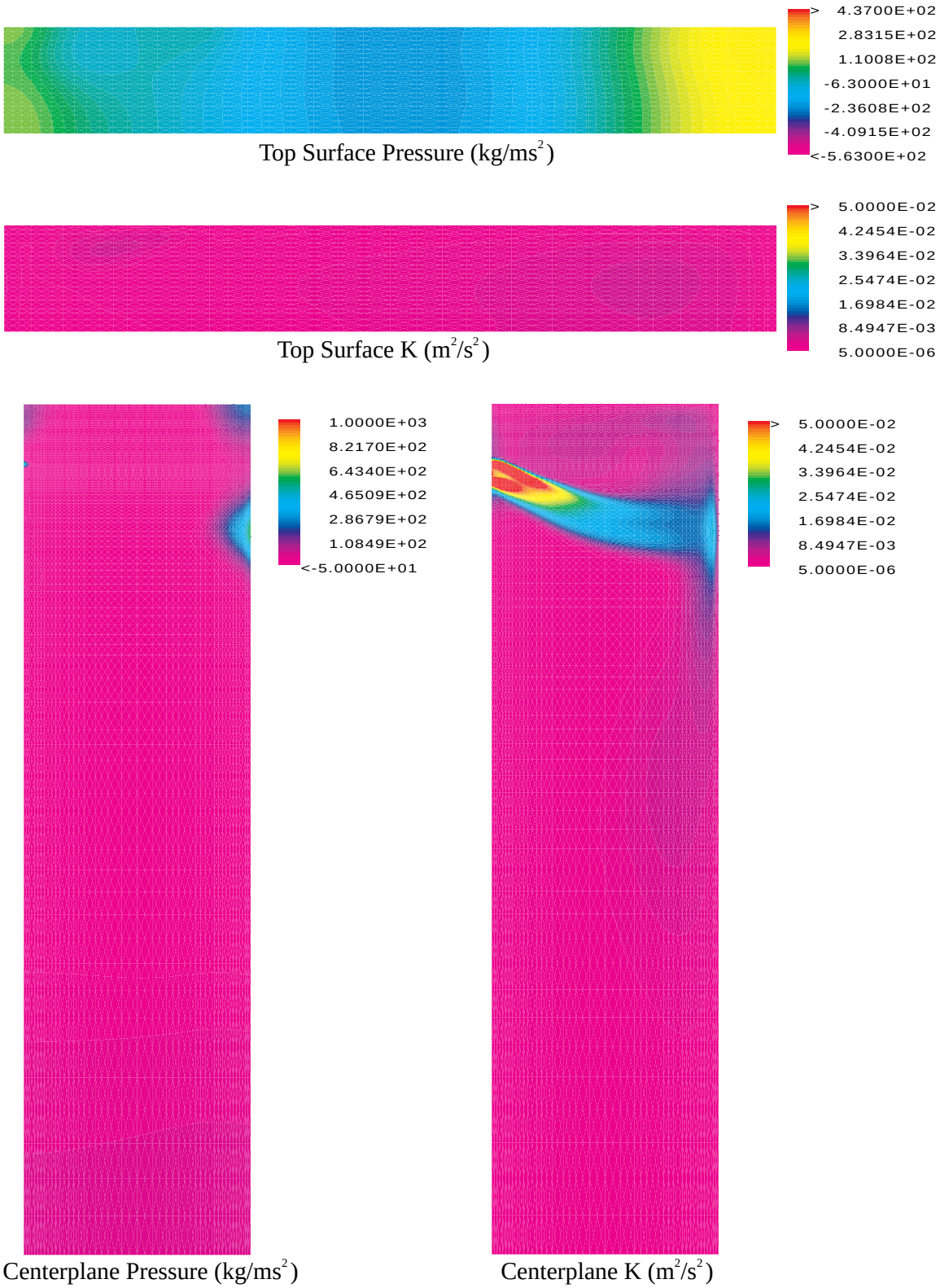

Figure E.70. Case 18. Width 1.60 m, 0% Gas.

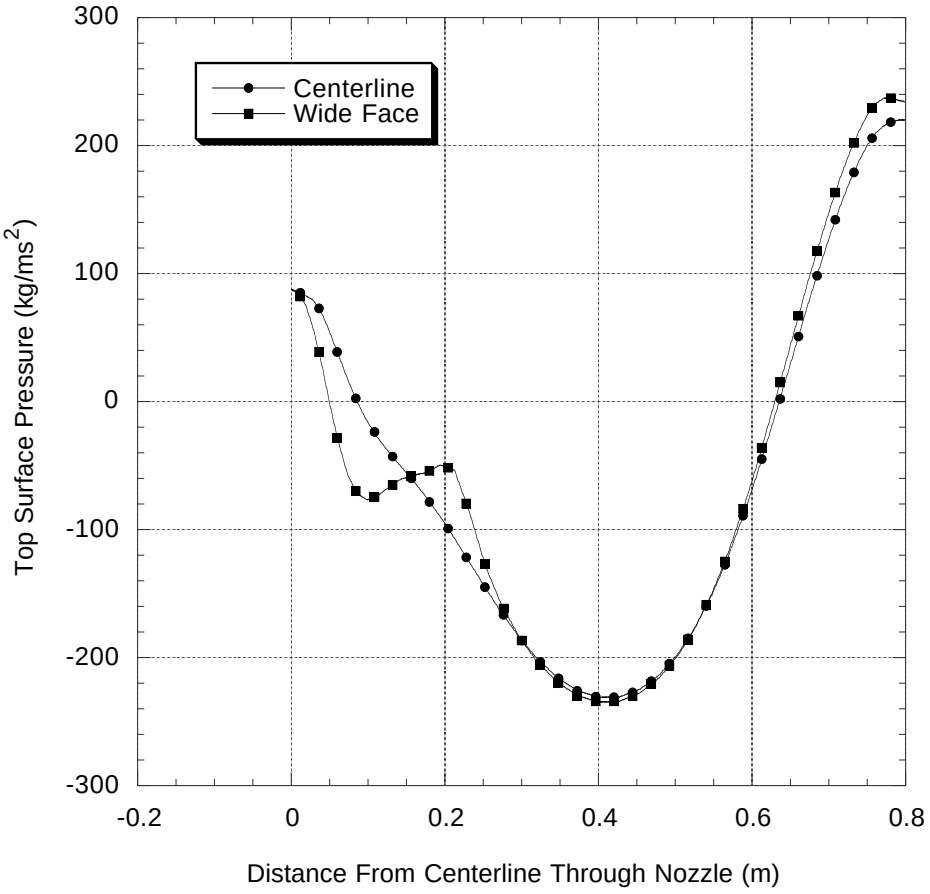

Figure E.71. Case 18. Centerplane and Wide Face Top Surface Pressure. Width 1.60 m, 0% Gas.

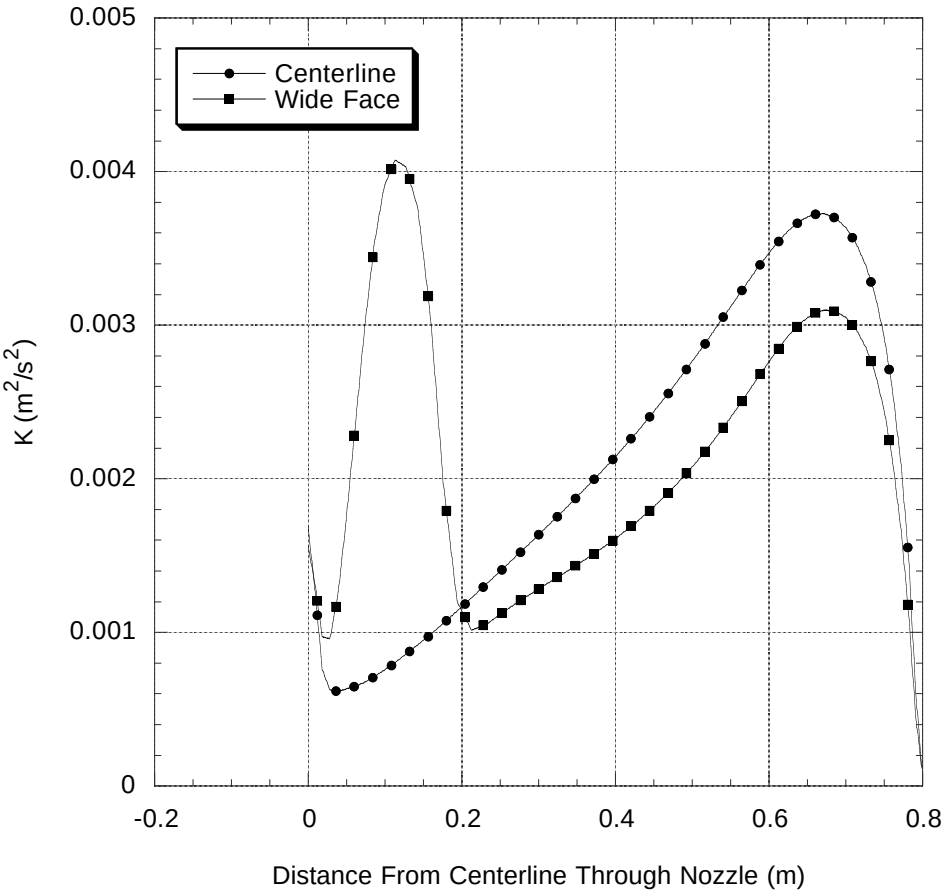

Figure E.72. Case 18. Centerplane and Wide Face Turbulent Kinetic Energy (K). Width 1.60 m, 0% Gas.

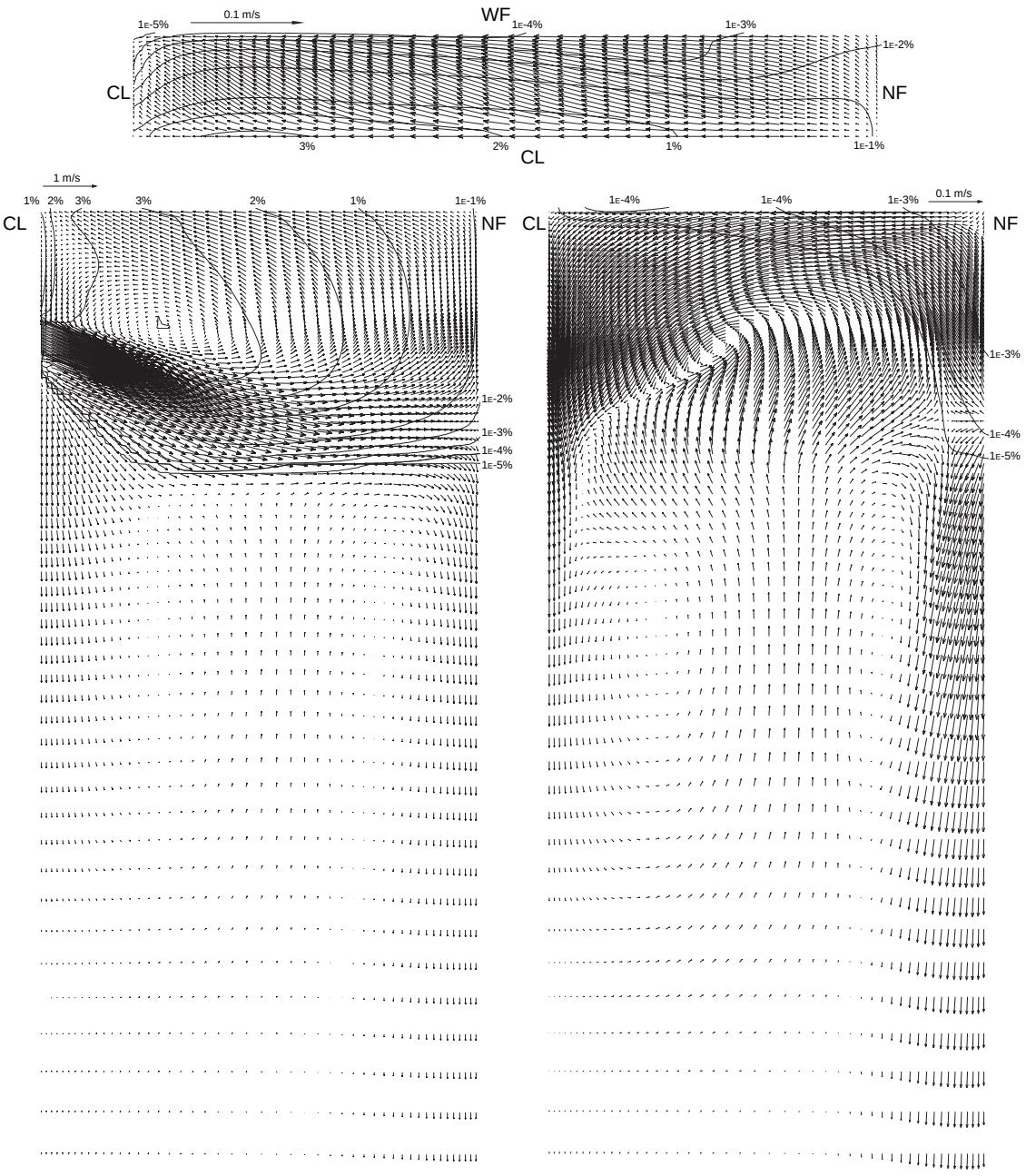

Figure E.73. Case 19. Centerplane (left), Wide Face (right) and Top Surface (top) Velocity. Width 1.60 m, 1 mm Bubble Diameter, 6% Gas.

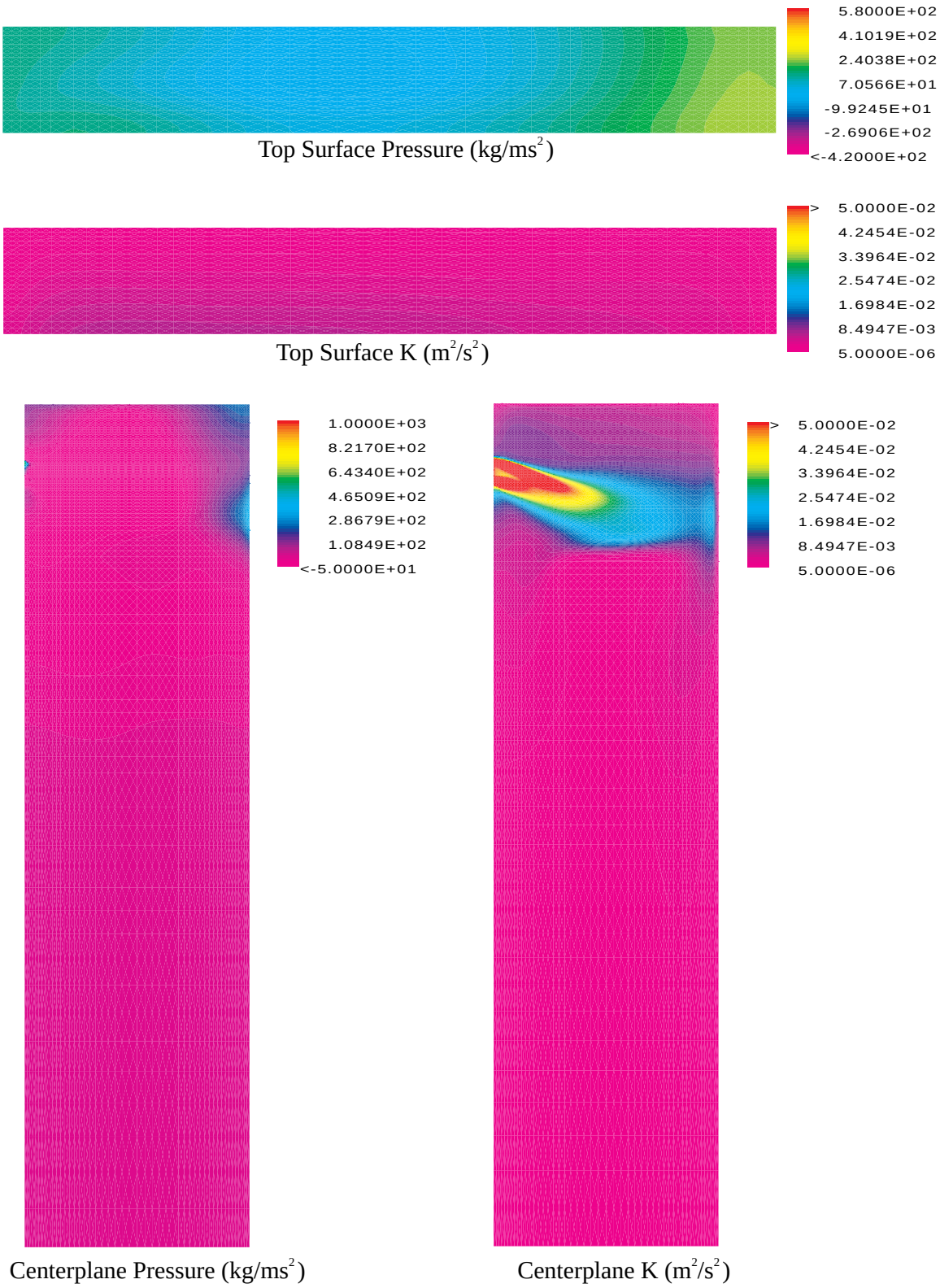

Figure E.74. Case 19. Width 1.60 m, 1 mm Bubble Diameter, 6% Gas.

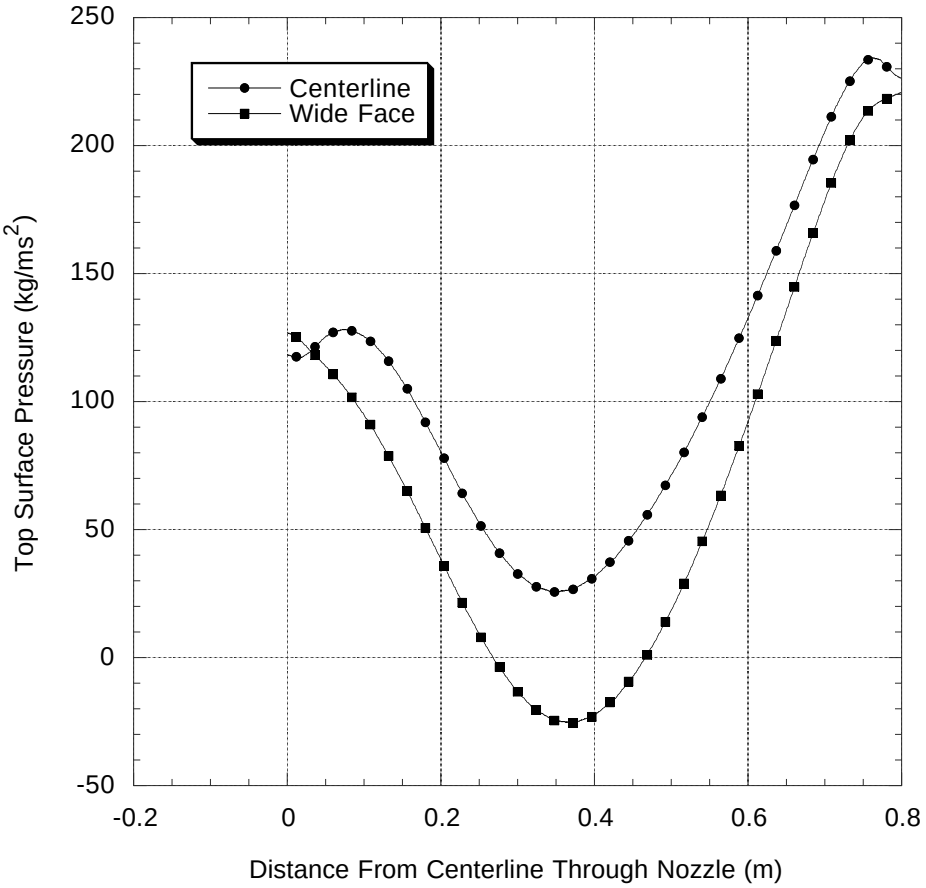

Figure E.75. Case 19. Centerplane and Wide Face Top Surface Pressure. Width 1.60 m, 1 mm Bubble Diameter, 6% Gas.

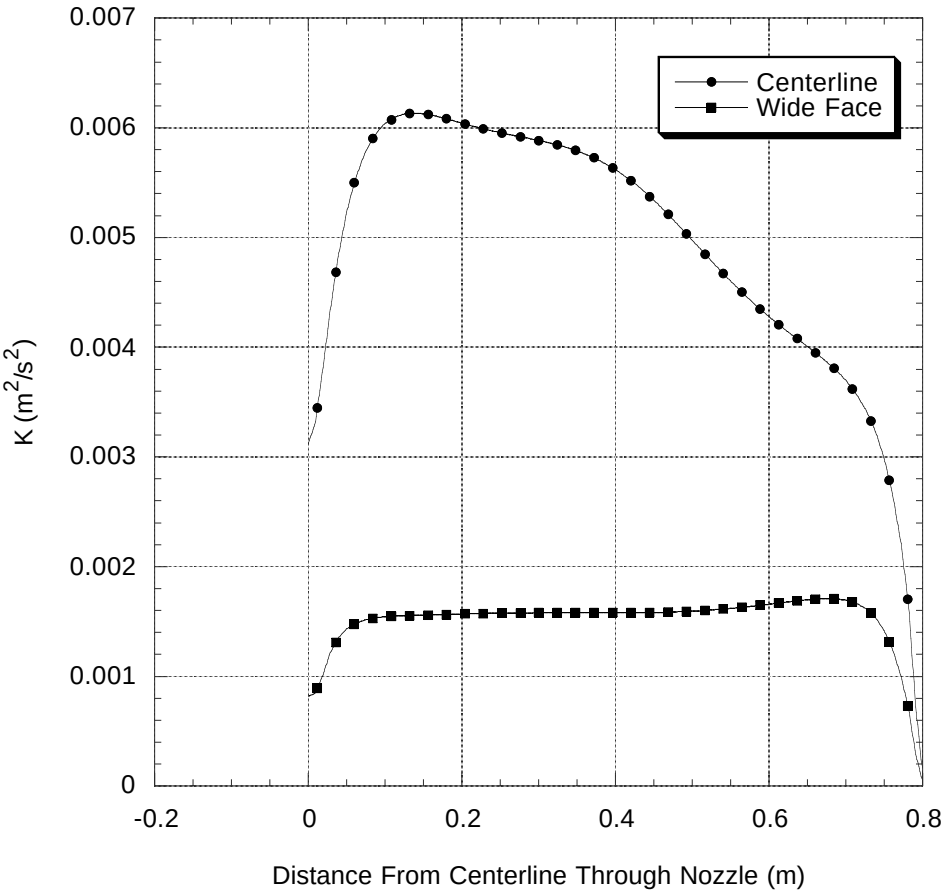

Figure E.76. Case 19. Centerplane and Wide Face Turbulent Kinetic Energy (K). Width 1.60 m, 1 mm Bubble Diameter, 6% Gas.

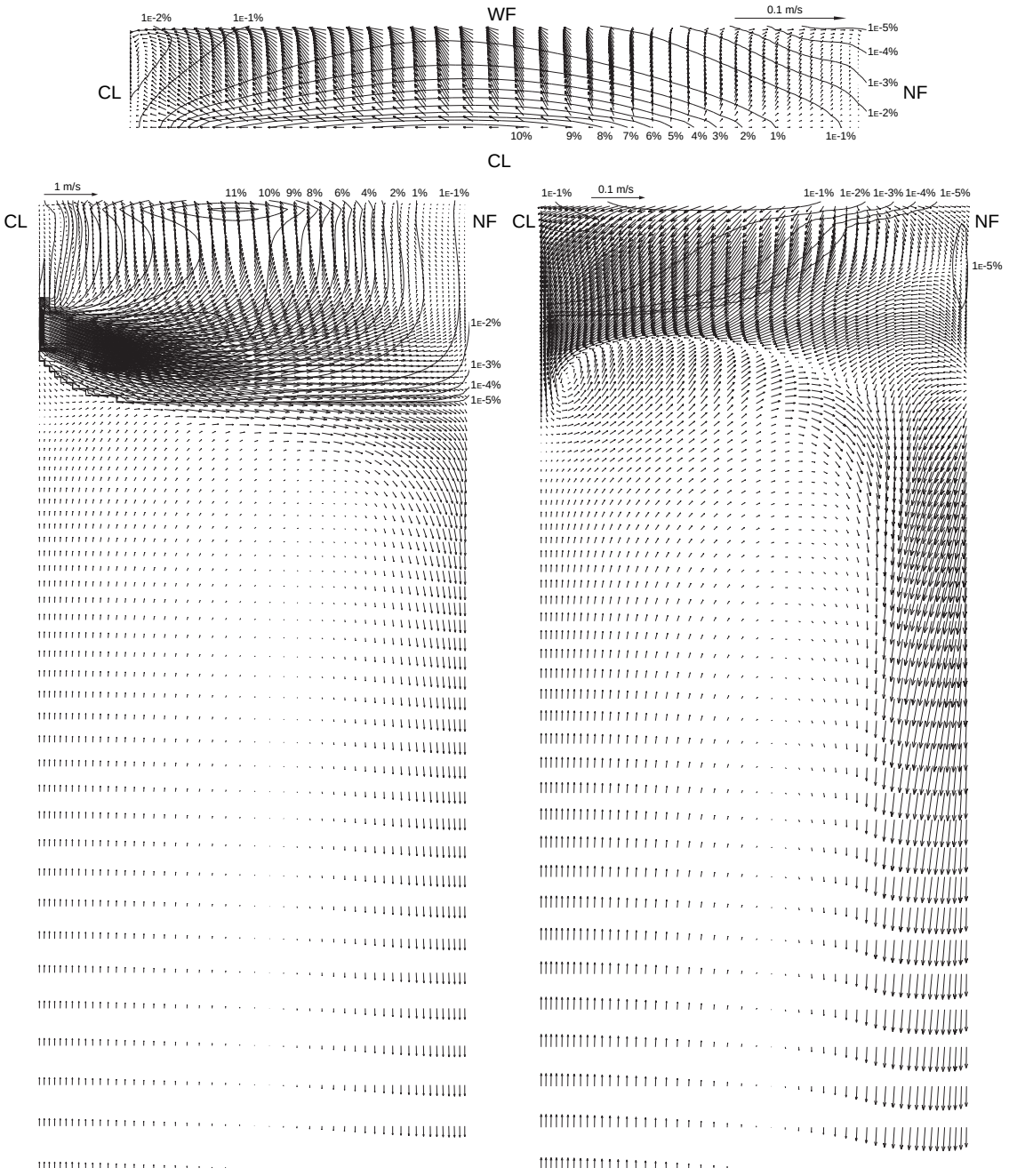

Figure E.77. Case 20. Centerplane (left), Wide Face (right) and Top Surface (top) Velocity. Width 1.60 m, 1 mm Bubble Diameter, 20% Gas.

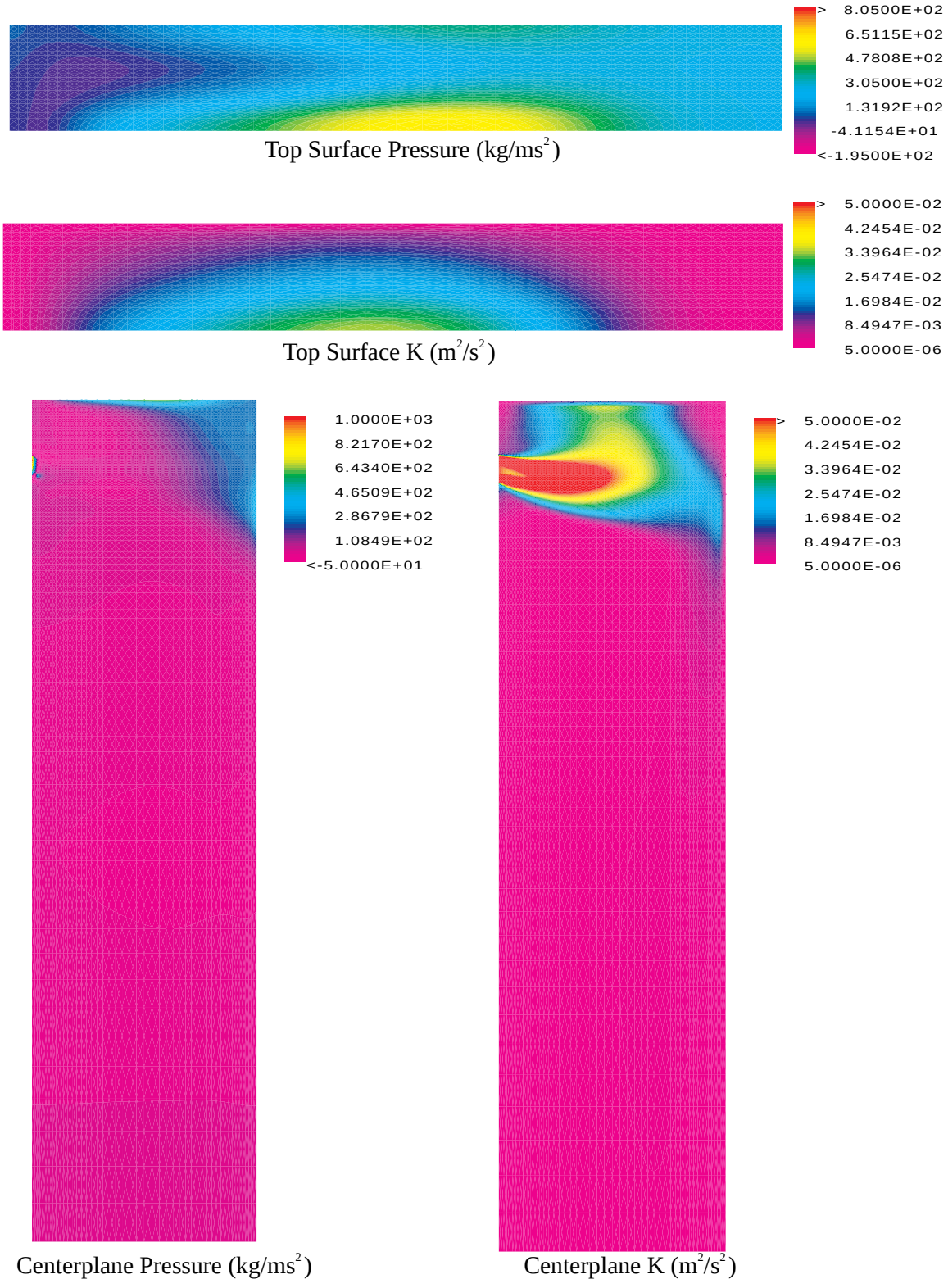

Figure E.78. Case 20. Width 1.60 m, 1 mm Bubble Diameter, 20% Gas.

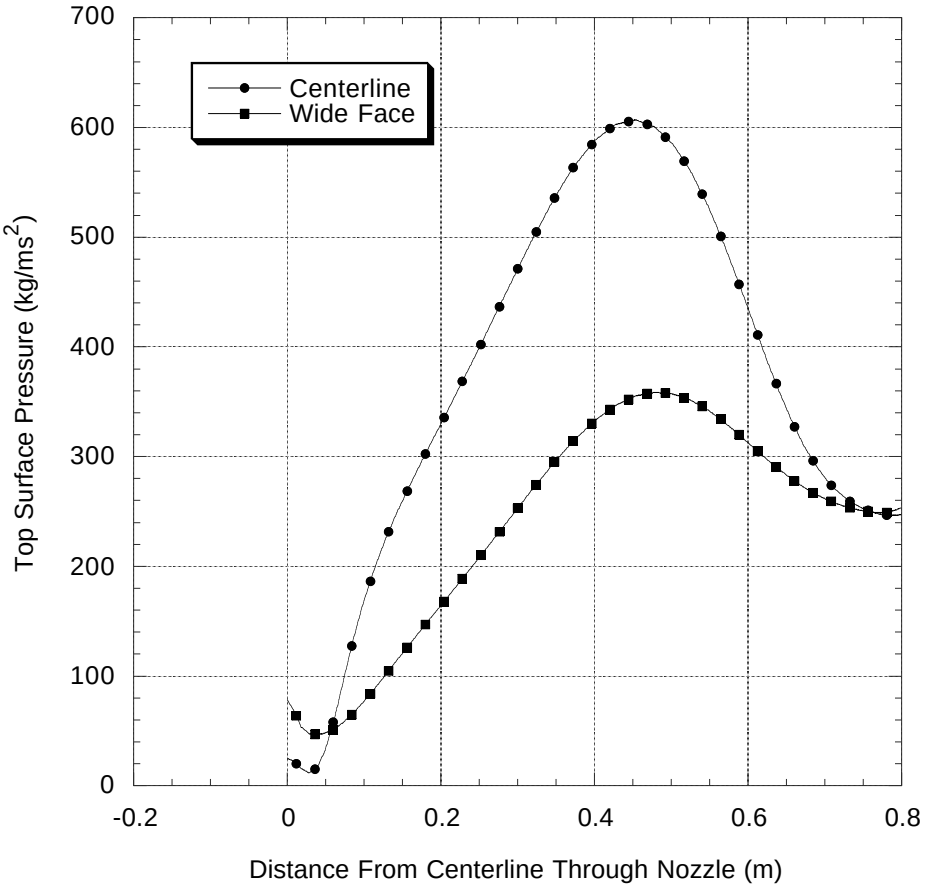

Figure E.79. Case 20. Centerplane and Wide Face Top Surface Pressure. Width 1.60 m, 1 mm Bubble Diameter, 20% Gas.

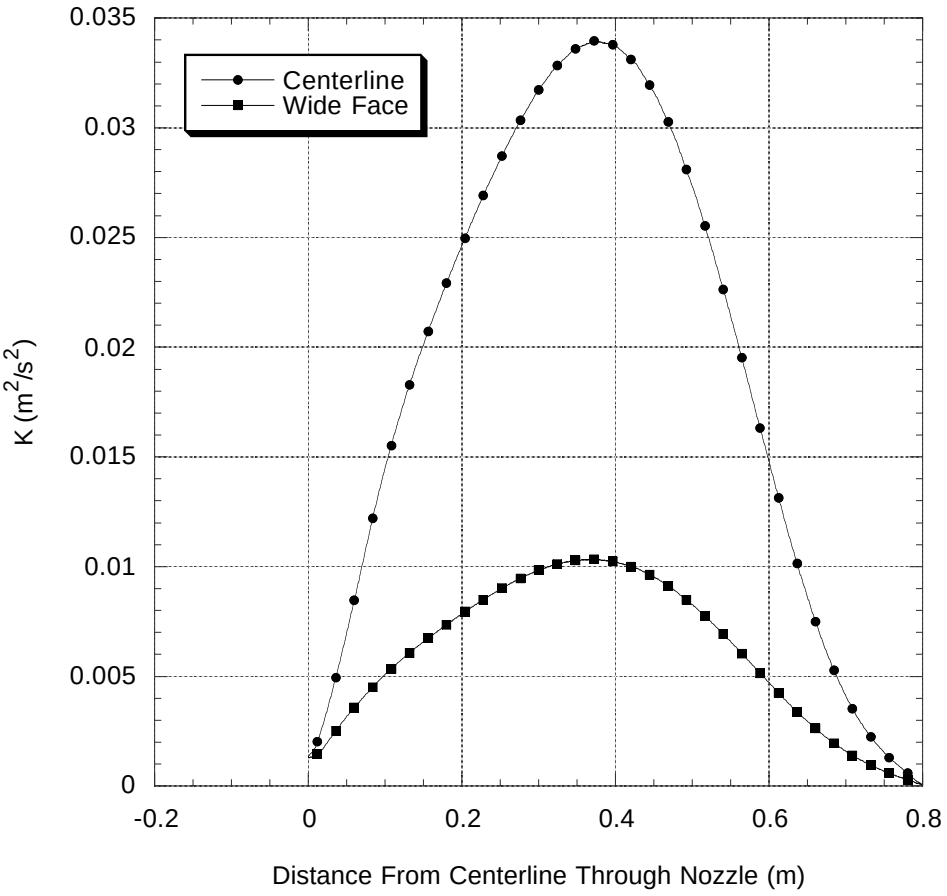

Figure E.80. Case 20. Centerplane and Wide Face Turbulent Kinetic Energy (K). Width 1.60 m, 1 mm Bubble Diameter, 20% Gas.

Appendix F. Sample Command File for Multiphase Model Using CFX

```
>>CFX4
   >>OPTIONS
     THREE DIMENSIONS
     BODY FITTED GRID
     CARTESIAN COORDINATES
     TURBULENT FLOW
     ISOTHERMAL FLOW
     INCOMPRESSIBLE FLOW
     BUOYANT FLOW
     STEADY STATE
     USER SCALAR EQUATIONS 1
     NUMBER OF PHASES 2
   >>USER FORTRAN
     USRSRC
     USRTRN
   >>VARIABLE NAMES
     U VELOCITY 'U VELOCITY'
     V VELOCITY 'V VELOCITY'
     W VELOCITY 'W VELOCITY'
     PRESSURE 'PRESSURE'
     VOLUME FRACTION 'VOLUME FRACTION'
     DENSITY 'DENSITY'
     VISCOSITY 'VISCOSITY'
     K 'K'
     EPSILON 'EPSILON'
     USER SCALAR1 'YPLUS'
 >>MODEL DATA
   >>AMBIENT VARIABLES
     K 0.0502
     EPSILON 0.4570
   >>TITLE
     PROBLEM TITLE 'INLAND MULTIPHASE FLOW MODEL'
   >>PHYSICAL PROPERTIES
     >>BUOYANCY PARAMETERS
       PHASE NAME 'PHASE1'
       ALL PHASES
       GRAVITY VECTOR 0.000000E+00 0.000000E+00 -9.800000E+00
     >>FLUID PARAMETERS
       VISCOSITY 5.5500E-03
       DENSITY 7.0200E+03
     >>FLUID PARAMETERS
       PHASE NAME 'PHASE2'
       VISCOSITY 7.4200E-05
       DENSITY 5.5900E-01
     >>MULTIPHASE PARAMETERS
       >>PHASE DESCRIPTION
         PHASE NAME 'PHASE1'
         LIQUID
         CONTINUOUS
       >>PHASE DESCRIPTION
         PHASE NAME 'PHASE2'
         GAS
         DISPERSE
         MEAN DIAMETER 1.0000E-03
       >>MULTIPHASE MODELS
         >>MOMENTUM
           INTER PHASE TRANSFER
           SINCE
       >>INTER PHASE TRANSFER MODELS
         >>MOMENTUM
           FIRST PHASE NAME 'PHASE1'
           SECOND PHASE NAME 'PHASE2'
           >>PARTICLE MODEL
             ALLEN
     >>TURBULENCE PARAMETERS
       >>TURBULENCE MODEL
         PHASE NAME 'PHASE1'
         TURBULENCE MODEL 'K-EPSILON'
```

```
        PARTICLE INDUCED TURBULENCE 'NONE'
      >>TURBULENCE MODEL
        PHASE NAME 'PHASE2'
        TURBULENCE MODEL 'LAMINAR'
        PARTICLE INDUCED TURBULENCE 'NONE'
>>SOLVER DATA
  >>PROGRAM CONTROL
    MAXIMUM NUMBER OF ITERATIONS 1000
    MASS SOURCE TOLERANCE 1.0000E-06
    ITERATIONS OF TURBULENCE EQUATIONS 1
    ITERATIONS OF VELOCITY AND PRESSURE EQUATIONS 1
    ITERATIONS OF TEMPERATURE AND SCALAR EQUATIONS 1
    ITERATIONS OF HYDRODYNAMIC EQUATIONS 1
    SOLVER DEBUG PRINT STREAM 20
  >>DEFERRED CORRECTION
    K START 2001
    K END 2001
    EPSILON START 2001
    EPSILON END 2001
  >>UNDER RELAXATION FACTORS
    ALL PHASES
    U VELOCITY 7.0000E-01
    V VELOCITY 7.0000E-01
    W VELOCITY 7.0000E-01
    PRESSURE 1.0000E+00
    VOLUME FRACTION 1.0000E+00
    VISCOSITY 1.0000E+00
    K 7.0000E-01
    EPSILON 7.0000E-01
>>MODEL BOUNDARY CONDITIONS
  >>INLET BOUNDARIES
    PHASE NAME 'PHASE1'
    PATCH NAME 'NOZZLE INLET'
    U VELOCITY 1.0620E+00
    V VELOCITY 0.0000E+00
    W VELOCITY -4.2700E-01
    VOLUME FRACTION 1.0000E+00
    K 0.0502
    EPSILON 0.4570
  >>INLET BOUNDARIES
    PHASE NAME 'PHASE2'
    PATCH NAME 'NOZZLE INLET'
    U VELOCITY 1.0620E+00
    V VELOCITY 0.0000E+00
    W VELOCITY -4.2700E-01
    VOLUME FRACTION 1.0000E-08
  >>PRESSURE BOUNDARIES
    PHASE NAME 'PHASE1'
    PATCH NAME 'OUTLET'
    PRESSURE 0.0000E+00
    VOLUME FRACTION 1.0000E+00
  >>PRESSURE BOUNDARIES
    PHASE NAME 'PHASE2'
    PATCH NAME 'OUTLET'
    PRESSURE 0.0000E+00
    VOLUME FRACTION 1.0000E-08
  >>WALL BOUNDARIES
    PHASE NAME 'PHASE1'
    PATCH NAME 'TOP SURFACE'
    U VELOCITY 0.0000E+00
    V VELOCITY 0.0000E+00
    W VELOCITY 0.0000E+00
  >>WALL BOUNDARIES
    ALL PHASES
    PATCH NAME 'WIDE FACE'
    U VELOCITY 0.0000E+00
    V VELOCITY 0.0000E+00
    W VELOCITY 0.0000E+00
  >>WALL BOUNDARIES
    ALL PHASES
    PATCH NAME 'NARROW FACE'
    U VELOCITY 0.0000E+00
    V VELOCITY 0.0000E+00
    W VELOCITY 0.0000E+00
>>OUTPUT OPTIONS
  >>FRONTEND PRINTING
```

```
    NO TOPOLOGY STRUCTURE
  >>PRINT OPTIONS
    >>WHAT
      NO VARIABLES
>>STOP
```

Appendix G. Sample Output File for Multiphase Model Using CFX

```
CFX-4.2 started on  Fri Aug 14 17:12:27 CDT 1998

This job was run on :  thor
The command line was: /usr/local/apps/cfd/cfx/v4.2/bin/runsolve4 -rel 4.2 -dir
/scratch-sif2/dcreech/multiphase/inland/bubble/.cfx4_tmpdir -c m01.fc -fort m01
.f -restart m01.dmp -geom m01.geo -dynam

User Fortran:
-------------
               degas
               injgas
               usrsrc
               usrtrn

  >>CFX4
    >>OPTIONS
      THREE DIMENSIONS
      BODY FITTED GRID
      CARTESIAN COORDINATES
      TURBULENT FLOW
      ISOTHERMAL FLOW
      INCOMPRESSIBLE FLOW
      BUOYANT FLOW
      STEADY STATE
      USER SCALAR EQUATIONS 1
      NUMBER OF PHASES 2
    >>USER FORTRAN
      USRSRC
      USRTRN
    >>VARIABLE NAMES
      U VELOCITY 'U VELOCITY'
      V VELOCITY 'V VELOCITY'
      W VELOCITY 'W VELOCITY'
      PRESSURE 'PRESSURE'
      VOLUME FRACTION 'VOLUME FRACTION'
      DENSITY 'DENSITY'
      VISCOSITY 'VISCOSITY'
      K 'K'
      EPSILON 'EPSILON'
      USER SCALAR1 'YPLUS'
  >>MODEL DATA
    >>AMBIENT VARIABLES
      K 0.0502
      EPSILON 0.4570
    >>TITLE
      PROBLEM TITLE 'INLAND MULTIPHASE FLOW MODEL'
    >>PHYSICAL PROPERTIES
      >>BUOYANCY PARAMETERS
        PHASE NAME 'PHASE1'
        ALL PHASES
        GRAVITY VECTOR 0.000000E+00 0.000000E+00 -9.800000E+00
      >>FLUID PARAMETERS
        VISCOSITY 5.5500E-03
        DENSITY 7.0200E+03
      >>FLUID PARAMETERS
        PHASE NAME 'PHASE2'
        VISCOSITY 7.4200E-05
        DENSITY 5.5900E-01
      >>MULTIPHASE PARAMETERS
        >>PHASE DESCRIPTION
          PHASE NAME 'PHASE1'
          LIQUID
          CONTINUOUS
        >>PHASE DESCRIPTION
          PHASE NAME 'PHASE2'
          GAS
```

```
        DISPERSE
        MEAN DIAMETER 1.0000E-03
      >>MULTIPHASE MODELS
        >>MOMENTUM
          INTER PHASE TRANSFER
          SINCE
      >>INTER PHASE TRANSFER MODELS
        >>MOMENTUM
          FIRST PHASE NAME 'PHASE1'
          SECOND PHASE NAME 'PHASE2'
          >>PARTICLE MODEL
            ALLEN
    >>TURBULENCE PARAMETERS
      >>TURBULENCE MODEL
        PHASE NAME 'PHASE1'
        TURBULENCE MODEL 'K-EPSILON'
        PARTICLE INDUCED TURBULENCE 'NONE'
      >>TURBULENCE MODEL
        PHASE NAME 'PHASE2'
        TURBULENCE MODEL 'LAMINAR'
        PARTICLE INDUCED TURBULENCE 'NONE'
 >>SOLVER DATA
   >>PROGRAM CONTROL
     MAXIMUM NUMBER OF ITERATIONS 1000
     MASS SOURCE TOLERANCE 1.0000E-06
     ITERATIONS OF TURBULENCE EQUATIONS 1
     ITERATIONS OF VELOCITY AND PRESSURE EQUATIONS 1
     ITERATIONS OF TEMPERATURE AND SCALAR EQUATIONS 1
     ITERATIONS OF HYDRODYNAMIC EQUATIONS 1
     SOLVER DEBUG PRINT STREAM 20
   >>DEFERRED CORRECTION
     K START 2001
     K END 2001
     EPSILON START 2001
     EPSILON END 2001
   >>UNDER RELAXATION FACTORS
     ALL PHASES
     U VELOCITY 7.0000E-01
     V VELOCITY 7.0000E-01
     W VELOCITY 7.0000E-01
     PRESSURE 1.0000E+00
     VOLUME FRACTION 1.0000E+00
     VISCOSITY 1.0000E+00
     K 7.0000E-01
     EPSILON 7.0000E-01
 >>MODEL BOUNDARY CONDITIONS

PERMANENT WORKSPACE ALLOCATED
  TYPE      TOTAL SET   TOTAL USED
REAL         22666880      9480198
INTEGER      11333440      4114066
CHARACTER        1438          748
SUMMARY OF RESTART DUMP FILE
------------------------------------------------------------------------
FILE PRODUCED BY CFX-4.2
TIME 08:51:50  DATE 14 AUG 98
----
NUMBER OF VARIABLES            28
NUMBER OF PHASES                2
NUMBER OF BLOCKS                6
NUMBER OF CELLS            114534
NUMBER OF BOUNDARY NODES    25090
NUMBER OF TIME STEPS            1
----
INITIAL GUESS TAKEN FROM A FILE
----
FLOW OPTIONS
   STEADY STATE
   INCOMPRESSIBLE FLOW
   TURBULENT FLOW
   ISOTHERMAL
   CARTESIAN COORDINATES
ACTIVE VARIABLES
   U VELOCITY
   V VELOCITY
   W VELOCITY
```

```
   PRESSURE
   VOLUME FRACTION
   DENSITY
   VISCOSITY
   K
   EPSILON
   YPLUS
------------------------------------------------------------------------
END OF SUMMARY
RESTART USING LAST DATA GROUP

   >>INLET BOUNDARIES
     PHASE NAME 'PHASE1'
     PATCH NAME 'NOZZLE INLET'
     U VELOCITY 1.0620E+00
     V VELOCITY 0.0000E+00
     W VELOCITY -4.2700E-01
     VOLUME FRACTION 1.0000E+00
     K 0.0502
     EPSILON 0.4570
   >>INLET BOUNDARIES
     PHASE NAME 'PHASE2'
     PATCH NAME 'NOZZLE INLET'
     U VELOCITY 1.0620E+00
     V VELOCITY 0.0000E+00
     W VELOCITY -4.2700E-01
     VOLUME FRACTION 1.0000E-08
   >>PRESSURE BOUNDARIES
     PHASE NAME 'PHASE1'
     PATCH NAME 'OUTLET'
     PRESSURE 0.0000E+00
     VOLUME FRACTION 1.0000E+00
   >>PRESSURE BOUNDARIES
     PHASE NAME 'PHASE2'
     PATCH NAME 'OUTLET'
     PRESSURE 0.0000E+00
     VOLUME FRACTION 1.0000E-08
   >>WALL BOUNDARIES
     PHASE NAME 'PHASE1'
     PATCH NAME 'TOP SURFACE'
     U VELOCITY 0.0000E+00
     V VELOCITY 0.0000E+00
     W VELOCITY 0.0000E+00
   >>WALL BOUNDARIES
     ALL PHASES
     PATCH NAME 'WIDE FACE'
     U VELOCITY 0.0000E+00
     V VELOCITY 0.0000E+00
     W VELOCITY 0.0000E+00
   >>WALL BOUNDARIES
     ALL PHASES
     PATCH NAME 'NARROW FACE'
     U VELOCITY 0.0000E+00
     V VELOCITY 0.0000E+00
     W VELOCITY 0.0000E+00
 >>OUTPUT OPTIONS

LINEAR SOLVER - BLOCK DEPENDENCY INFORMATION:

PERCENTAGE OF WELL ORDERED BLOCKS   100.0000
ORDERING USED
  6    1    4    5    2    3

   >>FRONTEND PRINTING
     NO TOPOLOGY STRUCTURE
   >>PRINT OPTIONS
     >>WHAT
       NO VARIABLES
 >>STOP
```

```
*************************************************************************
*                                                                       *
*                                                                       *
*                                                                       *
*                                                                       *
*                                                                       *
*               CCCCC   FFFFFF  XX    XX            444                 *
*              CCCCCCC  FFFFFF   XX  XX            4444                 *
*              CC       FF        XXXX            44 44                 *
*              CC       FFFFFF     XX     ====    44  44                 *
*              CC       FFFFFF    XXXX           44444444               *
*              CCCCCCC  FF       XX  XX          44444444               *
*               CCCCC   FF      XX    XX              44                 *
*                                                                       *
*                                                                       *
*                                                                       *
*                     3D LAMINAR AND TURBULENT FLOW                     *
*                          PREDICTION PROGRAM                           *
*                                                                       *
*                             VERSION  4.2                              *
*                                                                       *
*                                                                       *
*                                                                       *
*                                                                       *
*                                                                       *
*                           CFX-4 PROGRAM                               *
*                      COPYRIGHT AEA TECHNOLOGY PLC                     *
*        DISTRIBUTED ONLY ON THE BASIS OF STRICT CONFIDENTIALITY.       *
*                     CONFIDENTIALITY TO BE MAINTAINED                  *
*                                                                       *
*                                                                       *
*************************************************************************



  ***  INLAND MULTIPHASE FLOW MODEL                                  ***


     RUN AT  17:12:56  ON  14:08:98



     3-DIMENSIONAL  2-PHASE FLOW PREDICTION USING CFX-4


  FLOW OPTIONS
     TURBULENT FLOW
     STEADY STATE
     INCOMPRESSIBLE  FLOW
     NO. OF ADDITIONAL SCALAR EQUATIONS =    1
     BUOYANT FLOW, GRAVITY VECTOR =     0.000E+00    0.000E+00   -9.800E+00
                   BUOYANCY REFERENCE DENSITY   =   7.020E+03

  BUOYANCY PARAMETERS FOR PHASE    1

  BUOYANCY PARAMETERS FOR PHASE    2

  FLUID FLOW PROPERTIES

  PROPERTIES FOR PHASE    1
     DENSITY           =   7.020E+03    SET BY >> FLUID PARAMETERS
     LAMINAR VISCOSITY =   5.550E-03    SET BY >> FLUID PARAMETERS

  PROPERTIES FOR PHASE    2
     DENSITY           =   5.590E-01    SET BY >> FLUID PARAMETERS
     LAMINAR VISCOSITY =   7.420E-05    SET BY >> FLUID PARAMETERS

  HEAT AND MASS TRANSFER PROPERTIES
     CALORICALLY PERFECT FLUID

  PROPERTIES FOR PHASE    1
```

```
PROPERTIES FOR PHASE    2

TURBULENCE PROPERTIES

   TURBULENCE MODEL DETAILS FOR PHASE    1
   MODEL = STANDARD K-EPSILON

   TURBULENT PRANDTL NUMBERS AND LOG LAYER CONSTANTS

  VARIABLE                       PRT        ELOG      XYPLUS
  --------                       ---        ----      ------
  VELOCITY                   1.000E+00   9.793E+00   1.123E+01
  K                          1.000E+00
  EPSILON                    1.217E+00

   TURBULENCE MODEL DETAILS FOR PHASE    2
   MODEL = LAMINAR

   MODEL PARAMETERS
        C1     =  1.440    C2     =  1.920    C3     =  0.000
        CMU    =  0.090    CAPPA  =  0.419

MULTIPHASE PARAMETERS

   PHASE DESCRIPTIONS
   PHASE    1   TYPE = LIQUID  CONTINUOUS
   PHASE    2   TYPE = GAS     DISPERSE     MEAN DIAMETER =   1.000E-03

   MULTIPHASE MODELS
      IPSA   = INTER PHASE TRANSFER     HOMOG  = HOMOGENEOUS
      EXPLIC = EXPLICIT                 PARTIC = PARTICLE MODEL
      MIXTUR = MIXTURE MODEL            STRATI = STRATIFIED MODEL

   EQUATION                   MODEL
   --------                   -----
   MOMENTUM                   IPSA    SINCE
   TURBULENCE                 IPSA    SINCE
   CONCENTRATIONS             IPSA    SINCE

   INTER PHASE TRANSFER BETWEEN PHASE1     AND PHASE2

   EQUATION                   MODEL
   --------                   -----
   MOMENTUM                   PARTIC
                              DRAG MODEL = ALLEN
                              PARTICLE CONCENTRATION IS : DILUTE

WALL BOUNDARY CONDITIONS FOR PHASE    1
   SYNTHETIC BOUNDARY CONDITIONS
   LOGARITHMIC WALL PROFILES
   DEFAULT NO SLIP BOUNDARY CONDITIONS

WALL BOUNDARY CONDITIONS FOR PHASE    2
   NATURAL BOUNDARY CONDITIONS
   QUADRATIC WALL PROFILES
   DEFAULT NO SLIP BOUNDARY CONDITIONS

GEOMETRY AND GRID
   NON-ORTHOGONAL MODE
   CARTESIAN COORDINATES IN PHYSICAL SPACE

SOLUTION PROCEDURE OPTIONS
   SIMPLE ALGORITHM
   USING SIMPLEC CORRECTION, ALPHA =  1.000000

      FDS  = DIFFERENCING SCHEME         RDFC = RESIDUAL REDUCTION FACTOR
      URF  = UNDER RELAXATION FACTOR     MNSL = MINIMUM NUMBER OF ITERATIONS
      DTF  = FALSE TIME STEP             MXSL = MAXIMUM NUMBER OF ITERATIONS
      CRNT = COURANT NUMBER              MOL  = DIFFERENCE MOLECULE IN SOLVER
      METH = SOLVER METHOD               EXT  = ORDER OF TIME EXTRAPOLATION
      TYPE = VARIABLE TYPE

   SOLUTION PARAMETERS FOR PHASE    1

   EQUATION            FDS     URF     DTF      CRNT      METH     TYPE           EXT
```

```
     --------              ---     ---     ---      ----      ----     ----             ---
     U VELOCITY            HDS     0.70   0.0E+00   0.0E+00   ST3D     UNBOUNDED        0
     V VELOCITY            HDS     0.70   0.0E+00   0.0E+00   ST3D     UNBOUNDED        0
     W VELOCITY            HDS     0.70   0.0E+00   0.0E+00   ST3D     UNBOUNDED        0
     PRESSURE              CDS     1.00   0.0E+00   0.0E+00   ICCG     UNBOUNDED        0
     VOLUME FRACTION       UDS     1.00   0.0E+00   0.0E+00   ST3D     SIGN DEFINITE    0
     K                     HDS     0.70   0.0E+00   0.0E+00   LRLX     SIGN DEFINITE    0
     EPSILON               HDS     0.70   0.0E+00   0.0E+00   LRLX     SIGN DEFINITE    0

     EQUATION              RDFC    MNSL    MXSL    MOL
     --------              ----    ----    ----    ---
     U VELOCITY            0.250      1       5   7-PT
     V VELOCITY            0.250      1       5   7-PT
     W VELOCITY            0.250      1       5   7-PT
     PRESSURE              0.100      1      30   7-PT
     VOLUME FRACTION       0.250      1       5   7-PT
     K                     0.250      1       5   7-PT
     EPSILON               0.250      1       5   7-PT

     SOLUTION PARAMETERS FOR PHASE    2

     EQUATION              FDS     URF     DTF      CRNT      METH     TYPE           EXT
     --------              ---     ---     ---      ----      ----     ----            --
-
     U VELOCITY            HDS     0.70   0.0E+00   0.0E+00   ST3D     UNBOUNDED        0
     V VELOCITY            HDS     0.70   0.0E+00   0.0E+00   ST3D     UNBOUNDED        0
     W VELOCITY            HDS     0.70   0.0E+00   0.0E+00   ST3D     UNBOUNDED        0
     PRESSURE              CDS     1.00   0.0E+00   0.0E+00   ICCG     UNBOUNDED        0
     VOLUME FRACTION       UDS     1.00   0.0E+00   0.0E+00   ST3D     SIGN DEFINITE    0
     K                     HDS     0.70   0.0E+00   0.0E+00   LRLX     SIGN DEFINITE    0
     EPSILON               HDS     0.70   0.0E+00   0.0E+00   LRLX     SIGN DEFINITE    0

     EQUATION              RDFC    MNSL    MXSL    MOL
     --------              ----    ----    ----    ---
     U VELOCITY            0.250      1       5   7-PT
     V VELOCITY            0.250      1       5   7-PT
     W VELOCITY            0.250      1       5   7-PT
     PRESSURE              0.100      1      30   7-PT
     VOLUME FRACTION       0.250      1       5   7-PT
     K                     0.250      1       5   7-PT
     EPSILON               0.250      1       5   7-PT

   MULTIPHASE DAMPING OF THE RHIE-CHOW CORRECTION TERM

      RESIDUAL MASS FLOW  =  1.000E-06


 REAL BOUNDARY CONDITIONS


      ***       ALL WALLS HAVE DEFAULT BOUNDARY CONDITIONS           ***
      ***                   OF ZERO VELOCITY                         ***


 FLOW BOUNDARIES


 NO. OF INLET BOUNDARY GROUP NUMBERS =    1
    GROUP NO.   PHASE NO.   FLOW IN
         1           1      8.499E+00
         1           2      6.768E-12

 NO. OF PRESSURE BOUNDARY GROUP NUMBERS =    1


 TOTAL FLOW INTO REGION THROUGH INFLOW/OUTFLOW BOUNDARIES:
      INLETS                                =  8.499E+00
      OUTLETS                               =  0.000E+00

 ******** USRTRN - INLET **********
   NISURF=          30 JISURF=     4130621
   IWORK(JISURF)=      114535
   IWORK(JISURF+NISURF-1)=      114564
   TOTAL AREA OF INLET =  1.1400053E-03
```

```
  INJECTOR
   AIR  FLOW RATE  (kg/s)=      9.8095654E-05
   AIR  FLOW RATE  (kg/m^2*s)=  8.6048417E-02
   JET  VELOCITY    (m/s)=   1.062000      0.1000000     -0.4270000

 ******** USRTRN - OUTLET *********
  NDSURF=         920 JDSURF=     4130651
  IWORK(JDSURF)=      125025
  IWORK(JDSURF+NDSURF-1)=      125944


MONITORING POINT AT (  2,  5, 20) IN BLOCK: BLOCK-NUMBER-1
 ITER  I------------ABSOLUTE RESIDUAL SOURCE SUMS------------I I------------------FIELD
VALUES AT MONITORING POINT------------------I
   NO.   UMOM    VMOM    WMOM    MASS    VFRC    TKIN    EDIS    U VEL.    V VEL.    W
VEL.    PRESS.    VFRAC       K        EPS.
                                                                    USR 1
  PHASE: PHASE1
    1  3.52E-5 3.58E-5 1.44E-3 4.01E-4 1.79E-4 2.62E-5 3.72E-4  3.058E-01-9.736E-03
8.798E-02 3.959E+00 9.269E-01 3.815E-02 1.076E-01
                                                                    0.000E+00

  PHASE: PHASE2
    1  6.00E-1 6.52E-1 2.71E+1 4.01E-4 2.03E-4 0.00E+0 0.00E+0  3.053E-01-8.333E-03
2.128E-01 3.959E+00 7.311E-02 5.020E-02 4.570E-01
                                                                    0.000E+00
```

Iterations 2 through 999 have been cut for space

```
  PHASE: PHASE1
 1000  7.38E-6 2.43E-6 9.46E-6 1.83E-5 3.54E-6 1.47E-6 3.34E-5  4.219E-01-1.131E-02
1.493E-01-2.040E+01 9.090E-01 4.707E-02 1.514E-01
                                                                    0.000E+00

  PHASE: PHASE2
 1000  9.17E-3 7.48E-3 2.79E-3 1.83E-5 2.56E-6 0.00E+0 0.00E+0  4.216E-01-9.226E-03
2.695E-01-2.040E+01 9.098E-02 5.020E-02 4.570E-01
                                                                    0.000E+00



 #### WARNING FROM SUBROUTINE FLOCAL ####
 UNDER RELAXATION OF DEFERRED CORRECTION IS
 LESS THAN 1.0 AT THE END OF ITERATIONS
 VALUE FOR K   0.0000E+00 VALUE FOR EPSILON   0.0000E+00

 AVERAGE REDUCTION FACTOR ACHIEVED BY LINEAR SOLVERS


          PHASE NUMBER      1
      U RESIDUALS   (PHASE  1)           8.6E-03
      V RESIDUALS    (PHASE 1)           3.4E-02
      W RESIDUALS    (PHASE 1)           5.8E-03
     MASS SOURCE RESIDUALS              1.9E-01
  VFRAC RESIDUALS    (PHASE 1)           2.3E-01
     TE RESIDUALS   (PHASE  1)           1.1E-01
     ED RESIDUALS   (PHASE  1)           2.0E-01

          PHASE NUMBER      2
      U RESIDUALS   (PHASE  2)           8.8E-02
      V RESIDUALS    (PHASE 2)           9.5E-02
      W RESIDUALS    (PHASE 2)           7.3E-02
     MASS SOURCE RESIDUALS              1.9E-01
  VFRAC RESIDUALS    (PHASE 2)           2.2E-01
     TE RESIDUALS   (PHASE  2)           0.0E+00
     ED RESIDUALS   (PHASE  2)           0.0E+00



                     MAXIMUM NUMBER OF ITERATIONS EXCEEDED, ITERATIONS TERMINATED
  *** MASS BALANCE ***

  AIR
    INFLOW  (kg/s) =  9.8095632E-05
```

```
   OUTFLOW (kg/s) =  9.8081284E-05
   % ERROR        = -1.4626735E-02

 WATER
   INFLOW  (kg/s) =   8.499010
   OUTFLOW (kg/s) =  -8.500278
   % ERROR        =  -200.0149


 * * * * * * * * * *             MASS FLOW THROUGH INLETS     * * * * * * * * * *


TOTAL MASS FLOW THROUGH INLETS FOR PHASE   1  =    8.499E+00 KG/S
TOTAL MASS FLOW THROUGH INLETS FOR PHASE   2  =    6.768E-12 KG/S


 * * * * * * * * * *      MASS FLOW THROUGH PRESSURE BOUNDARIES  * * * * * * * * * *


TOTAL MASS FLOW THROUGH PRESSURE BOUNDARIES FOR PHASE   1  =   -8.500E+00 KG/S
TOTAL MASS FLOW THROUGH PRESSURE BOUNDARIES FOR PHASE   2  =    4.197E-11 KG/S


 * * * * * * * * * * * * * * * * * * * * * * * * * * * * * * * * * * * * * * * * * * * * * * *

          RATIO OF RESIDUALS FROM SECOND AND LAST ITERATIONS

         PHASE NUMBER      1
                            U RESIDUALS   (PHASE  1)          4.9E+01
                            V RESIDUALS    (PHASE 1)          7.6E+01
                            W RESIDUALS    (PHASE 1)          1.8E+02
                           MASS SOURCE RESIDUALS              8.5E+01
                         VFRAC RESIDUALS    (PHASE 1)          1.8E+01
                           TE RESIDUALS   (PHASE  1)          1.8E+01
                           ED RESIDUALS   (PHASE  1)          9.5E+00

         PHASE NUMBER      2
                            U RESIDUALS   (PHASE  2)          1.8E+01
                            V RESIDUALS    (PHASE 2)          1.1E+01
                            W RESIDUALS    (PHASE 2)          5.0E+02
                           MASS SOURCE RESIDUALS              8.5E+01
                         VFRAC RESIDUALS    (PHASE 2)          3.6E+01
                           TE RESIDUALS   (PHASE  2)          0.0E+00
                           ED RESIDUALS   (PHASE  2)          0.0E+00


 TOTAL REAL      WORKSPACE USED =   18435371
 TOTAL INTEGER   WORKSPACE USED =    4474304
 TOTAL CHARACTER WORKSPACE USED =        967


 TOTAL CPU TIME =    4.057E+04  SECONDS

CFX-4.2 finished on Sat Aug 15 08:02:20 CDT 1998
```

References

1. D.T. Stone, (MS Thesis Thesis, University of Illinois at Urbana-Champaign, .

2. J. Herbertson, O.L. He, P.J. Flint, R.B. Mahapatra, in 74th Steelmaking Conference Proceedings, 74, ISS, Warrendale, PA, 1991), 171-185.

3. W.H. Emling, T.A. Waugaman, S.L. Feldbauer, A.W. Cramb, "Subsurface Mold Slag Entrainment in Ultra-Low Carbon Steels," in Steelmaking Conference Proceedings, 77, (Chicago, IL: ISS, Warrendale, PA, 1994), 371-379.

4. R. McDavid and B.G. Thomas, "Flow and Thermal Behavior of the Top-Surface Flux/ Powder Layers in Continuous Casting Molds," Metallurgical Transactions B, 27B (4) (1996), 672-685.

5. X. Huang and B.G. Thomas, "Modeling Transient Flow Phenomena in Continuous Casting of Steel," (1998),

6. B.G. Thomas, X. Huang and R.C. Sussman, "Simulation of Argon Gas Flow Effects in a Continuous Slab Caster," Metall. Trans. B, 25B (4) (1994), 527-547.

7. N. Bessho, R. Yoda, H. Yamasaki, T. Fujii, T. Nozaki, S. Takatori, "Numerical Analysis of Fluid Flow in the Continuous Casting Mold by a Bubble Dispersion Model," Iron Steelmaker, 18 (4) (1991), 39-44.

8. G.A. Panaras, A. Theodorakakos and G. Bergeies, "Numerical Investigation of the Free Surface in a Continuous Steel Casting Mold Model," Metallurgical and Materials Transactions, 29B (No. 5) (1998), 1112-1126.

9. J. Anagnostopoulos and G. Bergeles, "3-D Modeling of the Flow and the Interface Surface in a Continuous Casting Mold Model," Metallurgical and Materials Transactions, (1998), (in press).

10. B.G. Thomas, A. Dennisov and H. Bai, "Behavior of Argon Bubbles during Continuous Casting of Steel," in Steelmaking Conference Proceedings, 80, (Chicago, IL: ISS, Warrendale, PA., 1997), 375-384.

11. Y. Shang, "Statistics on Pencil-Pipe and Blister Defects" (Report, University of Illinois at Urbana Champaign, 1996).

12. R.I.L. Guthrie, "Physical and Mathematical Models for Ladle Metallurgy Operations" (Paper presented at Mathematical Modeling of Materials Processing Operations, Palm Springs, CA, 1987, The Minerals, Metals, and Materials Society, Warrendale, PA), 447-482.

13. F. Najjar, "Finite Element Modeling of Turbulent Fluid Flow and Heat Transfer Through Bifurcated Nozzles in Continuous Steel Slab Casters" (Masters Thesis, University of Illinois at Urbana-Champaign, 1990).

14. F.M. Najjar, B.G. Thomas and D.E. Hershey, "Turbulent Flow Simulations in Bifurcated Nozzles: Effects of Design and Casting Operation," Metallurgical Transactions B, 26B (4) (1995), 749-765.

15. AEA Technology, "CFX4.2 Solver," 1997),

16. R. McDavid, "Fluid Flow and Heat Transfer Behavior of Top-Surface Flux Layers in Steel Continuous Casting" (Masters Thesis, University of Illinois at Urbana-Champaign, 1994).

17. H. Schlichting, Boundary-Layer Theory, (New York, NY: McGraw Hill, 1979).

18. J. Nikuradse, "Gesetzmaßigkeit der Turbulenenten Stromung in Glatten Rohren," Forsehg. Arb. Ing. Wed., 356 (1932),

19. B.G. Thomas, L.M. Mika and F.M. Najjar, "Simulation of Fluid Flow Inside a Continuous Slab Casting Machine," Metallurgical Transactions, 21B (1990), 387-400.

20. H. Bai and B.G. Thomas, ""Two-Phase Fluid Flow in Continuous Casting Nozzles" (Report, University of Illinois at Urbana-Champaign, 1998), Report to Continuous Casting Consortium.

21. B.G. Thomas, B. Ho and G. Li, "CON1D User's Manual" (Report, University of Illinois, 1994).

22. B.G. Thomas, R.J. O'Malley and D.T. Stone, "Measurement of temperature, solidification, and microstructure in a continuous cast thin slab" (Paper presented at *Modeling of Casting, Welding, and Advanced Solidification Processes VIII*, San Diego, CA, 1998, TMS), 1185-1199.

23. E.A. Mizikar, "Mathmatical heat transfer model for solidification of continuously cast steel slabs," (No. 239) (1967), 1747-1753.

24. B.G. Thomas and X. Huang, "Effect of Argon on Fluid Flow in a Continuous Slab Casting Mold" (Paper presented at 76th Steelmaking Conference, Dallas, TX, 1993, Iron and Steel Society).

25. D.E. Hershey and B.G. Thomas, "Turbulent flow of steel through continuous casting nozzles using 3D finite element models" (Paper presented at 10th Process Technology Conference, Toronto, Canada, April 5-8, 1992, The Iron and Steel Society, Warrendale, PA).

26. P. Andrzejewski, K.-U. Kohler and W. Pluschkeli, "Model investigations on the fluid flow in continuous casting moulds of wide dimensions," 63 (6) (1992), 242-246.

27. K. Tabata and e. al., "Gas Injection Methods at Tundish Slide gate Valve for Continuous Casting" (Report No. Vol 31, Shinagawa Technical Report, 1988).

28. X. Huang and B.G. Thomas, "Modeling Transient Flow Phenomena in Continuous Casting of Steel," in 35th Conference of Metallurgists, 23B, C. Twigge-Molecey, eds., (Montreal, Canada: CIM, 1996), 339-356.

29. A. Cramb, "Slag Entrainment" (Paper presented at Continuous Casting of Steel Billets, Blooms and Slabs, Vancouver, 1997, The University of British Columbia), No. 1, H1-H20.